

Marta Angulo Martínez

# El factor climático en la erosión del suelo: erosividad de la lluvia en la cuenca del Ebro

Departamento  
Geografía y Ordenación del Territorio

Director/es  
Beguería Portugués, Santiago

<http://zaguan.unizar.es/collection/Tesis>



Tesis Doctoral

**EL FACTOR CLIMÁTICO EN LA EROSIÓN DEL  
SUELO: EROSIVIDAD DE LA LLUVIA EN LA  
CUENCA DEL EBRO**

Autor

Marta Angulo Martínez

Director/es

Beguería Portugués, Santiago

**UNIVERSIDAD DE ZARAGOZA**  
Geografía y Ordenación del Territorio

2012



# El factor climático en la erosión del suelo: EROSIVIDAD DE LA LLUVIA EN LA CUENCA DEL EBRO



MARTA ANGULO MARTÍNEZ  
Director: Santiago Beguería Portugués

Universidad de Zaragoza - Facultad de Filosofía y Letras  
Dpto. de Geografía y Ordenación del Territorio

Imagen portada: Erosion caused by soil compaction, canton of Bern, Switzerland.  
Volker Prasuhn 

Imagen contra portada: Estación de medida de la energía de la lluvia y erosión por salpicadura. Estación Experimental Aula Dei-CSIC, Zaragoza

Universidad de Zaragoza – Facultad de Filosofía y Letras  
Dpto. de Geografía y Ordenación del Territorio

El factor climático en la erosión del suelo: erosividad de la lluvia en la cuenca del  
Ebro

Por  
Marta Angulo Martínez

Memoria para optar al grado  
De Doctora en Geografía por la  
Universidad de Zaragoza

Zaragoza, Diciembre 2011

Este trabajo ha contado con la dirección del Dr. Santiago Beguería Portugués, Científico Titular del Consejo Superior de Investigaciones Científicas en la Estación Experimental de Aula Dei (EEAD-CSIC).

La realización de esta Tesis ha sido posible gracias a una ayuda predoctoral del programa JAEpredoc del Consejo Superior de Investigaciones Científicas financiada por CSIC y FEDER, y con financiación de los proyectos de investigación: MEDEROCAR (CGL2008-00831/BTE), EROMED (CGL2011-25486) y DISDROSPEC (CGL2011-24185) financiados por la Comisión Interministerial de Ciencia y Tecnología (CICYT) y FEDER, y Grupo de Excelencia E68 financiado por el Gobierno de Aragón y FEDER.

El Doctor Santiago Beguería Portugués, Científico Titular del Consejo Superior de Investigaciones Científicas en la Estación Experimental de Aula Dei (EEAD-CSIC), Zaragoza, España.

CERTIFICA:

Que Doña Marta Angulo Martínez ha realizado bajo mi dirección el trabajo que, para optar al grado de Doctora en Geografía, presenta con el título:

“El factor climático en la erosión de suelo: erosividad de la lluvia en la cuenca del Ebro”, y

Que el trabajo se ajusta a los objetivos establecidos en el Proyecto de Tesis Doctoral aprobado el 15 de Julio de 2011, por el Departamento de Geografía y ratificado por la Comisión de Doctorado el 7 de Septiembre de 2011.

Y para que así conste, firmo la presente Certificación en Zaragoza a 02 de Marzo de 2012 para los efectos que sean oportunos.

Fdo. Santiago Beguería Portugués

*A mis abuelos,  
a mis padres,  
a mi hermana.*

## Agradecimientos:

Entiendo el ejercicio de investigación como una construcción colectiva, compuesta tanto por el acceso a instrumentos y soportes materiales y bibliográficos como la red de personas que forman el trampolín sobre el que cada individuo se impulsa. Ortega y Gasset dijo que somos nosotros y nuestras circunstancias, también nuestras colectividades. Con estas palabras quiero expresar mi agradecimiento a nodos importantes en esa red de colectividades que de una u otra manera han permitido la realización de esta tesis doctoral.

Expreso pues mi agradecimiento a aquellos que me formaron durante la licenciatura en la Universidad Autónoma de Madrid, muy especialmente al área de geografía física y, sobre todo a Juan Antonio González por su calidad personal y por saber transmitirme la curiosidad necesaria para querer saber más.

A los que me han acogido en Zaragoza, porque aquí empezó el viaje de verdad un verano de 2007 cuando conocí a Sergio Vicente y a Santiago Beguería en el primer curso de estadística climática. Entonces fui afortunada, al poder unirme a este grupo de aguerridos capitanes, Sergio, Nacho López y Santiago, dispuestos a navegar entre las inclemencias del tiempo y los movimientos de la atmósfera, caprichosos en la carestía de lluvias, en copiosas nevadas o energicas tormentas. Me enrolé bajo las órdenes de Santiago como grumetilla inexperta, pero con la inmensa suerte de contar con uno de los mejores capitanes: arriesgado, visionario y dispuesto, con un excelente humor contra viento y marea, haciendo del día a día y de cualquier difícil tarea, algo fácil y con muchas posibilidades. Esta tesis es el resultado de nuestro buen hacer conjunto, pero sobretodo le doy gracias a Santi por todo lo que me ha enseñado y que es en realidad la base para seguir trabajando en investigación con el rigor científico necesario.

Otros muchos han aportado experiencia y conocimientos para diseñar la hoja de ruta, entre ellos: Teodoro Lasanta, Jose M<sup>a</sup> García Ruiz y Ana Navas que dieron su beneplácito y consejos, a la vez que otros compañeros: Luis Carlos Alatorre, Álvaro Cabezas, Manuel López, David Moret, Estela Nadal, Noemí Lana, Leticia Gaspar y otros muchos.

Quiero expresar también mi agradecimiento al equipo del CSIRO Land & Water de Canberra, con quienes pasé 4 meses con el fin de descubrir nuevos métodos que me permitiesen conocer la lluvia de todo el globo y a cualquier altitud. En este caso, bajo las órdenes de Albert Van Dijk, pero de nuevo, muchos otros se implicaron en mi tormentosa causa. Agradezco especialmente la ayuda de Luigi Renzullo, Tim Raupach, Peter Dyce, Adrian Chappell y Tim McVivar, su sentido del humor y sus ganas por compartir y transmitir.

Agradezco a las colectividades de las que he formado parte el compañerismo y las ganas de trabajar gratuitamente por un mundo diferente y mejor: Colectivo Pedalea, Decrecimiento Aragón, Bike-polo Zaragoza, y Radio Topo.

Todo mi agradecimiento va también para los amigos que han aguantado mi temporal de lluvia todo este tiempo y de nueva cuña: Juan, Maribel, Silvia, Ana, Dani, Borja, Edurne, Diego, Nuria, Sofía, Chabi, Alfonso, Marieta, Noé y José Manuel y a todos a los que llevo en el corazón.

*Finalmente, mis circunstancias, mi colectividad más próxima es mi familia, Alberto, Ana, Lara, Pedro y Martina, os agradezco la paciencia, la constancia y el espíritu crítico y de realización que me habéis inculcado.*

*Abí donde las nubes  
enseñan el agua a los cometas  
hay semillas que abogan,  
contra todo pronóstico,  
por quebrantar la uniformidad  
de la arcilla.*

Diego J. Colás

### Monólogo de Isabel viendo llover en Macondo

*“Llovió durante toda la tarde en un solo tono. En la intensidad uniforme y apacible se oía caer el agua como cuando se viaja toda la tarde en un tren. Pero sin que lo advirtiéramos, la lluvia estaba penetrando demasiado hondo en nuestros sentidos. Mi madrastra y yo volvimos a contemplar el jardín. La tierra áspera y parda de mayo se había convertido durante la noche en una substancia oscura y pastosa, parecida al jabón ordinario. Un chorro de agua comenzaba a correr por entre las macetas. “Creo que en toda la noche han tenido agua de sobra”, dijo mi madrastra. Y yo noté que había dejado de sonreír y que su regocijo del día anterior se había transformado en una seriedad laxa y tediosa”.*

Gabriel García Márquez; Cien años de soledad

## Índice de contenidos

<b>1.</b>	<b>Bloque I: Marco conceptual, antecedentes y perspectivas sobre el factor climático en la erosión del suelo</b>	<b>1</b>
1.1	La erosión del suelo como problema medioambiental	3
1.2	Factores de la erosión del suelo	5
1.3	La lluvia como agente erosivo	8
1.4	Estudio del tamaño y velocidad de las gotas de lluvia	10
1.5	Relación entre la intensidad de la lluvia y el tamaño, velocidad y energía cinética de los eventos de lluvia	13
1.6	Climatología de la energía cinética	19
1.7	Índices de erosividad de la lluvia	21
1.8	Fronteras de conocimiento sobre erosividad de la lluvia	23
1.9	El estudio de la erosividad de la lluvia en el ámbito español	26
1.10	Objetivos y estructura de la tesis	29
1.11	Referencias bibliográficas	31
<b>2.</b>	<b>Bloque II: Estudio climatológico de la erosividad de la lluvia en la Cuenca del Ebro</b>	<b>41</b>
2.1	Introduction	43
2.2	Study area	45
2.3	Rainfall erosivity by RUSLE R factor	49
2.4	Database	50
2.5	Validation criteria	61
2.6	Estimating rainfall erosivity from daily precipitation records: a comparison among methods using data from the Ebro Basin (NE Spain)	63
2.7	Mapping rainfall erosivity at the regional scale: a comparison of interpolation methods in the Ebro Basin (NE Spain)	87
2.8	Rainfall erosivity cartography at annual and seasonal scale for the period 1955-2006	117
2.9	Do atmospheric teleconnection patterns influence rainfall erosivity? A study of NAO, MO and WeMO in NE Spain, 1955-2006. 0020	125
2.10	Trends in rainfall erosivity (1955-2006) over the Ebro Basin (NE Spain)	159
2.11	References	175
<b>3.</b>	<b>Bloque III: Estudio experimental de la erosividad de la lluvia: validación de índices a partir de datos empíricos</b>	<b>189</b>

3.1	Introduction	191
3.2	Experimental setup	192
3.3	Splash erosion under natural rainfall on three soil types in NE Spain	199
3.4	On the reliability of rainfall erosivity indices: a comparison between observed and estimated rainfall kinetic energy from natural events.	213
3.5	References	225
<b>4.</b>	<b>Valoración de los resultados de la investigación y conclusiones generales</b>	<b>231</b>
4.1	Introduction	233
4.2	Principales aportaciones de la tesis doctoral	235
4.3	Valoración crítica	237
4.4	Perspectivas futuras	239
4.5	Conclusiones finales	240
4.6	Referencias	241

## Índice de figuras

<b>Figura 1.1:</b> Vulnerabilidad frente a la erosión hídrica. Basado en la combinación del mapa global de los biomas terrestres y el mapa global de suelos. Fuente: USDA-NRCS (1998) -----	6
<b>Figura 1.2:</b> Riesgo de erosión hídrica acelerada debida a causas antrópicas. Basado en la combinación entre el mapa global de vulnerabilidad frente a la erosión hídrica y el mapa de densidad de población en 1994. Fuente: USDA-NRCS (1998). -----	6
<b>Figura 1.3:</b> Relación entre la intensidad de lluvia y el diámetro mediano de las gotas ( $D_{50}$ ). Fuente: Hudson (1995). -----	14
<b>Figura 1.4:</b> Formación y desarrollo de las gotas de lluvia. Adaptado de Horstmeyer (2008). -----	16
<b>Figura 1.5:</b> Relación entre energía cinética ( $EC$ ) e intensidad de la lluvia ( $I$ ) según tres modelos alternativos. Datos experimentales obtenidos en la Estación Experimental de Aula Dei (Zaragoza: $41^{\circ}43'31''N / 0^{\circ}48'39''O$ ; 230 m.a.s.l.) Resolución temporal de la toma de datos: 1 min. -----	17
<b>Figura 1.6:</b> Histogramas de frecuencias de la intensidad de lluvia por zonas climáticas. Fuente: Hudson, 1995. -----	21
<b>Figure 2.1:</b> General view of the study area. -----	45
<b>Figure 2.2:</b> Land uses map; (Corine Land Cover, 2005). -----	46
<b>Figure 2.3:</b> Mean annual rainfall (1955-2006). -----	47
<b>Figure 2.4:</b> Rainfall observatories used in the study area -----	50
<b>Figure 2.5:</b> Spatial distribution for the alpha parameter -----	53-56
<b>Figure 2.6:</b> Spatial distribution for the beta parameter. -----	57-60
<b>Figure 2.7:</b> Monthly distribution among the analyzed observatories for parameter $\alpha$ from the Richardson et al. (1983) exponential relationship -----	73
<b>Figure 2.8:</b> Monthly distribution among the analyzed observatories for parameter $\beta$ from the Richardson et al. (1983) exponential relationship.-----	73
<b>Figure 2.9:</b> Comparison between observed $R$ values (ordinate axis) and those estimated by various methods (abscissa axis): A) model A; B) model B; C) model	

C; D) model D; and E) model E. Line of best fit (continuous diagonal line), and regression line (dashed)----- 75

**Figure 2.10:** Spatial distribution of estimated R values by: *Model A; Model B*. These maps can be compared to Figure 2.20 ----- 76-77

**Figure 2.11:** Comparison between observed R values (ordinate axis) and those estimated by various methods (abscissa axis): F) model F; G) model G; and H) model H. Line of best fit (continuous diagonal line ), and regression line (dashed)

----- 79

**Figure 2.12:** Spatial distribution of estimated R values by: *Model F; Model G; Model H*. These maps can be compared to Figure 2.20----- 81

**Figure 2.13:** Empirical semivariograms (circles) and fitted semivariogram Gaussian models (lines) of the rainfall erosivity indices: A) R factor; B)  $EI_{30}$  index. Range parameters are: 10.98 km (R factor) and 13.05 km ( $EI_{30}$  index)

----- 97

**Figure 2.14:** Rainfall erosivity maps (RUSLE R factor; MJ mm ha<sup>-1</sup> h<sup>-1</sup> y<sup>-1</sup>) for the Ebro Basin: a) inverse distance weighting surface; b) spline with tension ( $\varphi = 5000$ ); c) smoothing spline ( $\varphi = 400$ ) ----- 99-101

**Figure 2.15:** Rainfall erosivity maps (average  $EI_{30}$  index of the erosive events; MJ mm ha<sup>-1</sup> h<sup>-1</sup>) for the Ebro Basin: a) inverse distance weighting surface; b) spline with tension ( $\varphi = 5000$ ); c) smoothing spline ( $\varphi = 400$ )----- 102-104

**Figure 2.16:** Comparison between observed (ordinate axis) and predicted (abscissa axis) values for the interpolation methods used for the spatial distribution of the R factor, line of perfect fit (continuous) and regression line (dashed). a) inverse distance weighting ( $r=2$ ); b) smoothing spline ( $\varphi = 400$ ); c) splines with tension ( $\varphi = 5000$ ); d) ordinary kriging; e) ordinary kriging with anisotropy; f) universal kriging; g) co-kriging; h) regression model (GLS); i) regression-kriging-----107

**Figure 2.17:** Comparison between observed (ordinate axis) and predicted (abscissa axis) values for the different interpolation methods used for the spatial distribution of the  $EI_{30}$  index, line of perfect fit (continuous) and regression line (dashed). a) inverse distance weighting ( $r=2$ ); b) smoothing spline ( $\varphi = 400$ ); c) splines with tension ( $\varphi = 5000$ ); d) ordinary kriging; e) ordinary kriging with

anisotropy; f) universal kriging; g) co-kriging; h) regression model (GLS); i) regression-kriging -----	108
<b>Figure 2.18:</b> Local uncertainty modeled by Gaussian geostatistical simulation (GGS) for the R factor: mean of R factor and standard error of R factor (MJ mm ha <sup>-1</sup> h <sup>-1</sup> y <sup>-1</sup> ) -----	111
<b>Figure 2.19:</b> Local uncertainty modeled by Gaussian geostatistical simulation (GGS) for the of $EI_{30}$ index: mean of $EI_{30}$ index and standard error of $EI_{30}$ index (MJ mm ha <sup>-1</sup> h <sup>-1</sup> )-----	112
<b>Figure 2.20:</b> Mean annual rainfall erosivity for the period 1955-2006 (MJ mm ha <sup>-1</sup> h <sup>-1</sup> y <sup>-1</sup> ) -----	117
<b>Figure 2.21:</b> Monthly rainfall erosivity (Ei; MJ mm ha <sup>-1</sup> h <sup>-1</sup> month <sup>-1</sup> ) and rainfall (mm) regimes in the study area -----	118
<b>Figure 2.22:</b> Mean monthly rainfall erosivity for spring months (MJ mm ha <sup>-1</sup> h <sup>-1</sup> month <sup>-1</sup> ) during the period 1955-2006 in the Ebro basin (NE Spain) -----	120-123
<b>Figure 2.23:</b> Sea-level pressure points used to calculate the daily atmospheric indices. -----	127
<b>Figure 2.24:</b> Daily time series of NAOi, WeMOi, MOi and rainfall erosivity for the observatory X9987 (Ebro Delta) between 01/01/2001 and 31/03/2001. Red and blue regions indicate positive and negative phases according to the three teleconnection indices, which were used to construct time series of daily rainfall erosivity-----	129
<b>Figure 2.25:</b> Relative differences in median daily rainfall erosivity (MJ mm ha <sup>-1</sup> day <sup>-1</sup> ) at <b>annual</b> scale during negative and positive days of the atmospheric circulation indices for the period 1955-2006. Masked areas indicate no significant difference-----	133
<b>Figure 2.26:</b> Monthly relative differences in median daily rainfall erosivity (MJ mm ha <sup>-1</sup> day <sup>-1</sup> ) during negative and positive days of the atmospheric circulation indices for the period 1955-2006. Masked areas indicate no significant difference -----	135-146
<b>Figure 2.27:</b> L-moments ratio diagram, comparing empirical L-moment ratios (L-skewness and L-kurtosis) with the ones of several widely used extreme value	

distributions: Generalized Extreme Value (GEV), Log-Normal (LN), Pearson III (PIII) and Pareto (GP) -----147

**Figure 2.28:** Expected extreme daily rainfall erosivity ( $\text{MJ mm ha}^{-1} \text{h}^{-1} \text{d}^{-1}$ ) during winter (September-April) corresponding to a return period of 10 years under **negative days** of the atmospheric circulation indices.----- 150-151

**Figure 2.29:** Standard error associated to the expected extreme daily rainfall erosivity ( $\text{MJ mm ha}^{-1} \text{h}^{-1} \text{d}^{-1}$ ) during winter (September-April) corresponding to a return period of 10 years under **negative days** of the atmospheric circulation indices.----- 152-153

**Figure 2.30:** Return period curves for Ebro river delta (observatory X9987) of the winter (September-April) extreme daily rainfall erosivity under positive and negative days of the indices analysed. Grey line represents the extreme daily rainfall erosivity values under the different days of the indices for a return period of 10y, cartographied for all the observatories in figure 2.27. -----154

**Figure 2.31:** Per decade change of annual rainfall erosivity during the period 1955-2006 ( $\text{MJ mm ha}^{-1} \text{h}^{-1} \text{y}^{-1}$ ). Black circles indicate data series for which the trend was significant at the 95% confidence level-----162

**Figure 2.32:** Per decade change of seasonal rainfall erosivity (spring and summer) during the period 1955-2006 ( $\text{MJ mm ha}^{-1} \text{h}^{-1} \text{y}^{-1}$ ). Black circles indicate data series for which the trend was significant at the 95% confidence level.

----- 163-164

**Figure 2.33:** Boxplots of trends in the number of daily rainfall erosivity events classified by quintiles of daily erosivity over the whole period 1955-2006.

-----165

**Figure 2.34:** Per decade change in the number of daily rainfall erosivity events corresponding to the first (Q1) and fifth (Q5) quintiles for the period 1955-2006. Black circles indicate significant trends at the 95% confidence level.

-----166

**Figure 2.35:** Per decade change in the number of daily rainfall erosivity events in **spring** corresponding to the first (Q1) and fifth (Q5) quintiles for the period 1955-2006. Black circles indicate significant trends at the 95% confidence level.

----- 167-170

**Figure 2.36:** Temporal evolution of October to March NAO, WeMO and MO indices obtained from average daily indices. Source: Vicente-Serrano et al., 2009.

----- 173

**Figure 3.1:** Example of a disdrometric record: one-minute values of rainfall intensity and unit energy flow (left axis) and cumulative rain and energy (dotted line and red axis) for one rainfall event ----- 195

**Figure 3.2:** Experimental scheme at the Experimental Station of Aula Dei-CSIC (41°43'30"N, 0°48'39"O. 230 m. a.s.l.). Soil plots dimensions: 14 1 m. The circles indicate the placement of the Morgan's splash cups. LPM is the Laser Precipitation Monitor recording rainfall properties every minute ----- 198

**Figure 3.3:** Soil splash ( $\text{g m}^{-2}$ ) boxplots by soil type sorted by the amount collected. The boxes indicate the 25<sup>th</sup> and 75<sup>th</sup> percentiles, the thick line indicates the median (50<sup>th</sup> percentile), the whiskers are extreme observations (highest/lowest observation which is not more/less than 1.5 times the interquartile range from the box), and the circles indicate outlier observations (observations which are higher/lower than 1.5 times the interquartile range from the box) ----- 206

**Figure 3.4:** Scatter plot of soil splash vs. rainfall erosivity index  $EI_{30}$  ( $\text{MJ mm ha}^{-1} \text{h}^{-1}$ ); Both variables are log-transformed. Soil types are indicated by symbols: Cambisol (circle), Solonchak (cross) and Gypsisol (triangle) ----- 207

**Figure 3.5:** Rainfall erosivity ( $EI_{30}$ ) for events with soil splash sediment (T) and events without it (F) ----- 209

**Figure 3.6:** Monitoring rainfall intensity at 1-minute (grey line) and 15-minutes (black line) time resolution. Reducing the sampling frequency from one to 15 minutes has the effect of smoothing the time series of rainfall intensity, loosing the peak intensities that are shown in the high-frequency record. This could have an effect in the calculation of  $I_{30}$ , dificulting the comparison between models calibrated from records of varying time frequency ----- 217

**Figure 3.7:** Histograms of event's kinetic energy,  $E$ , maximum 30-minutes intensity,  $I_{30}$ , and erosivity index,  $EI_{30}$  ----- 218

**Figure 3.8:** Comparison between observed (ordinate axis) and predicted (abscissa axis) values of rainfall erosivity,  $EI_{30}$  (circles). Line of perfect fit (continuous) and regression line (dashed) ----- 219

**Figure 3.9:** Comparison between erosivity properties ( $E$ ,  $I_{30}$  and  $EI_{30}$ ) from observations at 1-minute (ordinate axis) and 15-minutes (abscissa axis) time resolution. Observed values (LPM), and estimations by three empirical models. Line of perfect fit (continuous) and regression line (dashed) -----223

## Índice de tablas:

<b>Tabla 1.1:</b> Valores de diámetro mediano de gotas de lluvia ( $D_{50}$ ) obtenidos en varios estudios experimentales. -----	11
<b>Tabla 1.2:</b> Funciones empíricas para estimar la velocidad terminal de las gotas de lluvia, $V_T$ ( $\text{m s}^{-1}$ ), en función de su diámetro, $D$ (mm.) -----	12
<b>Tabla 1.3.</b> Relaciones matemáticas entre la energía cinética ( $EC$ ) y la intensidad de la lluvia ( $I$ ); $a$ y $b$ son coeficientes empíricos. . -----	16
<b>Tabla 1.4:</b> Relaciones empíricas entre la energía cinética, $EC$ ( $\text{MJ ha}^{-1} \text{ mm}^{-1}$ ) e intensidad de la lluvia, $I$ ( $\text{mm h}^{-1}$ ) en distintos lugares, con indicación del rango de intensidad de los datos utilizados (n.c.: no consta). -----	18
<b>Tabla 1.5:</b> Algunos grupos de investigación sobre erosión de suelo en España, síntesis a partir de García Ruiz y López Bermúdez (2009). -----	26-27
<b>Table 2.1:</b> Acronyms and definition of the selected indices from the daily precipitation series. -----	69
<b>Table 2.2:</b> Accuracy measurements for the R factor models: means and standard deviations of the observed and predicted values -----	74
<b>Table 2.3:</b> Correlation coefficients between the observed R factor and several precipitation intensity indices. See Table 2.1 for definition of the indices -----	78
<b>Table 2.4:</b> Regression coefficients and variance, and regression analysis for the precipitation intensity indices (see Table 2.1) and the modified Fournier index (MFI). -----	79
<b>Table 2.5:</b> Accuracy measurements for the R factor models: mean and standard deviation of the observed and predicted values, and cross-validation statistics -----	109
<b>Table 2.6:</b> Accuracy measurements for the mean $EI_{30}$ index: mean and standard deviation of the observed and predicted values, and cross-validation statistics -----	109
<b>Table 2.7:</b> Number and proportion of series with significant differences in annual and monthly erosivity between positive and negative days of the atmospheric circulation indices (Wilcoxon-Mann-Witney test) -----	132

<b>Table 2.8:</b> Number and proportion of series with significant trends at the 95% confidence level-----	132
<b>Table 2.9:</b> Number and proportion of series with trends in the number of events in the first quintile (Q1) significant at the 95% confidence level -----	167
<b>Table 2.10:</b> Number and proportion of series with trends in the number of events in the first quintile (Q5) significant at the 95% confidence level -----	168
<b>Table 3.1:</b> Laser Precipitation Monitor classification of drop diameter and velocity -----	193
<b>Table 3.2:</b> Laser Precipitation Monitor variables recorded in real time every minute -----	193
<b>Table 3.3:</b> Soil types properties -----	197
<b>Table 3.4:</b> Properties of rainfall events registered and corresponding soil splash: n° of event; was it erosive (Y) or not (N: splash was negligible, less than 0.25 g m <sup>-2</sup> ); D: total time during which splash cups were deployed (hours); D <sub>eff</sub> : total time of rain registered at the monitoring site (hours); P: total rainfall (mm); E: total kinetic energy (MJ ha <sup>-1</sup> mm <sup>-1</sup> ); I <sub>30</sub> : maximum intensity in 30 minutes (mm h <sup>-1</sup> ); EI <sub>30</sub> : rainfall erosivity index (MJ mm ha <sup>-1</sup> h <sup>-1</sup> ); mean soil splash by soil type (g m <sup>-2</sup> ): CA = Cambisol, GA= Gypsisol, SA = Solonchak. Events eliminated due to loss of data are not shown -----	204
<b>Table 3.5:</b> Linear Mixed-Effects analysis summary. Only significant covariates are shown. -----	208
<b>Table 3.6:</b> Erosivity properties of natural rainfall events registered at 1-minute time intervals: total kinetic energy E (MJ ha <sup>-1</sup> ), maximum intensity in 30 minutes I <sub>30</sub> (mm h <sup>-1</sup> ) and rainfall erosivity EI <sub>30</sub> (MJ mm ha <sup>-1</sup> h <sup>-1</sup> ); measured values and estimations by the RUSLE (-R), Van Dijk (-VD), and Cerro (-C) methods -----	220
<b>Table 3.7:</b> Erosivity properties of natural rainfall events registered at 15-minute time intervals: total kinetic energy E (MJ ha <sup>-1</sup> ), maximum intensity in 30 minutes I <sub>30</sub> (mm h <sup>-1</sup> ) and rainfall erosivity EI <sub>30</sub> (MJ mm ha <sup>-1</sup> h <sup>-1</sup> ); measured values and estimations by the RUSLE (-R), Van Dijk (-VD), and Cerro (-C) methods -----	221

**Table 3.8:** Validation statistics of rainfall erosivity index  $EI_{30}$  estimations for 37 natural rainfall events, measured at 1-minute time frequency: bias (mean, standard deviation, mean bias error) and goodness-of-fit statistics (mean absolute error, correlation,  $r^2$ , Willmott's D, Nash-Sutcliffe) ----- 222

**Table 3.9:** Mean and standard deviation of observed and estimated erosivity  $EI_{30}$  for 37 rainfall events, recorded at 1-minute and at 15-minutes time resolution

---

----- 222



# Bloque I

## Marco conceptual: antecedentes y perspectivas sobre el factor climático en la erosión del suelo.

"Si he logrado ver más lejos, ha sido porque he subido a hombros de gigantes". —Isaac Newton

### Resumen

En este bloque se revisan los trabajos precedentes relacionados con la lluvia como agente erosivo del suelo, sentando las bases epistemológicas que enmarcan y cimentan esta tesis doctoral. En primer lugar, se contextualiza la erosión del suelo como un problema medio ambiental de primer orden, del que se empezó a tomar conciencia y a cuantificar a partir de la 2<sup>a</sup> mitad del siglo XX. La cuantificación de los procesos permitió el desarrollo de modelos empíricos, tanto para la determinación de la pérdida de suelo global, como específicamente para la descripción de la capacidad erosiva de la lluvia. Éstos últimos están basados en la energía cinética de las gotas, fundamental para estimar, por ejemplo la erosión por impacto (*splash*). Los estudios empíricos encontraron una relación entre la energía cinética y la intensidad del evento (EC-I) a escalas temporales de alta resolución, permitiendo la estimación de la energía de la lluvia a partir de relaciones matemáticas en función de la intensidad. En las siguientes páginas y especialmente en la sección 1.5 se presenta una detallada revisión de todas las propuestas investigadas. Asimismo, el estudio de los resultados empíricos obtenidos en distintos lugares los relaciona con las características atmosféricas, climáticas y geográficas propias de los eventos de lluvia. Se plantean también las fronteras en el conocimiento de la erosividad de la lluvia, relacionadas con el avance instrumental en los métodos de detección de la energía de la lluvia, mediante satélite y radar. Finalmente, se plantean los objetivos y estructura de la tesis.



## Abstract

In this part previous studies related with rainfall erosivity as causal soil erosion factor are reviewed. First of all, soil erosion background as first order environmental problem is set up. Society and scientists started taking it into account and quantifying it since 1950's. Quantification allowed developing soil loss empirical models, and more specifically rainfall erosivity determination. This last is based in the raindrop's kinetic energy, related to *splash* erosion, together with rainfall volumen and intensity. All these parameters are related one to each other, and depend on atmospheric, climatic and geographical characteristics, as revealed by the reviewed investigations. Frontiers in rainfall erosivity studies are drafted. Finally, in order to determine our contribution, the objectives and structure of the thesis are presented.



## 1.1. La erosión del suelo como problema medioambiental

La erosión es el conjunto de procesos responsables de la meteorización de los materiales de la superficie terrestre (roca, sedimento o suelo), el transporte de las partículas sólidas generadas por ésta y su sedimentación en otros lugares del paisaje. La erosión tiende a disminuir las diferencias de energía potencial determinadas por el relieve, y por tanto es uno de los principales agentes de modelado de la superficie terrestre. La erosión es un proceso natural y necesario para los ecosistemas (el transporte de sedimento es fundamental para la dinámica y mantenimiento de los ecosistemas fluviales y deltaicos, por ejemplo), y en condiciones naturales existe en general un equilibrio entre los procesos de erosión y los de formación de suelo o regolito. Sin embargo la erosión se ve en ocasiones acelerada como consecuencia del uso antrópico del territorio, resultando en un balance negativo entre los procesos de formación y de pérdida de suelo.

El suelo es la capa geológica capaz de sostener el crecimiento de la vegetación y los cultivos, y su degradación o desaparición se puede considerar como irreversible a escala temporal humana. Este hecho convierte al suelo en un recurso no renovable y tremadamente valioso, y sitúa la erosión acelerada del suelo como un importante problema ambiental para el sostenimiento de la civilización. Se estima que las actividades humanas (agrícolas, ganaderas y forestales, excluyendo la urbanización) son la causa de tasas de erosión entre 1 y 2 órdenes de magnitud superiores a las naturales, representando un importante problema para la sostenibilidad de la producción mundial de alimentos (Montgomery, 2007). Así, se calcula que en los últimos 40 años alrededor de un tercio de los suelos agrícolas de la Tierra han visto reducida su productividad debido a la erosión acelerada (Almorox-Alonso et al., 2010). En España, aproximadamente el 50% de los suelos agrícolas presentan un riesgo medio-alto de degradación por erosión (OECD, 2001; Boardman, 2006). La prevención de la erosión acelerada del suelo requiere la puesta en marcha de medidas de protección y conservación del suelo, que exigen un sólido conocimiento de los factores y procesos que determinan la erosión.

Aunque el papel de la erosión acelerada en el declive de las civilizaciones históricas es ampliamente reconocido (Montgomery, 2008), la toma de conciencia de la gravedad de la erosión acelerada en los tiempos actuales se produjo



probablemente en la década de los años 30 del siglo XX, después de varios años de intensa sequía en el centro de los EEUU que arruinaron cosechas y dejaron desnudos a los suelos ya degradados por el exceso de laboreo, siendo fácilmente erosionados por efecto del viento y las lluvias torrenciales. Este periodo de erosión acelerada, conocido como el '*dust bowl*', arruinó a muchos agricultores que tuvieron que desplazarse a otras regiones, y fue causa de importantes problemas medioambientales. Como consecuencia se creó el *U.S. Soil Conservation Service*, con el objetivo de estudiar los procesos erosivos y determinar las mejores estrategias de conservación de suelos y cultivos.

En España la preocupación por la erosión de suelo y su deterioro y por la desaparición de la cubierta vegetal comenzó a hacerse patente durante el siglo XX. Marca un hito histórico, tanto en España como en el contexto europeo la *Ley de Montes* de 1863, que constituyó el primer código forestal español centrado en la mejora, el fomento y la repoblación de los montes públicos. Esta ley no llegó a ponerse en marcha hasta 1874, continuando vigente hasta 1957. Fruto de la misma es la primera repoblación forestal en Europa en 1900 en Sierra Espuña (Murcia). Sin embargo, en España no se iniciaron estudios cuantitativos sobre la erosión del suelo hasta los años 50 del siglo XX, aunque a partir de ese momento se ha convertido en un tema de investigación de gran relevancia como demuestra el estudio retrospectivo de García Ruiz y López Bermúdez (2009). Así, en 1955 se instalaron por el Servicio de Conservación de Suelos las primeras parcelas experimentales de erosión del suelo, muy similares a las del SCS estadounidense. Este proyecto fue abandonado en 1967 sin que se publicara ningún resultado. En 1970 se utilizó el método de Fournier (1960) para evaluar la degradación específica en las cuencas con grandes presas. También en esta época se utilizó el modelo USLE (Wischmeier & Smith, 1959) y sus versiones revisadas (MUSLE: Wischmeier & Smith, 1978; RUSLE: Renard et al., 1997) con el fin de poner en marcha proyectos de restauración hidrológico-forestal. A comienzos de los años 80 y primeros de los 90, el Instituto para la Conservación de la Naturaleza (ICONA), en el marco del proyecto LUCDEME y del *Plan nacional de restauración hidrológico-forestal y de control de erosión* promueve un estudio piloto sobre paisajes erosivos en el sureste español, elaborándose asimismo cartografías de la erosión hídrica en España y de los estados erosivos en las grandes cuencas hidrográficas, con el objetivo de evaluar los procesos de erosión, desertificación y degradación del suelo. El estudio culmina en 2003 con la publicación de los *Mapas de los*



*Estados Erosivos; resumen nacional*, que se suman a otras publicaciones de relevancia como *La agresividad de la lluvia en España, valores del factor R de la Ecuación Universal de Pérdida de Suelo* (ICONA, 1988). Más recientemente el Ministerio de Medio Ambiente promovió, a través del Real Decreto 1415/2000 de 21 de julio, la realización de un *Inventario Nacional de Erosión del Suelo* (INES). Los objetivos de este trabajo son: i) localizar, cuantificar y analizar la evolución de los fenómenos erosivos, delimitar las áreas prioritarias de actuación y definir y valorar las actuaciones que deben llevarse a cabo; ii) formar un sistema de datos de fácil acceso que posibilite la educación y la participación ciudadana; iii) constituir un elemento de la red europea de información y comunicación medioambiental; y iv) proporcionar indicadores paneuropeos sobre gestión sostenible de los bosques. El método de evaluación empleado es la RUSLE.

## 1.2. Factores de la erosión del suelo

Los factores que intervienen en la erosión del suelo se pueden agrupar en tres conjuntos (Morgan, 2005): i) relacionados con los procesos de intercambio de energía entre la atmósfera y los materiales de la superficie terrestre a través de los agentes erosivos capaces de movilizar las partículas del suelo como la precipitación o el viento (erosividad); ii) relacionados con la resistencia que opone el suelo a ser erosionado, determinada por las características físicas y químicas propias de cada suelo (erodibilidad); iii) derivados de las características protectoras de la cubierta vegetal o de las medidas de protección y conservación llevadas a cabo por los agricultores.

Entre los agentes erosivos la acción eólica queda en general restringida a zonas áridas mientras que la erosión hídrica es el principal causante de la pérdida de suelo en las zonas húmedas y subhúmedas, lo que comprende una fracción sustancial de las tierras emergidas (Figura 1.1). Las áreas más afectadas por la erosión hídrica son las zonas de montaña, las zonas climáticas de borde como el Mediterráneo, o las zonas tropicales.

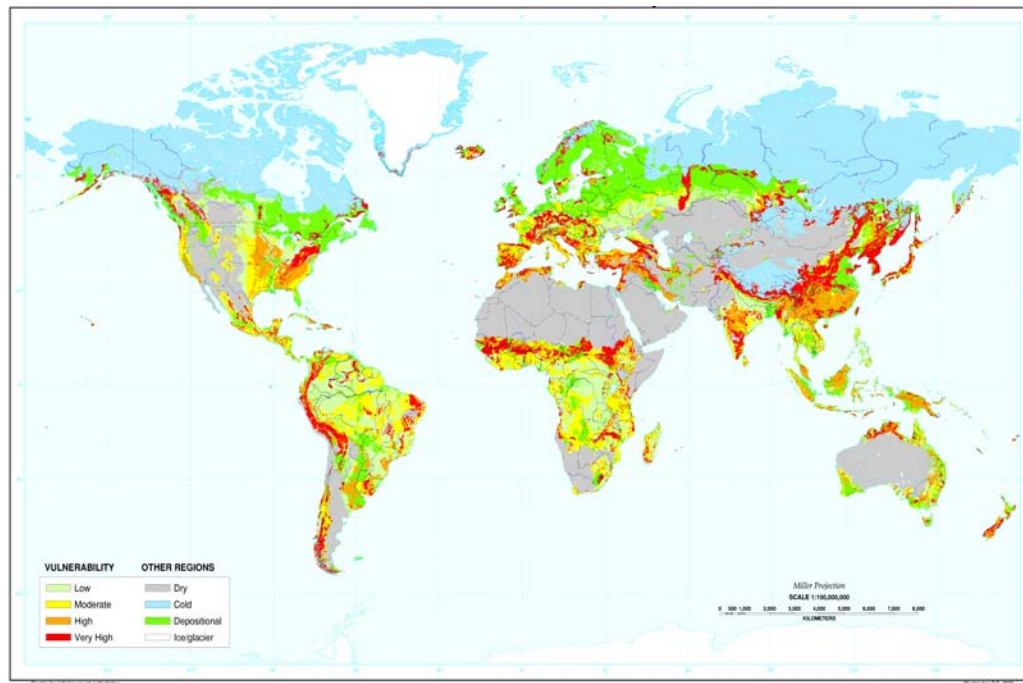


Figura 1.1: Vulnerabilidad frente a la erosión hídrica. Basado en la combinación del mapa global de los biomas terrestres y el mapa global de suelos. Fuente: USDA-NRCS (1998)

El riesgo de erosión hídrica aumenta en función del uso del suelo y de la presión antrópica sobre el mismo (Figura 1.2). La densidad de población así como la presión sobre el territorio debido a la sobreexplotación del suelo es el denominador común de las zonas que presentan un mayor riesgo.

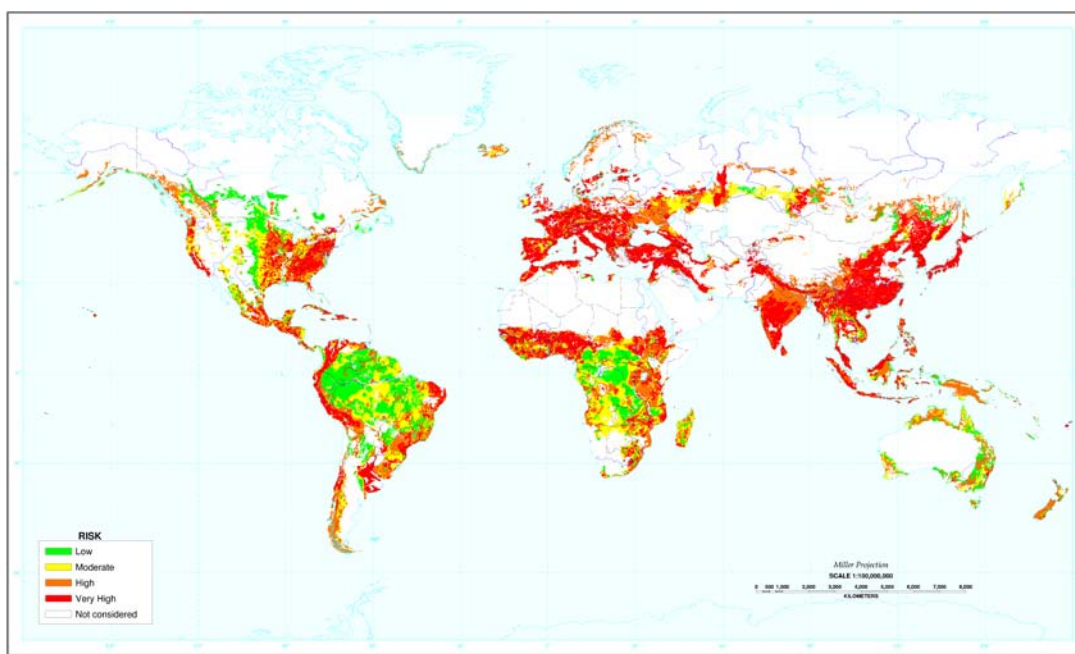


Figura 1.2: Riesgo de erosión hídrica acelerada debida a causas antrópicas. Basado en la combinación entre el mapa global de vulnerabilidad frente a la erosión hídrica y el mapa de densidad de población en 1994. Fuente: USDA-NRCS (1998).



La determinación de los factores que condicionan la erosión posibilitó el desarrollo de métodos empíricos para determinar las tasas de erosión por unidad de superficie y tiempo. De todos ellos el más conocido y utilizado es la Ecuación Universal de Pérdida de Suelo (USLE, por sus siglas inglesas) y sus derivados y modificaciones (MUSLE, RUSLE). La USLE es una ecuación paramétrica de carácter predictivo desarrollada por el SCS de los Estados Unidos (Wischmeier y Smith 1958) a partir de datos de unas 8000 parcelas distribuidas a lo largo del centro-oeste de los EEUU.

La USLE permite estimar la erosión hídrica promedio que se produce en una parcela agrícola a partir de la multiplicación de una serie de parámetros correspondientes con los factores relacionados con la erosión de suelo: la erosividad de la lluvia ( $R$ ), la erodibilidad del suelo ( $K$ ), la longitud de la ladera ( $L$ ), la pendiente ( $S$ ), la cubierta vegetal ( $C$ ) y las prácticas de conservación ( $P$ ).

La formulación de la USLE es:

$$A = R \cdot K \cdot L \cdot S \cdot C \cdot P,$$

siendo  $A$  la pérdida media anual de suelo ( $Mg\ ha^{-1}\ a^{-1}$ ).

El modelo USLE ha sido ampliamente utilizado y criticado. El propio autor (Wischmeier, 1965) fue prudente en cuanto a su aplicación y uso debido al empirismo del que es resultado, indicando que únicamente debería aplicarse a zonas que tengan características similares a aquellas donde se calibró. Además hay que tener en cuenta que los resultados de la USLE son aplicables únicamente a unidades espaciales de tamaño parcela, ya que no tiene en cuenta procesos de transporte y sedimentación que se producen en unidades mayores (laderas y cuencas). El modelo tiende a la sobreestimación de la erosión a escala de cuenca, como se ha puesto de relieve en numerosas investigaciones (p. ej., Almorox et al., 1994). En este sentido la mayor crítica que se puede hacer es al mal uso de la ecuación al forzarla para obtener resultados para los cuales no fue diseñada, como por ejemplo para la estimación de tasas de aterramiento en embalses.



### 1.3. La lluvia como agente erosivo

Como se desprende de la formulación del modelo USLE, y como han puesto de relieve numerosos estudios empíricos, la acción de la lluvia es uno de los principales factores de la erosión hídrica. La lluvia actúa como agente erosivo a través de dos mecanismos: el impacto de las gotas y la tensión ejercida por la escorrentía, con los consiguientes efectos de disagregación de partículas (meteorización), su transporte y sedimentación.

El proceso erosivo de la lluvia se inicia por el efecto de la salpicadura de las gotas de lluvia (ingl. *rain splash*). Al impactar contra la superficie del suelo desnudo las gotas desencadenan dos mecanismos: i) la compactación y la formación de una costra incipiente, y ii) la desagregación de las partículas del suelo (Hudson, 1995) y su transporte a favor de la pendiente por un proceso de difusión o escorrentía (Morgan, 2005). La erosión producida por el impacto de las gotas depende no solo de las características de éstas, sino también de las propiedades físicas y químicas del suelo (Park et al., 1982). Además, se ve influenciada por características dinámicas en el tiempo como las condiciones de humedad del suelo y de la costra superficial. En efecto, en suelos muy húmedos o sellados por la costra se forma una película de agua superficial (encharcamiento) que influye sobre la erosión por salpicadura, haciendo que ésta sea máxima cuando el espesor de la película es aproximadamente igual al grosor de las gotas de lluvia. Al aumentar el espesor de esta lámina de agua, en cambio, disminuye el efecto disgregador de las gotas incidentes, convirtiéndose en un elemento disipador de la energía de las gotas, y por tanto protector frente a la erosión (Morgan, 2005).

El agua que fluye a favor de la pendiente se denomina escorrentía y produce también la desagregación de las partículas del suelo y, fundamentalmente, su transporte. La escorrentía se produce cuando el suelo se satura o bien cuando la intensidad de la lluvia supera la velocidad de infiltración.

De estos dos procesos erosivos—el impacto de las gotas y la escorrentía—es el impacto de las gotas sobre el suelo o sobre una delgada película de agua el principal agente iniciador de la erosión hídrica (Sempere Torres, 1994; Hudson, 1995; Morgan, 2005).

Los primeros estudios sobre erosión de suelo ya percibieron esta circunstancia, como por ejemplo el trabajo de Ellison (1944), quien con datos de lluvia cada 30



minutos estableció la primera formulación empírica sobre la pérdida de suelo producida por la erosión por salpicadura:

$$SL = kV^{4.33} D^{1.07} I^{0.65}, \quad (1.1)$$

donde  $SL$  es la pérdida de suelo (g),  $k$  es una constante empírica,  $V$  la velocidad de caída de las gotas (pies por segundo),  $D$  el diámetro de las gotas (mm), e  $I$  la intensidad de la lluvia (pulgadas por hora). De estos factores,  $k$  puede considerarse un factor de erodibilidad dependiente de las características del suelo;  $I$  modula la erosión en función de la cantidad de lluvia por intervalo de tiempo. La inclusión de  $V$  y  $D$  constituye una aproximación a la energía cinética de las gotas de lluvia, ya que asumiendo una forma esférica de las mismas el diámetro  $D$  se relaciona directamente con su masa. Otro de los primeros ejemplos es la formulación propuesta por Bisal (1960):

$$SL = kDV^{1.4}, \quad (1.2)$$

donde la velocidad  $V$  se mide en  $\text{m s}^{-1}$ .

A partir de la observación, los trabajos citados ya reconocieron la importancia fundamental del tamaño y velocidad de caída de las gotas de lluvia en la cantidad de suelo erosionado. La erosividad de la lluvia se debe, por tanto, a la transferencia de energía que se produce cuando las gotas de lluvia impactan sobre los agregados del suelo. Desde consideraciones puramente físicas la energía cinética de una gota de lluvia,  $EC$  (J), se puede estimar como (Roldán, 2006):

$$EC = \frac{1}{12} 10^{-3} \pi \rho V_i^2 D_i^3, \quad (1.3)$$

donde  $\rho$  es la densidad del agua ( $1 \text{ g cm}^{-3}$ ),  $D_i$  es el diámetro de una esfera con el volumen equivalente al de la gota de lluvia (cm), y  $V_i$  es la velocidad terminal de caída ( $\text{m s}^{-1}$ ). Esta última depende del radio de la gota siguiendo la ley de Stockes:

$$V_i = \frac{F}{12\pi\eta D_i}, \quad (4)$$

donde  $F$  es el rozamiento ( $\text{Pa s}^{-1}$ ), y  $\eta$  representa la viscosidad del fluido ( $\text{kg m}^{-1} \text{s}^{-1}$ ).

Como se puede apreciar, según las ecuaciones (3) y (4) la energía cinética depende mayormente del tamaño de la gota. La validez de este modelo se basa en dos importantes supuestos: i) que las gotas de lluvia tienen una forma esférica, y ii) que la velocidad de caída de las gotas es igual a la velocidad terminal. Aunque en



la realidad estos dos supuestos no se cumplen de manera estricta se trata de una simplificación relativamente razonable, lo que ha motivado la realización de numerosos estudios sobre la variabilidad del tamaño de las gotas de lluvia.

#### 1.4. Estudio del tamaño y velocidad de las gotas de lluvia

Los primeros estudios experimentales sobre el tamaño de las gotas de lluvia se remontan a finales del siglo XIX (Wiesner, 1895). La metodología empleada era un papel de filtro teñido en el que quedaban señaladas las circunferencias correspondientes a las gotas de lluvia (ingl. *drop splash*), existiendo una relación empírica entre el diámetro de la mancha y el de la gota. Algunos trabajos han criticado este método por sobreestimación del tamaño de las gotas en eventos de elevada intensidad (Hall, 1970; Carter et al., 1974), aunque es un método que se ha seguido utilizando (Cerdá, 1997; Nyssen, 2005).

Otro método de gran difusión es el conocido como “método de las bolitas de harina” o *flour pellets* (Bently, 1904), basado en la captura de las gotas de lluvia en un recipiente lleno de harina. Las gotas, al impactar contra la harina, crean formas que representan el tamaño de éstas. Una vez finalizado el experimento se seca la harina y se separan los moldes de las gotas por un tamiz de 210 µm. Al igual que en el caso anterior, el método se debe calibrar previamente en el laboratorio. Este método ha sido considerado el más fiable hasta hace relativamente poco tiempo y aún hoy es probablemente el más extendido permitiendo comparaciones entre los resultados obtenidos en diferentes lugares, (Jayawardena y Rezaur, 2000). Otros métodos de captura utilizan un tanque con aceite aprovechando la diferencia entre las densidades de los dos fluidos (McCool et al., 1978; De Luna et al., 2000).

En las últimas décadas se ha avanzado en la utilización de aparatos capaces de monitorizar las gotas de lluvia, como por ejemplo los basados en fotografía o vídeo de alta frecuencia (Mutchler y Hansen, 1970; Mutchler, 1971). También se han desarrollado aparatos específicos para la medición de las características de las gotas de lluvia: los disdrómetros. Los primeros ~~disdrómetros acústicos~~—se basan en la onda de presión generada por el impacto de las gotas sobre una superficie (Joss y Waldvogel, 1967). Los disdrómetros ópticos, de desarrollo más reciente, se basan en el oscurecimiento de un haz de luz láser infrarroja al ser atravesado por las gotas de lluvia (Cerro et al., 1998; Fernández-Raga et al., 2010). Los métodos más recientes video de alta resolución,



disdrómetro óptico—permiten medir no sólo el tamaño de las gotas de lluvia, sino también su velocidad e incluso su forma, lo que ha permitido disponer de mediciones más precisas de la energía cinética.

La comparación entre los valores característicos de tamaño de gota medidos en distintos lugares de la Tierra refleja una elevada variabilidad geográfica (Tabla 1.1).

Tabla 1.1: Valores de diámetro mediano de gotas de lluvia ( $D_{50}$ ) obtenidos en varios estudios experimentales.

Fuente	Localización	$D_{50}$ (mm)
Kowal (1972), Kowal y Hassam (1976, 1978)	Samaru, Norte Nigeria	2.34 – 4.86
Aina et al., (1977)	Ibadan, Nigeria	1.9 – 4.5
Salako et al., (1995)	East Nigeria	2.3
Osuji (1989)	Ibadan, Nigeria	2 – 3.5 (max. 5.46)
Jayawardena y Rezaur (2000)	Hong Kong	2.23 – 4.48
Cerdà (1997)	Valencia, España	0.25 – 2.69

En general puede diferenciarse entre las zonas tropicales donde se registran las mayores intensidades y tamaños de gota y las zonas templadas o de latitudes medias en las que las lluvias son menos intensas y las gotas de menor tamaño.

Algunos autores, considerando que el estadístico  $D_{50}$  ofrece una información limitada acerca de la distribución de tamaños de las gotas de lluvia, han buscado ajustar los datos a funciones de distribución teóricas. Los primeros estudios propusieron una distribución exponencial (Marshall y Palmer, 1948). Los dos parámetros que controlan la curva exponencial estarían relacionados por un lado con la intensidad de la lluvia mediante una función potencial, y por otro con el número de gotas por unidad de volumen de aire ( $N_o$ ,  $\text{mm}^{-1} \text{ m}^{-3}$ ). Se ha argumentado con posterioridad que la distribución exponencial no es adecuada ya que tiende a sobreestimar el número de gotas en las colas de la distribución, tanto asociadas a los tamaños inferiores (Waldvogel, 1974) como a los superiores (Joss y Gori, 1978). Como consecuencia se han propuesto otras distribuciones de frecuencias como la Exponencial generalizada, la Gamma, la log-Normal o la Weibull. A pesar de las distintas propuestas, no se ha llegado a una conclusión clara sobre la distribución de frecuencias de las gotas de lluvia, y es posible que



existen diferencias a este respecto en función de los mecanismos genéticos de la lluvia, sistemas de medición, u otros aspectos.

Respecto a la velocidad terminal de las gotas, es conocido que fenómenos como el viento pueden alterar ésta alejándola de los valores teóricos de la ecuación (4) (Hudson, 1995). Los experimentos de Laws (1941) encontraron que, en promedio, las gotas de lluvia impactaban en el suelo al 95% de su velocidad terminal teórica, lo que invalidaría el supuesto de velocidad terminal en que se basan muchos modelos. A partir de mediciones de eventos reales, varios autores han propuesto diferentes expresiones empíricas (Tabla 1.2).

Tabla 1.2: Funciones empíricas para estimar la velocidad terminal de las gotas de lluvia,  $V_T$  ( $\text{m s}^{-1}$ ), en función de su diámetro,  $D$  (mm.)

Fuente	Ecuación
Uplinger (1981)	$V_T = 48.54D e^{-1.95D}$
Atlas y Ulbrich (1977)	$V_T = 1.767D^{0.67}$
Van Dijk et al (2002)	$V_T = 0.0561D^3 - 0.912D^2 + 5.03D - 0.254$

Estudios recientes, sin embargo, han revelado que son frecuentes los casos de gotas de tamaño pequeño a mediano con velocidades superiores en más de un orden de magnitud a la velocidad terminal teórica de las gotas en función de su tamaño (Montero-Martínez et al., 2009). La presencia de gotas a velocidad super-terminal se incrementa en los casos de lluvias de gran intensidad y con gotas muy grandes, por lo que se ha propuesto que las gotas super-terminales proceden de la ruptura de gotas grandes a poca altura de la superficie, de manera que las pequeñas gotas generadas conservan todavía el momento de la gota antes de la ruptura. En cualquier caso, se está lejos aún de tener un conocimiento general acerca de la velocidad terminal de las gotas, por lo que los estudios experimentales con aparatos de medida capaces de determinar la velocidad de las gotas, como los disdrómetros ópticos, son todavía muy relevantes (p. ej. Bloemink and Lanzinger, 2005; Brawn and Upton, 2008; Fernández-Raga et al., 2009).

Los datos disponibles sobre la distribución de frecuencias de tamaños y velocidades de las gotas de lluvia, ya sea a partir de métodos tradicionales o de



modernos aparatos de medida, son muy escasos y se circunscriben al ámbito espacial y temporal de experimentos científicos concretos. Aunque estos experimentos han permitido llegar a conclusiones valiosas, resultan insuficientes para determinar las características erosivas de la lluvia en un lugar o una región determinados. Ello ha motivado la realización de un gran número de trabajos dedicados a la búsqueda de relaciones entre las características de las gotas de lluvia (incluida su energía cinética) y otras propiedades de la lluvia de más fácil determinación, como su intensidad.

### **1.5. Relación entre intensidad de lluvia y el tamaño, velocidad y energía cinética de los eventos de lluvia**

La intensidad de la lluvia es un parámetro que se recoge de forma habitual en la mayoría de las estaciones meteorológicas, a diferencia de la distribución de frecuencias del tamaño de gotas que se ha estudiado en pocos lugares y durante períodos temporales limitados. Como consecuencia se han dedicado muchos estudios a encontrar expresiones matemáticas que permitan relacionar la distribución de frecuencias de los tamaños de gota (ingl. *drop size distribution, DSD*) o el diámetro mediano ( $D_{50}$ ) con la intensidad de la lluvia.

Probablemente los primeros estudios sean los realizados en Europa por Lenard (1904) y Defaut (1905). La coincidencia entre los resultados obtenidos en estos estudios seminales y nuevos datos experimentales registrados en Norteamérica permitió a Laws y Parsons (1943) formular la primera relación matemática entre el tamaño de gotas y la intensidad de la lluvia, para lo que eligieron una función potencial:

$$D_{50} = 2.23I^{1.82}, \quad (1.5)$$

donde  $D_{50}$  es el diámetro mediano de las gotas de lluvia medidas en un intervalo de tiempo determinado, generalmente 30 min e  $I$  es la intensidad de la lluvia medida durante el mismo intervalo de tiempo. Estos y otros estudios iniciales se realizaron a partir de eventos de intensidad baja a moderada, lo que condujo a la formulación de un modelo general de tipo potencial al existir una correlación positiva entre la intensidad de la lluvia y el tamaño de las gotas a lo largo de todo el rango de medidas (Best, 1950):



$$D_{50} = aI^b, \quad (1.6)$$

donde  $a$  y  $b$  son constantes calibradas con datos empíricos.

A partir de las investigaciones de Hudson (1963) en ambientes tropicales, en cambio, se conoce que el diámetro de las gotas de lluvia alcanza un valor máximo asociado a intensidades de lluvia en torno a los  $70\text{-}100 \text{ mm h}^{-1}$ , y que a partir de dicho valor la relación entre tamaño e intensidad se estabiliza o incluso se hace negativa (Figura 1.3).

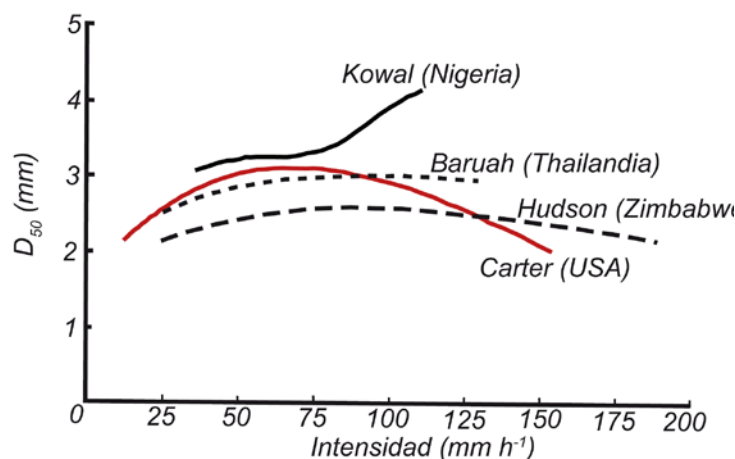


Figura 1.3: Relación entre la intensidad de lluvia y el diámetro mediano de las gotas ( $D_{50}$ ). Fuente: Hudson (1995).

Esta no linealidad en la relación entre intensidad de lluvia y tamaño de las gotas se puede explicar por el proceso de formación y desarrollo de las gotas de lluvia (Figura 1.4).

El proceso se inicia con la formación de pequeñas gotas de diámetro muy pequeño cuando las moléculas de agua se adhieren entre sí tanto por la condensación, convirtiéndose en cristales de hielo, como en torno a impurezas y núcleos higroscópicos presentes en la atmósfera. Las pequeñas gotas permanecen suspendidas en la nube debido a la resistencia al aire y a posibles vientos ascendentes, hasta alcanzar por crecimiento y coalescencia un tamaño de unos 0.2 mm, momento a partir del cual comienza su caída vertical atraídas por la gravedad terrestre. Durante su trayecto hacia la superficie continúan agrandándose en función de la cantidad de humedad de la masa de aire por la que se desplazan y por coalescencia con otras gotas, lo que explica que una mayor intensidad de lluvia (y por tanto mayor densidad de gotas por volumen de aire) produzca un mayor crecimiento de las gotas. La resistencia que ofrece el aire



inestabiliza las gotas en su base modificando la forma esférica de éstas, hasta que al llegar a un determinado tamaño en torno a los 5 o 6 mm de diámetro esta inestabilidad produce la rotura de las gotas en otras más pequeñas (Sempere Torres, 1994). Varios autores han señalado el cambio en la forma de las gotas en función del tamaño del diámetro pasando, a partir de 1 mm, de tener una forma asemejable a una esfera a otra más próxima a la elipse (Teschl et al., 2008). Este hecho se ha de tener en cuenta a la hora de estimar la energía cinética (ecuación 2), de no ser así se produce una sobreestimación que Fernández-Raga et al. (2010) han cuantificado en un 50% sobre la real.

En el proceso de formación de las gotas unas se crean a expensas de las otras y, por tanto, la existencia de una gota grande sólo es posible si hay una gradación de gotas más pequeñas, explicándose así la distribución de frecuencias de los tamaños de gota observadas. Durante un evento de lluvia y en fracciones de tiempo y espacio pequeños existe una gran variabilidad de gotas de diferentes tamaños. Los estudios empíricos reflejan que a intensidades bajas hay mayor variabilidad que a intensidades mayores (Van Dijk et al., 2002).

La distribución de los tamaños de gota tiene una gran variabilidad espacial, en relación con factores geográficos como la altitud, la latitud, la proximidad a masas de agua, etc. Estos factores limitan la obtención de una única expresión aplicable a distintas localidades geográficas.

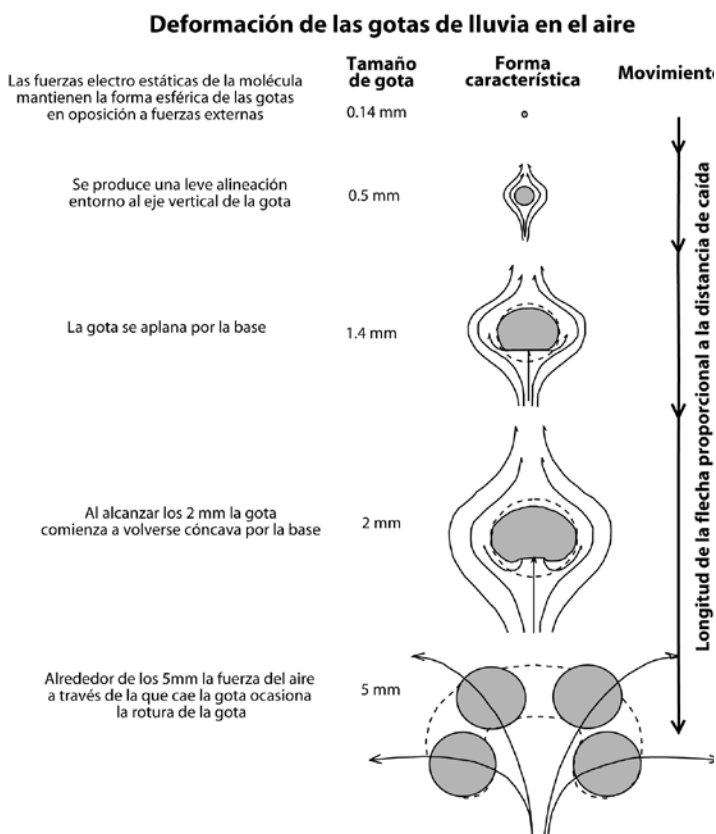


Figura 1.4: Formación y desarrollo de las gotas de lluvia.

Adaptado de Horstmeyer (2008).

La DSD y sus velocidades asociadas se combinan entre sí a través de la energía cinética,  $EC$ . Ya que, como hemos visto, estos parámetros están relacionados con la intensidad. Un buen número de trabajos han tratado de relacionar la  $EC$  con la intensidad de la lluvia; esto permitiría calcular la energía cinética de los eventos de lluvia a partir de registros de intensidad de la lluvia relativamente habituales. Se han empleado principalmente tres tipos de relaciones, basadas en las funciones logarítmica, potencial y exponencial (Tabla 1.3).

Tabla 1.3. Relaciones matemáticas entre la energía cinética ( $EC$ ) y la intensidad de la lluvia ( $I$ );  $a$  y  $b$  son coeficientes empíricos.

Tipo de función matemática	Ecuación
Potencial	$EC = aI^b$
Logarítmica	$EC = a + b \log I$
Exponencial	$EC = e_{\max} [1 - a \exp(-bI)]$



La utilización de uno u otro modelo tiene importantes repercusiones tanto teóricas como prácticas, como demuestra la Figura 1.5.

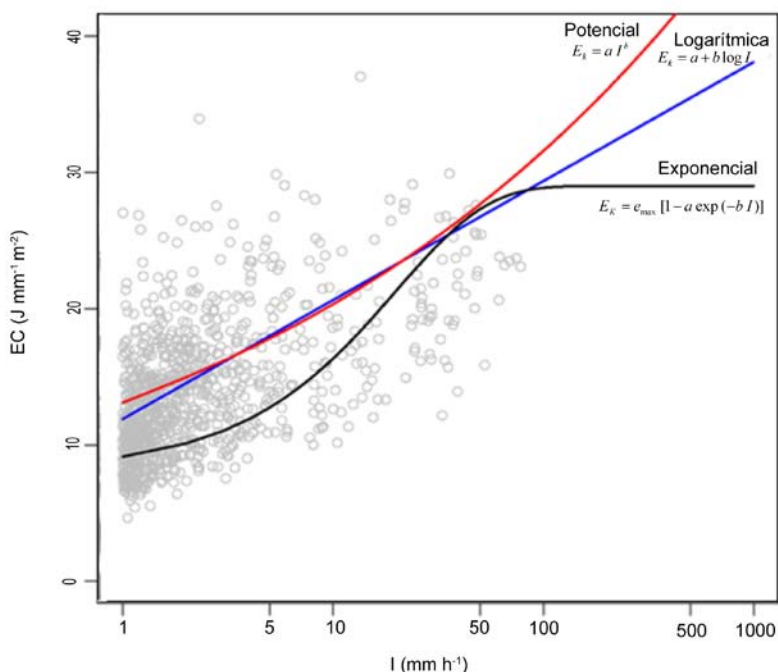


Figura 1.5: Relación entre energía cinética ( $EC$ ) e intensidad de la lluvia ( $I$ ) según tres modelos alternativos. Datos experimentales obtenidos en la Estación Experimental de Aula Dei (Zaragoza:  $41^{\circ}43'31''N / 0^{\circ}48'39''O$ ; 230 m. a.s.l.). Resolución temporal de la toma de datos: 1 min.

Los modelos potencial y logarítmico (los más antiguos en su formulación) estiman la energía cinética relativamente bien para bajas intensidades de lluvia, pero la sobreestiman a intensidades elevadas, sin existir un límite superior. Sin embargo los estudios experimentales realizados con posterioridad sugieren que en la naturaleza la  $EC$  no se incrementa indefinidamente sino que se estabiliza a partir de unos determinados valores de intensidad (Hudson, 1963; Baruah, 1973; Carter et al., 1974; Kinnell, 1980; Rosewell, 1986; Brown and Foster, 1987). El modelo exponencial consigue un mejor ajuste a intensidades elevadas, ya que presenta una asíntota a partir de un determinado valor, aunque puede subestimar ligeramente los valores de  $EC$  a intensidades bajas. Numerosos autores han estudiado la relación entre ambas variables a partir de los modelos descritos, como se resume en la Tabla 1.4. Conviene indicar que en todos los casos es necesario disponer de datos de intensidad de lluvia con una frecuencia de 30 minutos o superior.



Tabla 1.4: Relaciones empíricas entre la energía cinética,  $EC$  ( $\text{MJ ha}^{-1} \text{mm}^{-1}$ ) e intensidad de la lluvia,  $I$  ( $\text{mm h}^{-1}$ ) en distintos lugares, con indicación del rango de intensidad de los datos utilizados (n.c.: no consta).

Fuente	Localidad	Ecuación	Rango de intensidad ( $\text{mm h}^{-1}$ )
USLE; Wischmeier & Smith 1978; basado en Laws and Parsons (1943)	EE.UU.	$EC = 0.0119 + 0.0873 \log_{10} I$	0.4–144
Marshall and Palmer (1948)	Canadá	$EC = 0.0895 + 0.0844 \log_{10} I$	0–23
Hudson (1965)	Zimbawe	$EC = 0.298 (1 - 4.29/I)$	n.c.
Carter et al. (1974)	Sur y centro EE.UU.	$EC = 0.1132 + 0.0055I - 0.005 \cdot 10^{-2} I^2 + 0.00126 \cdot 10^{-4} I^3$	<260
Zanchi y Torri (1980)	Italia, Toscana	$EC = 0.0981 + 0.1125 \log_{10} I$	1–140
Park et al. (1982)	EE.UU	$EC = 0.2111 * I^{1.156}$	n.c.
Bolline et al., (1984)	Bélgica	$EC = 0.123 + 0.56 * I$	0.3–39
Rosewell (1986)	New South Wales, Australia	$EC = 0.29 (1 - 0.6 e^{-0.04I})$	1–146
Rosewell (1986)	Queensland, Australia	$EC = 0.26 (1 - 0.7 e^{-0.035I})$	1–161
RUSLE; Brown and Foster (1987)	Sur EE.UU	$EC = 0.29 (1 - 0.72 e^{-I/20})$	0–250
Onaga et al. (1988)	Okinawa, Japón	$EC = 0.0981 + 0.106 \log_{10} I$	4–103
Brandt (1990)	EE.UU.	$EC = 0.895 + 0.844 \log_{10} I$	n.c.
Sempere Torres et al. (1992)	Cévennes, Francia	$EC = 0.34 * I - 0.19$	n.c.
Coutinho y Tomas (1995)	Portugal	$EC = 0.29 (1 - 0.72 e^{-0.34I})$	0–120
Cerro et al. (1998)	Barcelona, España	$EC = 0.384 (1 - 0.54 e^{-0.029I})$	1–150
Uijlenhoet y Stricker (1999)	Canadá	$EC = 0.072 * I^{1.32}$	<23
Jayawardena and Rezaur (2000)	Hong Kong	$EC = 0.369 (1 - 0.69 e^{-0.038I})$	12–120
Van Dijk et al (2002)	Universal	$EC = 0.283 (1 - 0.52 e^{-0.042I})$	n.c.
Usón y Ramos (2001)	España	$EC = 0.34 * I - 0.18$	0–20
Roldán, M. (2006)	Madrid, España	$EC_{\min} = 65 - e^{(-9.8679 \cdot 10^{-5} I^2 - 4.987 \cdot 10^{-3} I + 4.1779)}$	47.5



Entre todos los estudios citados únicamente el de Van Dijk et al. (2002) propuso una relación universal utilizando datos de estudios previamente publicados. Entre los estudios que estos autores analizaron consideraron 12 como adecuados en función de la longitud de las series y la precisión en la toma de datos. A su vez compararon las estimaciones proporcionadas por la relación obtenida con esos 12 estudios y otros 10 más, obteniendo buenas aproximaciones en la mayoría de los lugares. Las diferencias encontradas las achacaron a diferencias en los sistemas de medida y a la longitud del periodo de observación, así como al peso que tiene el factor local (relieve, génesis de la lluvia) en la energía cinética. A pesar de su universalidad el modelo de Van Dijk et al. (2002) no ha sido ampliamente utilizado, a diferencia del propuesto por Wischmeier y Smith (1958) o la versión revisada de Renard et al. (1997).

## 1.6. Climatología de la energía cinética

A pesar de los errores de medición muchas de las diferencias entre las distintas relaciones  $EC(I)$  obtenidas en diferentes lugares se pueden atribuir a diferencias en las características atmosféricas y físicas de la precipitación, así como a rasgos geográficos del entorno que modifican dichas características. Tanto el tamaño de las gotas de lluvia como su velocidad terminal dependen de factores atmosféricos como la temperatura del aire y la presión atmosférica, de manera que la energía cinética de las gotas a 500 m de altura es alrededor de un 4-5% mayor que a nivel del mar, un 8-10% a 1000 m. y un 44-61% a 4000 m (Van Dijk et al., 2002). Esta diferencia se incrementa con el tamaño de la gota. La  $DSD$  y sus consiguientes energías cinéticas están relacionadas con la temperatura de la masa de aire, de forma que el  $D_{50}$  podría calcularse a través de una relación potencial con la temperatura (Zanchi y Torri, 1980), aunque esta relación puede manifestar también diferentes tipos de situaciones atmosféricas (Van Dijk et al., 2002). Otros estudios revelan diferencias en la  $DSD$  asociadas a frentes fríos o frentes ocluidos, (Kinnell, 1973).

Uno de los primeros estudios exhaustivos a este respecto es el de Carter et al. (1974), quienes analizaron mediante *flour pellets* 181 eventos de lluvia en Baton Rouge (Louisiana) y 315 en Holly Springs (Carolina del Norte) durante el periodo 1964-1972. Evaluaron la influencia de parámetros meteorológicos como: i) la temperatura del aire, ii) la estación del año y iii) la duración de las tormentas. Sus



análisis mostraron que las gotas de lluvia precipitadas a temperaturas del aire superiores a 18.3°C eran significativamente más grandes que en condiciones más frías, lo que explicaba las diferencias estacionales observadas. Estos autores también constataron la influencia de la duración de los eventos, ya que con una duración inferior a 1 hora las gotas eran significativamente mayores que en eventos de mayor duración. Estas relaciones mostraron la importancia de los mecanismos de generación de la lluvia (ingl. *cloud microphysics*) en las características de las gotas. Otras variables analizadas como: i) la humedad relativa, ii) el momento del día en el que se produce el evento, o iii) el tamaño de la tormenta no mostraron diferencias significativas respecto al tamaño de gotas. Sin embargo, este hecho también se puede deber al tamaño relativamente pequeño de la muestra utilizada.

En general se observa que las condiciones atmosféricas influyen en el tamaño de las gotas produciéndose un gradiente desde frentes cálidos, relacionados con tamaños de gota más pequeños y eventos de lluvia generalmente más duraderos y de menor intensidad, a frentes ocluidos y fríos, vinculados con eventos de lluvia de mayor intensidad (Van Dijk et al., 2002).

Los estudios revelan también una influencia de los factores geográficos. Por ejemplo, la diferencia entre frentes fríos y cálidos se atenúa en regiones costeras y se incrementa en zonas continentales, lo cual hace necesario establecer dos relaciones *EC(I)* diferentes, (Rosewell, 1986). La comparación de valores publicados por diversos autores confirma el incremento general de los valores de *EC* promedio desde la costa hacia el interior: Brisbane ( $26.4 \text{ J m}^{-2} \text{ mm}^{-1}$ ) en la costa australiana, en oposición a Gunnedah ( $28.2 \text{ J m}^{-2} \text{ mm}^{-1}$ ) en el interior de Australia, (Rosewell, 1986); Carolina del Norte ( $24.6 \text{ J m}^{-2} \text{ mm}^{-1}$ ) en comparación con New Jersey ( $25.1 \text{ J m}^{-2} \text{ mm}^{-1}$ ), (McIsaac, 1990); Japón ( $23.7 \text{ J m}^{-2} \text{ mm}^{-1}$ ), (Mihara, 1952); Trinidad ( $24.7 \text{ J m}^{-2} \text{ mm}^{-1}$ ), (Ker, 1954).

Los estudios experimentales enfocados a cuantificar el efecto de la orografía en el tamaño de las gotas reflejan un descenso en el tamaño de las mismas con la altitud (Blanchard, 1953; McIsaac, 1990). Esto se ha explicado por el hecho de que a medida que las gotas de lluvia pasan de capas atmosféricas altas y frías a otras más cálidas próximas a la superficie las gotas más pequeñas tienden a evaporarse, prevaleciendo por tanto las gotas de mayor tamaño que proporcionan valores mayores de *EC* (Blanchard, 1953; Beard, 1977).



Por su parte, diferencias en los mecanismos genéticos de la precipitación en las zonas tropicales y zonas de latitudes medias tienen como resultado lluvias más erosivas en las primeras con respecto a las segundas (Figura 1.6). Estas diferencias pueden ser también estacionales, haciendo difícil el establecimiento de modelos únicos que relacionen la *EC* con otros parámetros simples como la intensidad de la lluvia.

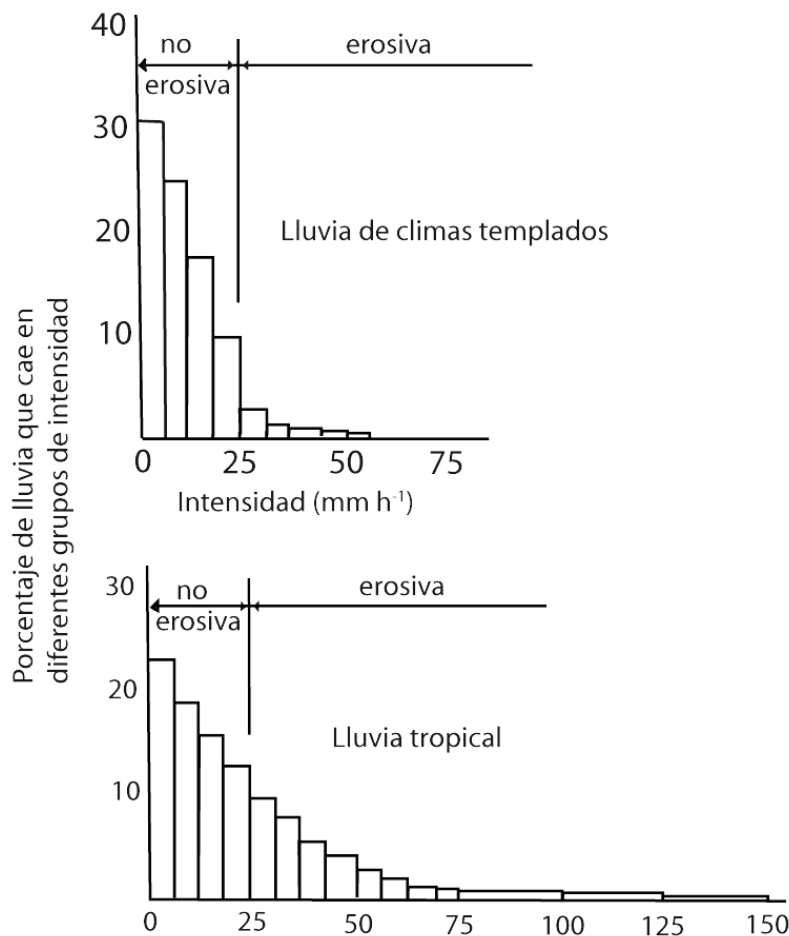


Figura 1.6: Histogramas de frecuencias de la intensidad de lluvia por zonas climáticas. Fuente: Hudson, 1995.

## 1.7. Índices de erosividad de la lluvia

Como se ha indicado en Apartado 1.3, la acción erosiva de la lluvia depende fundamentalmente de la energía cinética, pero también de otras características del evento de lluvia como el volumen total precipitado, por su influencia en procesos como el encharcamiento. Diversos autores se han esforzado por definir índices de erosividad basados en las características de la lluvia.



El índice de erosividad más extendido es sin duda el factor R del modelo USLE/RUSLE (Wischmeier, 1958; Wischmeier y Smith, 1978; Brown y Foster, 1987), constituido por el promedio anual de la erosividad de los eventos de lluvia:

$$R = \frac{1}{n} \sum_{j=1}^n \sum_{k=1}^{m_j} (EI_{30})_k , \quad (1.7)$$

donde  $n$  es el número de años,  $m_j$  es el número de eventos erosivos del año  $j$ , y  $EI_{30}$  es el índice de erosividad de cada evento  $k$  ( $\text{MJ mm ha}^{-1} \text{ h}^{-1}$ ), calculado como:

$$EI = EI_{30} = \left( \sum_{r=1}^o e_r v_r \right) I_{30} , \quad (1.8)$$

donde  $e_r$  y  $v_r$  son, respectivamente, la energía cinética unitaria de la lluvia ( $\text{MJ ha}^{-1} \text{ mm}^{-1}$ ) y la cantidad de lluvia (mm) durante un periodo de tiempo  $r$  e  $I_{30}$  es la intensidad máxima en 30 minutos ( $\text{mm h}^{-1}$ ). La energía unitaria,  $e_r$ , se estima para cada intervalo de tiempo como:

$$e_r = 0.29 [1 - 0.72 \exp(-0.05 i_r)] , \quad (1.9)$$

donde  $i_r$  es la intensidad de la lluvia en el intervalo de tiempo ( $\text{mm h}^{-1}$ ). Esta última ecuación responde a las modificaciones introducidas por Brown y Foster (1987). Asimismo, Elwell y Stocking (1975) proponen no aplicar el cálculo de  $EI_{30}$  para los eventos de lluvia inferiores a 12.7 mm, estando separados de otros eventos en al menos 6h, a no ser que se registren intensidades de 6.35 mm en 15 minutos o superiores.

Algunos autores han observado que el índice  $EI_{30}$  sobreestima la erosividad de la lluvia en climas tropicales. Estudios en África demostraron que se requieren intensidades superiores a 25  $\text{mm h}^{-1}$  para erosionar el suelo, por lo que se propuso utilizar sólo los valores de  $EI_{30}$  por encima de dicho umbral ( $KE > 25$ ) (Hudson, 1971). Morgan (1977) propuso el uso de un umbral de  $KE > 10$  para Europa.

Los estudios de Lal (1976) en Nigeria no observaron un buen ajuste con ninguno de los índices referidos, lo cual motivó el desarrollo del índice  $AI_m$ ,

$$AI_m = \sum_{i=1}^{12} \left[ \sum_{l=1}^n A I_{\max} \right] , \quad (1.10)$$



donde  $\mathcal{A}$  es la cantidad de lluvia registrada por evento e  $I_m$  la intensidad máxima en 7.5 minutos,  $n$  es el número de eventos por mes.

De estos índices el más ampliamente utilizado es el  $EI_{30}$ . La principal desventaja de este índice y de otras ecuaciones similares es la necesidad de contar con series de lluvia continuas y lo suficientemente largas a una resolución temporal mínima de 15 minutos, aconsejándose por lo menos una longitud mínima de 20 años (Renard et al., 1997; Verstraeten et al., 2006). Este tipo de información no suele estar disponible con una adecuada cobertura espacio-temporal. Por ello se ha recurrido a la estimación de la erosividad de la lluvia a partir de registros de lluvia de menor frecuencia, desde la lluvia media anual (Renard y Freimund, 1994), mensual (Yu and Rosewell, 1996a, b and c, Yu et al., 2001), diaria o incluso de evento (Richardson et al., 1983, Bagarello and D'Assaro, 1994, Petkovsek and Mikos, 2004, Angulo-Martínez y Beguería, 2009b), o a partir del índice modificado de Fournier (Arnoldus, 1977; Renard y Freimund, 1994).

En realidad todas estas aproximaciones están basadas en relaciones potenciales del tipo:

$$EI = aP^b, \quad (1.11)$$

donde  $EI$  es la erosividad de la lluvia,  $P$  es la lluvia a escala anual, mensual, diaria o de evento o el índice de Fournier, y  $a$  y  $b$  son parámetros empíricos.

## 1.8. Fronteras de conocimiento sobre la erosividad de la lluvia

La importancia de estudiar la erosividad de la lluvia como un factor fundamental para plantear medidas de conservación del suelo es ampliamente reconocida. Los trabajos más recientes han ahondado en determinar la erosividad de la lluvia en un número creciente de lugares del planeta, tratando de recabar más datos que permitan ampliar la escala espacial de trabajo y así poder determinar relaciones universales entre ésta y las dinámicas atmosféricas y los factores geográficos. La elaboración de cartografías de erosividad de la lluvia adquiere por ello un valor fundamental, aunque hasta el momento pocos trabajos se han ocupado de esta tarea y por ejemplo no se han estudiado a fondo cuáles son las técnicas estadísticas más adecuadas para estudiar la distribución espacial de esta variable. Asimismo, son escasos los trabajos orientados a determinar la existencia de tendencias temporales relacionadas con la variabilidad de los mecanismos



atmosféricos generadores de lluvia, o los posibles efectos del cambio climático sobre la erosividad de la lluvia. Una de las razones para este hecho radica en el esfuerzo de experimentación necesario para determinar con precisión la erosividad de la lluvia. No sólo se han de medir la distribución de los tamaños de gota y su velocidad, sino también la cantidad de suelo que se erosiona, para lo que se requiere la instalación y seguimiento de parcelas experimentales. Estos hechos han limitado la toma de datos a lugares puntuales y a periodos temporales irregulares.

Recientemente se están desarrollando estimaciones globales de la intensidad de lluvia a partir de datos de satélites geoestacionarios—basados en algoritmos sobre el espectro infrarrojo y visible a partir del brillo de las nubes dependiente de su contenido en hielo—y de microndas pasivas de los satélites de la órbita terrestre próximos a la Tierra que llevan incorporados radares para la detección de la lluvia (Gruber y Levizzani, 2008). Desde la puesta en marcha de la *Tropical Rainfall Measurement Mission* de la NASA (<http://trmm.gsfc.nasa.gov/>) en 1997 se han desarrollado una serie de productos de estimación de la lluvia a escala global. Entre ellos TMPA 3B42 (Huffman et al., 2007) proporciona datos de lluvia global cada 3 horas y TMPA 3B43 datos mensuales a partir de TMPA 3B42 corregido con las medidas registradas en diversas estaciones de superficie. Los datos están disponibles desde 1998 con una resolución espacial de 0.25° de latitud y longitud. Estos productos abren una línea de trabajo novedosa ya que permiten obtener estimaciones de la lluvia en cualquier lugar de la Tierra, independientemente de la red de observación. La literatura científica ya incluye varios trabajos utilizando estos datos para el estudio de la precipitación. En relación con la erosividad de la lluvia existe el trabajo pionero de Vrieling et al. (2010) en el que se estima la erosividad de la lluvia en el continente africano a partir de esta fuente de datos y se compara con datos de observatorios puntuales. Sus conclusiones son buenas para la estimación de la erosividad anual, pero no tanto en lo que respecta al índice  $EI_{30}$ , ya que este depende de la energía y la intensidad de la lluvia a una resolución temporal mínima de 30 minutos, que queda completamente diluida en las estimaciones satelitales cada 3h, a lo que se suma el error inherente a la detección de la lluvia a frecuencias temporales altas. Existen otros productos satelitales a mejor resolución temporal, de todos ellos CMORPH (*Climate Prediction Center Morphing Method* del Centro de Predicción Climática NOAA/NCEP; Joyce et al., 2004) proporciona estimaciones de lluvia



globales cada 30 minutos a una resolución espacial aproximada de 8 km, con resultados equiparables en validez a los obtenidos por TMPA 3B42.

Quizá un paso intermedio necesario en la estimación de la erosividad de la lluvia con datos de satélite sea la utilización del radar meteorológico, debido a la mejor cobertura espacial y temporal de éstos. En España la red radar de la Agencia Española de Meteorología (AEMET: <http://www.aemet.es/es/eltiempo/observacion/radar>) proporciona datos cada 10 minutos, contando con un total de 15 radares regionales desde hace aproximadamente 20 años. El radar meteorológico funciona emitiendo radiación que al impactar contra un obstáculo, en este caso las gotas de agua presentes en las nubes y en la lluvia, retorna parcialmente hacia la fuente. A la medida del retorno parcial de energía se la denomina reflectividad, y constituye la información que se utiliza para estimar la cantidad de agua líquida presente en la atmósfera. La reflectividad se corresponde con la densidad de gotas que se encuentran en suspensión y por tanto, de manera indirecta, con la intensidad de precipitación que se está produciendo. Para convertir los datos de reflectividad del radar en intensidad de lluvia se utiliza una relación exponencial  $Z(R)$  (Marshall y Palmer, 1948):

$$Z = aR^b, \quad (1.12)$$

siendo  $Z$  la reflectividad ( $\text{mm}^6 \text{ m}^{-3}$ ) y  $R$  la lluvia ( $\text{mm h}^{-1}$ ), y  $a$  y  $b$  coeficientes empíricos. Los disdrómetros ópticos proporcionan el valor de  $Z$  en función de los datos de la *DSD* que se recogen en superficie, permitiendo establecer relaciones con los datos de altura del radar. Fernández-Raga et al. (2009) analizaron la situación de la atmósfera durante 24h del evento más lluvioso de 2006 en León. Sus resultados permitieron diferenciar episodios de lluvia convectiva y estratiforme durante el evento, observando una concordancia entre los datos de superficie y el radar meteorológico.

El estudio de la erosión del suelo ha de incluir información no solo sobre la cantidad e intensidad de la lluvia sino, también sobre la *DSD* de las gotas de lluvia y sobre todo la energía cinética de las gotas al impactar contra la superficie (Sharma et al., 1991; Cerro et al., 1998; Fernández-Raga et al. 2009), además de las características físico-químicas del suelo (Moss and Green, 1983, Kinnell, 1991, Leguédois et al., 2005).



## 1.9. El estudio de la erosividad de la lluvia en el ámbito español

En España el estudio de la erosividad de la lluvia se ha realizado como uno de los factores que intervienen en la erosión hídrica, siendo importante el cómputo global de suelo erosionado más que las propiedades físicas de la precipitación. A mediados de los 80 se comenzó a crear una red de estaciones experimentales, que a partir de los 90 se financia en el marco del proyecto RESEL (Red de Estaciones Experimentales de Seguimiento y Evaluación de la Erosión y la Desertificación), inicialmente por el ICONA y más tarde por la Dirección General de Conservación de la Naturaleza y la Dirección General para la Biodiversidad del Ministerio de Medio Ambiente, dentro del proyecto LUCEDME de Lucha Contra la Desertificación en el Mediterráneo (García Ruiz y López Bermúdez, 2009). A modo de ejemplo, los objetivos de los estudios sobre la erosión de suelos en parcelas incluyen (Bryan, 1991): i) identificar umbrales en el volumen e intensidad de la lluvia para la generación de escorrentía y transporte de sedimento; ii) estudiar procesos hidrológicos, como la variabilidad espacial de la tasa de infiltración; iii) comparar los efectos erosivos de diferentes cultivos, rotaciones y técnicas de laboreo y prácticas de conservación de suelo; iv) comparar el efecto de diferentes factores topográficos (pendiente, exposición, longitud de la ladera) y de la pedregosidad sobre la pérdida de suelo y sobre el funcionamiento de la escorrentía. A la monitorización en parcelas se unió la monitorización en cuencas hidrográficas de tamaños entre 5 y 300 ha. Esto proporcionó un cambio de escala y como consecuencia del marco conceptual y de los objetivos de estudio, que en este caso abordan la evolución de los caudales y el transporte de sedimento en función de cambios en la cubierta vegetal, usos de suelo o clima. Las condiciones son más próximas a la dinámica natural. Los principales equipos de investigación que han desarrollado estos estudios son:

Tabla 1.5: Algunos grupos de investigación sobre erosión de suelo en España. Síntesis a partir de García Ruiz y López Bermúdez (2009).

Centro	Localización	Parcela	Cuenca
Centro de Edafología y Biología Aplicada del Segura-CEBAS	Murcia	X	X
Departamento de Geografía de la Universidad de Murcia		X	
Centro de Investigaciones sobre Desertificación-CIDE	Valencia	X	



Centro	Localización	Parcela	Cuenca
Departamento de Geografía de la Universidad de Valencia		X	X
Instituto Pirenaico de Ecología	Zaragoza	X	X
Departamento de Ciencias de la Tierra de la Universidad de Zaragoza		X	X
Centro de Ciencias Medioambientales	Toledo	X	
Instituto Madrileño de Investigación Agraria y Alimentaria	Madrid	X	
Departamento de Edafología de la Universidad de Santiago de Compostela	Santiago de Compostela	X	
Departamento de Edafología de la Universidad de la Laguna	Tenerife	X	X
Instituto de Ciencias de la Tierra Jaume Almera	Cataluña		X
Centro de Investigaciones Ecológicas y Aplicaciones Forestales (CREAF). Universidad Autónoma de Barcelona	Cataluña		X
Departamento de Geografía Física de la Universidad de Barcelona	Cataluña		X
Departamento Ecología de la Universidad de Alicante	Alicante		X
Servicio de Estructuras Agrarias del Gobierno de Navarra	Navarra		X
Grupo de Hidrogeología de la Facultad de Ciencia y Tecnología de la Universidad del País Vasco (Guipúzcoa)	País Vasco		X
Grupo de Investigación en Recursos Hídricos de la Universidad de Salamanca	Salamanca		X
Estación Experimental de Zonas Áridas	Almería		X
Departamento de Geografía de la Universidad de Extremadura	Cáceres		X
Departamento de Ciencias de la Tierra de la Universidad de las Islas Baleares	Mallorca		X

A pesar del esfuerzo de experimentación e instrumentación realizado no se ha incluido la monitorización de las propiedades físicas de la lluvia, a excepción de ensayos puntuales con simuladores de lluvia que exponen al suelo a intensidades generalmente muy elevadas durante períodos de tiempo relativamente cortos con el objetivo de determinar la respuesta de los suelos frente a la lluvia, la capacidad de infiltración y la profundidad del frente de humectación. Navas et al. (1990) publicaron los datos de calibración para ensayos de simulación de lluvia a intensidades de  $48 \text{ mm h}^{-1}$  y  $58 \text{ mm h}^{-1}$ , con distintos tamaños de gota medidos en lluvia natural en la depresión del Ebro.



Para la estimación de la erosividad de la lluvia generalmente se ha recurrido a aproximaciones empíricas como el factor R de la USLE y su relación con intensidades de lluvia diaria recogidas en la red de estaciones pluviométricas de la Agencia de Meteorología Española (Domínguez-Romero et al., 2007; Angulo-Martínez y Beguería, 2009b) o intensidades pluviográficas recogidas por las Confederaciones Hidrográficas (ICONA, 1988; Angulo-Martínez et al., 2009a). A partir de estas aproximaciones teóricas diversos autores han estudiado las dinámicas estacionales e interanuales de la erosividad de la lluvia. Domínguez-Romero et al. 2007 detectaron para las estaciones de Córdoba, Sevilla, Huelva y Cádiz, una diferencia en la dinámica estacional de la erosividad de la lluvia entre los observatorios costeros y los interiores. Asimismo, Angulo-Martínez et al. (2009a) observaron un gradiente positivo en sentido NW-SE en la cuenca del Ebro, así como una distribución diferencial de la erosividad a lo largo del año. López-Vicente et al. (2008) identificaron cuatro periodos erosivos en una zona de montaña del Pirineo Central Español en función de los factores de la RUSLE, encontrando que la máxima erosión coincidía con el periodo de máxima erosividad de la lluvia unido a la época con escasa cobertura vegetal.

En el estudio llevado a cabo por González-Hidalgo et al. (2007) a partir de datos publicados sobre erosión de suelo a escala diaria en áreas del Mediterráneo occidental, se constató que la tasa de erosión anual depende de unos pocos eventos erosivos al año. Este hecho está en concordancia con los estudios de Martínez-Casasnovas et al. (2002), aunque la erosividad producida por todos los eventos a lo largo del año influye en la pérdida de nutrientes en el suelo. Las tendencias observadas en los últimos 50 años sobre la erosividad de la lluvia en el nordeste del territorio español han mostrado una tendencia regresiva (Angulo-Martínez et al., 2009c; De Luis et al., 2010), aunque este hecho puede estar relacionado con la predominancia de periodos de fases positivas de la Oscilación del Atlántico Norte u otros índices de teleconexión atmosférica responsables de la precipitación en este área (Angulo-Martínez y Beguería, enviado).

En cuanto al análisis de la relación entre tamaños de gota y energía cinética con el fin de aportar relaciones con la intensidad que reflejen las propiedades físicas de la lluvia han sido pocos los estudios realizados, no habiéndose utilizado hasta la fecha las ecuaciones propuestas en los mismos, salvo en el campo científico. Resaltan a este respecto los trabajos de Cerro et al. (2008) a partir de datos obtenidos en Barcelona con disdrómetro óptico, la formulación aportada por



Usón y Ramos (2001) para climas mediterráneos, y el estudio de Roldán (2006) en Madrid a partir de disdrómetro acústico.

El trabajo más completo en la determinación de la erosividad del suelo en España ha sido el realizado por Fernández-Raga et al. (2010), quienes combinaron los datos de pérdida de suelo recogidos experimentalmente por dos colectores de *splash* junto con medidas de *DSD* y *EC* a partir de disdrómetro óptico.

En resumen, el estudio de la erosividad de la lluvia aborda diversos campos de conocimiento, combinando desarrollos y estudios propios de física de la atmósfera con geomorfológicos y edafológicos junto con estadísticos y climatológicos. Esta amplitud y variabilidad de puntos de vista han complicado el desarrollo de estudios, que sin embargo debe ser completado dada la importancia del objeto de estudio a la hora de establecer medidas de conservación del suelo que resulten realmente prácticas.

## 1.10. Objetivos y estructura de la Tesis Doctoral

El objetivo principal de esta Tesis Doctoral es profundizar en el estudio de la erosividad de la lluvia en un área climática de transición con características oceánicas, mediterráneas y continentales: la cuenca del Ebro.

Este objetivo general se desglosa en los siguientes objetivos concretos:

1. Proponer un modelo de la relación entre la erosividad de la lluvia y la lluvia diaria,  $EI(I)$ , en la cuenca del Ebro con el fin de desarrollar una base de datos cubriendo el periodo 1955-2006.
2. Valorar las relaciones existentes entre la erosión de suelo y la erosividad de la lluvia a partir de registros experimentales obtenidos en parcelas monitorizadas en el centro del valle del Ebro.
3. Analizar las dinámicas espacio-temporales de la erosividad de la lluvia en la cuenca del Ebro y determinar los factores geográficos y climáticos que influyen en esta variable.
4. Investigar las relaciones existentes entre los principales patrones de circulación atmosférica que influyen en la climatología de esta área, tales como la Oscilación del Atlántico Norte (NAO), la Oscilación Mediterránea (MO) y la Oscilación del Mediterráneo Occidental (WeMO), y la erosividad de la lluvia.



5. Proponer una ecuación  $EC(I)$  para la cuenca del Ebro a partir de los datos obtenidos mediante disdrómetro óptico en el centro del valle del Ebro.

En función de estos objetivos, el contenido de la tesis se estructura en 4 bloques: el primero aborda el marco conceptual sobre la erosividad de la lluvia. El segundo está dedicado al estudio climatológico de la erosividad de la lluvia. En él se abordan los objetivos 1, 3 y 4. El tercer bloque está dedicado al estudio experimental de la erosividad de la lluvia, abordando los objetivos 2 y 5. Finalmente, en el bloque IV se realiza una valoración crítica de todo el estudio y se aportan las conclusiones finales.

En la redacción de esta tesis se han utilizado indistintamente las lenguas castellana e inglesa. El castellano se ha empleado en los bloques I y IV, de introducción y síntesis, mientras que en los bloques de análisis (II y III) se usa el inglés. El motivo es que los bloques centrales de la Tesis están basados en artículos ya publicados o en fase de evaluación, en revistas de difusión internacional de habla inglesa. Se ha preferido mantener el lenguaje original en el que se han redactado los trabajos.

Cada bloque consta de un breve resumen en castellano e inglés junto con una introducción que permite contextualizarlo dentro del marco global del estudio, de esta forma, aunque se haya compartimentado la tesis en bloques temáticos se mantiene una estructura e hilo conductor general.

Otro aspecto a reseñar es la decisión de repartir el listado bibliográfico entre los bloques que componen la Tesis. Aunque ello conlleva la inevitable repetición de algunas referencias, ha permitido separar la bibliografía por grandes bloques temáticos, lo que añade valor al listado.



## 1.11. Referencias bibliográficas

- Almorox Alonso, J., López Bermúdez, F., Rafaelli, S. 2010. *La degradación de los suelos por erosión hídrica. Métodos de estimación*. Edit.um Ediciones de la Universidad de Murcia. Murcia, 384 pág.
- Almorox, J., De Antonio, R., Saa, A., Díaz, M.C., Gascó, J.M. 1994. *Métodos de estimación de la erosión hídrica*. Editorial Agrícola Española, 152 pág. Madrid
- Angulo-Martínez, M., López-Vicente, M., Vicente-Serrano, S.M., Beguería, S., 2009a. Mapping rainfall erosivity at a regional scale: a comparison of interpolation methods in the Ebro Basin (NE Spain). *Hydrology and Earth Systems Science*, 13, 1907-1920.
- Angulo-Martínez, M., Beguería, S., 2009b. Estimating rainfall erosivity from daily precipitation records: A comparison among methods using data from the Ebro Basin (NE Spain). *Journal of Hydrology*, 379, 111-121.
- Angulo-Martínez, M., Vicente-Serrano, S.M., Beguería, S., 2009c. Tendencias en la erosividad de la lluvia (1955-2006) en la cuenca del Ebro. En Romero Díaz, A., Belmonte Serrano, F. Alonso Sarria, F., López Bermúdez, F. (eds). 2009. *Avances en estudios sobre desertificación. Aportaciones al congreso internacional sobre desertificación en memoria del profesor John B. Thornes*. Servicio de publicaciones de la Universidad de Murcia. 511-515.
- Angulo-Martínez, M., Beguería, S., 2011. Do atmospheric teleconnection patterns influence rainfall erosivity? A study of NAO, MO and WeMO in NE Spain, 1955-2006. *Journal of Hydrology*, (enviado).
- Arnoldus, H.M.J. Methodology used to determine the maximum potential average annual soil loss due to sheet and rill erosion in Morocco. *FAO Soils Bulletin*, 34: 39-51. 1977
- Atlas, D., Ulbrich, C.W. 1977. Path and area integrated rainfall measurement by a microwave attenuation in the 1-3 cm band. *Journal of Applied Meteorology*, 16: 1322-1331
- Bagarello, V., D'Asaro, F., 1994. Estimating single storm erosion index. *Transactions of the American Society of Agricultural Engineers*, 37, 3, 785-791.
- Baruah, P.C., 1973. *An investigation of drop size distribution of rainfall in Thailand*. MSc Thesis no. 528, Asian Institute of Technology, Bangkok.



- Beard, K.V. 1977. Terminal velocity adjustment for cloud and precipitation drops aloft. *Journal of Atmospheric Sciences*, 34: 1293–1298.
- Bentley, W.A. 1904. Studies of raindrops and raindrop phenomena, *Monthly Weather Review* 32: 450–456.
- Best, A.C., 1950. The size distribution of raindrops. *Quart. J. r. Meteorological Society*. 76: 16-36.
- Bisal, F., 1960. The effect of raindrop size and impact velocity on sand splash. *Canadian Journal of Soil Science*, 40: 242-245.
- Blanchard, D.C. 1953. Raindrop size distributions in Hawaiian rains. *Journal of Meteorology*, 10: 457–473
- Bloemink, H.I., Lanzinger, E., 2005. Precipitation type from the Thies disdrometer. WMO Technical Conference on Meteorological and Environmental Instruments and Methods of Observation (TECO-2005) Bucharest: Romania, 3(11). 4-7 May.
- Boardman, J. Poesen, J. 2006. *Soil erosion in Europe*. Chichester: Wiley. ISBN 978-0-470-85910-0
- Bolinne, A., Florins, P., Hecq, P., Homerin, D., Renard, V., Wolfs, J.L. 1984. Etude de l'énergie des pluies en climat tempéré océanique d'Europe Atlantique. *Z. Geomorph.* N.F., 27-35.
- Bowen, E.G. 1951. Radar observations of rain and their relation to mechanisms of rain formation. *Journal of Atmospheric and Terrestrial Physics*, 1 (3): 125-140.
- Brandt, C.J. 1990. Simulation of size distribution and erosivity raindrops and throughfall drops. *Earth Surface Processes*, 15: 687-698
- Brown, D., Upton, G., 2008. Estimation of an atmospheric gamma drop size using disdrometer data. *Atmospheric Research*. 87, 66-79.
- Brown, L.C., Foster, G.R., 1987. Storm erosivity using idealized intensity distributions. *Transactions of the ASAE*, 30 (2): 379-386.
- Carter, C.E.; Greer, J.D.; Braud, H.J.; Floyd, J.M. 1974. Raindrop characteristics in South Central United States. *Transactions of the ASAE*, 17(6): 1033-1037
- Cerdà, A. 1997. Rainfall drop size distribution in the Western Mediterranean basin, Valencia, Spain. *Catena*, 30(2-3), 169-182.



- Cerro, C., Bech, J., Codina, B., Lorente, J. 1998. Modeling rain erosivity using disdrometric techniques. *Soil Science Society of America Journal*, 62 (3) 731-735
- Coutinho, M.A., Tomás, P.P. 1995 Characterization of raindrop size distributions at the Vale Formoso Experimental Erosion Center. *Catena* 25: 187–197.
- Defant, A., 1905. Gesetzmässigkeiten in der Verteilung der verschiedenen Tropfengrössen bei Regenfällen. *Akademie d. Wissenschaften, Vienna, Math.-Naturwiss. Klasse, Sitzungsberichte*, 114, 585-646.
- De Luis, M.; González-Hidalgo, J.C.; Longares, L.A. 2010: Is rainfall erosivity increasing in the Mediterranean Iberian Peninsula? *Land Degradation and Development*, 21, 139-144.
- De Luna, E., Laguna, A., Giráldez, J.V. 2000. The role of olive trees in rainfall erosivity and runoff and sediment yield in the soil beneath. *Hydrology and Earth System Sciences*, 4(1), 141-153
- Domínguez-Romero, L., Ayuso Muñoz, J.L., García Marín, A.P. 2007. Annual distribution of rainfall erosivity in western Andalusia, southern Spain. *Journal of Soil and Water Conservation* 62 (6): 390-401.
- Ekern, P.C. 1953. Problems of raindrop impact erosion. *Agricultural engineering*, 34(1), 23-25
- Elwell, H.A., Stocking, M.A. 1975. Parameters for estimating annual runoff and soil loss from agricultural lands in Rhodesia. *Water Resources Research*, 11(4): 601-605.
- Ellison, W.D. 1944. Studies of raindrop erosion. *Agricultural Engineering* 25(4-5): 131-136, 181-182.
- Fernández-Raga, M., Castro, A., Palencia, C., Calvo, A.I., Fraile, R. 2009. Rain events on 22 October 2006 in León (Spain): Drop Size Spectra. *Atmospheric Research*, 93, 619-635.
- Fernández-Raga, M., Fraile, R., Keizer, J.J., Varela Teijeiro, M.E., Castro, A., Palencia, C., Calvo, A.I., Koenders, J., Da Costa Marques, R.L. 2010. The kinetic energy of rain measured with an optical disdrometer: an application to splash erosion. *Atmospheric Research*, 96 (2-3), 225-240.
- Fournier, F. 1972. *Soil conservation*. Nature and Environment series. Council Eur., p. 194.



García Ruiz, J.R. and López Bermúdez, F. 2009. *La erosión del suelo en España*. Sociedad Española de Geomorfología. Zaragoza, 441 pág.

González-Hidalgo, J.C., Peña-Monnè, J.L., de Luis, M. 2007. A review of daily soil erosion in western Mediterranean areas. *Catena*, 71: 193-199

Gunn, R. and Kinzer, G.D. 1949. The terminal velocity of fall for water drops in stagnant air. *Journal of Meteorology*. 6, 243-248.

Gruber, A., Levizzani, V., 2008. Assessment of Global Precipitation Products. WCRP-128, WMO/TD No. 1430. *World Climate Research Programme*, p. 50.

Hall, M.J., 1970. Use of stain method in determining the drop size distribution of coarse liquid sprays. *Transations of ASAE* 30, 33-37, 41.

Horstmeyer (2008). Formación y desarrollo de las gotas de lluvia.

<http://www.shorstmeyer.com/wxFAQs/float/dropdeform.html>

Hudson, N.W., 1963. Raindrop size distribution in high intensity rainstorms. *Rhodesian journal of agricultural research*, 1: 6-11.

Hudson, N.W., 1965. *The influence of rainfall on the mechanics of soil erosion*. MSc Thesis, University of Cape Town, Cape Town, South Africa.

Hudson, N.W. 1971. *Soil Conservation*, Batsford Ltd, London, 388 pp

Hudson, N.W. 1995. *Soil conservation*. Third Edition. Batsford. London 304pp.

Huffman, G.J., Adler, R.F., Bolvin, D.T., Gu, G., Nelkin, E.J., 373 Bowman, K.P., Hong, Y., Stocker, E.F., Wolff, D.B., 2007. The TRMM Multisatellite Precipitation Analysis (TMPA): Quasi-global, multiyear, combined-sensor precipitation estimates at fine scales. *Journal of Hydrometeorology* 8, 38-55.

ICONA. 1988. *Agresividad de la lluvia en España. Valores del factor R de la Ecuación Universal de Pérdida de Suelo*, Ministerio de Agricultura, pesca y alimentación, España.

Jayawardena, A.W., Rezaur, R.B., 2000. Measuring drop size distribution and kinetic energy of rainfall using a force transducer. *Hydrological Processes* 14, 37-49.

Joss, J., Waldvogel, A. 1967. Ein Spektrograph für Niederschlagstropfen mit automatischer Auswertung. *Pure and Applied Geophysics PAGEOPH*, 68(1): 240-246.



- Joss, J., Gori, E. 1978. Shapes of raindrop size distributions. *Journal of Applied Meteorology*, 17: 1054-1061.
- Joyce, R.J., Janowiak, J.E., Arkin, P.A., Xie, P. 2004. CMORPH: a method that produces global precipitation estimates from passive microwave and infrared data at high spatial and temporal resolution. *Journal of Hydrometeorology*, 5, 487-503.
- Ker, A. D. R. 1954. *The measurement of rainfall intensity, drop-size distribution and impactive force*, unpublisish. thesis Dip. Trop. Agric., Trinidad
- Kinnell, P.I.A. 1973. The problem of assessing the erosive power of rainfall from meteorological observations. *Soil Science Society of America Proceedings*, 37: 617 – 621
- Kinnell, P.I.A., 1980. Rainfall intensity-kinetic energy relationships for soil loss prediction. *Soil Science Society of America Proceedings*, 45: 153-155.
- Kowal, J. 1972., Effect of an exceptional storm on soil conservation at Samaru, Nigeria. *Samaru Research Bulletin*. 141, *Institute of Agricultural Research.*, Samaru, Nigeria, pp. 163-172.
- Kowal, J.M., Kassam, A.H., 1976. Energy and instruments intensity of rainstorms at Samaru, northern Nigeria. *Tropical Agriculture*. 53, 185-198.
- Kowal, J.M., Kassam, A.H., 1978. *Agricultural Ecology of Savanna: A Study of West Africa*. Clarendon Press, Oxford, UK, 403 pp.
- Lal, R. 1976. Soil erosion on alfisols in Western Nigeria. III. Effects of rainfall characteristics. *Geoderma* 16: 389–401
- Lal, R. 1998. Drop size distribution and energy load of rainstorms at Ibadan, western Nigeria. *Soil and Tillage Research*, 48 (1-2), 103-114.
- Laws, J.S., Parsons, D.A. 1943. Relation of raindrop size to intensity. *Transactions of American Geophysical Union*, 24: 452-460
- Laws, J.O. 1941. Measurements of the fall velocity of water drops and raindrops. *Transactions of American Geophysical Union*, 22 (3), 709-721.
- Lenard, P. 1904. Über Regen. *Meteor. Z.*, 21, 248-262.
- López-Vicente, M., Navas, A., Machin, J.: Identfyng erosive periods by using RUSLE factors in mountain fields of the Central Spanish Pyrenees, *Hydrology Earth Systems Sciences*, 12, 1-13, 2008.



- Marshall, J.S., Palmer, W.M. 1948. Relation of raindrop size to intensity. *Journal of Meteorology*, 5, 165-166
- Martinez-Casasnovas, J.A., Ramos, M.C., and Ribes-Dasi, M., 2002. Soil erosion caused by extreme rainfall events: mapping and quantification in agricultural plots from very detailed digital elevation models. *Geoderma*, 105(1-2): 125-140.
- McCool, D.K., Robinette, M.J., King, J.T., Molanu, M., Young, J.L., 1978. Raindrop characteristics in the Pacific Northwest. *Transactions of American Geophysical Union*, 59 (abstract).
- McIsaac, G.F. 1990. Apparent geographic and atmospheric influences on raindrop sizes and rainfall kinetic energy. *Journal of Soil and Water Conservation*. 45: 663 – 666.
- Mihara, Y. 1952. Raindrop and soil erosion. *Bulletin of the National Institute of Agricultural Science Japan*, series A n°1.
- Montero-Martínez, G., Kostinski, A.B., Shaw, R.A., García-García, F. 2009. Do all raindrops fall at terminal speed?, *Geophysical Research Letters*, 36, L11818.
- Montgomery, D.R. (2007) Soil erosion and agricultural sustainability. *PNAS* 104: 13268-13272.
- Montgomery, D. 2008. *The Erosion of Civilizations* (1st ed.). University of California Press. ISBN 978-0-520-25806-8
- Morgan, R.P.C., 1977. Soil erosion in the United Kingdom: field studies in the Silsoe area, 1973–75. *National College of Agricultural Engineering Silsoe Occasional Paper* 4.
- Morgan, R.P.C., 2005. *Soil erosion and conservation*. Third edition, Blackwell publishing, Oxford, UK. 303 p.
- Mutchler, C.K., Hansen, L.M., 1970. Splash of a waterdrop at terminal velocity. *Transactions of American Geophysical Union* 31, 836-842.
- Mutchler, C.K., 1971. Splash droplet production by water drop impact. *Water Resource Research*, 7, 1024-1030.
- Navas, A., Alberto, F., Machín, J., Galán, A. 1990. Design and operation of a rainfall simulator for field studies of runoff and soil erosion. *Soil Technology*, 3: 385-397.



- Nyssen, J., Vandenreyken, H., Poesen, J., Moeyersons, J., Deckers, J., Haile, M., Salles, C., Govers, G. 2005. Rainfall erosivity and variability in the Northern Ethiopian Highlands. *Journal of Hydrology*. 311: 172-187.
- Onaga, K., Shirai, K., Yoshinaga, A., 1988. Rainfall erosion and how to control its effects on farmland in Okinawa. In: Rimwanich, S. (Ed.), *Land Conservation for Future Generations*. Department of Land Development, Bangkok, pp. 627–639.
- Osoji, G.E. 1989. Raindrop characteristics in the humid tropics. *Journal of Environmental Management*. 28 (3): 227-233.
- Park, S.W.; Mitchell, J.K.; Bubenzer, G.D. 1982. Splash erosion modelling: physical analysis. *Transactions of the ASAE*. 25: 357-361.
- Petkovsek, G., Mikos, M. 2004. Estimating the R factor from daily rainfall data in the sub-Mediterranean climate of southwest Slovenia. *Hydrological sciences journal*, 49 (5): 869-877.
- Renard, K.G., Freimund, J.R. 1994. Using monthly precipitation data to estimate the R-factor in the revised USLE. *Journal of Hydrology*, 157, 287-306.
- Renard, K.G., Foster, G.R., Weesies, G.A., McCool, D.K., Yoder, D.C. 1997. Predicting Soil Erosion by Water: A Guide to Conservation Planning with the Revised Universal Soil Loss Equation (RUSLE). *USDA Agricultural Handbook No. 703*, USDA, Washington, DC (1997) 384 pp.
- Richardson, C.W., Foster, G.R., Wright, D.A., 1983. Estimation of Erosion Index from Daily Rainfall Amount. *Transactions of the ASAE*, 26, 153-160.
- Roldan Soriano, M. 2006. *El poder de la lluvia. Características de la lluvia y erosividad. Nueva formulación para la estimación de la erosividad. Aplicación al cálculo del factor R de la USLE*. Organismo Autónomo de Parques Nacionales. Ministerio de Medio Ambiente. Madrid 125 pág.
- Rosewell, C.J. 1986. Rainfall kinetic energy in Eastern Australia. *Journal of Climate and Applied Meteorology*, 25: 1695–1701
- Salako, F.K., Ghuman, B.S., Lal, R. 1995. Rainfall erosivity in South-Central Nigeria. *Soil Technology*, 7(4), 279-290.
- Sempere Torres, D., Creutin, J.D., Salles, C., Delrieu, G. 1992. Quantification of soil detachment by raindrop impact: performances of classical formulae of kinetic energy in Mediterranean storms. *Erosion and sediment transport monitoring programmes*



in river basins. J. Bogen, D.E. Walling and T. Day, Eds. IAHS Publ. No. 210, 115-124.

Sempere Torres, D., Porrà, J.M., Creutin, J.D. 1994. A general formulation for Raindrop Size Distribution. *Journal of Applied Meteorology*, 33: 1494-1502.

Seuffert, O., Busche, D., Löwe, P. 1999. Rainfall structure – rainfall erosivity: new concepts to solve old problems. *Petermanns Geographische mitteilungen*, 143 (5-6): 475-490.

Soil Survey Division, World Soil Resources (1998).

<http://soils.usda.gov/use/worldsoils/mapindex/erosh2o.html>

Soil Survey Division, World Soil Resources (1998); Tobler, W., Deichman,V., Gottsegen, J. y Maloy, K. 1995. *The global demography project. Technical report TR-95-6*. National Centre for geographic information analysis. Univ. Santa Barbara.  
<http://soils.usda.gov/use/worldsoils/mapindex/eh2orisk.html>

Teschl, F., Randeu, W.L., Schönhuber, M., Teschl, R., 2008. Simulation of polarimetric radar variables in rain at S-, C- and X-band wavelengths. *Advances in Geosciences*. 16, 27-32.

Uijlenhoet, R. and J. Stricker. 1999. A consistent rainfall parametrization based on the exponential raindrop size distribution. *Journal of Hydrology*, 218, 101-127.

Uplinger, C. W., 1981: A new formula for raindrop terminal velocity. *20th Conference of Radar Meteorology. American Meteorology Society*, Boston (USA), 389-391.

Usón, A., Ramos, M.C. 2001. An improved rainfall erosivity index obtained from experimental intererill soil losses in soil with a Mediterraenan climate. *Catena* , 43: 293-305

Van Dijk, A.I.J.M., Bruijnzeel, L.A., Rosewell, C.J. 2002. Rainfall intensity-kinetic energy relationships: a critical literature appraisal. *Journal of Hydrology*, 261, 1-23.

Verstraeten, G., J. Poesen, G. Demarée, and C. Salles (2006), Long-term (105 years) variability in rain erosivity as derived from 10-min rainfall depth data for Ukkel (Brussels, Belgium): Implications for assessing soil erosion rates, *Journal of Geophysical Research*, 111, D22109.

Vrieling, A., Sterk, G., de Jong, S.M. 2010. Satellite-based estimation of rainfall erosivity for Africa. *Journal of Hydrology*, 395: 235-241



- Waldvogel, A., 1974. The No jump of raindrop spectra. *Journal of Atmospheric Science*, 31, 1069–1078.
- Wiesner, J., 1895. Beiträge zur Kenntnis des tropischen Regens. Sitzungsberichte der kaiserlichen Akademie der Wissenschaften in Wien, mathematisch-naturwissenschaftliche Classe 104, 1397–1434
- Wischmeier, W.H., Smith, D.D., 1958. Rainfall energy and its relationships to soil loss. *Transactions of the American Geophysical Union*, 39: 285-291
- Wischmeier, W.H. 1962: Rainfall erosion potencial. *Agricultural engineering*, 43(4), 212-215-225.
- Wischmeier WH & Smith DD. 1965. Predicting rainfall erosion losses from cropland east of the Rocky Mountains. *Agriculture Handbook 282, USDA, Washington, DC.*
- Wischmeier, W.H., Smith, D.D., 1978. Predicting Rainfall Erosion Losses. *Agriculture Handbook 537, USDA, Washington, DC.*
- Yu, B., Hashim, G.M., Eusof, Z., 2001. Estimating the R-factor with limited rainfall data: a case study from peninsular Malaysia. *Journal of Soil and Water Conservation*, 56: 101-105
- Yu, B., Rosewell, C.J., 1996a. An assessment of daily rainfall erosivity model for New South Wales. *Australian Journal of Soil Research*, 34, 139-152
- Yu, B., Rosewell, C.J., 1996b. A robust estimator of the R factor for the Universal Soil Loss Equation. *Transactions of the ASAE*, 39, 559-561
- Yu, B., Rosewell, C.J., 1996c. Rainfall erosivity estimation using daily rainfall amounts for South Australia. *Australian Journal of Soil Research*, 34, 721-733
- Zanchi, C., Torri, D. 1980. Evaluation of rainfall energy in Central Italy. In: M. De Boodt and D. Gabriels, Editors, *Assessment of Erosion*, Wiley, Chichester, pp. 133–142.





## Bloque II

### Estudio climatológico de la erosividad de la lluvia en la cuenca del Ebro

"If we begin with certainties, we shall end in doubts, but if we begin with doubts, and are patient in them, we shall end in certainties"—Francis Bacon.

"Better a subjective model of uncertainty than an illusion of certainty"—André Journel, 1994

#### Resumen

Este bloque aborda el estudio climático de la erosividad de la lluvia en la cuenca del Ebro durante el periodo 1955-2006. En primer lugar se presentan las características fundamentales del área de estudio y las bases de datos utilizadas. La erosividad de la lluvia para el periodo 1997-2006 se ha estimado siguiendo la metodología de cálculo del factor R de la RUSLE. A partir de esta base de datos revisamos una serie de métodos que nos permitan estimar la erosividad de la lluvia diaria mediante datos de precipitación diaria para el periodo 1955-2006, creando así la base de datos principal para el análisis climático. Se explora el comportamiento espacial de la variable en la zona de estudio a través de distintos métodos de interpolación, constatando una elevada variabilidad e incertidumbre espacial que estriba la dependencia de observaciones puntuales. El estudio climatológico se centra en primer lugar en la evaluación de la influencia de los índices de NAO, MO y WeMO sobre la erosividad diaria de la lluvia, resultando en una clara influencia de estos índices en fase negativa, especialmente MO y WeMO, sobre la erosividad de la lluvia, fundamentalmente hacia el Mediterráneo. Esta influencia es más evidente en el caso de los eventos extremos. En segundo lugar se evalúan las tendencias de la erosividad de la lluvia a escala anual, mensual y diaria durante 1955-2006. Detectamos una tendencia decreciente de la erosividad de la lluvia a escala anual y estacional, como consecuencia de una disminución en la ocurrencia de eventos elevados y extremos mientras que los eventos con menor capacidad erosiva han aumentado en los últimos 52 años.



## Abstract

In this part the climatic characteristics of rainfall erosivity in the Ebro basin for the period 1955-2006 are analysed. First of all, study area characteristics and used databases are presented. Rainfall erosivity for the period 1997-2006 has been estimated by the RUSLE R factor methodology. With this rainfall erosivity database several methods for the estimation of daily rainfall erosivity from daily precipitation records are compared, resulting in the creation of the daily rainfall erosivity database for the period 1955-2006 needed for the climatic analysis. The spatial distribution of rainfall erosivity in the Ebro basin is analysed with several interpolation techniques. Rainfall erosivity shows high spatial variability and uncertainty, as a consequence of the dependence on local observations. The climatic study is focused on atmospheric teleconnection patterns influence, NAO, MO and WeMO, on daily rainfall erosivity. Negative phases of the indices, especially MO and WeMO, are related with higher rainfall erosivity values, especially towards the Mediterranean. This influence is more evident for rainfall erosivity extreme values. Finally, trends in annual, seasonal and daily rainfall erosivity for the period 1955-2006 are evaluated. Generalized decreasing trend is found at annual and seasonal scale, explained by decreasing of occurrence in the higher daily rainfall erosivity events whilst the lowest one have increased frequency. High spatial variability at monthly and daily scale is found.



## 2.1 Introduction

Rainfall is a major cause of soil erosion, given the extraordinary importance of soil detachment processes due to drop impact and runoff shear. Compared to other natural factors such as the relief or the soil characteristics, rainfall erosivity has very little or null possibility of modification by humans, so it represents a natural environmental constrain that limits and conditions land use and management. In the context of climate change, the effect of altered rainfall characteristics on soil erosion is one of the main concerns of soil conservation studies. Hence, the estimation of rainfall erosivity may contribute to a better prediction of soil erosion. Rainfall erosivity links the physical properties of the raindrops as a consequence of rainfall generating processes and their impact on the soil surface. Rainfall erosivity is responsible for changes in the soil properties due to crusting, disruption of aggregates, removal of nutrient-rich particles, etc. It represents one of the main mechanisms of soil degradation in semiarid landscapes where vegetation is scarce. Its influence depends on the soil characteristics, topography and land use, as well as on other features of the rainfall regime (D'Odorico et al. 2001). Rainfall erosivity estimates are thus of paramount importance for estimation of soil erosion rates through space and time. It is well known that several very intense rainfall events are responsible for the largest proportion of soil erosion and sediment delivery. Hence, estimating rainfall erosivity is central to assessment soil erosion risk.

Numerous studies using natural and simulated rainfall have investigated the role of drop size distribution on the detachment of soil particles. The measurements involved are difficult to perform, and reported data are consequently very limited both spatially and temporally. In addition, measurements of natural rainfall properties, for comparison with simulated rain, are scarce (Dunkerley, 2008). This has encouraged studies relating more conventional rainfall indices, such as the maximum intensity during a period of time, to overall rainfall energy or directly to soil detachment rates. Examples of such indices of rainfall erosivity are the USLE R factor, which summarizes all the erosive events quantified by the  $EI_{30}$  index occurred along the year (Wischmeier, 1959, Wischmeier and Smith, 1978, Brown and Foster, 1987), the modified Fournier index for Morocco (Arnoldus, 1977), the  $KE > 25$  index for southern Africa (Hudson, 1971), and the AIM index for Nigeria (Lal, 1976). Among these the most extensively used is the USLE/RUSLE R factor (Wischmeier, 1959, Wischmeier and Smith, 1978,



Brown and Foster, 1987, Renard *et al.*, 1997). At many sites worldwide the R factor has been shown to be highly correlated with soil loss (Van der Knijff et al., 2000, Diodato, 2004, Shi et al., 2004, Hoyos et al., 2005, Curse et al., 2006, Onori et al., 2006, Domínguez-Romero et al., 2007).

One of the main disadvantages in seeking to employ the RUSLE R factor is the need for a relatively continuous rainfall data series, with a time resolution of at least 15 min (pluviograph data). Information of this nature is rarely available with good spatial and temporal coverage. In section 2.6 several methods of estimating rainfall erosivity based on different data sources are reviewed, showing that reasonably accurate estimations can be obtained from daily rainfall data if at least a relatively short data base of high frequency data is available.

In many studies the rainfall erosivity calculation is reduced to at-site analysis. An improvement focus on the reduction of the risk of erosion in landscape management and conservation planning is to obtain continuous maps for large areas as a preliminary step to evaluate the hazard. For this purpose a common procedure is the mapping of at-site estimated rainfall erosivity index values by means of interpolation techniques (e.g., Prudhome and Reed, 1999; Weisse and Bois, 2002). In section 2.7 several interpolation methods including global, local and mixed approaches, are compared in order to determine which one describes better the spatial distribution of the average  $EI_{30}$  index and the R factor.

In section 2.8 rainfall erosivity cartography at annual and seasonal scale for the period 1955-2006 are presented.

There is an increasing interest on assessing the impacts of climate change. Global warming is certain, but changes in rainfall parameters are not well understood (López-Moreno et al., 2010). Previous work has shown that the spatial and temporal variability of rainfall intensity can be explained by coupled modes of atmospheric circulation patterns (Hurrell, 1995; Jones et al., 1997; Hurrell et al., 2003). Since rainfall erosivity is related with rainfall, in section 2.9 the influence of atmospheric teleconnection patterns as North Atlantic Oscillation, Mediterranean Oscillation and Western Mediterranean Oscillation on daily rainfall erosivity for the period 1955-2006 is analysed. In addition, in section 2.10, annual, seasonal and daily rainfall erosivity trends for the period 1955-2006 are evaluated. These results are crucial in order to compare them with climate model predictions. However, all these studies are restricted to rainfall erosivity indices calibrated



empirically in other regions, therefore uncertain results are expected although nowadays are the best possible to obtain.

## 2.2. Study area

The study area covers most of the north-east of Spain (Figure 2.1). It corresponds to the Ebro Basin, encompassing an area of about 85,000 km<sup>2</sup>. The Ebro valley is an inner depression surrounded by high mountain ranges. It is limited to the North by the Cantabrian Range and the Pyrenees, with maximum elevations above 3000 m a.s.l. The Iberian range closes the Ebro valley to the South, with maximum elevations in the range of 2000-2300 m. a.s.l. To the East, parallel to the Mediterranean coast, the Catalan Coastal Range closes the Ebro valley, with maximum elevations between 1000 and 1200 m a.s.l.



Figure 2.1: General view of the study area



Mountains represent 12% of the study area. The main activity in terms of surface is agriculture, representing approximately 38% of the land use. It is extended around the Ebro valley occupying a broader area close to the Mediterranean coast. (Figure 2.2). Agricultural soils remain uncovered in most cases during winter. Consequently, rainfall is the principal agent of soil erosion at that time, and during all year for fruit trees cultivations (frutales) and vineyards (viñedos).

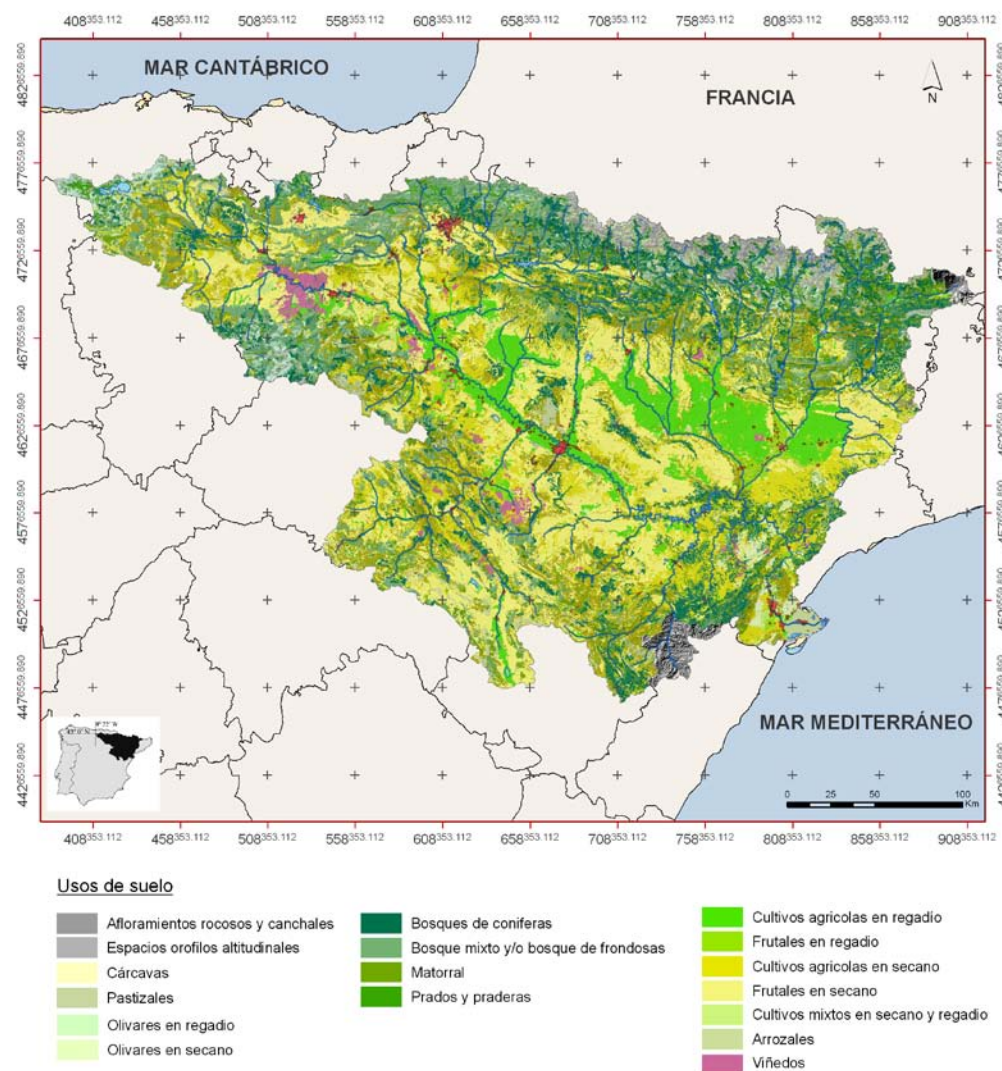


Figure 2.2: Land uses map; (Corine Land Cover, 2005)

The climate is influenced by the Cantabric and Mediterranean Seas and the effect of the relief on rainfall and temperature. The bordering mountain ranges isolate the central valley blocking the maritime influence, resulting in a continental climate which experiments arid conditions (Cuadrat, 1991; Lana and Burgueño, 1998; Creus 2001; Vicente-Serrano 2005). A climatic gradient in the NW-SE



direction is remarkable, determined by the strong Atlantic influences in the north and north-west of the area during large part of the year and the Mediterranean influence to the east. Mountain ranges add complexity to the climate of the region. The Pyrenees extend the Atlantic influence to the east by increasing rainfall, whereas the Cantabrian Range, which runs parallel to the Atlantic coastland in the NW, is a barrier to the humid flows and has a noticeable climate contrast between the north (humid) and the south (dry) slopes.

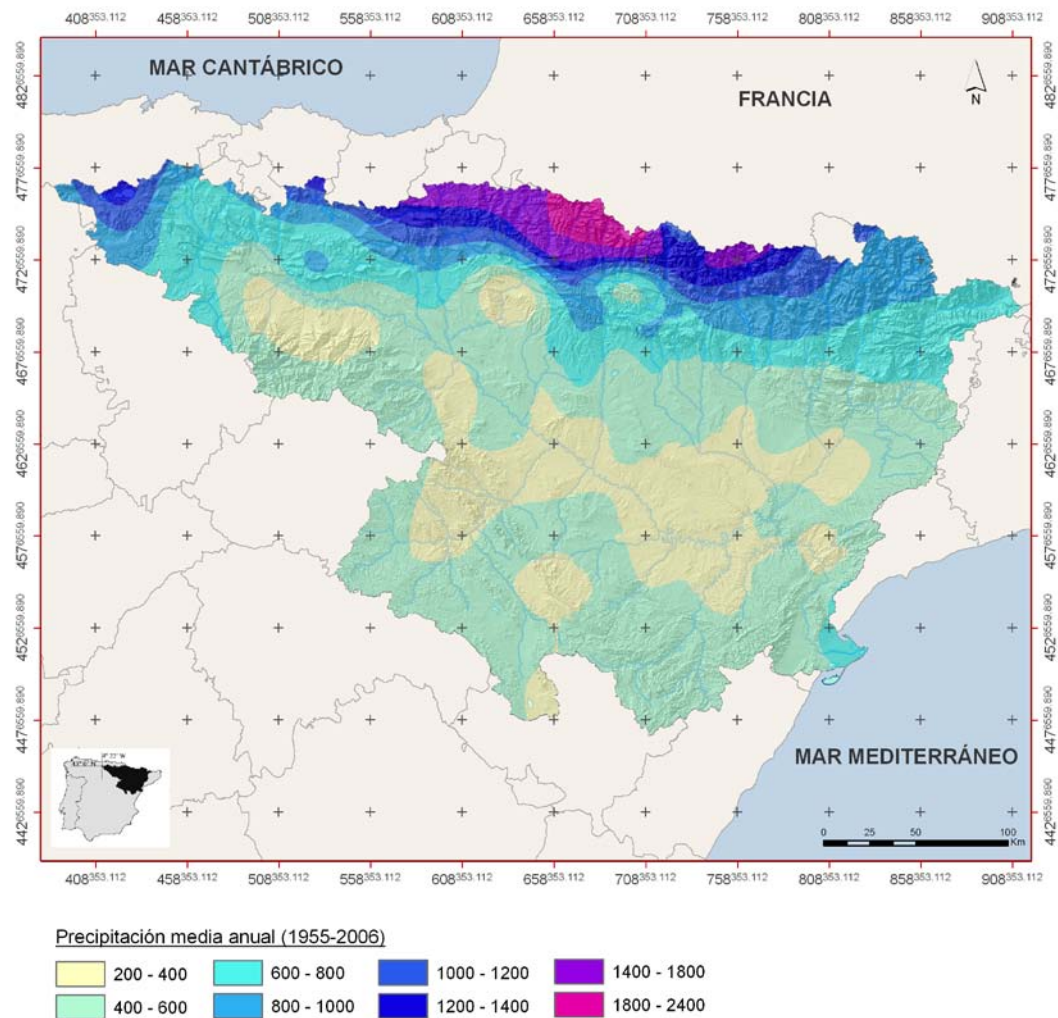


Figure 2.3: Mean annual rainfall (1955-2006).

The rainfall regime shows strong seasonality (Garrido and García, 1992), which involves not only the amount of rainfall but also its physical cause (frontal or convective). Rainfall in the inland areas is characterised by alternating wet and dry periods as a consequence of the seasonal displacement of the polar front and its associated pressure systems. Inter-annual variability of rainfall can be very high,



and drought years can be followed by torrential rain events which last for many days (Martín-Vide, 1994).

Close to the Mediterranean Sea the rainfall amount also increases as a consequence of the maritime influence. Nevertheless, the rainfall frequency, intensity and seasonality are very different compared to the areas in the North, where rainfall is frequent but rarely very intense, with the exception of the mountains (García-Ruiz *et al.*, 2000). The most extreme rainfall events are recorded along the Mediterranean seaside (Llasat, 2001; Romero *et al.*, 1998; Peñarrocha *et al.*, 2002).

Due to its complex climatology as a consequence of being a meteorological border region and the contrasted relief, the Ebro Basin has a long history of social, economic and environmental damage caused by extreme rainfall events (García-Ruiz *et al.* 2000, Lasanta 2003, Llasat *et al.* 2005).



### 2.3. Rainfall erosivity by RUSLE R factor

Daily  $EI_{30}$  values for the period 1997–2006 were calculated using rainfall intensity data recorded every 15 minutes (database 2.4-i), and the RUSLE model. The RUSLE model uses the Brown and Foster (1987) approach for calculating the average annual rainfall erosivity,  $R$  ( $\text{MJ mm ha}^{-1} \text{ h}^{-1} \text{ y}^{-1}$ ):

$$R = \frac{1}{n} \sum_{j=1}^n \sum_{k=1}^{m_j} (EI_{30})_k \quad (2.1)$$

where  $n$  is the number of years of the record,  $m_j$  is the number of erosive events for a given year  $j$ , and  $EI_{30}$  is the rainfall erosivity index of a single event  $k$  ( $\text{MJ mm ha}^{-1} \text{ h}^{-1}$ ). Thus, the  $R$  factor is the average value of the annual cumulative  $EI_{30}$  over a given period. The rainfall erosivity of a single event  $EI_{30}$  is calculated as follows:

$$EI_{30} = \left( \sum_{r=1}^o e_r v_r \right) I_{30}, \quad (2.2)$$

where  $e_r$  and  $v_r$  are, respectively, the unit rainfall energy ( $\text{MJ ha}^{-1} \text{ mm}^{-1}$ ) and the rainfall volume (mm) during a time period  $r$ , and  $I_{30}$  is the maximum rainfall intensity in a 30 min period during the event ( $\text{mm h}^{-1}$ ). The unit rainfall energy ( $e_r$ ) is calculated for each time interval as:

$$e_r = 0.29 [1 - 0.72 \exp(-0.05 i_r)] \quad (2.3)$$

where  $i_r$  is the rainfall intensity during the time interval ( $\text{mm h}^{-1}$ ).



## 2.4. Database

For this study two databases were used (Figure 2.4):

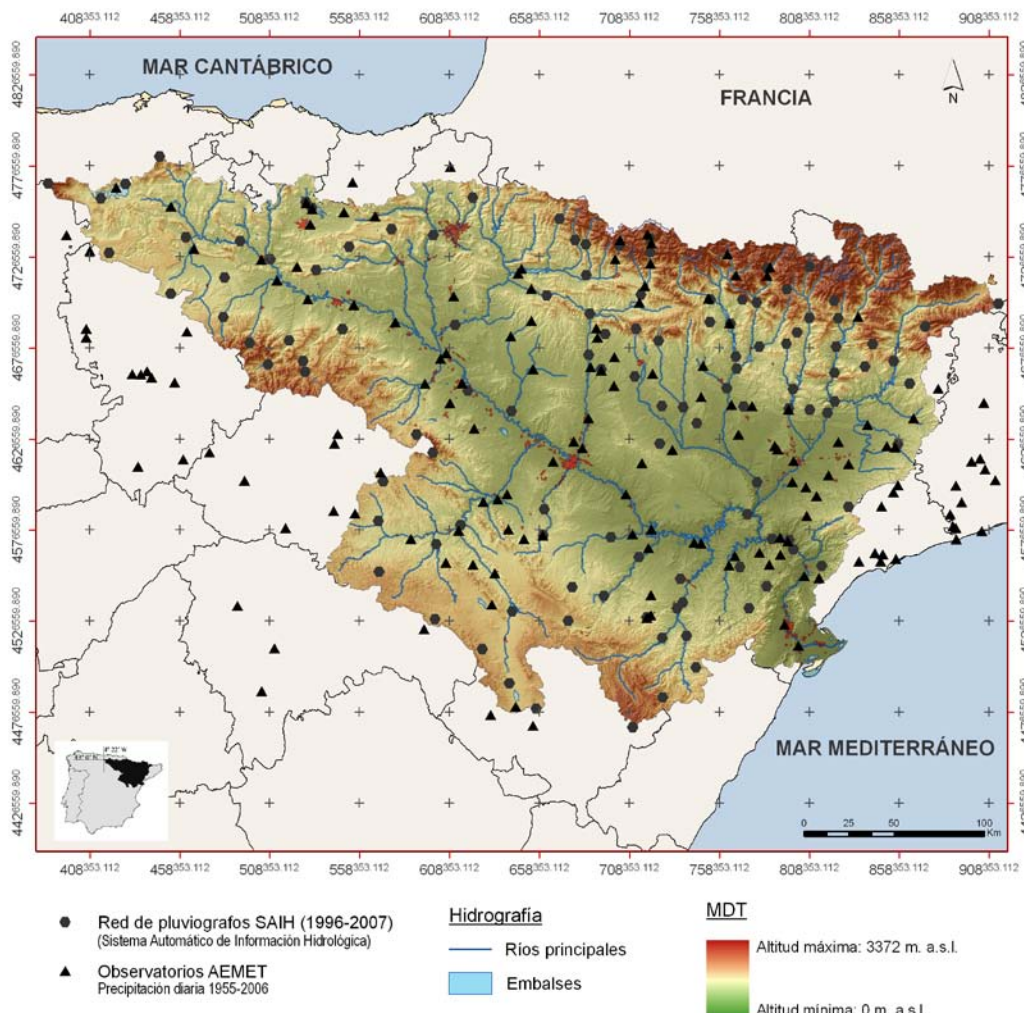


Figure 2.4: Rainfall observatories used in the study area.

- i) The first database consisted of 111 rainfall series from the Ebro Hydrographical Confederation automatic hydrological information network system (SAIH). Each station provides rainfall data at a time resolution of 15 min. The system started on 1997, and is the only dense network providing sub-daily resolution data in the region. We used all available series covering the period 01/01/1997 to 31/12/2006.

The rainfall series were subject to a quality control process that allowed identifying wrong records due to system failures. These records were replaced by the corresponding ones from a nearby station. This allowed creating a database of erosive events (EEDB). The erosive events were



determined by the RUSLE criterion: an event is considered erosive if at least one of two conditions holds: i) the cumulative event's rainfall is greater than 12.7 mm, or ii) the cumulative event's rainfall has at least one intensity peak greater than 6.35 mm in 15 minutes. Two consecutive events are considered different from each other if the cumulative rainfall in a period of 6 hours is greater than 1.27 mm. In the present study we have considered all the rainfall events with rainfall above 0 mm as erosive events. This threshold was used for calibrating the models; otherwise we could not do monthly calibration, (see section 2.5 for details of the models).

A daily erosivity database was constructed from the events database. Thus, if there were more than one erosive event in a given day their values were summed up to give a total daily erosivity. This involved some 2% of the original dataset composed by 66,486 events. In a few cases (0.66% of all erosive events), an erosive event occurred during two or more consecutive days. In those cases the event was assigned to the day with the highest rainfall. This procedure was preferred to splitting up the erosive event, which would have altered the rainfall erosivity value.

- ii) The second database consisted of 156 daily rainfall series from the Spanish meteorological agency (AEMET), with daily (0600 to 0600 hours, local time) rainfall amounts for the period 1955-2006. Rainfall time series were debugged via a process that included reconstruction, gap filling, quality control and homogeneity testing (Vicente-Serrano et al. 2009a). The SAIH dataset (i) had the adequate time resolution for computing rainfall erosivity, but only covered eleven years. The AEMET dataset has the adequate length for undertaking climatological studies, but its coarser time resolution does not allow to directly computing rainfall erosivity. Therefore, we used a transformation for estimating daily erosivity values from daily rainfall amounts (Angulo-Martínez and Beguería, 2009, also explained in detail in section 2.6).

Daily erosivity was computed from the SAIH dataset ( $EI_{SAIH}$ ) following the RUSLE methodology (Renard et al. 1997). Daily rainfall amounts were also calculated from the SAIH dataset ( $P_{SAIH}$ ). This allowed fitting



an exponential relationship between both variables (Richardson et al., 1983):

$$EI_m = a_m P^{b_m} + \varepsilon, \quad m = \{1, \dots, 12\}, \quad (2.4)$$

where  $a$  and  $b$  are empirical parameters and  $\varepsilon$  is a random, normally distributed error. Parameters  $a$  and  $b$  are adjusted month-by-month ( $m$ ) to take account of seasonal variations in rainfall characteristics. Parameter estimation was achieved by weighted least squares (WLS) regression after a logarithmic transformation of the terms in equation (1). Weights were assigned to the observations in order to reduce the excessive influence of small erosive events during parameterization. Spatial interpolation of the parameters  $a_m$  and  $b_m$  by splines allowed obtaining local values of these parameters over the study area (Fig. 2.5 and 2.6). This allowed applying equation (1) to the daily rainfall values of the AEMET dataset, to obtain a daily erosivity database for the period 1955-2006. Annual and monthly cumulative values of the RUSLE R factor were obtained by aggregating the daily  $EI_{30}$  values.

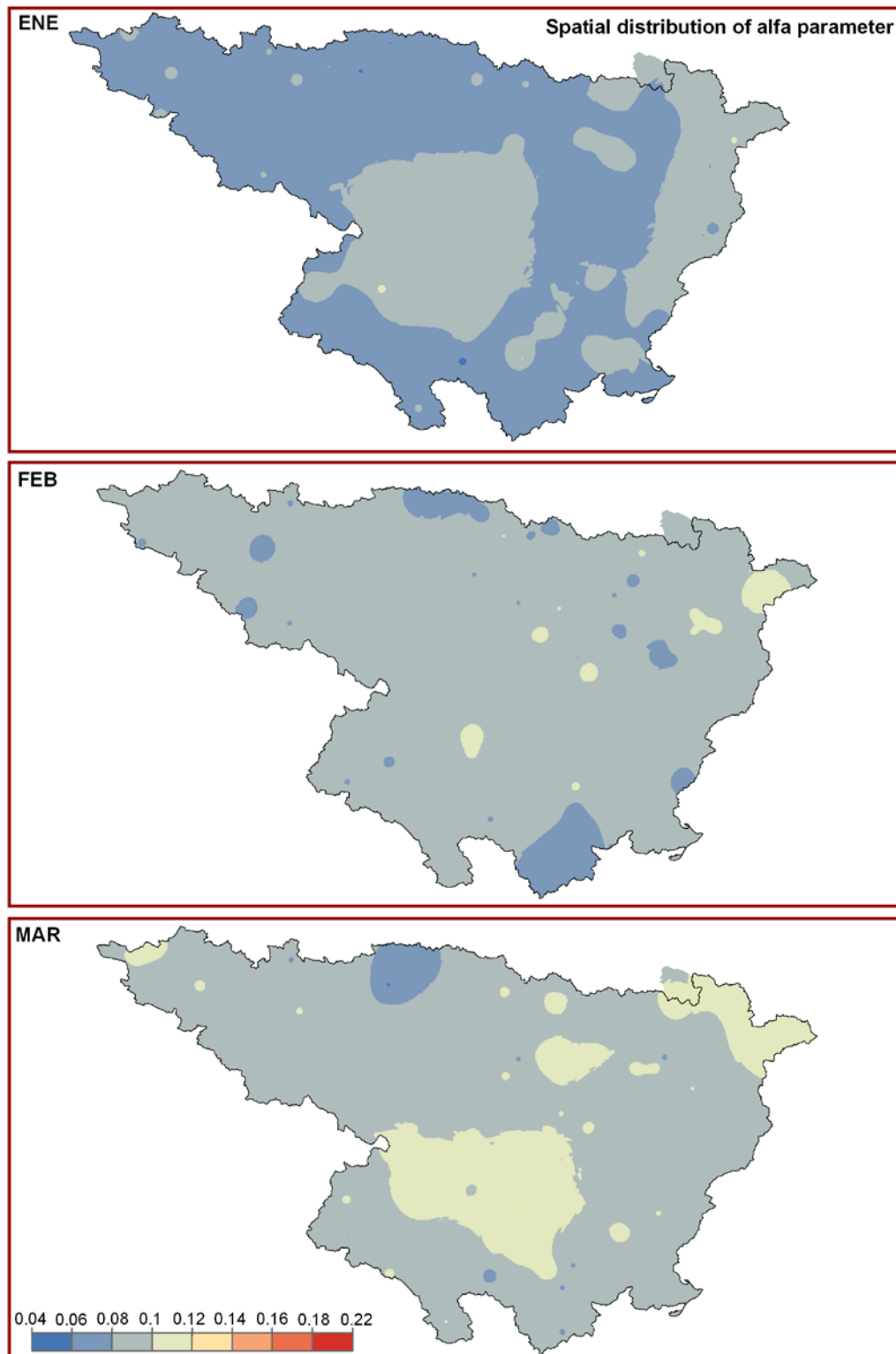


Figure 2.5: Spatial distribution of the **alpha** parameter in January, February and March.

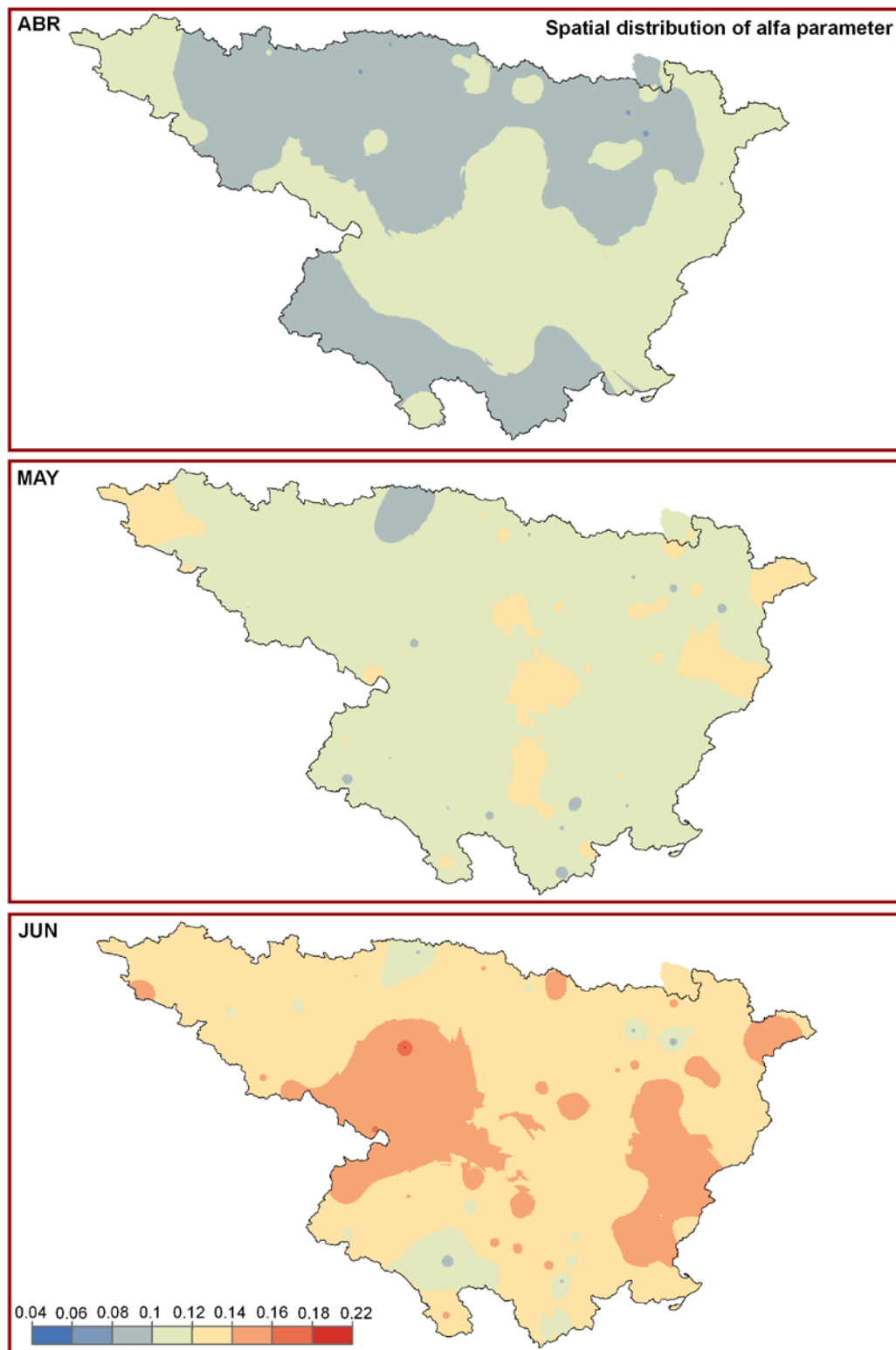


Figure 2.5 (cont.): Spatial distribution of the **alpha** parameter in April, May and June.

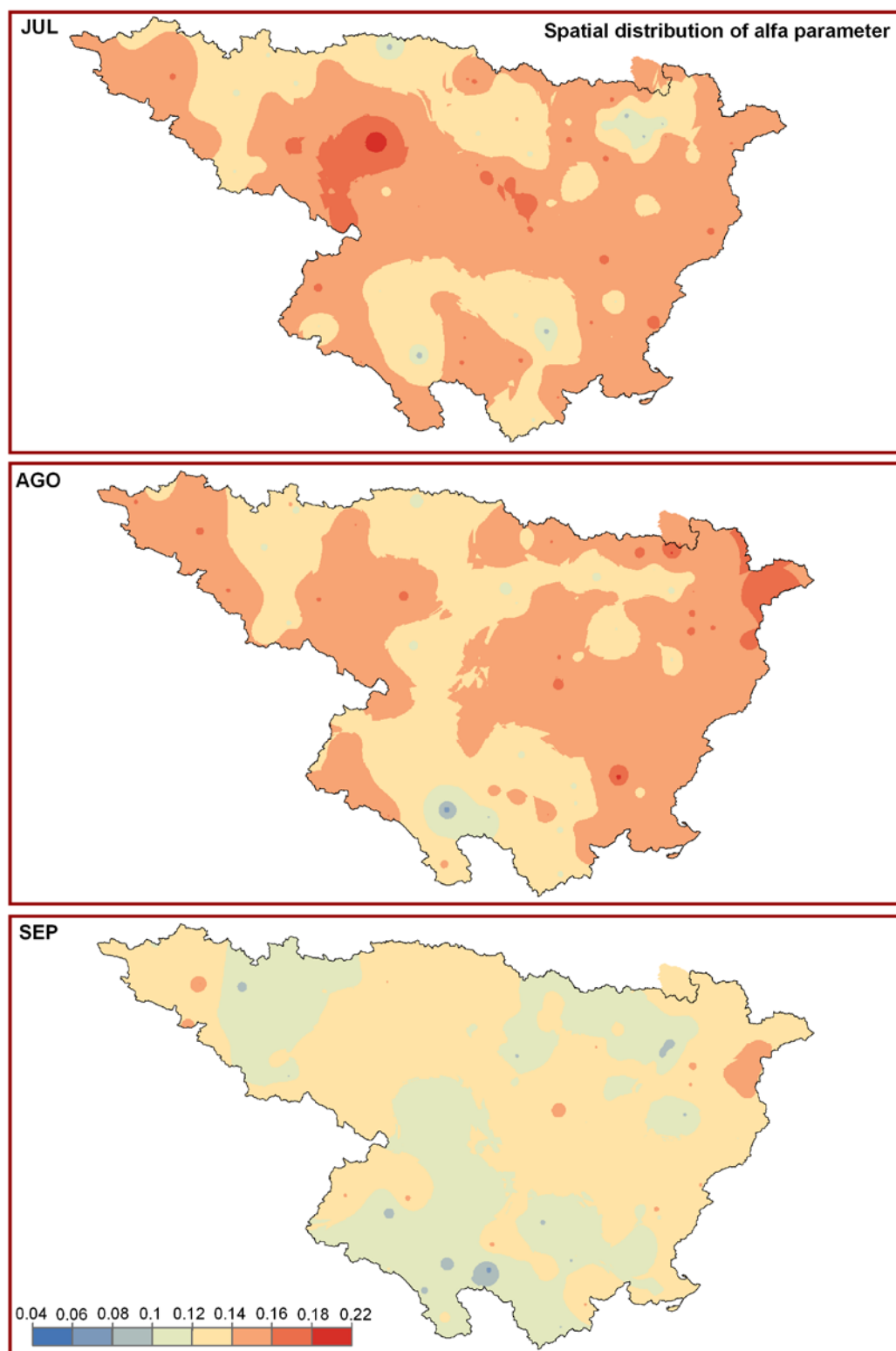


Figure 2.5 (cont.): Spatial distribution of the **alpha** parameter in July, August and September.

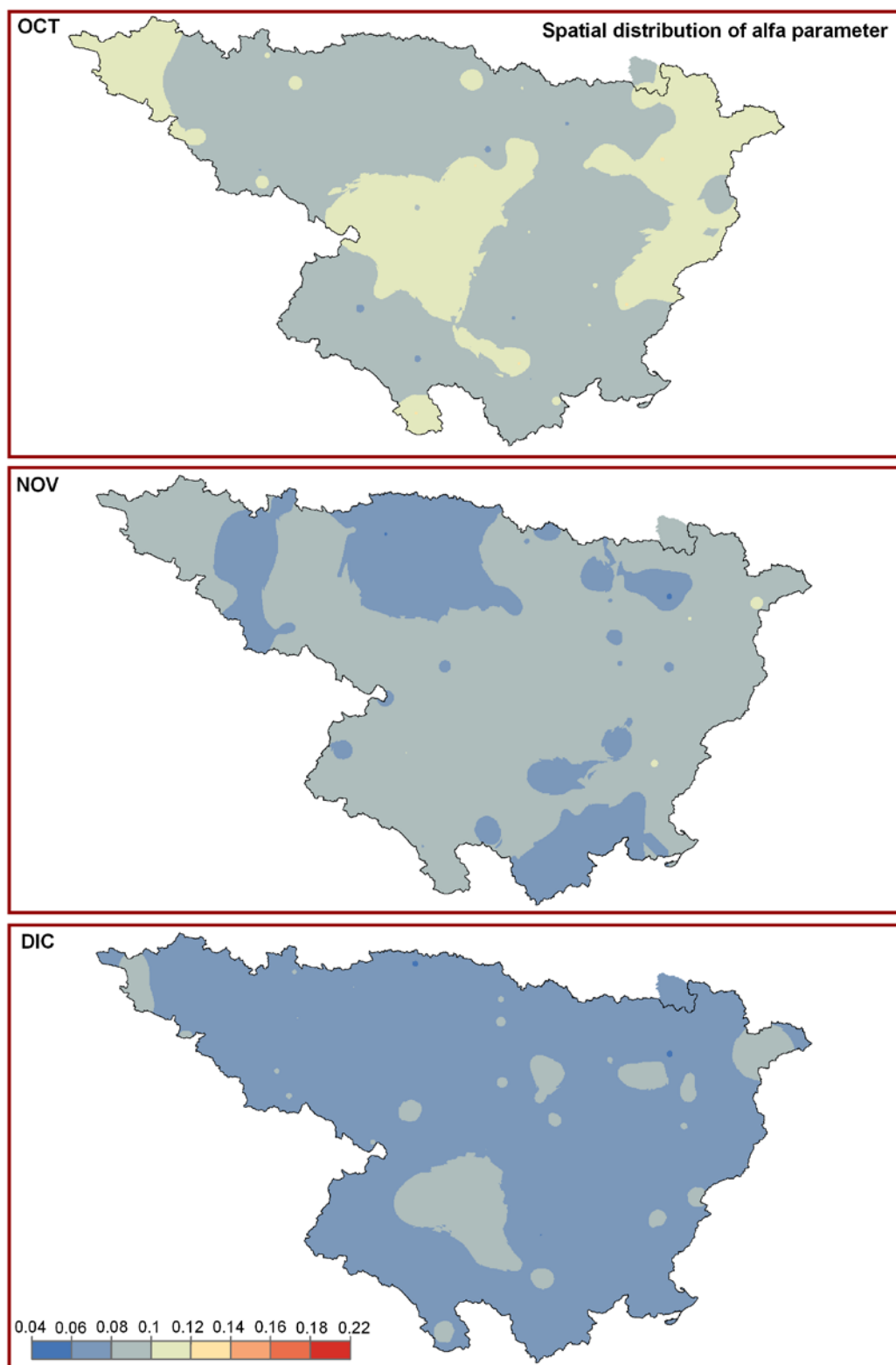


Figure 2.5 (cont.): Spatial distribution of the **alpha** parameter in October, November and December.

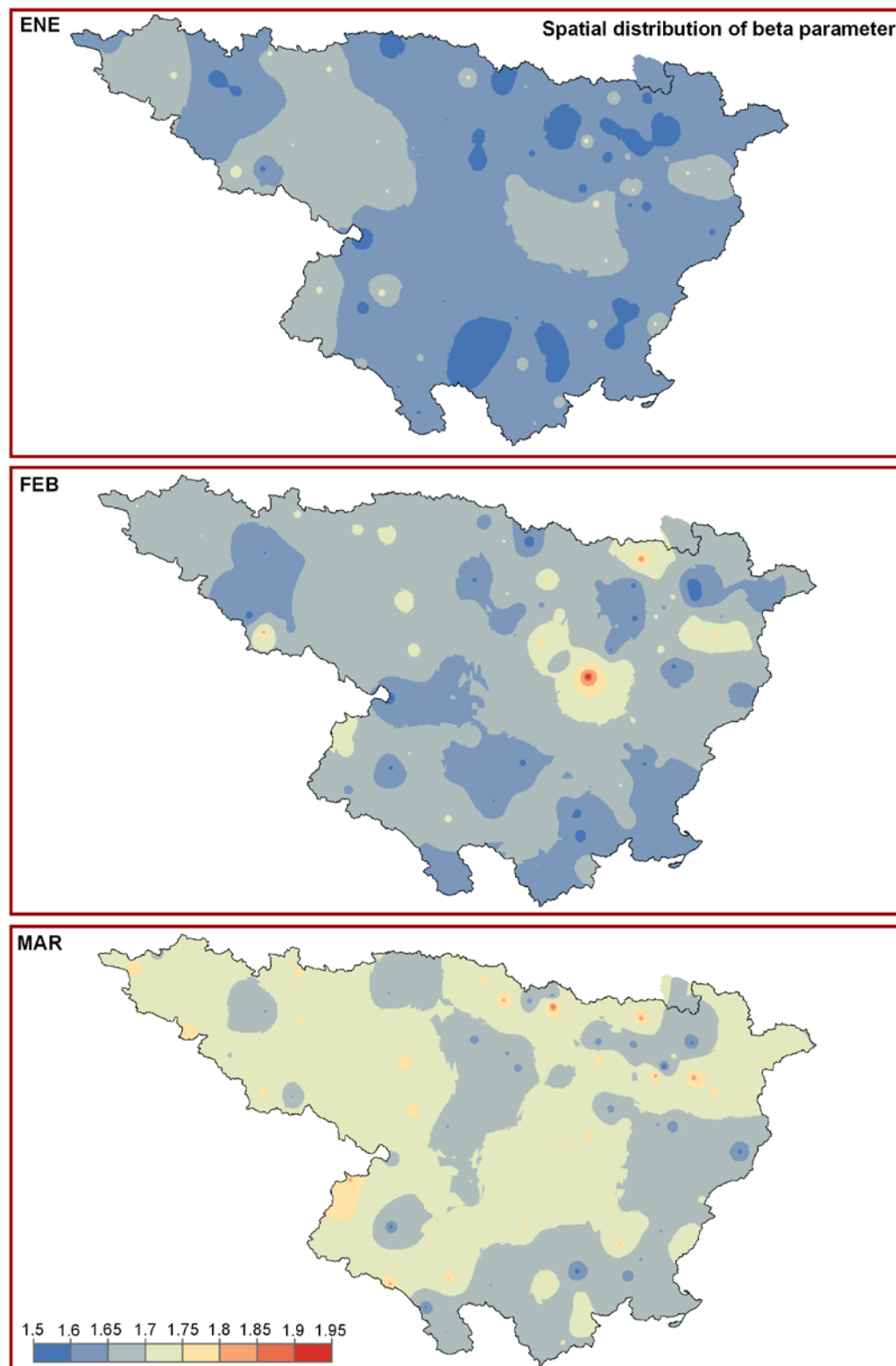


Figure 2.6: Spatial distribution for the **beta** parameter in January, February and March.

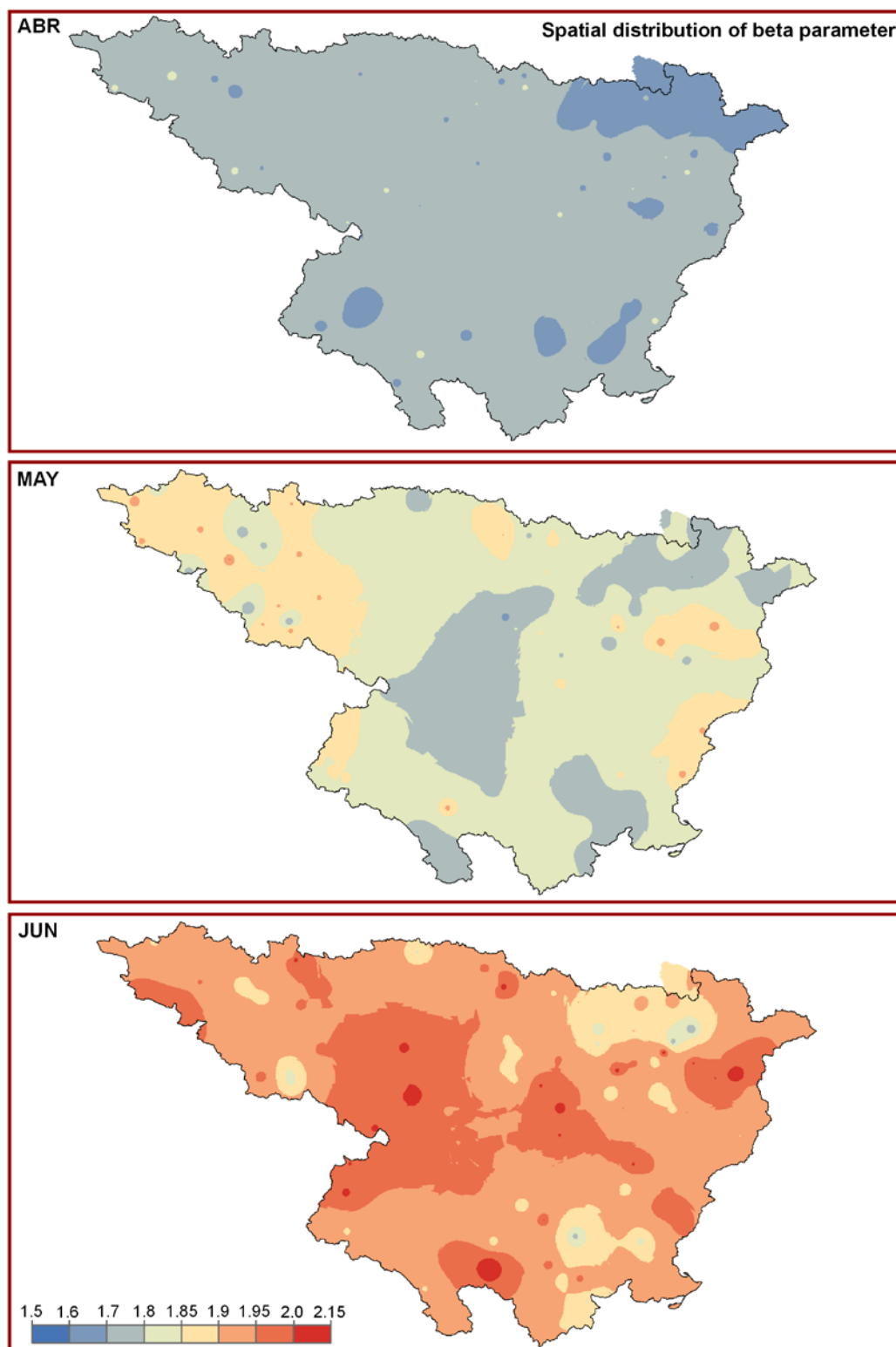


Figure 2.6 (cont.): Spatial distribution for the **beta** parameter in April, May and June.

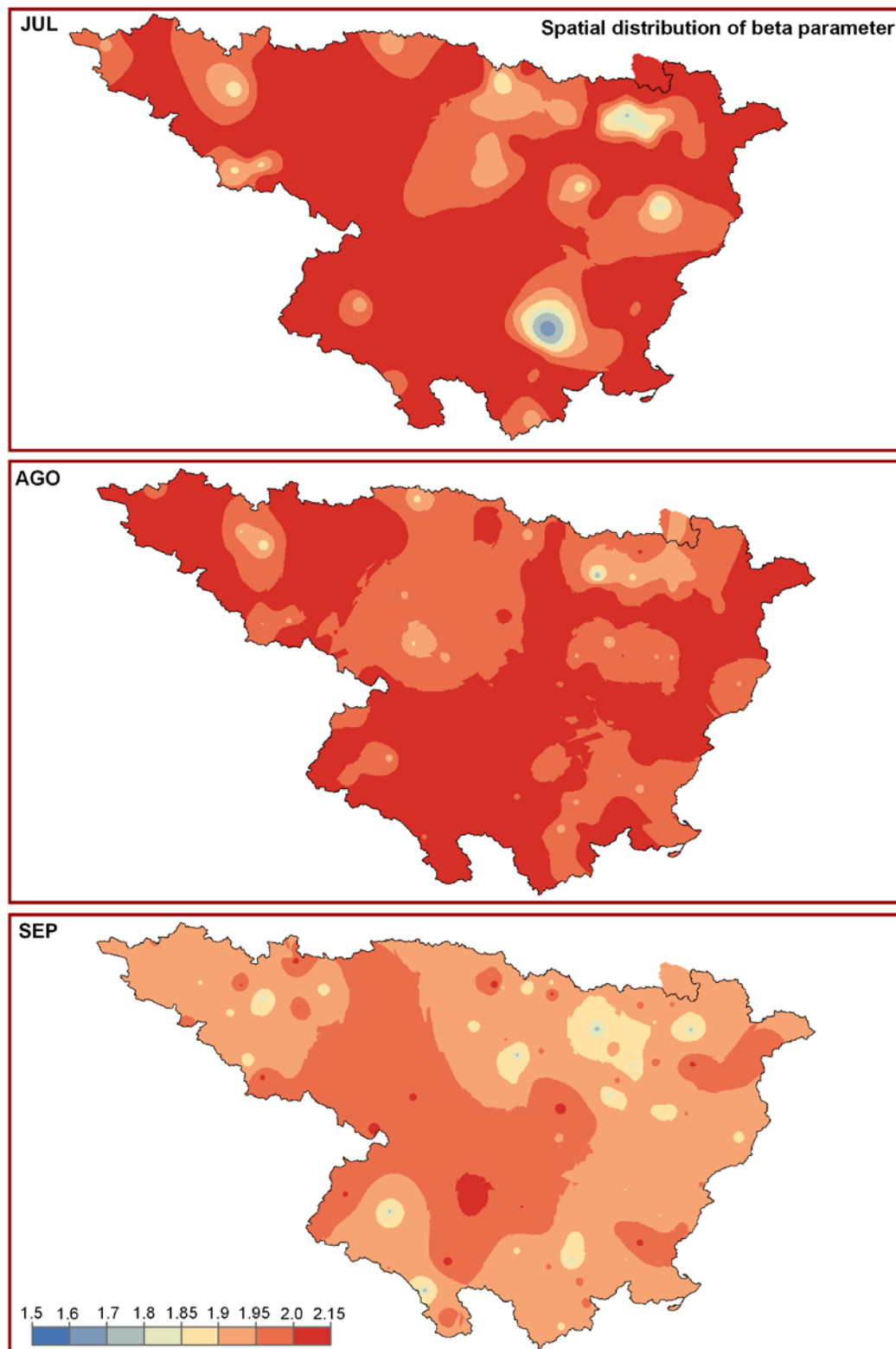


Figure 2.6 (cont.): Spatial distribution for the **beta** parameter in July, August and September.

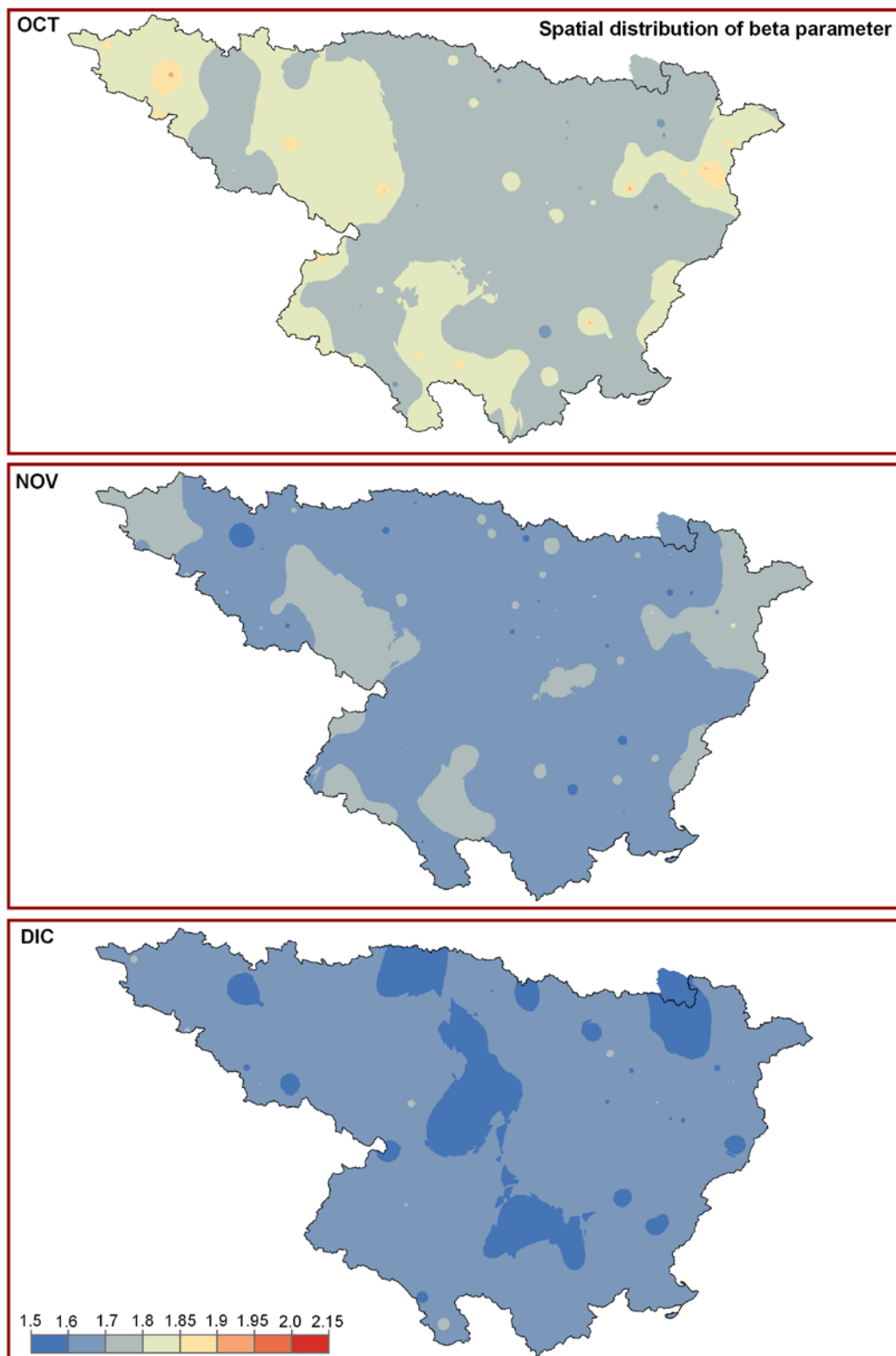


Figure 2.6 (cont.): Spatial distribution for the **beta** parameter in October, November and December.



## 2.5. Validation criteria

In several sections (2.6, 2.7 and 3.4) we compare observed and estimated values obtained by different models and procedures in order to validate the estimates obtained and the reliability of the method. The validation criteria used are based on standard descriptive measurements of centrality and dispersion, and on several error and goodness-of-fit statistics. Among the former we selected i) the mean bias error ( $MBE$ ), which is centered around zero and is an indicator of prediction bias; and ii) the mean absolute error ( $MAE$ ), which is a measure of the average error. As goodness-of-fit measures we used: i) the  $NS$  coefficient of efficiency (Nash and Sutcliffe, 1970), which indicates how close scatters of predicted values are to the line of best fit (this is similar to the coefficient of determination  $R^2$ , without being highly affected by outlier data); and ii) the agreement index  $D$  (Willmott, 1981), which scales the magnitude of the variables, retains the mean information and does not amplify the outliers. We avoided using the root mean square error (RMSE) because it is highly biased by outlier observations, and also because it is difficult to discern whether it reflects the average error or the variability of the squared errors (Willmott and Matsuura, 2005).

The equations for these statistics are:

$$MBE = N^{-1} \sum_{i=1}^N (P_i - O_i), \quad (2.5)$$

$$MAE = N^{-1} \sum_{i=1}^N |P_i - O_i|, \quad (2.6)$$

$$D = 1 - \frac{\sum_{i=1}^N (P_i - O_i)^2}{\sum_{i=1}^N (|P_i| + |O_i|)^2}, \quad (2.7)$$

$$NS = 1 - \frac{\sum_{i=1}^N (O_i - P_i)^2}{\sum_{i=1}^N (P_i - P_m)^2}, \quad (2.8)$$

where  $N$  is the number of data in the sample,  $O$  are the observed data,  $O_m$  is the mean of the observed data,  $P$  are the predicted data,  $P_m$  is the mean of the predicted data,  $O_m'$  is the mean of the observed data, and  $P_i' = P_i - O_m$  and  $O_i' = O_i - O_m$ .

The validity of the empirical models was also evaluated graphically by means of goodness-of-fit plots.





## 2.6 Estimating rainfall erosivity from daily rainfall records: a comparison among methods using data from the Ebro Basin (NE Spain)<sup>1</sup>

Attempts to predict rainfall erosivity from mean annual rainfall and/or mean monthly rainfall have provided results that are quite coarse, but these have been extensively cited in the scientific literature (Banasik and Górska 1994, Renard and Freimund 1994, Yu & Rosewell 1996c, Ferro et al. 1999). Renard and Freimund (1994) provided a succinct summary of methods for estimating the R factor in various parts of the world, and also developed a new set of relationships for calculating the R factor using mean annual rainfall data and the modified Fournier index.

Daily weather records with good spatial and temporal coverage that adequately represent rainfall characteristics are usually available for most locations. Because of the high temporal and spatial variability of rainfall erosivity, accurate records based on long data series are required. Attempts to accurately predict rainfall erosivity from daily rainfall records or storm events (Richardson et al. 1983, Bagarello and D'Assaro 1994, Petkovsek and Mikos 2004), or from monthly rainfall (Yu and Rosewell 1996a, b and c, Yu et al. 2001), have been based largely on exponential relationships.

As the origin of rainfall erosivity is linked to climate dynamics, there is a need to apply climate analysis methodologies to the study of the erosivity factor. However, long series of rainfall erosivity data are required if consistent results are to be obtained. Daily rainfall erosivity models bridge the gap between climate change scenarios based on general and regional circulation models, and the implications of these scenarios for some land degradation processes (Yu and Rosewell 1996b). In addition, a daily rainfall erosivity model would have potential application in many erosion constructs, as the daily model would provide robust predictions of rainfall erosivity.

The aim of this study was to review existing methodologies for predicting the R factor, and to compare estimates obtained using these methodologies with R factor values calculated by the RUSLE procedure. The study was conducted using data from a dense network of observatories distributed in a climatically

---

<sup>1</sup> This section is based in the article: Angulo-Martínez, M., Beguería, S., 2009. Estimating rainfall erosivity from daily precipitation records: A comparison among methods using data from the Ebro Basin (NE Spain). *Journal of Hydrology*, 379, 111-121



complex region (the Ebro Basin, NE Spain), and covers the period 1997–2006, (section 2.4-i). The methodology described has the potential to be applied to longer daily rainfall data bases, which could improve estimates of the spatial coverage of rainfall erosivity in the Ebro basin with respect to both long-term average erosivity and seasonal distribution thereof. The proposed methodology can be applied in many parts of the world where short time series of high-resolution rainfall data coexist with long series at a daily resolution.

### 2.6.1 Rainfall erosivity estimating methodologies based on daily rainfall intensity data

*Model A: The Richardson et al. (1983) exponential model*

Event rainfall erosivity values ( $EI$ ) are usually well fitted to the event rainfall amount ( $P$ ) by an exponential relationship (Richardson et al. 1983):

$$EI = a P^b + \varepsilon, \quad (2.9)$$

where  $a$  and  $b$  are empirical parameters and  $\varepsilon$  is a random, normally distributed error. The  $R$  factor, equal to the annual cumulative  $EI$ , is obtained by adding all event values. The parameters  $a$  and  $b$  can be adjusted month-by-month to take account of intra-annual variations in rainfall characteristics. This leads to the more general expression:

$$EI_m = a_m P^{b_m} + \varepsilon, \quad (2.10)$$

where  $m = \{1, \dots, 12\}$  represents the month of the year being evaluated. The exponential relationship has been applied to event (Richardson et al. 1983, Posch and Rekolainen 1993), daily (Bagarello and D'Asaro 1994) and even monthly data (Yu and Rosewell 1996a; Petkovsek and Mikos 2004). In all these studies parameter  $a$  was the only variable, and parameter  $b$  was assumed to be stationary across the year.

Parameter estimation in the Richardson et al. (1983) model is achieved by ordinary least squares (OLS) regression after a logarithmic transformation of the terms in equation (2.9). OLS regression offers an analytical solution to minimizing the sum of squared errors, SSE:



$$SSE_m = \sum_{m=1}^M (E_m - \hat{E}_m)^2, \quad (2.11)$$

where  $E_m$  and  $\hat{E}_m$  are the observed and predicted cumulative rainfall erosivity for month  $m$ , respectively,  $\hat{E}_m$  is the predicted cumulative rainfall erosivity for the month, and  $M$  is the number of months for which data are available.

#### *Model B: The Richardson et al. (1983) exponential model by weighted least squares*

A problem with the method of Richardson et al. (1983) is that it tends to underestimate systematically the R factor values. This has been pointed out by a number of authors, and it has been usually attributed to the logarithmic transformation of the variables to allow parameter estimation by OLS (Richardson et al. 1983, Elsenbeer et al. 1993, Posch and Rekolainen 1993). However, we believe that the R factor is underestimated mainly because parameter estimation by OLS is based on minimizing the squared errors *at the daily or rainfall event scale*, resulting in excessive significance being placed on many small events that do not contribute materially to the cumulative annual erosivity. In fact, many studies have shown the paramount importance of the contribution of very few, but intense, daily rainfall events to total annual rainfall erosivity.

In order to avoid excessive influence of small erosive events during parameterization of the Richardson et al. (1983) model, we have also tried an alternative parameterization method based on weighted least squares regression (WLS). In WLS weights can be assigned to the observations in order to modify their influence on the fitting process. In this case, the weights  $w_i$  were computed as the inverse of the empirical frequency of the observations:

$$w_i = \left( \frac{i}{n} \right)^{-1}, \quad (2.12)$$

where  $i$  is the order of the observation after the series has been sorted in ascending order, and  $n$  is the number of observations in the series.



### Model C: The Yu and Rosewell model

Using the equation of Richardson et al. (1983) requires a logarithmic transformation of the data, which usually leads to underestimation of erosivity and bias when the predicted values are transformed back to the original scale (Richardson et al. 1983, Elsenbeer et al. 1993, Posch and Rekolainen 1993). In addition, individual regression equations must be developed for each month (Posch and Rekolainen, 1993) or season (Richardson et al., 1983), resulting in a large number of parameters. Yu and Rosewell (1996a) proposed an alternative equation based on the Richardson et al. (1983) method, in which the seasonal variation of parameter  $\alpha$  (termed  $\alpha$  in their study) was modeled parametrically using a periodic function:

$$EI = \alpha \left[ 1 + \eta \cos\left(2\pi \frac{1}{12}m - \omega\right) \right] P^\beta \quad \nabla P > P_0, \quad (2.13)$$

where  $\eta$  controls the amplitude of the intra-annual variation of  $\alpha$ , and  $\omega$  controls the phase, i.e. the month of the year for which the value of  $\alpha$  is maximum. The periodic function modifying parameter  $\alpha$  allows introduction of seasonal effects such as varying storm types, using a reduced number of parameters in comparison with the method of Richardson et al. (1983). Equation 7 is evaluated at the daily time scale, and only those values of daily rainfall greater than a threshold value  $P_0$  are considered. A value of 0.0 mm is usually valid for  $P_0$  when daily data are used. The parameter  $\omega$  is kept constant, depending on the month registering the highest erosivity for a given rainfall amount.

To minimize bias in the estimated erosivity values, Yu and Rosewell (1996a) recommended using parameter estimates without data transformation. The adjustment between the observed and predicted values is done by using an iterative algorithm minimizing the sum of squared errors.



### *Model D: A modified Yu and Rosewell model*

Application of the original model of Yu and Rosewell—*Model C*—only allows intra-annual variation of parameter  $\alpha$ . An alternative model could allow periodic variation in parameter  $\beta$  while parameter  $\alpha$  is kept stationary:

$$EI = \alpha P^{\beta[1+\eta \cos(2\pi \frac{1}{12}m-\omega)]}, \quad (2.14)$$

### *Model E: The five-parameter modified Yu and Rosewell model*

A logical extension of *Model D* would be to allow intra-annual variation in both  $\alpha$  and  $\beta$ :

$$EI = \alpha \left[ 1 + \eta_\alpha \cos(2\pi \frac{1}{12}m - \omega) \right] P^{\beta[1+\eta_\beta \cos(2\pi \frac{1}{12}m-\omega)]}, \quad (2.15)$$

where  $\eta_\alpha$  and  $\eta_\beta$  control the amplitude of the variation of  $\alpha$  and  $\beta$ , respectively. In the previous formulation the phase parameter  $\omega$  is kept equal for both  $\alpha$  and  $\beta$ . The parameters  $\alpha$ ,  $\beta$ ,  $\eta_\alpha$  and  $\eta_\beta$  were estimated by minimizing the sum of squared errors as described above.

Since equations (2.9), (2.10) and (2.11) are highly non-linear no analytical solution is available, and an iterative method has to be used for minimizing the SSE. In this case a genetic algorithm (*Pikaia*; Charbonneau 1995, Metcalfe and Charbonneau 2003) was used to determine the best values for parameters  $\alpha$ ,  $\beta$ ,  $\eta_\alpha$  and  $\eta_\beta$ , depending on the model. Parameter  $\omega$  can be estimated directly from the observations as:

$$\omega = \frac{\pi}{6} m_{\max}, \quad (2.16)$$

where  $m_{\max}$  is the month registering the highest average erosivity for the complete record period.



## 2.6.2 Rainfall erosivity estimates based on monthly rainfall and annual rainfall indices

Other approaches exist to estimate rainfall erosivity without daily rainfall data. As a consequence of the relationship between rainfall erosivity and rainfall intensity, alternative ways to calculate the impact of rainfall on soil are based on the rainfall concentration, for example by applying the modified Fournier index, or by regression of the RUSLE R factor upon different rainfall intensity statistics calculated at the annual level.

### *Model F: Rainfall intensity indices*

Annual rainfall erosivity has been related to several rainfall intensity indices calculated at the annual level (Table 2.1). A common indicator of high rainfall erosivity values is the mean annual rainfall (Renard and Freimund 1994). Several studies have highlighted the relationship between the R factor and occasional heavy rainfall events recorded during a year (Martínez-Casanovas et al. 2002, González-Hidalgo et al. 2007, Angulo-Martínez et al. 2009). Rainfall erosivity can also be related to several rainfall intensity indices that are also correlated with the presence and duration of dry spells. Since there are many alternative indices to regress upon, it is wise to perform a multiple regression analysis to find an optimum estimator of the R index of the form:

$$R = b_0 + \sum_1^n b_n x_n + \varepsilon, \quad (2.17)$$

where  $b_0 - b_n$  are regression coefficients and  $x_1 - x_n$  are independent variables.

For model selection (identification of the significant variables) in the present study we used a forward stepwise method based on the Akaike's information criterion (Venables and Ripley 2002). A ten-fold cross-validation procedure was used, which involved repeating the stepwise method ten times, each time omitting one-tenth of the sample from the analysis (Breiman and Spector 1992). In an ideal situation all ten repetitions should yield the same set of significant variables, indicating high reliability of the model. A robust regression procedure was used to avoid the excessive influence of outlier observations present in the data. This involved assigning to each observation a weight that was inversely



proportional to its influence on the model fitting process (Marazzi 1993). The R statistical analysis package (R Development Core Team 2008) was used for the regression analysis.

Table 2.1. Acronyms and definition of the selected indices from the daily rainfall series.

Acronym	Definition	Units
P	Total rainfall	mm
WD	Number of wet days (rainfall >1mm)	days
PI	Simple daily intensity (P/WD)	mm
C90	Annual 90th percentile	mm
R90N	Nº of events with rainfall greater than long-term 90th percentile (P90)	days
R90T	Percentage of total rainfall from events above P95	%
C95	Annual 95th percentile	mm
R95N	Nº of events with rainfall greater than long-term 90th percentile (P95)	days
R95T	Percentage of total rainfall from events above P95	%
C99	Annual 99th percentile	mm
R99N	Nº of events with rainfall greater than long-term 90th percentile (P99)	days
R99T	Percentage of total rainfall from events above P99	%
R1GD	Greatest day total rainfall	mm
R3GD	Greatest 3-day total rainfall	mm
R5GD	Greatest 5-day total rainfall	mm
R7GD	Greatest 7-day total rainfall	mm
R9GD	Greatest 9-day total rainfall	mm
R11GD	Greatest 11-day total rainfall	mm
R13GD	Greatest 13-day total rainfall	mm
R15GD	Greatest 15-day total rainfall	mm
R17GD	Greatest 17-day total rainfall	mm
R19GD	Greatest 19-day total rainfall	mm
R21GD	Greatest 21-day total rainfall	mm
WSM	Max nº of consecutive wet days (rainfall >1mm)	days
DSM	Max nº of consecutive dry days (rainfall <1mm)	days
WS	Average Max nº of consecutive wet days (rainfall >1mm)	days
DS	Average Max nº of consecutive dry days (rainfall <1mm)	days
RS	Ratio (WS/DS)	



### Model G: The modified Fournier index

Estimation of the annual rainfall erosivity using the modified Fournier index has been proposed when only monthly rainfall data are available (Arnoldus 1977) i.e.:

$$MFI = \sum_{i=1}^{i=12} \frac{P_i^2}{P}, \quad (2.18)$$

where  $P_i$  is the mean monthly rainfall of the month  $i$  and  $P$  is the mean annual rainfall. The relationship between  $MFI$  and the R factor showed better adjustment following an exponential distribution (Ferro et al. 1999). The R factor values can be estimated from the  $MFI$  using the following equation:

$$R = aMFI^b + \varepsilon, \quad (2.19)$$

where  $a$  and  $b$  are empirical parameters and  $\varepsilon$  is a random, normally distributed error.

The Fournier index has been used in several recent studies (Apaydin et al. 2006, Gabriels 2006). The application of this model yielded the following equation for the study area:

$$R = 21.56MFI^{0.927}, \quad (2.20)$$

### Model H: The F index (Ferro et al. 1991)

A modification in the  $MFI$  for estimating rainfall erosivity has been proposed by Ferro et al. (1991):

$$F_F = \frac{P}{12} \left[ \frac{\sum_{j=1}^N P_j [1 + CV^2(p_{i,j})]}{\sum_{j=1}^N P_j} \right] = \sum K_i \frac{P}{12}, \quad (2.21)$$

where  $P_j$  is the annual rainfall amount of the year  $j$ ,  $CV$  is the variation coefficient of the month  $i$  from the year  $j$ ,  $K_i$  is a constant depending on the month  $i$ , and  $P$  is the mean annual rainfall of the study period

In this case, the value  $K$  is an indicator of the monthly rainfall distribution in the year. The best adjustment between  $F_F$  index and the R factor was achieved with



an exponential distribution—i.e. eq. 15—(Ferro et al. 1999). In the study area the R factor values were obtained by using the following equation:

$$R = 0.0542 F_F^{1.412}, \quad (2.22)$$

### 2.6.3. Validation

The resulting rainfall erosivity prediction models were assessed using a set of validation statistics that compared the observed and estimated values of the R factor. We used a set of goodness-of-fit statistics described in section 2.5 including: i) the mean and the standard deviation of the predicted and observed values, as a measure of centrality and dispersion, and ii) the *NS* coefficient of efficiency (Nash and Sutcliffe, 1970), which indicates how close scatters of predicted values are to the line of best fit. This validation statistic is commonly used in rainfall erosivity studies (Yu et al., 2001, Petkovsek and Mikos, 2004). In addition we used two error statistics: i) the mean bias error (*MBE*), as indicator of prediction bias; and ii) the mean absolute error (*MAE*), as a measure of the average error. The validity of the models was also evaluated by goodness-of-fit plots and the comparison between the spatial distribution of the observed values and the spatial distribution of the R factor estimates from the different models. The R factor maps were obtained by spatial interpolation of the at-site points using smoothing splines for spatial interpolation.

### 2.6.4. Results

#### *Model A equation parameters*

We have analyzed the *a* and *b* parameters calibrated monthly using the exponential relationship of Richardson et al. (1983) in eq. (2.9) above. As explained earlier, further development of this model was largely dependent on how seasonal variation of the *a* and *b* parameters was modeled.



Rainfall erosivity displayed a very marked seasonal pattern that did not coincide with the seasonal variation in monthly rainfall. In principle, this is consistent with seasonal variation in the parameters of the exponential relationship. Figures 2.7 and 2.8 show the monthly distribution of parameters  $a$  and  $b$ . Differences between observatories were relatively small, and were usually noticed in the month during which maximum values were registered. Both parameters showed significant temporal variation within the year, following a periodic model. Minimum values were found in winter (December–January) and the maxima at the end of summer (July–August). This result supports the validity of the models of Yu and Rosewell (models C, D, and E).

Another noteworthy result is that both of the  $a$  and  $b$  parameters showed seasonal variation. As mentioned above, many studies have minimized the influence of parameter  $b$  by holding  $b$  constant throughout the year. This is because  $b$ , being an exponent, has a greater influence than has parameter  $a$  on the estimations, and hence is much more sensitive to calibration errors. However, our results show that both parameters varied significantly, supporting the hypothesis that a model incorporating such variation could yield better results. In this context, Figures 2.7 and 2.8 show that parameters  $a$  and  $b$  displayed very similar relative patterns, with minima and maxima that occurred in the same months and that differed only in the magnitude of variation. This supports the hypothesis that a model with one  $\omega$  parameter, which controls the phase of the periodic function, replacing both  $a$  and  $b$ , would be adequate (this is model E).

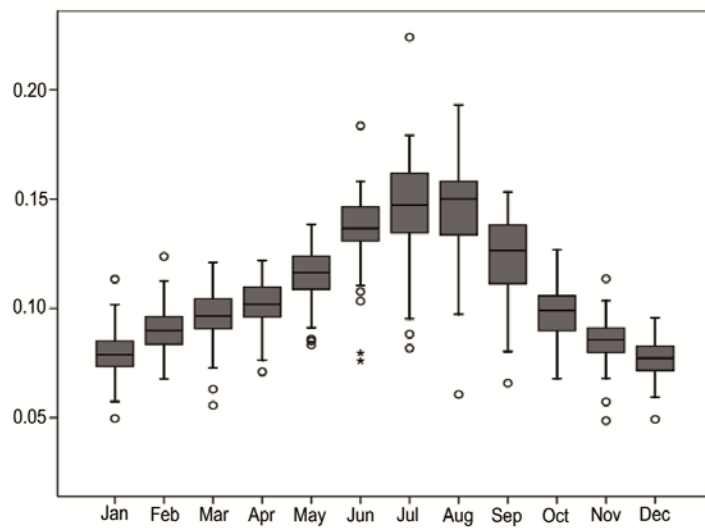


Figure 2.7: Monthly distribution among the analyzed observatories for parameter  $\alpha$  from the Richardson et al. (1983) exponential relationship.

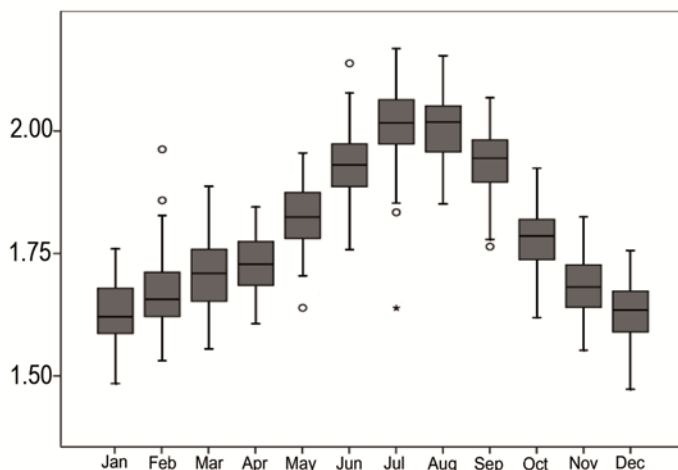


Figure 2.8: Monthly distribution among the analyzed observatories for parameter  $\beta$  from the Richardson et al. (1983) exponential relationship.

*Comparison between methods; Models based on daily data*

All the daily rainfall erosivity models yielded good results, as was made evident by the validation statistics (Table 2.2), goodness-of-fit plots (Figure 2.9), and by checking the spatial distribution of the R factor estimates (Figures 2.10). The models based on the Yu and Rosewell equations (models C, D, and E) were most satisfactory. Model C—the original Yu and Rosewell (1996a) equation—ranked best among them. The exponential relationship model of Richardson et al. (1983) fitted by the ordinary least squares method (model A) underestimated rainfall erosivity, as evidenced by all the validation statistics. However, the Richardson et al. (1983) model fitted by weighted least squares (Model B) showed better agreement, as evidenced by the validation statistics and the goodness-of fit plots (Table 2.2 and Figure 2.9, respectively). This result confirmed that the underestimation of model A, which has been attributed to the logarithmic transformation applied to the data by a number of authors, is in fact related to the utilization of a fitting algorithm that is sub-optimal for estimating the R factor, due the high importance of very few, but intense rainfall events.

Table 2.2. Accuracy measurements for the R factor models: means and standard deviations of the observed and predicted values.

	Mean	Standard dev.	MBE	MAE	NS
Observed	903.9	619.91	---	---	---
Model A	708.2	573.5	-194.4	205.9	0.745
Model B	774.8	628.5	-128.4	152.8	0.839
Model C	969.8	696.4	64.9	97.6	0.947
Model D	1000.2	729.3	95.0	132.4	0.909
Model E	998.2	697.9	93.0	124.5	0.910
Model F	1025.9	530.2	120.8	243.2	0.574
Model G	805.4	320.4	-97.6	329.6	-1.903
Model H	830.1	392.6	-73.2	293.6	-0.512

Looking at the goodness-of-fit plots (Figure 2.9), it is evident that model A resulted in significant under-estimation of the R factor, whereas model B provided better predictions. The models based on the Yu and Rosewell (1996a) equation, e.g. models C, D and E, had also a good agreement, although in general tended to over-estimate the R factor. Among the three parametric models the



differences were narrow; the best overall fit was given by the Yu and Rosewell original model—model C—followed by model E.

With respect to goodness-of-fit and error statistics (Table 2.2), all models based on daily data (A, B, C, D, and E) gave good results. Overall, model A ranked lowest, underestimating both the mean and the standard deviation of rainfall erosivity, and showing the strongest bias of all methods. This model also had the lowest goodness-of-fit statistic ( $NS$ ) of all models using daily data, and ranked closer to theoretically less refined methods, such as the regression method (model F). As a comparison, when using weighted least squares in the Richardson et al. (1983) model—Model B—better validation statistics were obtained. Among the models based on the equation of Yu and Rosewell (C, D, and E), model C was the best considering all the validation statistics altogether. Between models D and E, model E yielded the best results.

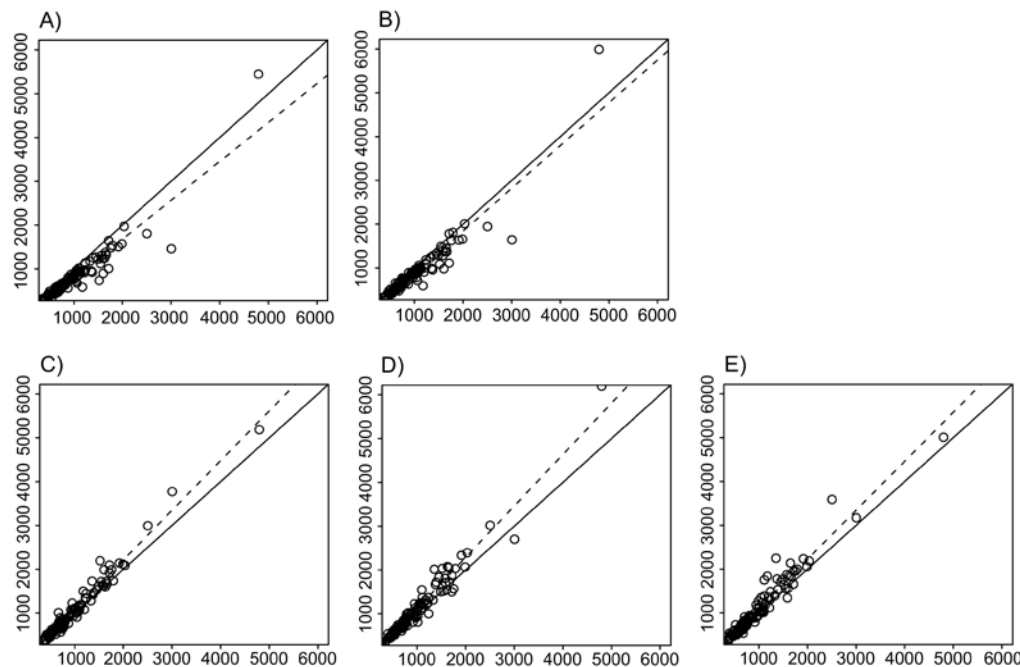


Figure 2.9: Comparison between observed  $R$  values (ordinate axis) and those estimated by various methods (abscissa axis): A) model A; B) model B; C) model C; D) model D; and E) model E. Line of best fit (continuous diagonal line), and regression line (dashed).

Finally, a comparison was made among the various methods in terms of the spatial distribution of rainfall erosivity (Figure 2.10). Based on these results we rejected models A and B which resulted in underestimation and a poor approximation to the observed values of rainfall erosivity (Figure 2.20).



Differences between the others models were hardly noticed, and all adequately reproduced the observed spatial pattern (Figure 2.20). However, it must be noted that interpolation techniques may increase underestimation.

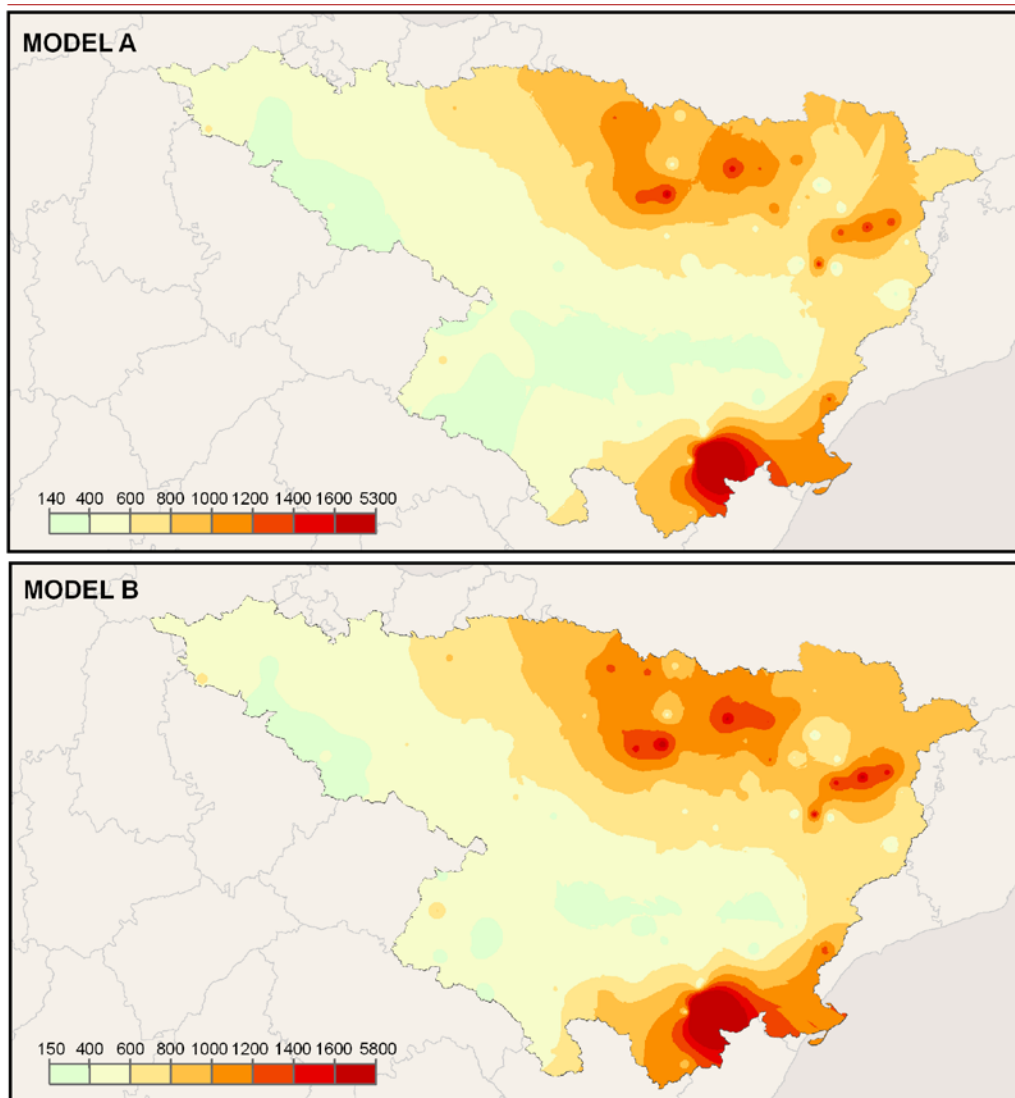


Figure 2.10: Spatial distribution of estimated R values by: *Model A*; *Model B*. These maps can be compared to Figure 2.20.

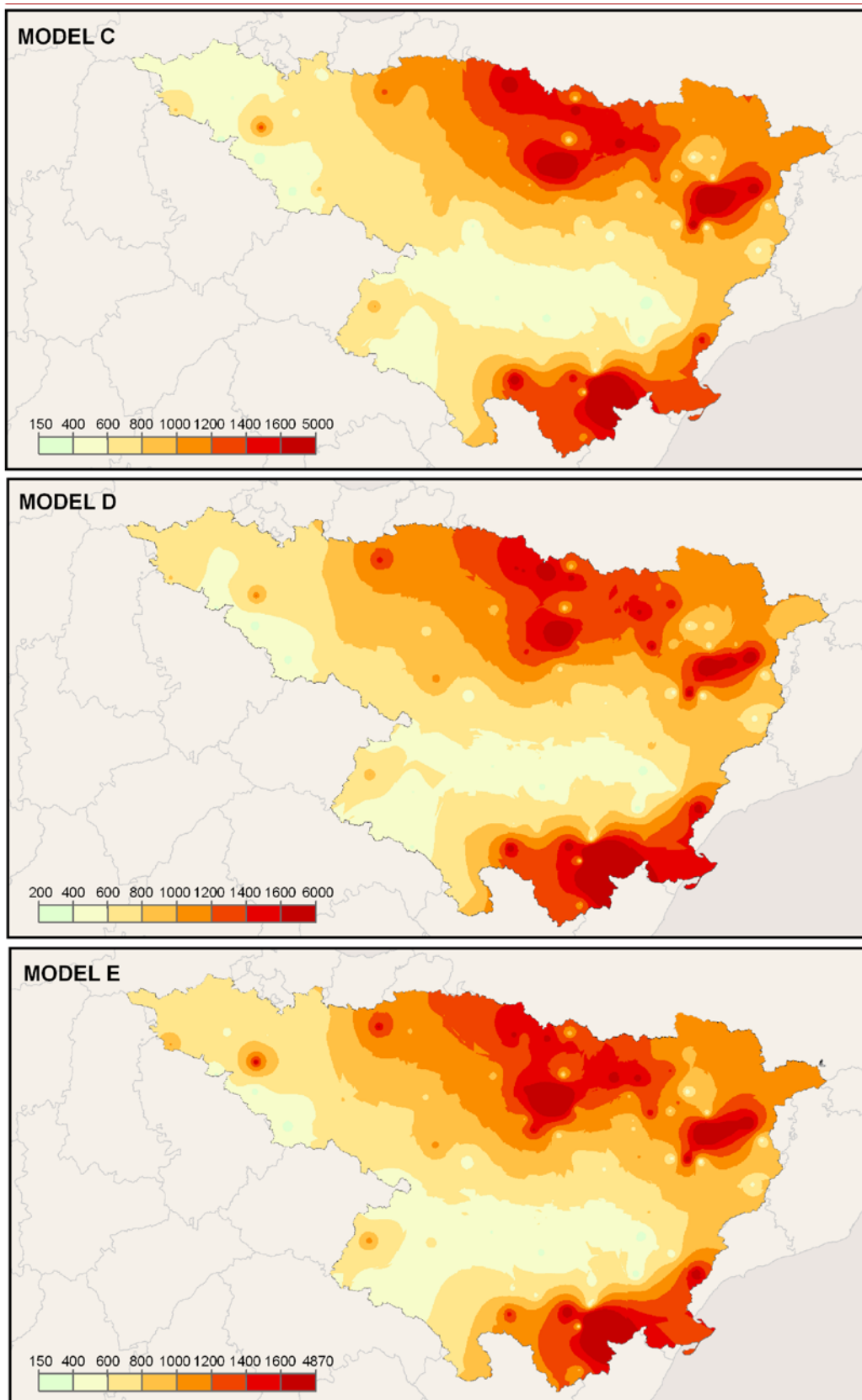


Figure 2.10 (cont.): Spatial distribution of estimated  $R$  values by: *Model C*; *Model D*; *Model E*.  
These maps can be compared to Figure 2.20.



### Comparison between models; Models based on monthly or annual rainfall intensity indices

An exploratory correlation analysis (Table 2.3) showed that high and significant correlations existed between rainfall erosivity on the one hand, and several rainfall intensity indices computed on an annual basis, on the other. The highest correlation coefficients were found with R3GD and R5GD; these are the amounts of rainfall accumulated during the three and five wettest days, respectively, confirming the hypothesis that very few events are responsible for a large part of annual rainfall erosivity.

Table 2.3. Correlation coefficients between the observed *R* factor and several rainfall intensity indices. See Table 2.1 for definition of the indices.

P	WD	PI	C90	R90N	R90T	C95
0.50*	0.042	0.79*	0.76*	0.047	0.18	0.80*
R95N	R95T	C99	R99N	R99T	R1GD	R3GD
0.036	0.19	0.80*	0.056	0.26*	0.79*	0.84*
R5GD	R7GD	R9GD	R11GD	R13GD	R15GD	R17GD
0.84*	0.82*	0.80*	0.79*	0.77*	0.75*	0.74*
R19GD	R21GD	WSM	DSM	WS	DS	RS
0.72*	0.71*	0.0068	0.10	0.094	0.049	0.044

\* significant at the confidence level  $\alpha=0.05$

The explanatory variables selected by the stepwise procedure were R5GD, WSM, and RS; the latter two figures are the maximum wet spell duration and the ratio between the average length of wet and dry spells (Table 2.4). It is notable that the regression analysis included two variables that did not show significant correlations with *R* when considered individually, although other indices that were probably highly correlated with R5GD were excluded. The selection of variables was remarkably constant during the jack-knife process, confirming the statistical significance of the three variables mentioned. In contrast, the correlations between the *R* factor and the modified Fournier index, and the *R* factor with the  $F_F$  index were very poor (Table 2.4), and yielded unsatisfactory results.



Table 2.4. Regression coefficients and variance, and regression analysis for the rainfall intensity indices (see Table 2.1) and the modified Fournier index (MFI).

Explanatory variables	$r^2$	Variables selected
Regression against rainfall intensity indices based on daily data	0.727	R5GD, WSM, RS
Modified Fournier Index	0.250	---
$F_F$ index	0.408	---

Figure 2.11 shows the goodness-of-fit plots for the three models. Underestimation occurred in all cases, particularly using the regression based on the Fourier index—model G. Among all models based on monthly or annual rainfall intensity indices model F yielded the best results, which were closer to those based on daily data and exponential relationships, although the values of all validation statistics were worse (Table 2.5). Estimation by model H—regression based on the  $F_F$  index—showed better agreement than using the original Fournier index, but still model F ranked best.

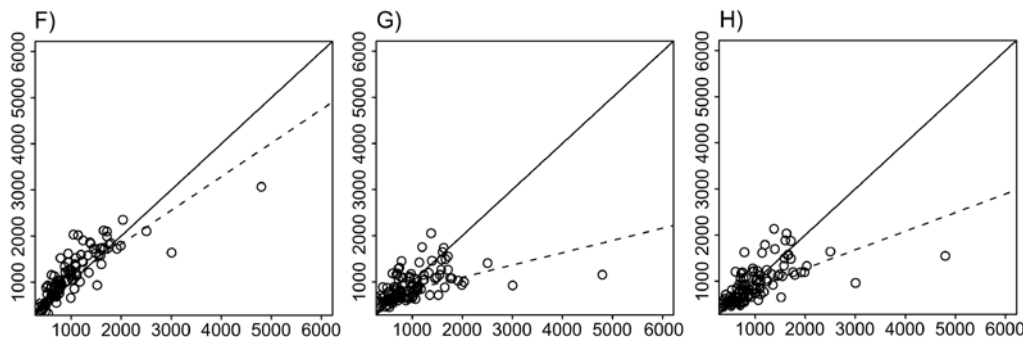


Figure 2.11: Comparison between observed R values (ordinate axis) and those estimated by various methods (abscissa axis): F) model F; G) model G; and H) model H. Line of best fit (continuous diagonal line), and regression line (dashed).

The validation statistics (Table 2.2) showed that the MFI regression afforded the poorest performance of all methods tested and, particularly, resulted in a marked underestimation of the standard deviation of rainfall erosivity, as well as the highest absolute error and the worst NS statistic. The rainfall intensity indices regression model—model F—was relatively poor compared to methods based on the Yu and Rosewell equation, although the validation statistics were almost as good as those for model A. Validation statistics obtained for Model H slightly



improved those from Model G, but this model still ranked very low to be considered a valid choice when other models are affordable.

Finally, the spatial distribution of the estimated R factor values determined by these methods (Figure 2.12) matched the observed pattern quite well (Figure 2.20) in the case of model F, but was very poor when model G and H were employed. This fact was especially evident for the highest values recorded at the southeast part of the region. Those high values corresponded to an extreme event recorded at the daily scale which is still disguised at the monthly level.

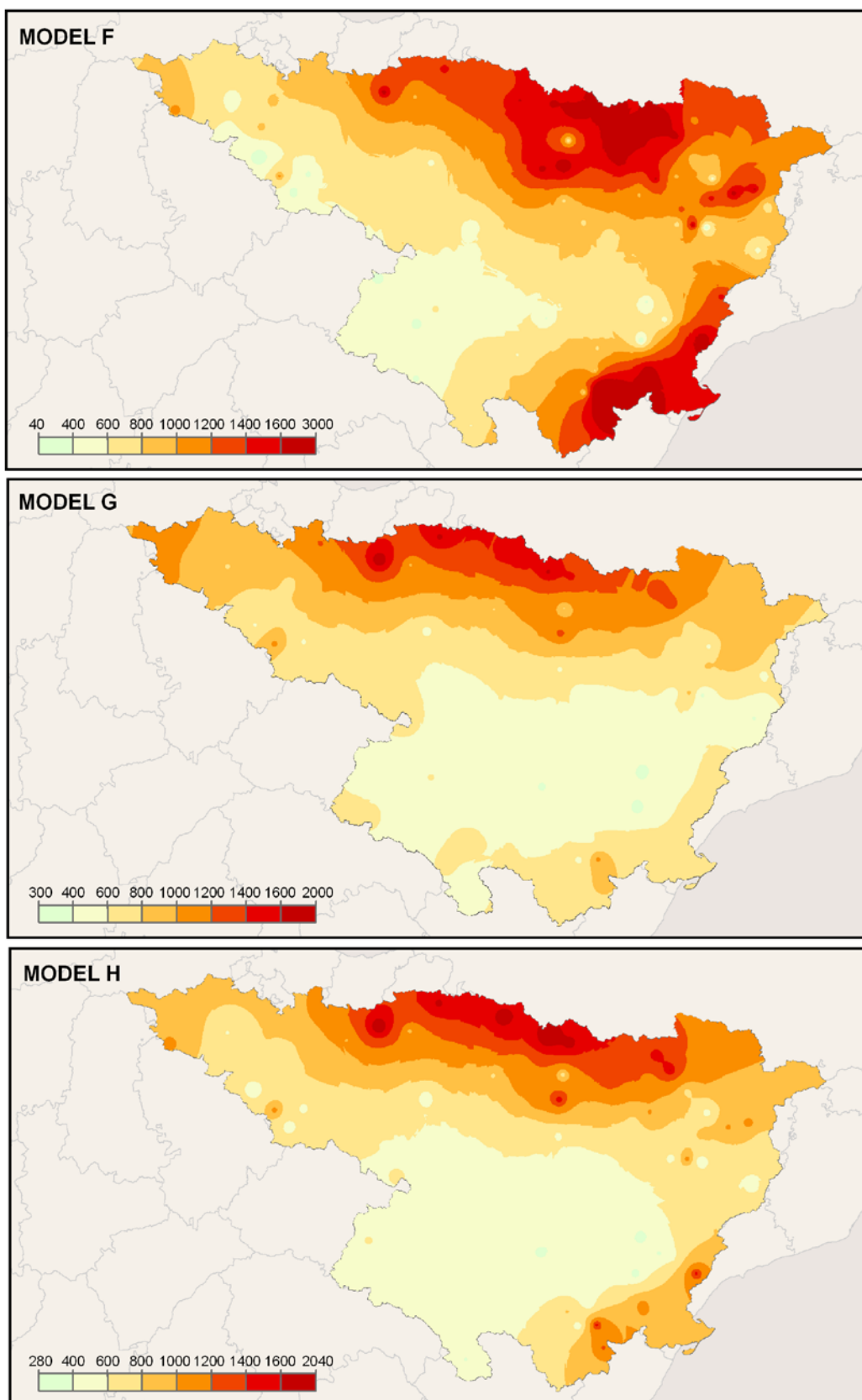


Figure 2.12: Spatial distribution of estimated R values by: *Model F*; *Model G*; *Model H*. These maps can be compared to Figure 2.20.



## 2.6.5. Discussion

Estimation of rainfall erosivity is of great importance for soil erosion assessment, and has important implications for agriculture and land planning. Rainfall erosivity is an indicator of rainfall aggressiveness, and depends both on the rainfall energy (raindrop size distribution and kinetic energy) and the intensity of the storm event. Rainfall in Mediterranean climates is characterized by great temporal variability and high, brief, intensity (storms). This latter characteristic particularly affects rainfall erosivity, which increases with greater occurrence of few, very intense, events (González-Hidalgo et al. 2007).

In this study we used the RUSLE R factor, calculated employing high resolution (15 min) rainfall data, as an indicator of rainfall erosivity, and compared R factor values with estimates obtained using alternative methods based on daily rainfall data and rainfall indices calculated on monthly and annual scales. This comparison was conducted to identify valid, spatially-distributed estimates of rainfall erosivity using the type of rainfall data that are most usually available.

Among the methods used to estimate the RUSLE R factor, the Yu and Rosewell (1996a) equation and variations thereof (models C, D and E) yielded the best results, and the data were consistent when tested using several statistical validation tools and by direct comparison of the maps of rainfall erosivity produced by each method. The main advantage of the Yu and Roswell method is that this approach allows investigators to reproduce seasonal variations in the relationship between daily rainfall and rainfall erosivity without a need to divide the data into monthly segments; this makes more efficient use of the information available. Although most previous studies assumed that the  $b$  coefficient remained constant throughout the year (Richardson et al. 1983, Bagarello and D'Asaro 1994, Petkovsek and Mikos 2004) our results demonstrate that both of the parameters  $a$  and  $b$  showed a periodic variation within the year. Moreover, the influence of parameter  $b$ , being an exponent, is greater than that of parameter  $a$ . This result drove directly to the proposal of two variants of the original model of Yu and Rosewell (1996a)—Models D and E. We compared three versions of the original model of Yu and Rosewell, in which only  $\alpha$ , only  $\beta$  or both  $\alpha$  and  $\beta$  were allowed to vary over the year by using a periodic function. Although the ability of the models to predict the R factor was supposed to increase with the model complexity, the validation statistics did not allow such a clear conclusion to be



drawn, since the original model of Yu and Rosewell (1996a) yielded results which were marginally better than the other two variants. Hence, even though there are strong theoretical evidences in favour of a model with both  $\alpha$  and  $\beta$  parameters allowed varying, for practical use we have to recommend the simplest formulation with only  $\alpha$  varying, that is, the original formulation of Yu and Rosewell (1996a). It is possible that a model with both parameters varying—model E—provides a better way to estimate the rainfall erosivity at a monthly or even a daily basis, although this hypothesis has not been tested in this work. Due to the high complexity and non-linearity of model E, it is also possible that better results would be obtained by using fitting methods other than the genetic algorithm used in this work. These possibilities, however, would need further testing and they have not been tested in this work, which is restricted to predicting the RUSLE R factor.

In contrast, the method based on the exponential relationship of Richardson et al. (1983) yielded unsatisfactory results, systematically underestimating the annual erosivity and the variance thereof. This outcome has been reported on many occasions, and has been attributed to the logarithmic transformation that is usually performed on the variables to allow parameter estimation by the least squares method. However, our results demonstrate that under-estimation of the R factor is caused by the sub-optimal character of the OLS algorithm. We have shown that when the weighted least squares method was applied—Model B—the underestimation was reduced very significantly. This fact confirmed that underestimation by the OLS algorithm is due to excessive significance being placed on many small events that do not contribute materially to the cumulative annual erosivity expressed by the R factor. In fact, the results of our analyses confirmed the paramount importance of the contribution of very few, but intense, daily rainfall events to total annual rainfall erosivity.

In the absence of daily rainfall data, other ways to estimate the R factor are based on regression upon intensity rainfall indices on monthly or annual scales. These are commonly available statistics that are readily obtainable through any meteorological service. Our results showed that the modified Fournier index or its modified form—the  $F_F$  index—are not appropriate for estimating the R factor and result in severe underestimation. The best alternative to using a daily-based approach was a multivariate linear model based on three indices (the cumulative



rainfall for the five days with most rain, the maximum wet spell duration, and the ratio between the length of the average wet and dry spells).

The parameter values obtained from models A and B in this study are similar to those obtained in several studies carried out in other Mediterranean areas (Bagarello and D'Asaro 1994, Petkovsek and Mikos 2004, D'Asaro et al. 2007). All those studies developed regional models based on exponential relationships upon daily rainfall amounts. One or more model parameters were considered spatially invariant and were maintained equal for all the stations in the study area. In this study we have preferred to perform an at-site analysis, i.e. calibrating all the model parameters individually for each station. This was recommended due to the existence of contrasting rainfall regimes within the study area, and also because regional variations were found in the values of the parameters when fitted individually for each site

There remain inherent limitations in the use of daily weather records for estimating the rainfall erosivity by the Revised Universal Soil Loss Equation. Erosivity includes kinetic energy and intensity measures that are poorly represented by daily rainfall values (Selker et al. 1990). Future research may provide better calibration of the Brown and Foster (1987) rainfall kinetic energy equation by measuring natural rainfall properties in any particular region.

### 2.6.6. Conclusions

In this study we have shown that good rainfall erosivity estimates can be obtained by using several methods based on daily rainfall data. The best model is the original formulation of Yu and Rosewell (1996a). The weighted least squares method applied to the Richardson et al. (1983) model is an accurate improvement to the original proposal. In this case underestimation was reduced very significantly, confirming that underestimation is due by treating all events as having the same erosion potential leading to excessive significance of many small events which do not contribute materially to the cumulative annual erosivity expressed by the R factor. When daily rainfall data are not available, good estimates can be achieved based on regression upon intensity rainfall indices on monthly or annual scales. These are commonly available statistics that are readily obtainable through any meteorological service. Our results showed that the



modified Fournier index or its modified form—the  $F_F$  index—are not appropriate for estimating the R factor and result in severe underestimation.





## 2.7. Mapping rainfall erosivity at the regional scale: a comparison of interpolation methods in the Ebro Basin (NE Spain)<sup>2</sup>

Soil erosion has become a major environmental threat due to the growth of the World's population, and is one of the main consequences of projected land use and climate change scenarios (Gobin *et al.* 2004). Studies on soil erosion started in the first decades of the 20<sup>th</sup> Century, and have increased in number and variety since then. Isolating the role of different natural and management factors on soil erosion has been one of the major research topics. The combination of those factors in the form of a parametric model allowed the development of tools such as the USLE (Wischmeier and Smith, 1978; Kinnell and Risse, 1998), which can be used for predicting the effect of different management strategies on soil erosion rates. The development of parametric models opened a new area of research, devoted to analyze the spatial variability of erosion causal factors. Maps showing the spatial distribution of natural and management related erosion factors are of great value in the early stages of land management plans, allowing identify preferential areas where action against soil erosion is more urgent or where the remediation effort will have highest revenue.

Mapping rainfall erosivity at regional and basin scale is still an emerging research question. Such maps allow for a better comprehension of the processes with geographical imprint as well as the application of these methodologies to large spatial areas. They are also an important step for large-scale soil erosion assessments, soil conservation management of natural resources, agronomy and agrochemical exposure risk assessments (Winchell *et al.* 2008). Early examples are the rainfall erosivity maps for the whole USA in the form of *isoerodent* maps or maps of the RUSLE R factor (Renard and Freimund, 1994). Other researchers have used regression techniques to elaborate spatially continuous maps of rainfall erosivity on the basis of other available data such as daily and monthly records of rainfall depth (ICONA, 1988).

With the advent of GIS packages and the generalization of spatial interpolation techniques, maps of environmental parameters such as those relevant for soil erosion have become frequent. For example, several authors have used GIS

---

<sup>2</sup> This section is based in the article: Angulo-Martínez, M., López-Vicente, M., Vicente-Serrano, S.M., Beguería, S., 2009. Mapping rainfall erosivity at a regional scale: a comparison of interpolation methods in the Ebro Basin (NE Spain). *Hydrology and Earth Systems Science*, 13, 1907-1920.



techniques to map the factors of the RUSLE equation by means of interpolation methods (Shi, 2004; Lim, 2005; Mutua, 2006; López-Vicente *et al.* 2008). There are a number of statistical methods available, such as regression models; local interpolators such as the inverse distance weighting (IDW) or thin-plate splines, or geostatistical techniques such as kriging (Burrough and McDonnell, 1998). Recent studies, mostly in the field of Climatology (e.g., Ninyerola and Pons, 2000; Vicente-Serrano *et al.* 2003; Beguería and Vicente-Serrano, 2006), highlighted the interest of finding the method with the best adjustment to the observed data.

There are few studies comparing among interpolation techniques for rainfall erosivity indices. Millward (1999) calculated the  $EI_{30}$  index at the monthly scale and the R factor with geostatistics and IDW techniques for the Algarve region (Southern Portugal). Hoyos (2005) observed that a local polynomial algorithm gave lower mean prediction errors than the IDW in the Colombian Andes. Goovaerts (1999) discussed the relation between rainfall erosivity and elevation in the comparison of three different geostatistical methods. None of these works provided a comprehensive comparison of mapping methods at the regional scale.

This work aims at comparing different interpolation methods to map the RUSLE R factor and the average  $EI_{30}$  index of the erosive events in the study area; the Ebro basin (NE Spain), a large and climatologically complex area. Results of rainfall erosivity cartography can be used as a reference for soil protection practices and discussion of the different interpolation methods will be of interest to enhance regional and basin cartography.

For this study we used database (i), described in section 2.4. Rainfall erosivity index  $EI_{30}$  and R factor were calculated using the methodology explained in section 2.3.

The average  $EI_{30}$ , is calculated as the mean erosivity of all rainfall events. Since the frequency distribution of  $EI_{30}$  is highly skewed (it follows a logarithmic law), the average  $EI_{30}$  is in fact most correlated with the highest erosive events. Maps showing the spatial distribution of the average  $EI_{30}$  index complement the information given by the R factor alone.



### 2.7.1. Spatial modelling

In many studies the rainfall erosivity calculation is reduced to at-site analysis. An improvement focus on the reduction of the risk of erosion in landscape management and conservation planning is to obtain continuous maps for large areas as a preliminary step to evaluate the hazard. For this purpose a common procedure is the mapping of at-site estimated rainfall erosivity index values by means of interpolation techniques (e.g., Prudhome and Reed, 1999; Weisse and Bois, 2002).

In this article several interpolation methods including global, local and mixed approaches, are compared in order to determine which one describes better the spatial distribution of the average  $EL_{30}$  index and the R factor. A leave-one-out cross-validation technique was used for validating the goodness of fit (Efron and Tibshirani, 1997).

For the regression-based models, a digital elevation model (DEM) and a digital coverage of the Iberian Peninsula coastline were used. Both were obtained from the Ebro Hydrographical Confederation (<http://www.chebro.es/>).

#### *Global methods*

The global method used was generalized least squares (GLS) multiple regression. Regression is a global approach to spatial interpolation, and it is based on finding empirical relationships between the variable of interest and other spatial variables. Regression-based techniques adapt to almost any space and usually generate adequate maps (Goodale *et al.* 1998; Vogt *et al.* 1997; Ninyerola *et al.* 2000). The relationships between climatic data and topographic and geographic variables have been extensively analyzed throughout the scientific literature, and regression-based models allow exploiting this relationship to produce maps of the climatic parameters. Some authors have shown the advantages of incorporating the information provided by ancillary data on mapping extreme rainfall probabilities (Beguería and Vicente-Serrano, 2006; Casas *et al.*, 2007). Regression methods can be especially adequate in large regions with complex atmospheric influences, such as the Ebro Valley (Daly *et al.*, 2002; Weisse and Bois, 2002; Vicente-Serrano *et al.*, 2003), or if the sample network is not dense enough for local interpolation methods (Dirks *et al.*, 1998).



GLS is an extension of the most common ordinary least squares (OLS) regression, which allows for autocorrelation in the dependent variable (Cressie, 1993). When dealing with spatial variables, it is common assumption that the observations are autocorrelated; this property forms, in fact, the basis of all geostatistical and mixed methods. The existence of autocorrelation in the residuals violates one of the main assumptions of OLS, thus making this technique not suitable for climatic variables with geographical imprint. This problem can be easily solved by using alternative regression techniques that account explicitly for spatial autocorrelation, such as GLS (Beguería and Pueyo, 2009). The differences between both methods can be easily explained by introducing their mathematical background. From the common OLS formula:

$$y = X\beta + \varepsilon, \quad (2.23)$$

where  $y$  is the dependent variable,  $X$  is a matrix of  $p$  independent variables (model matrix),  $\beta$  is a vector of  $p+1$  model coefficients to estimate, including a constant  $\beta_0$ , and  $\varepsilon$  is a vector of random errors. In OLS it is assumed that the errors are normally distributed with mean 0 and variance  $I:\varepsilon \sim N(0, \sigma^2 I)$ . In GLS, on the contrary, it is generally assumed that  $\varepsilon \sim N(0, \Sigma)$ , where the error variance-covariance matrix  $\Sigma$  is symmetric and positive-definite. Different diagonal entries in  $\Sigma$  correspond to non-constant error variances, while nonzero off-diagonal entries correspond to correlated errors. Since the error variance-covariance matrix  $\Sigma$  is not known, it must be estimated from the data along with the regression coefficients  $\beta$ . Due to the high number of elements of  $\Sigma$ , it needs to be approximated by a parametric model. In the case of spatial regression,  $\Sigma$  can be adequately parameterized by a semi-variogram model. The semi-variogram model explains the covariance between the errors based on the distance between pairwise observations. Since the semivariogram constitutes the basis of geostatistical interpolation methods, it is explained in depth in a further section (see section *Geostatistical interpolation methods*).

We used a set of independent variables at a spatial resolution of 100 m. Elevation is usually the main determinant of the spatial distribution of climatic variables. Nevertheless, other variables such as the latitude and longitude, or the incoming solar radiation may also have an influence on the distribution of erosive rains. All variables were derived from a DEM (UTM-30N coordinates). The incoming solar radiation is a spatially continuous variable that depends on the terrain aspect



(northern and southern slopes have low and high incoming solar radiation values, respectively). The annual mean incoming solar radiation was calculated following the algorithm of Pons and Ninyerola (2008). All these variables were processed in the MiraMon GIS package (Pons, 2006). Low-pass filters with radii of 5, 10 and 25 km were applied to elevation, slope and incoming solar radiation in order to measure the widest influence of these variables.

We used a Gaussian semivariogram model to parameterize the spatial autocorrelation between regression errors. As independent variables we used the spatial coordinates (longitude and latitude) in km and their squares ( $\text{km}^2$ ), the elevation (m a.s.l.), and the incoming solar radiation ( $\text{J d}^{-1}$ ). The R statistical analysis package (R Development Core Team, 2008) was used for the regression analysis.

### *Local methods*

In global methods, local variations are dismissed as random, unstructured noise, and the climatic map is created on the basis of general structure of the variable at all available points (Borrough and McDonnell, 1998). Local methods, on the contrary, use only the data of the nearest sampling points for climatic mapping. Since interpolated values at ungauged locations depend on the observed values, local methods strongly depend on a sufficiently dense and evenly spaced sampling network.

Two local methods were used: inverse distance weighting (IDW) and splines. The IDW interpolation is based on the assumption that the climatic value at an unsampled point  $\hat{z}(x)$  is a distance-weighting average of the climatic values at nearby sampling points  $\hat{z}(x_1), \hat{z}(x_2), \dots, \hat{z}(x_n)$ . Climatic values are more similar at closer distances, so the inverse distance ( $1/d_i$ ) between  $\hat{z}(x_i)$  and  $\hat{z}(x)$  is used as the weighting factor:

$$\hat{z}(x) = \frac{\sum_{i=1}^n z(x_i) d_{ij}^{-r}}{\sum_{i=1}^n d_{ij}^{-r}}, \quad (2.24)$$

where  $\hat{z}(x)$  is the predicted value,  $\hat{z}(x_i)$  is the climatic value at a neighbouring weather station,  $d_{ij}$  is the distance between  $\hat{z}(x)$  and  $\hat{z}(x_i)$ , and  $r$  is an empirical parameter. Models with  $r = 1, r = 2$  and  $r = 3$  were tested.



The splines method is based on a family of continuous, regular and derivable functions. Splines are similar to the equations obtained from the trend surfaces or regression-based methods, but they are fitted locally from the neighbouring points around the candidate location  $x$ . A new function is created for each location  $x$ , without loss of continuity properties among the curves. Smoothing or tension parameters can be specified, resulting in more or less smoothed maps. The predicted value  $\hat{z}(x)$  is determined by two terms:

$$z(x) = T(x) + \sum_{i=1}^n \lambda_j \psi_j(r_i), \quad (2.25)$$

where  $T(x)$  is a polynomial smoothing term, and the second term groups a series of radial functions where  $\psi_j(r_i)$  is a known group of functions, and  $\lambda_j$  represents the parameters (Mitasova *et al.*, 1995):

$$\psi(r_i) = -\left[ \ln\left(\frac{\varphi r_i}{2}\right) + E_i \left(\frac{\varphi r_i}{2}\right) + C_E \right], \quad (2.26)$$

where  $\varphi$  is the tension coefficient,  $C_E = 0.577215\dots$  is the Euler constant,  $E_i$  is the exponential integral function, and  $r_i$  is:

$$r_i = \sqrt{(x - x_i)^2 + (y - y_i)^2}, \quad (2.27)$$

The algorithms for fitting splines are quite complex but are currently standard in GIS packages. In this paper several spline interpolations were used as implemented in the ArcGIS 9.3 software. Tension and smoothing parameters were  $\varphi = 400$ ,  $\varphi = 5000$ ,  $T(x) = 0$  and  $T(x) = 400$ .

### *Geostatistical interpolation methods*

Kriging methods assume that the spatial variation of a continuous climatic variable is too irregular to be modelled by a continuous mathematical function, and its spatial variation could be better predicted by a probabilistic surface. This continuous variable is called a regionalized variable, which consists of a drift component and a random, spatially correlated component (Burrough and McDonnell, 1998). Hence, the spatially located climatic variable  $\hat{z}(x)$  is expressed by:



$$z(x) = m(x) + \varepsilon'(x) + \varepsilon'', \quad (2.28)$$

where  $m(x)$  is the drift component, i.e. the structural variation of the climatic variable,  $\varepsilon'(x)$  are the spatially correlated residuals, i.e. the difference between the drift component and the sampling data values, and  $\varepsilon''$  are spatially independent residuals. The predictions of kriging-based methods are currently a weighted average of the data available at neighbouring sampling points (weather stations). The weighting is chosen so that the calculation is not biased and the variance is minimal. A function that relates the spatial variance of the variable is determined using a semi-variogram model which indicates the semivariance ( $\gamma$ ) between the climatic values at different spatial distances.

The semivariogram describes the way in which similar observation values are clustered in space, in accordance with Tobler's first law of geography (Tobler, 1970). The semivariogram is therefore a measure of the dissimilarity of data pairs as the spatial separation between them increases (Deutsch and Journel, 1998). The semivariance is calculated for lagged sets of separation vectors  $h_u$  as half the mean squared pairwise difference between the  $N$  observed values within the spatial lag,  $u$ :

$$\gamma_u(h_u) = \frac{1}{2N(h_u)} \sum_{N(h_u)} [z(u) - z(u + h_u)]^2, \quad (2.29)$$

To summarize the autocorrelation in space, a product-sum covariance model was automatically fitted to the semivariogram. First, only the sample semivariograms,  $\gamma_{s,u}(h_s, \theta)$ , were considered. Valid semivariogram models were fitted to them, estimating automatically the partial range ( $\theta_u$ ) and sill ( $sill_u$ ) and adding a nugget discontinuity ( $\tau_u$ ) at the origin to reflect spatial uncertainty if required. Semivariogram models must be selected from a set of allowable functions that are conditionally negative definite (McBratney and Webster, 1986), i.e. spherical, exponential or gaussian models (Deutsch and Journel, 1998). There is some argument over the correct way to proceed in semivariogram model fitting (Diggle *et al.*, 2002; Goovaerts, 1997); we favoured automatically fitting by the OLS method, followed by adjustment by eye, to reduce the effect of outliers. The Gaussian function adjusted best. Predictions may improve depending in the number of neighbours included in the interpolation. Our data were not very sensible to the number of neighbours. A combination of 9 neighbours, including at least 3 fitted best.



Several types of kriging methods have been proposed, depending on how the drift component  $m(x)$  is modelled (see, e.g., the reviews by Isaaks and Strivastava, 1989; Goovaerts, 1997; Burrough and McDonnell, 1998). *Simple kriging* (SK) assumes a known constant trend (expected value),  $m(x) = 0$ , and relies on a covariance function. However, neither the expectation nor the covariance function are usually known, so simple kriging is seldom used. In *ordinary kriging* (OK), the most common type of kriging, an unknown constant trend is assumed,  $m(x) = E(z(x))$ , and the estimation relies on a semivariogram model which is estimated from the sample.

SK and OK both assume stationarity of the spatial field, i.e. that the expected value of the variable does not change in space. This is often not the case with climatic variables, which tend to show spatial trends due to differences in the exposure to the atmospheric factors. *Universal kriging* (UK) allows incorporating non-stationarity by assuming a general linear trend model,

$$m(x) = \sum_{k=0}^p \beta_k f(x), \quad (2.30)$$

where  $p$  defines the order of the polynomial model on the spatial coordinates of the point,  $f(x)$ . This process is often called trend removal, and it is interesting because it can capture a real spatial structure present in the data. However, it increases the complexity of the kriging model by adding more parameters for estimation. A two-dimensional quadratic surface, for example, adds five parameters beyond the intercept parameter that need to be estimated. As it is well known, the more parameters to be estimated, the more uncertain the model becomes.

Spatial structure can also arise in climatic data due to co-variation with other geographical factors such as the elevation or the solar incoming radiation. *Co-kriging* (CK) allows considering the influence of external variables (co-variates) by analysing the cross-correlation between the errors of the different variables,  $\varepsilon_1'(x)$ ,  $\varepsilon_2'(x)$ , etc.

Spatial correlation may occur at different distances when different directions are considered; this characteristic is called *anisotropy*. Since the Ebro basin has a marked NW-SE structure, the effect of including anisotropy in the model was also evaluated.



In our study we compared OK, UK and CK methods. The order of the trend removal component in UK was determined by the lowest root mean square error, computed by a leave-one-out bootstrap process. In the case of CK we used the elevation, as determined by a digital terrain model (DTM), as the spatially distributed co-variate; the kriging method used was the best one from the previous methods, i.e. OK and UK. All geostatistical analyses were done with the ArcGIS 9.3 software.

### *Mixed methods*

Mixed methods, also called “hybrid” (Hengl *et al.* 2004), are based on a combination of regression and local interpolation techniques or kriging, exploiting the ability of regression to relate the target variable to other spatially distributed variables and the spatial self-correlation acting at the local scale on most spatial variables. Alternative forms of mixed methods have been proposed in the last years for mapping environmental variables (Odeh *et al.*, 1994, 1995; Brown and Comrie, 2002; McBratney *et al.*, 2003; Hengl *et al.*, 2004; Ninyerola *et al.*, 2007; Vicente-Serrano *et al.*, 2007). These and other studies have demonstrated that mixed methods usually allow for more precise and detailed representations of the target variables.

There are several types of mixed interpolation methods which vary upon their procedure. When regression residuals ( $\epsilon$ ) are interpolated by means of kriging two methods can be used: i) in *kriging with external drift* (KED), the drift component is defined by regression upon some auxiliary variables and fitted together with the spatial distribution of the residuals (Wackernagel, 1998; Chiles and Delfiner, 1999); ii) in *regression-kriging* (RK) the drift and the residuals are fitted separately and then summed (Ahmed and Marsily, 1987; Odeh *et al.*, 1994, 1995). Other kind of mixed methods interpolate residuals using local methods as the inverse distance weighting interpolation or splines (Vicente-Serrano *et al.*, 2003; Ninyerola *et al.*, 2007).

In this study we used RK. To avoid misconceptions or sub-optimal solutions (Hengl *et al.* 2004), regression predictions were calculated by means of GLS (see section 2.4.1.), and then residuals surfaces were fitted by OK and added to the GLS predictions. The R statistical analysis package (R Development Core Team, 2008) was used for RK.



### 2.7.2. Local uncertainty assessment

Spatial modelling involves uncertainty associated to the continuous estimated surface. Estimating the standard error of the predictions is necessary for completing the spatial modelling. In the case of spatial variables the problem is more complex, since the standard error of the predictions is also a spatial variable (Goovaerts, 2001). In this study we have used the technique called Gaussian geostatistical simulation (GGS). GSS generates multiple, equally probable representations of the spatial distribution of the attribute under study. A normal score transformation is performed on the data so that it will follow a standard normal distribution ( $\text{mean} = 0$  and  $\sigma^2 = 1$ ). Conditional simulations are then run on this normally distributed data, and the results are back-transformed to obtain simulated output in the original units. Given a high enough number of simulations, its average will tend to equal the surface estimated by SK. The standard deviation of the simulations is taken as an estimator of the standard error of the estimated surface, from which confidence bands can be constructed. These representations provide a way to measure uncertainty for the unsampled locations taken all together in space rather than one by one (as measured by the kriging variance). We performed a series of 1000 conditioned simulations from an initial SK model with second order trend removal. GGS was performed with the ArcGIS 9.3 software.

### 2.7.3. Validation statistics

The resulting maps were compared by using a set of validation statistics described in section 2.5. A leave-one-out procedure was used, consisting in fitting the model  $n-1$  times— $n$  being the number of observations in the data set—, each time one observation is left out of the fitting sample. These observations are used to calculate the model residuals, i.e. the difference between the predicted and the observed values. Cross-validation techniques are preferred to more traditional split-sample procedures for estimating generalization error, since they allow an independent validation without sacrificing an important amount of data (Weiss and Kulikowski, 1991). Cross-validation is compulsory when comparing exact interpolators such as IDW or splines, which by definition give an exact value at the locations used for fitting the model, i.e. all residuals at these points are zero.



## 2.7.4 Results

The spatial structure of the data was initially assessed by empirical semivariograms, (Figure 2.13). Spatial autocorrelation was present for both variables at relatively short distances (less than 15 km). Above this distance the spatial autocorrelation disappeared, as it was also visible in the fitted Gaussian semivariogram models.

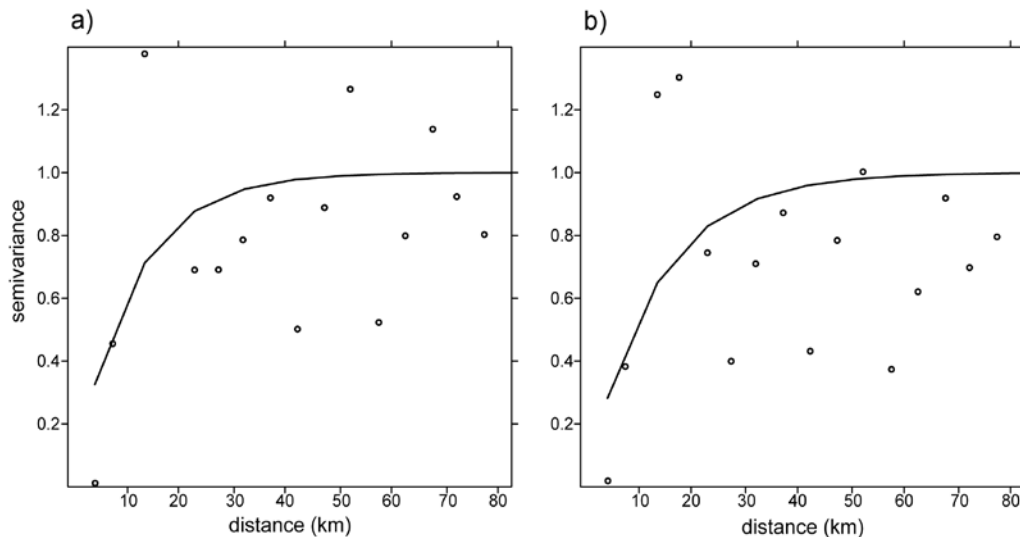


Figure 2.13: Empirical semivariograms (circles) and fitted semivariogram Gaussian models (lines) of the rainfall erosivity indices: A) R factor; B)  $EI_{30}$  index. Range parameters are: 10.98 km (R factor) and 13.05 km ( $EI_{30}$  index).

All interpolation methods were able to capture the regional distribution of the two rainfall erosivity parameters (Figures 2.14 y 2.15). Differences between interpolation methods were more evident for the  $EI_{30}$  index than for the R factor. The R factor was highest—from 1200 to 4500 MJ mm  $ha^{-1} h^{-1} y^{-1}$ —in two areas: i) in the Pyrenees Range at the north, especially in the central part; and ii) in the south-east mountainous part, corresponding to the Iberian Range and the southern east region. The lowest values—from 40 to 800 MJ mm  $ha^{-1} h^{-1} y^{-1}$ —appeared in the north-west of the area and in the centre of the Ebro River valley. The spatial distribution of the  $EI_{30}$  index was slightly different, showing a gradient from the north-west (Cantabrian Sea) to the south-east (Mediterranean Sea), modified to a certain extent by the relief. The highest values—from 70 to 190 MJ mm  $ha^{-1} h^{-1}$ —were found in the south-east corner, along the coast. Lower values—from 8 to 40 MJ mm  $ha^{-1} h^{-1}$ —are found close to the Cantabrian



Sea. This pattern is similar to the distribution of the extreme rainfall events in the region (Beguería *et al.*, 2009), and is an indicator of the  $EI_{30}$  index being closely related to the most intense rainfall events.

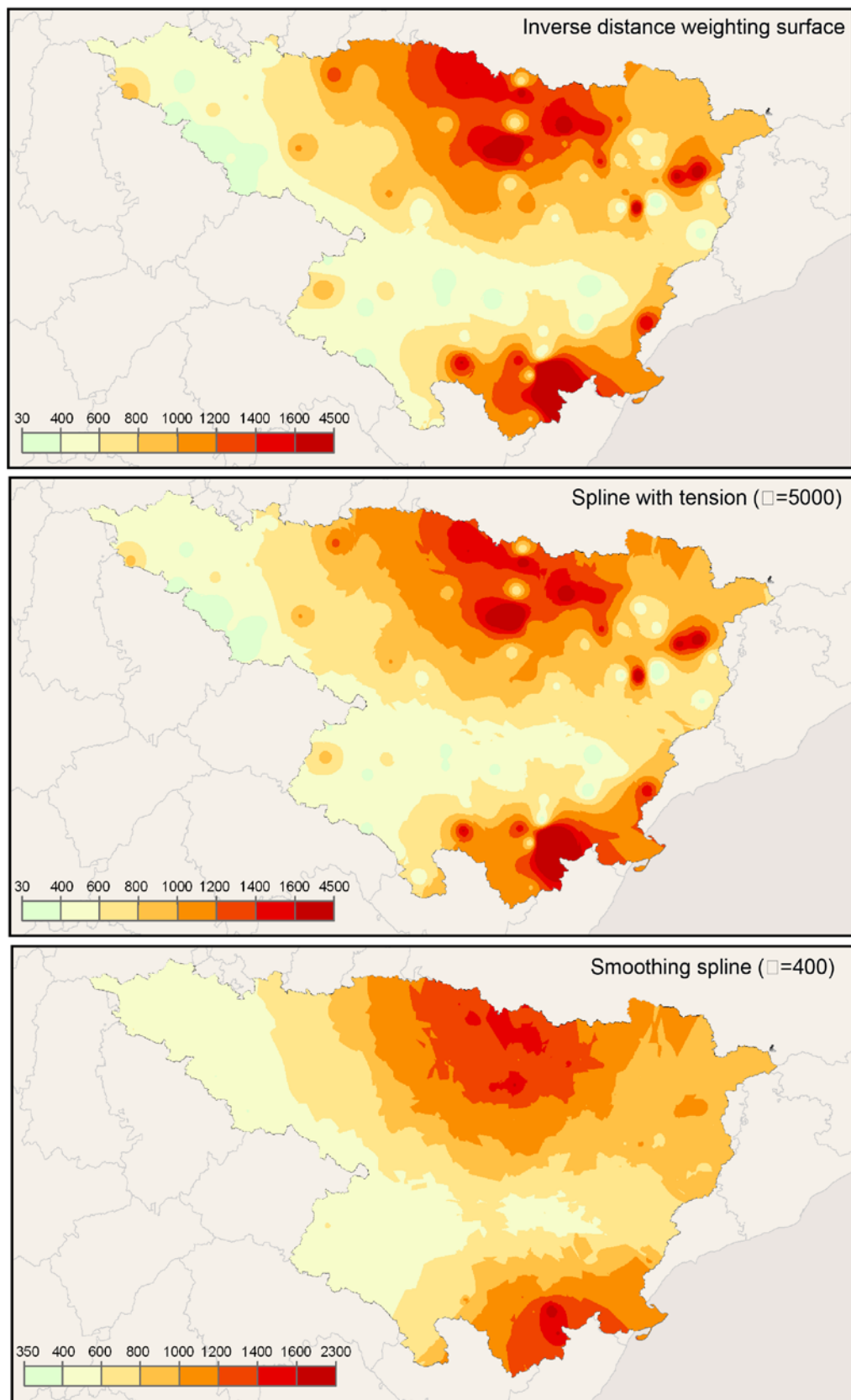


Figure 2.14: Rainfall erosivity maps (RUSLE R factor; MJ mm ha<sup>-1</sup> h<sup>-1</sup> y<sup>-1</sup>) for the Ebro Basin: a) inverse distance weighting surface; b) spline with tension ( $\varphi = 5000$ ); c) smoothing spline ( $\varphi = 400$ ).

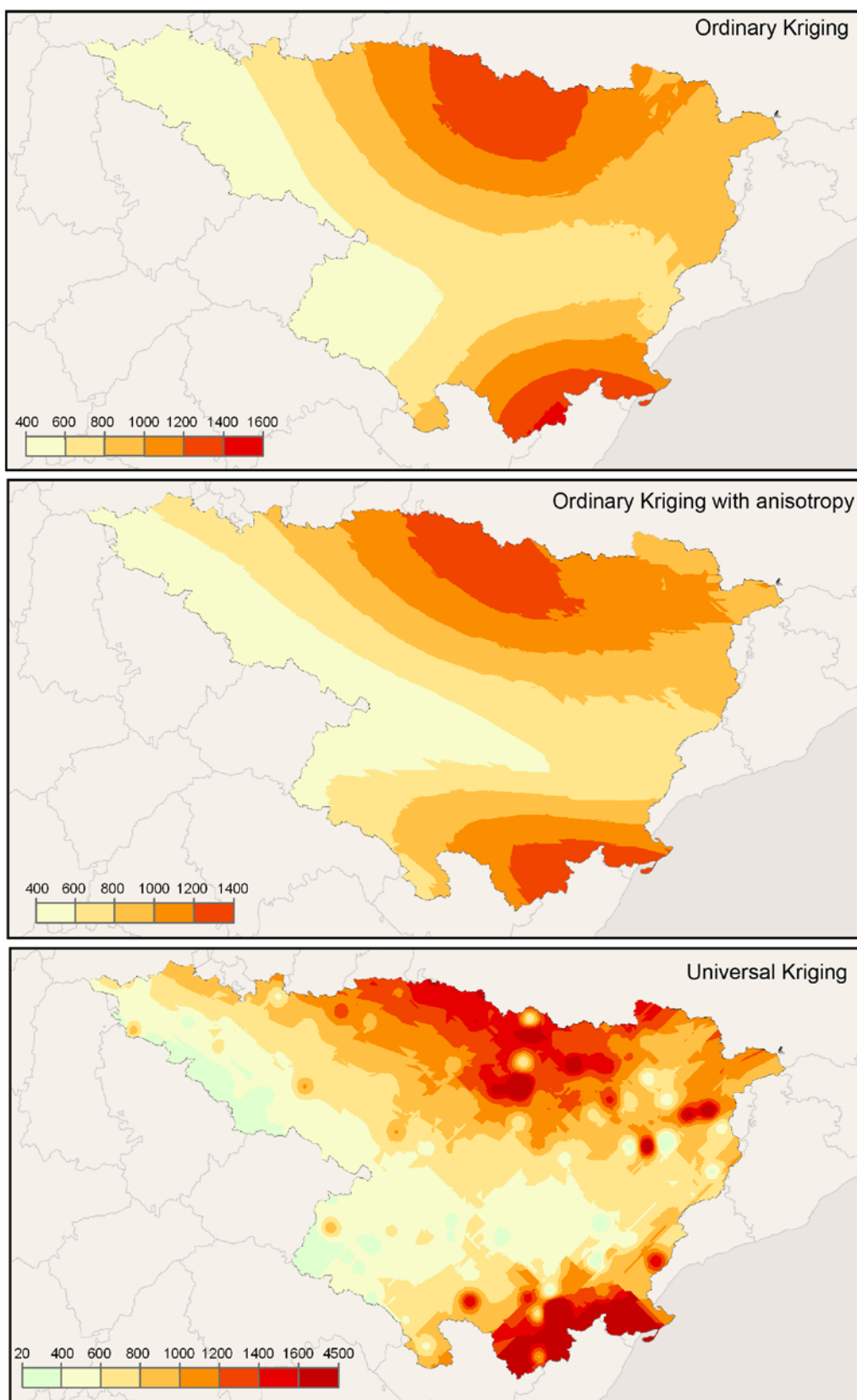


Figure 2.14 (cont.): Rainfall erosivity maps (RUSLE R factor;  $\text{MJ mm ha}^{-1} \text{h}^{-1} \text{y}^{-1}$ ) for the Ebro Basin: d) ordinary kriging (OK); e) ordinary kriging with anisotropy; f) universal kriging (UK).

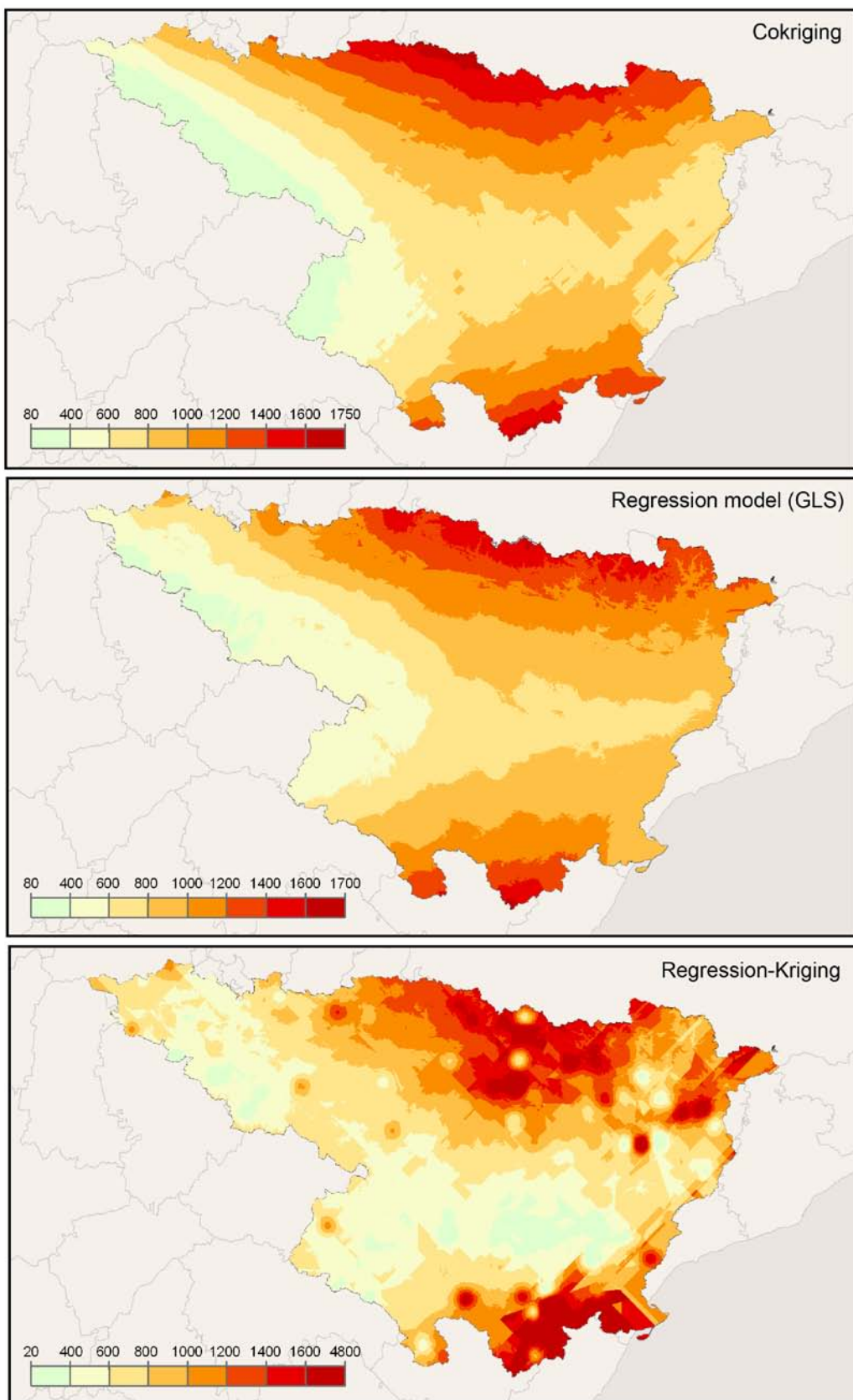


Figure 2.14 (cont.): Rainfall erosivity maps (RUSLE R factor; MJ mm ha<sup>-1</sup> h<sup>-1</sup> y<sup>-1</sup>) for the Ebro Basin: g) co-kriging (CK); h) regression model (GLS); i) regression-kriging (RK).

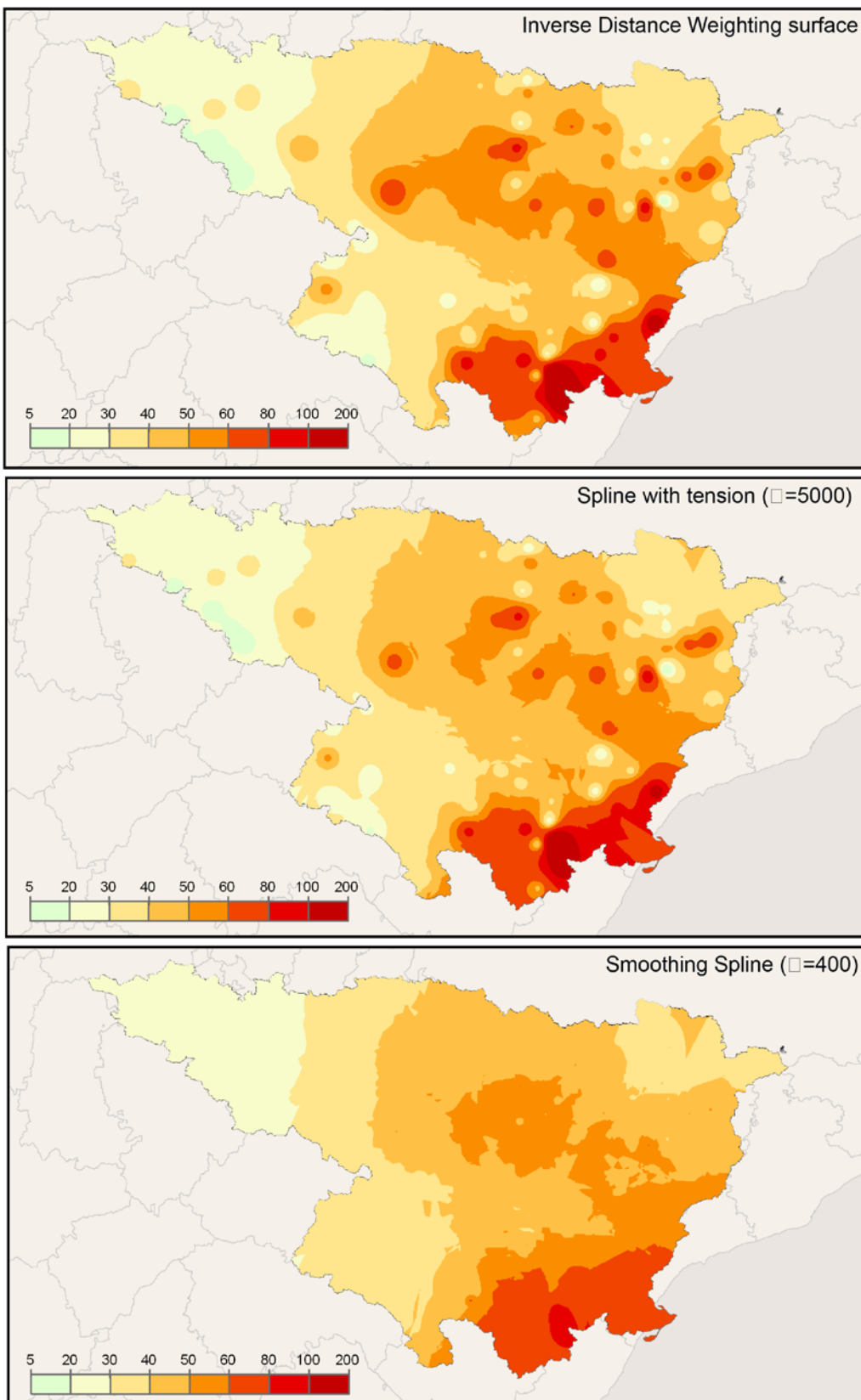


Figure 2.15: Rainfall erosivity maps (average *EI30* index of the erosive events; MJ mm ha<sup>-1</sup> h<sup>-1</sup>) for the Ebro Basin: a) inverse distance weighting surface; b) spline with tension ( $\varphi = 5000$ ); c) smoothing spline ( $\varphi = 400$ ).

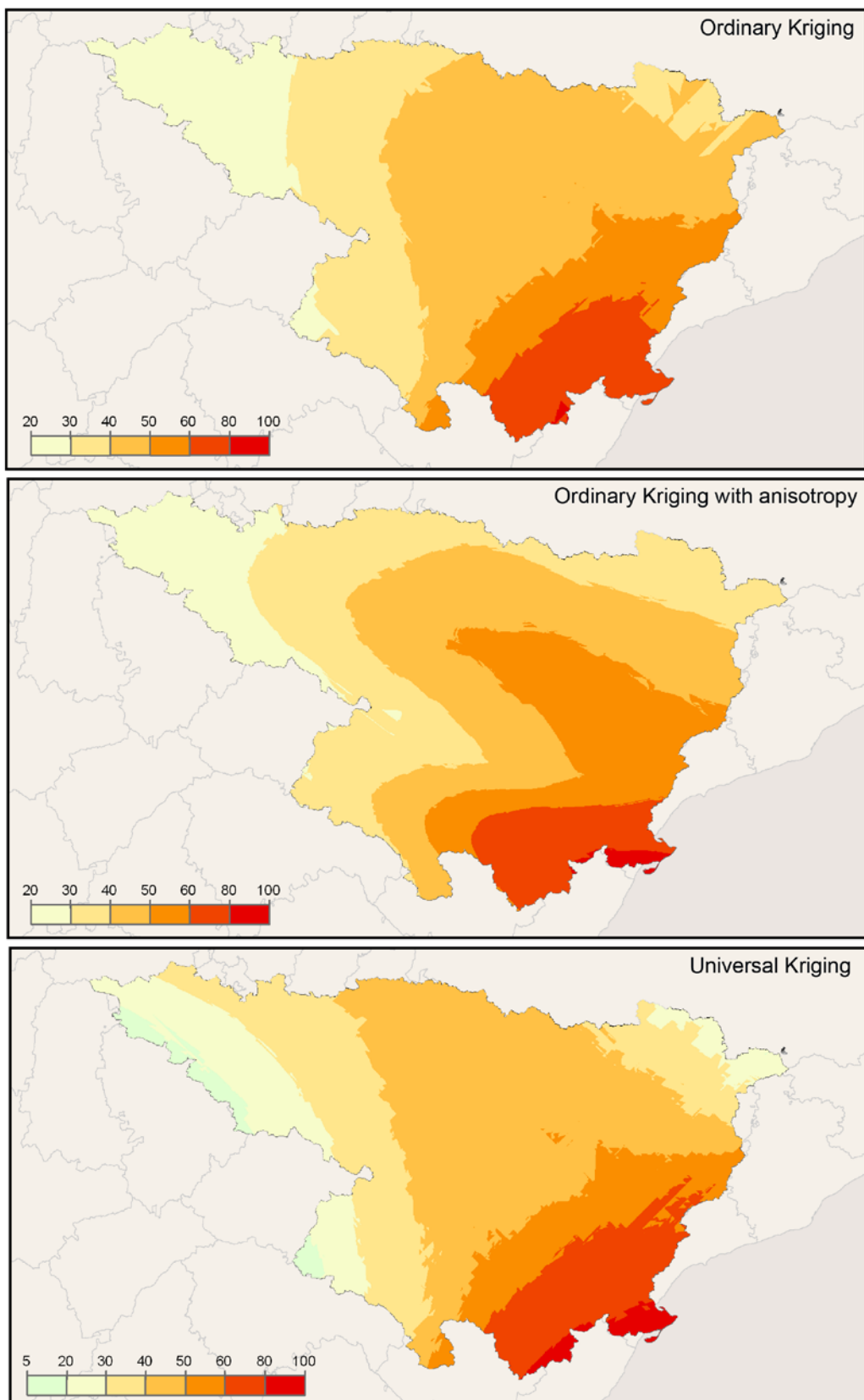


Figure 2.15 (cont.): Rainfall erosivity maps (average  $EI_{30}$  index of the erosive events;  $MJ mm ha^{-1} h^{-1}$ ) for the Ebro Basin: d) ordinary kriging (OK); e) ordinary kriging with anisotropy; f) universal kriging (UK).

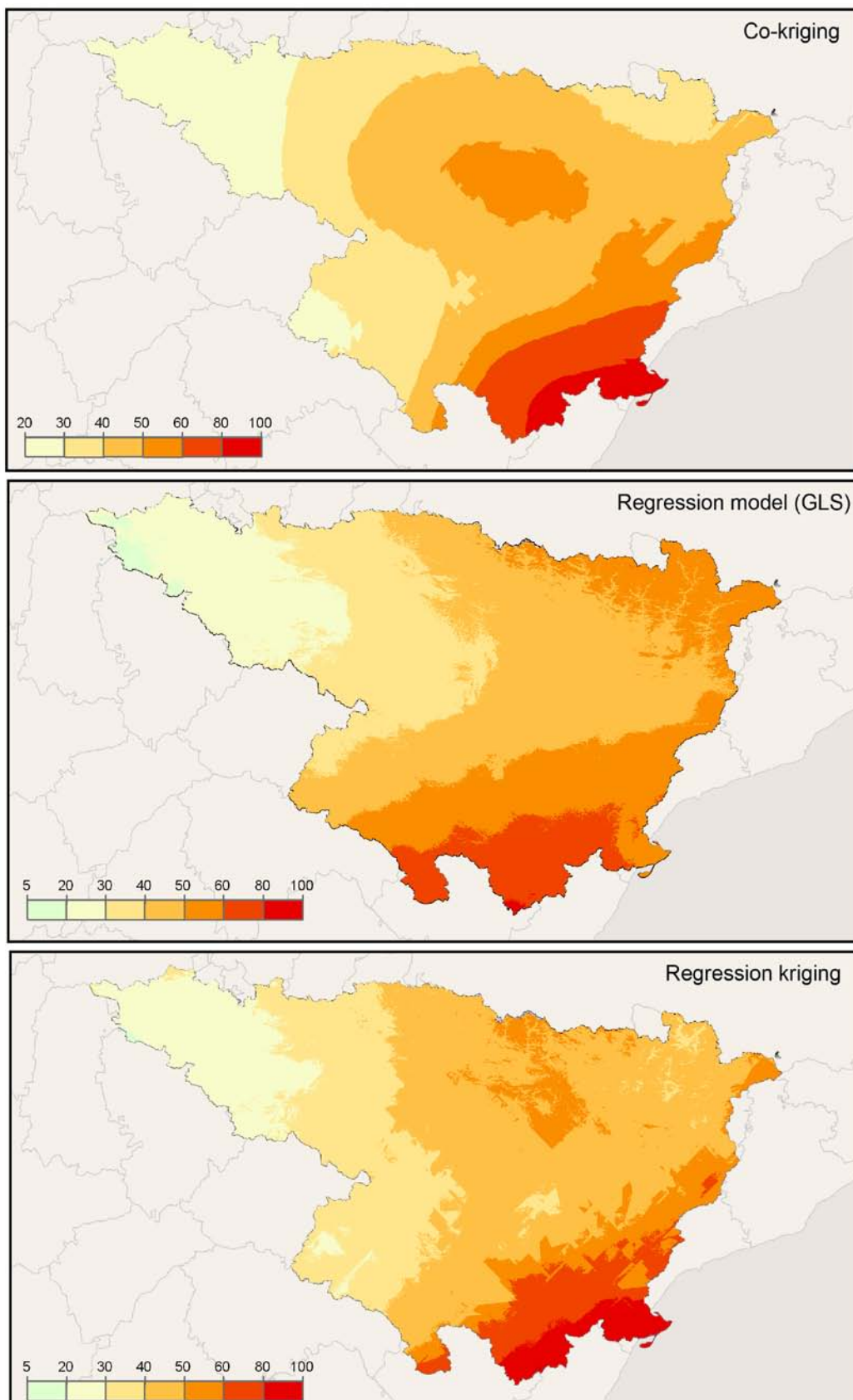


Figure 2.15 (cont.): Rainfall erosivity maps (average  $EI_{30}$  index of the erosive events; MJ  $mm\ ha^{-1}\ h^{-1}$ ) for the Ebro Basin: g) co-kriging (CK); h) regression model (GLS); i) regression-kriging (RK).



The spatial distribution of both indices over the study area can be explained to a large extent by the proximity to—or isolation from—the water masses (the Cantabrian and Mediterranean seas). The relief, with mountain ranges to the north, south and east of the region, modify this general pattern by increasing rainfall in those areas. Another effect of the relief is the isolation of the central area from the main rainfall sources, i.e. creating a zone of rain shadow.

Despite the general spatial pattern, differences were evident between the models. The maps produced by the local methods—IDW and Spline with tension—were very much influenced by individual observations. In most cases, local variance can be associated with the occurrence of anomalous events or very specific conditions, and might not reflect the general pattern adequately. The maps produced by these two methods varied slightly depending on the value of the  $r$  and  $\psi$  parameters (maps not shown), but in all cases they had this characteristic. The smoothed splines method, which includes a smoothing function to reduce excessive influence of local observations, produced a more regularized output.

Geostatistical methods—OK, OK with anisotropy and CK—produced much more smoothed results than the local methods, yet retaining a good degree of detail. Anisotropy modified only slightly the results from OK by orienting the estimated surface in the direction NW-SE. The R factor map resulting from UK—detrending the data by a second order polynomial—was very similar to the surfaces generated by local interpolators, i.e. it showed a high influence of local observations. The result of CK—OK with elevation as a covariate—showed only a marginal increase in detail with respect to OK.

The surface generated by GLS regression was similar to the CK surface. The regression models were significant at  $\alpha = 0.05$ , although the coefficient of determination ( $r^2$ ) of the models was not high (0.212 for the R factor and 0.218 for the  $EI30$  index). The only significant variables at  $\alpha = 0.05$  were the spatial coordinates, and just for the R factor, revealing the poor explanatory capacity of other auxiliary variables—elevation and solar radiation (Table 2.7). This was also evident by the low values of the beta coefficients of these two variables.

In the maps obtained by regression-kriging (RK) the influence of the interpolation of the residuals was evident. The predicted map was very similar to



the UK surface, especially in the case of the R factor. In the  $EI_{30}$  index maps the influence of elevation and radiation could be easily noticed.

Table 2.7. Results of the generalized least squares regression of the R factor and the  $EI_{30}$  index: regression coefficients, standardized coefficients and significance level for each independent variable.

Variable	Beta coeff.	Standardized coeff.	beta	Significance level
<b>R factor</b>				
longitude	14.411	2.658		0.023*
longitude <sup>2</sup>	-21.803	-2.582		0.219
latitude	-0.010	-2.380		0.041*
latitude <sup>2</sup>	0.003	2.744		0.191
elevation	0.087	0.047		0.579
solar radiation	-201.853	-0.031		0.732
<b><math>EI_{30}</math> index</b>				
longitude	0.255	1.132		0.304
longitude <sup>2</sup>	-0.849	-2.418		0.239
latitude	-0.0001	-0.861		0.432
latitude <sup>2</sup>	0.0001	2.166		0.291
elevation	0.003	0.045		0.593
solar radiation	0.691	0.003		0.977

\* variable is significant at confidence level  $\alpha = 0.05$

## 2.7.5. Validation

All methods underestimated the standard deviation of the R factor and the  $EI_{30}$  indices, resulting in relatively poor predictions (Tables 2.5 and 2.6). The observed standard deviation was 621.7 for the R factor, which varied in the range 40–4500 MJ mm ha<sup>-1</sup> h<sup>-1</sup> y<sup>-1</sup>, and 23.8 for  $EI_{30}$ , which varied in the range 8–190 MJ mm ha<sup>-1</sup> h<sup>-1</sup>. Compared with that, the standard deviation of the estimations ranged between 244.4 and 420.4 for R and 11.6 and 16.2 for  $EI_{30}$ . Consequently, all models had relatively large absolute errors, which were higher than 30% of the mean predicted value for most of them. Similarly, the values of the Willmott's *D* statistic were low. These facts reflect the high random character of both rainfall erosivity indices. The low performance of the models was mostly due to their inability to predict the highest values, especially those above 2000 MJ mm ha<sup>-1</sup> h<sup>-1</sup> y<sup>-1</sup> for R and 100 MJ mm ha<sup>-1</sup> h<sup>-1</sup> for  $EI_{30}$ , respectively. This can be clearly seen in the goodness of fit plots (Figures 2.16 and 2.17).

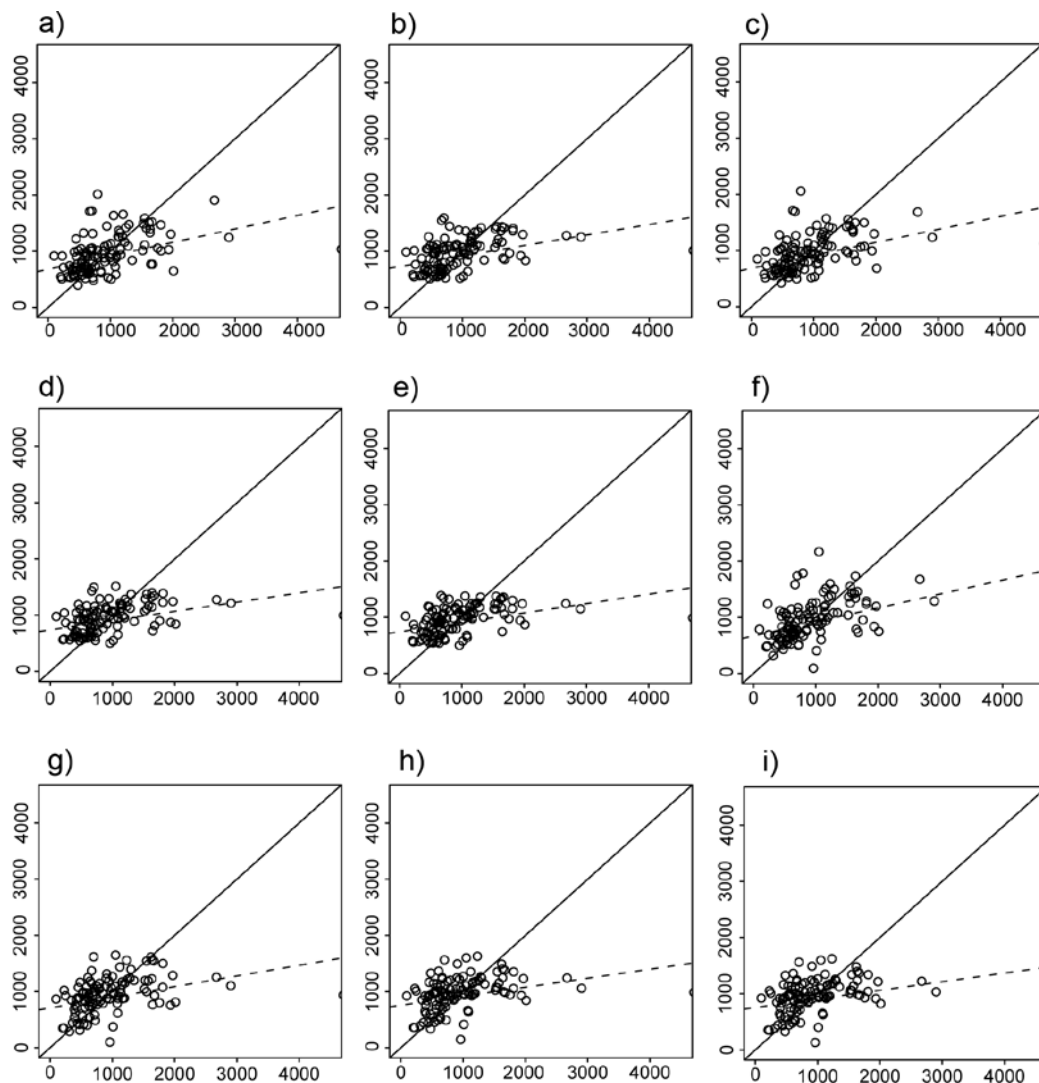


Figure 2.16: Comparison between observed (ordinate axis) and predicted (abscissa axis) values for the interpolation methods used for the spatial distribution of the R factor, line of perfect fit (continuous) and regression line (dashed). a) inverse distance weighting ( $r=2$ ); b) smoothing spline ( $\varphi = 400$ ); c) splines with tension ( $\varphi = 5000$ ); d) ordinary kriging; e) ordinary kriging with anisotropy; f) universal kriging; g) co-kriging; h) regression model (GLS); i) regression-kriging.

Differences between the models regarding the validation statistics were narrow, but allowed for a comparison. According to the validation statistics the local methods ranked best for both indices, showing highest Willmott's  $D$  values, and lowest MBE and MAE. The R factor was best predicted by inverse distance weighting with  $r=3$ , followed by universal kriging, whereas the  $EI_{30}$  index was best fitted by splines with tension ( $\varphi=5000$ ), followed by IDW with  $r=3$ . Geostatistical models yielded good results, especially Universal Kriging, equalled by Co-kriging (OK plus elevation) in the case of the  $EI_{30}$  index. The result of



including anisotropy in OK was only marginally better. Finally, regression based methods—GLS and RK—yielded the lowest validation statistics.

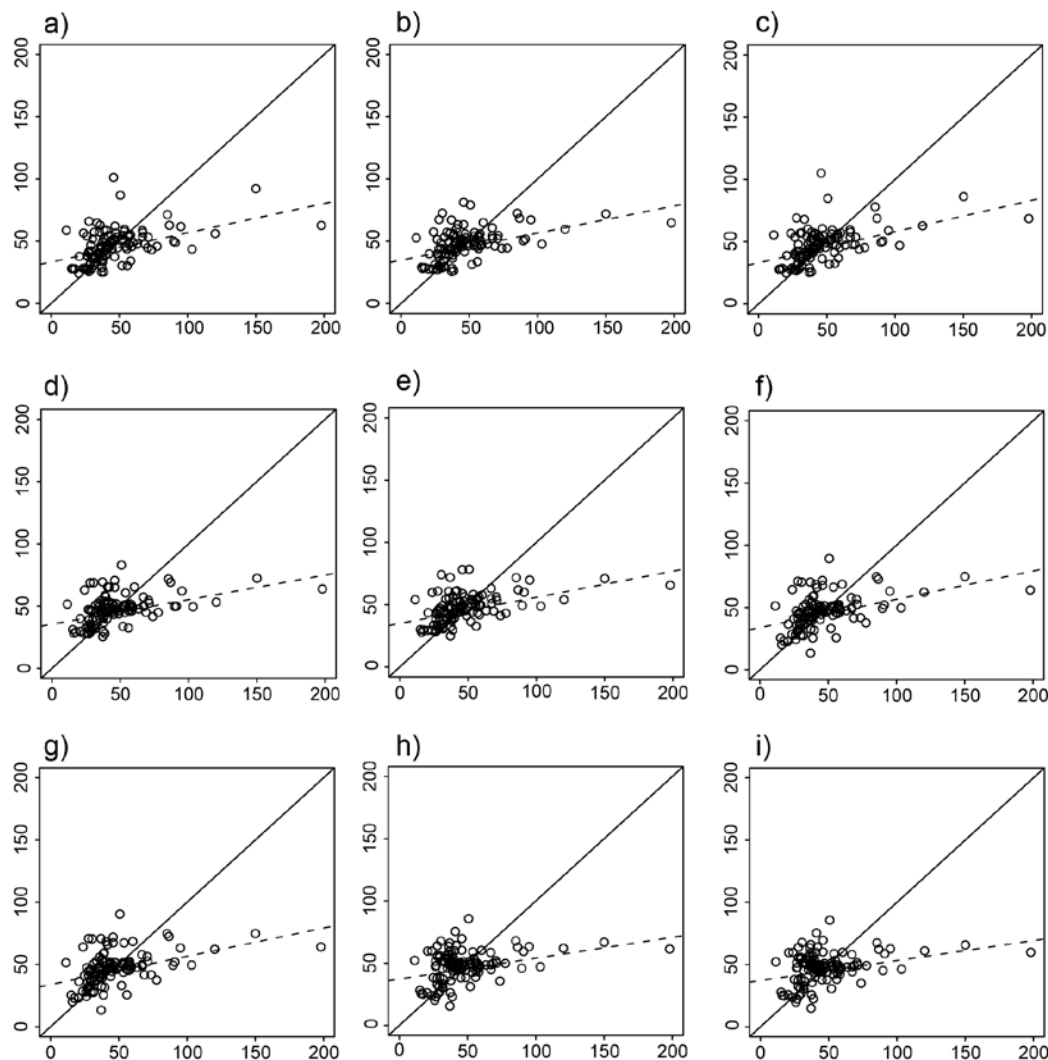


Figure 2.17: Comparison between observed (ordinate axis) and predicted (abscissa axis) values for the different interpolation methods used for the spatial distribution of the  $EI_{30}$  index, line of perfect fit (continuous) and regression line (dashed). a) inverse distance weighting ( $r=2$ ); b) smoothing spline ( $\varphi = 400$ ); c) splines with tension ( $\varphi = 5000$ ); d) ordinary kriging; e) ordinary kriging with anisotropy; f) universal kriging; g) co-kriging; h) regression model (GLS); i) regression-kriging.



Table 2.5: Accuracy measurements for the R factor models: mean and standard deviation of the observed and predicted values, and cross-validations statistics.

<b>Validation statistics</b>					
	<b>Mean</b>	<b>Standard deviation</b>	<b>MBE</b>	<b>MAE</b>	<b>Willmott's D</b>
Observed	891.40	621.77			
Predicted					
Inverse Distance Weighting ( $r = 1$ )	896.64	292.49	5.24	355.26	0.534
Inverse Distance Weighting ( $r = 2$ )	891.75	346.59	0.350	356.33	0.577
Inverse Distance Weighting ( $r = 3$ )	896.85	420.40	5.44	367.40	0.595
Smoothed splines [ $T(x,y) = 400$ ]	895.86	275.70	4.45	354.99	0.521
Splines with tension ( $\varphi = 400$ )	896.74	268.30	5.33	357.45	0.497
Splines with tension ( $\varphi = 5000$ )	890.21	324.54	-1.19	348.27	0.573
Ordinary kriging (OK)	885.37	252.11	-6.03	357.76	0.491
Ordinary kriging with anisotropy	890.06	244.41	-1.34	356.45	0.491
Universal kriging (UK)	890.60	359.08	-0.806	355.79	0.584
Co-kriging (OK + elev)	877.69	318.02	-13.71	369.52	0.513
Regression (GLS)	900.53	292.64	9.13	386.31	0.468
Regression-Kriging (GLS + residuals kriging)	910.60	292.02	19.20	385.16	0.480

Table 2.6: Accuracy measurements for the mean  $EI_{30}$  index: mean and standard deviation of the observed and predicted values, and cross-validations statistics.

<b>Validation statistics</b>					
	<b>Mean</b>	<b>Standard deviation</b>	<b>MBE</b>	<b>MAE</b>	<b>Willmott's D</b>
Observed	44.32	25.85			
Predicted					
Inverse Distance Weighting ( $r = 1$ )	44.23	12.17	-0.536	14.60	0.565
Inverse Distance Weighting ( $r = 2$ )	43.69	13.40	-0.635	14.62	0.582
Inverse Distance Weighting ( $r = 3$ )	43.82	16.22	-0.502	15.17	0.584
Smoothed splines [ $T(x,y) = 400$ ]	44.44	12.05	0.116	14.58	0.568
Splines with tension ( $\varphi = 400$ )	44.48	11.68	0.156	14.62	0.553
Splines with tension ( $\varphi = 5000$ )	44.11	13.40	-0.210	14.28	0.602
Ordinary kriging (OK)	44.18	11.57	-0.144	14.90	0.540
Ordinary kriging with anisotropy	44.23	11.60	-0.091	14.33	0.562
Universal kriging (UK)	43.93	13.38	-0.392	15.17	0.573
Co-kriging (OK + elev)	43.97	13.41	-0.357	15.18	0.573
Regression (GLS)	44.74	12.54	0.420	16.69	0.504
Regression-Kriging (GLS + residuals kriging)	45.18	12.51	0.853	16.62	0.515



### 2.7.6. Local uncertainty

The previous results evidenced the high level of uncertainty of the predictions of both erosivity indices. The uncertainty model, however, is also a spatial variable and can have strong differences between regions in the study area. The results of Gaussian geostatistical simulation (GGS) helped assessing spatial differences in the uncertainty model (Figure 2.18 and Figure 2.19). From 1000 equiprobable conditional simulations, mean and standard deviation surfaces were generated for the R factor and the  $EI_{30}$  index. Both surfaces showed the general pattern of their respective rainfall erosivity indices. Local uncertainty was quite high as showed by the standard error maps, where the magnitude of the error ranged between 10 and 100% of the mean value. The standard error increased rapidly for regions located more than  $\sim 15$  km away from any observatory, indicating that the range of the spatial influence of the observations was quite small. This was already suggested by the preliminary analysis of the semivariogram. From that distance, which was larger for the  $EI_{30}$  index than for the R factor, uncertainty distributed randomly.

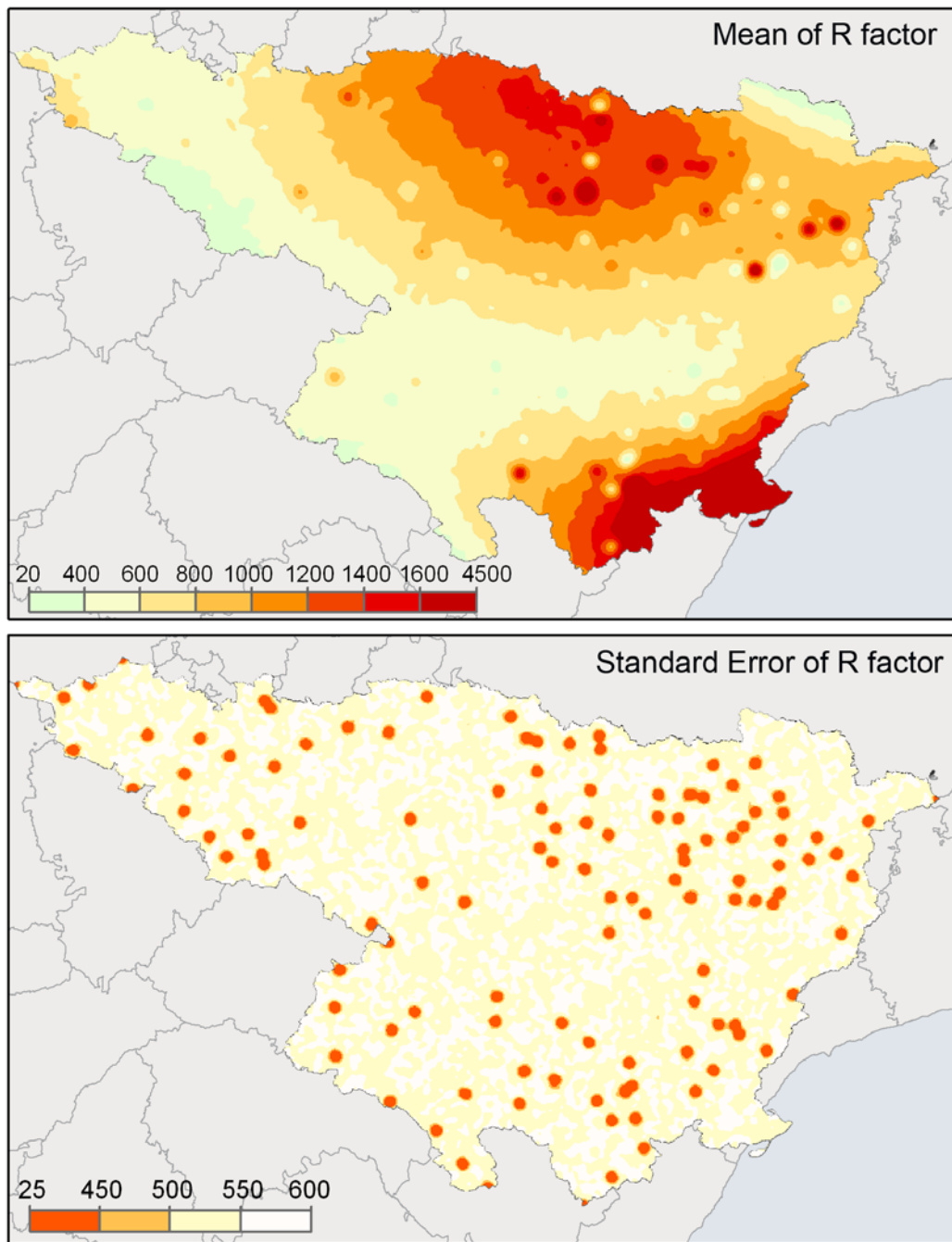


Figure 2.18: Local uncertainty modeled by Gaussian geostatistical simulation (GGS) for the R factor: mean of R factor and standard error of R factor ( $\text{MJ mm ha}^{-1} \text{h}^{-1} \text{y}^{-1}$ ).

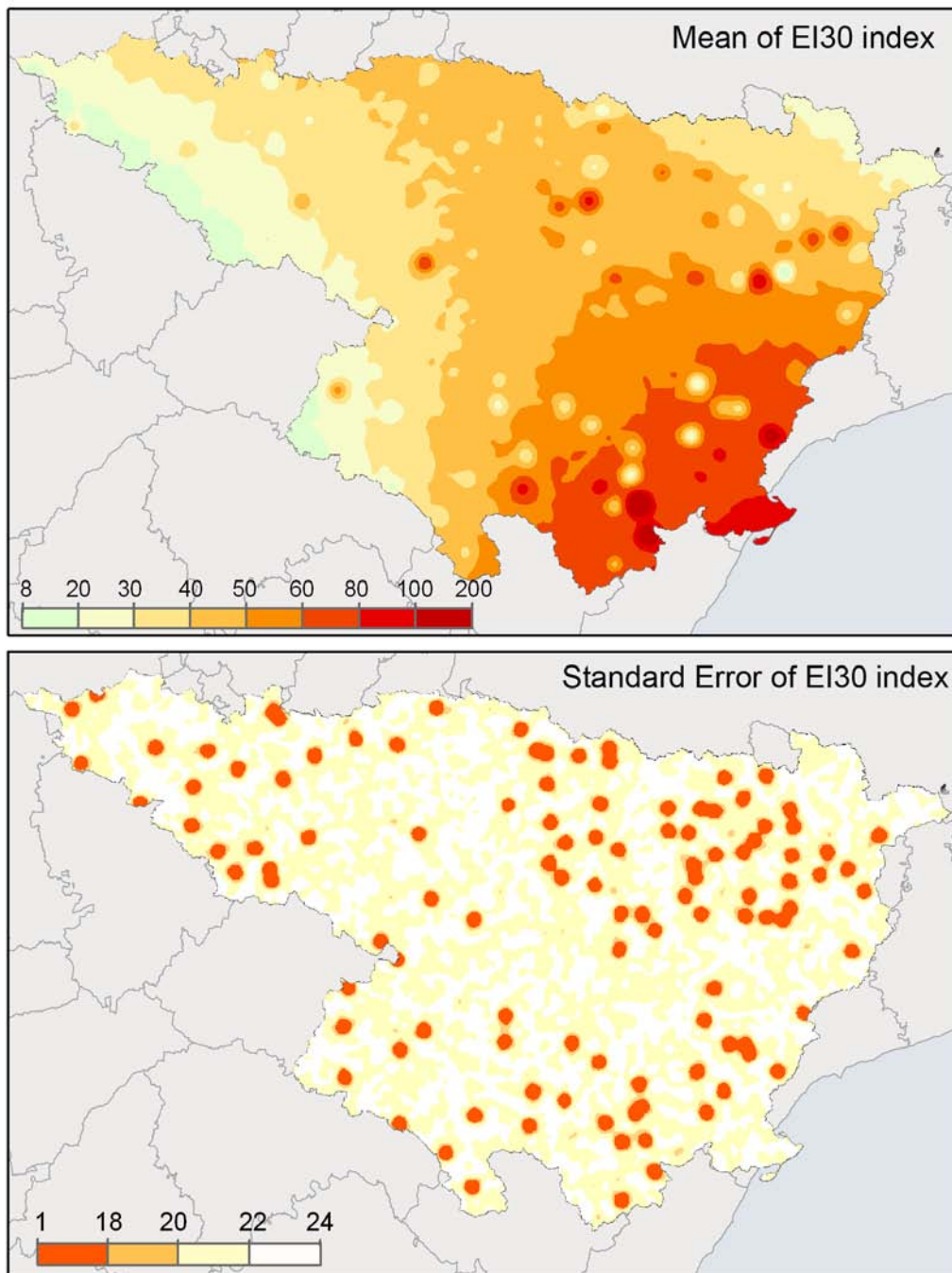


Figure 2.19: Local uncertainty modeled by Gaussian geostatistical simulation (GGS) for the  $EI_{30}$  index: mean of  $EI_{30}$  index and standard error of  $EI_{30}$  index ( $MJ \text{ mm}^{-1} \text{ h}^{-1}$ ).



## 2.7.7. Discussion

In this study we used the RUSLE R factor and the average  $EI_{30}$  index of the erosive events to assess the spatial distribution of rainfall erosivity on the northeast sector of the Iberian Peninsula. Both variables are characterized by a high temporal variability, especially in the Mediterranean area and in geographically complex regions (Leek and Olsen 2000; González-Hidalgo *et al.* 2007). During the initial stage of the analysis it was evident that close observatories could have very different values of R and  $EI_{30}$ , and this was confirmed by the analysis of the semivariogram.

Comparing both erosivity indices, the average  $EI_{30}$  index of the erosive events had larger variability than R, being more affected by the most extreme events. The spatial pattern of  $EI_{30}$  showed a clear northwest-southeast gradient. The highest values were found in the southern region, coinciding with the distribution of the peak intensity of extreme rainfall events for the same area (Beguería *et al.*, 2009). The spatial distribution of the R factor showed the highest values in the north and the south-east part, isolating the centre of the valley with low values. Previous works have analyzed the spatial distribution of the USLE R factor in Spain (ICONA, 1988). The value range and the spatial distribution are similar to the results of our study. There are differences however in the south-east corner along the Mediterranean coastland. The map of ICONA (1988) did not show the high erosivity values which were presented in our dataset. This discrepancy could be due to the different period of analysis, since the study of ICONA (1988) was based on data from the period 1966-1976, although this issue could not be assessed using the current dataset. Unfortunately, the technical brief attached to the map of ICONA did not report enough details allowing for a deeper comparison. The R factor values found for the area are similar to the ones published by other authors for the Mediterranean region: 697.4 to 3741.8 MJ mm  $ha^{-1} h^{-1} y^{-1}$  in Portugal (De Santos Loureiro and De Azevedo Coutinho, 2001); 471 and 3214 MJ mm  $ha^{-1} h^{-1} y^{-1}$  in Italy (Diodato, 2004); 339 to 818 MJ mm  $ha^{-1} h^{-1} y^{-1}$  in central Spain (Boellstorff and Benito, 2005); or 419.01 to 1124.36 MJ mm  $ha^{-1} h^{-1} y^{-1}$  in Sicily (Onori *et al.*, 2006). We are not aware of previous studies analyzing the spatial distribution of the average  $EI_{30}$  index.

Despite the high spatial variability of both indices, the mapping methods tested were able to capture the main spatial pattern of rainfall erosivity in the area. The



spatial distribution can be explained by seasonal atmospheric behaviour which causes the major stormy events. In the Pyrenees these events are related with south-western flows confronting the mountains triggering orographic rainfall in winter, and convective storms in summer. Close to the Mediterranean Sea the heating contrast between the atmosphere upper levels and continental and maritime surfaces, more intense during fall, generates intense storms. This is the principal cause of heavy rainfalls in the southeastern area (Llasat and Puigcerver 1997). These synoptic situations explain the spatial pattern of rainfall erosivity, which is linked to the most extreme events of the year. In addition, the strong relief adds complexity to the climate dynamics making more complex to obtain reliable models. It is responsible of orographic rainfall increase, and it also generates temperature differences in narrow spaces which contribute to the formation of convective cellules and local storms. Thus, the general pattern present in all rainfall erosivity maps show a clear north-west to south-east gradient, and marked local differences caused by the relief.

The comparison of several interpolation techniques yielded mixed results, since no single method arose as optimal according to all validation metrics, and the differences between models were narrow. Local interpolation methods yielded the best results overall, which can be explained by the very high spatial variability of rainfall erosivity as found in the preliminary semivariogram analysis. However, the maps produced by these methods masked the global pattern by introducing spatial noise due to the excessive weight given to local observations. Geostatistical methods were able to capture more general pattern ranking slightly lower from the local methods in the validation statistics. Among them, universal kriging (UK) ranked best and was able to capture local detail whereas conserving also the general pattern. Regression-based methods (GLS regression and regression-kriging) ranked lowest due to their most global character. Besides, the independent variables selected—elevation and solar radiation—did not have significant explanatory capacity. Regression-kriging ranked slightly better than regression-based methods, but their prediction was not better than that of UK.



## 2.7.8. Conclusions

The results obtained in the present study reflected the highly random character of rainfall erosivity, evaluated by both indices—the R factor and  $EI_{30}$  index. In general, the models were bad at predicting the highest values of both indices, due to the presence of outlier observations. The uncertainty of the predicted values can be explained by the natural climate variability in the study area, and also by the length of the analysis period. Other authors have reported high variability of soil erosion values in the Mediterranean region, both in space and time (González-Hidalgo *et al.*, 2007). Though, more information is needed for the assessment of the causal factors responsible of the high uncertainty present in all models. The quantification of uncertainty by means of Gaussian geostatistical simulation (GGS), expressed by standard error surfaces, allowed estimating confidence bands for the prediction surfaces. These cartographies constituted an important result for the applicability of the rainfall erosivity maps.

The results suggest that the database needs to be improved both in time (longer high-frequency rainfall series than 10 years of records: 1997-2006) and space (denser network). With respect to the length of the data series, it is generally accepted that a minimum of 20 years is desirable for rainfall erosivity analysis (Renard and Freimund, 1994; Renard *et al.*, 1997; Curse *et al.*, 2006; Verstraeten *et al.*, 2006). Unfortunately, there are very few data bases of high time resolution rainfall records and a good spatial coverage, as the one used in this work. Longer series are needed for reducing the strong influence of outlier observations. With respect to the spatial distribution of the data sets, the results showed spatial autocorrelation limited to a perimeter of ~15 km. This fact evidenced the need for improving the spatial coverage if better predictions are to be achieved.

The availability of high-quality environmental maps is a key issue for agricultural and hydrological management in many regions of the World. Rainfall erosivity maps can be of high relevance as a guidance for soil conservation practices, and also because they are usually part of erosion models such as the RUSLE. Recently, the RUSLE model has been implemented into GIS packages, integrating all the factors as different layers. Hence, the accuracy of the spatial surface of each factor is propagated to the outputs of the model. Compared to other climatic variables, rainfall erosivity is characterized by a high spatial and inter-annual variability, what makes mapping more difficult.





## 2.8 Rainfall erosivity cartography at annual and monthly scale for the period 1955-2006

The creation of a long daily rainfall erosivity database (1955-2006) allowed assessing the spatiotemporal evolution of this variable in the Ebro basin. The spatial distribution of the mean annual rainfall erosivity, estimated by the RUSLE R factor (Figure 2.20), is explained by the proximity to—or isolation from—the major water masses of the Cantabrian and the Mediterranean seas. The relief, with mountain ranges to the north, south, and east of the region, modifies this general pattern by increasing rainfall erosivity in those areas. Another effect of the relief is the isolation of the central area from the main rainfall sources through the creation of a rain shadow zone. All these influences result in a rather complex spatial pattern of erosivity.

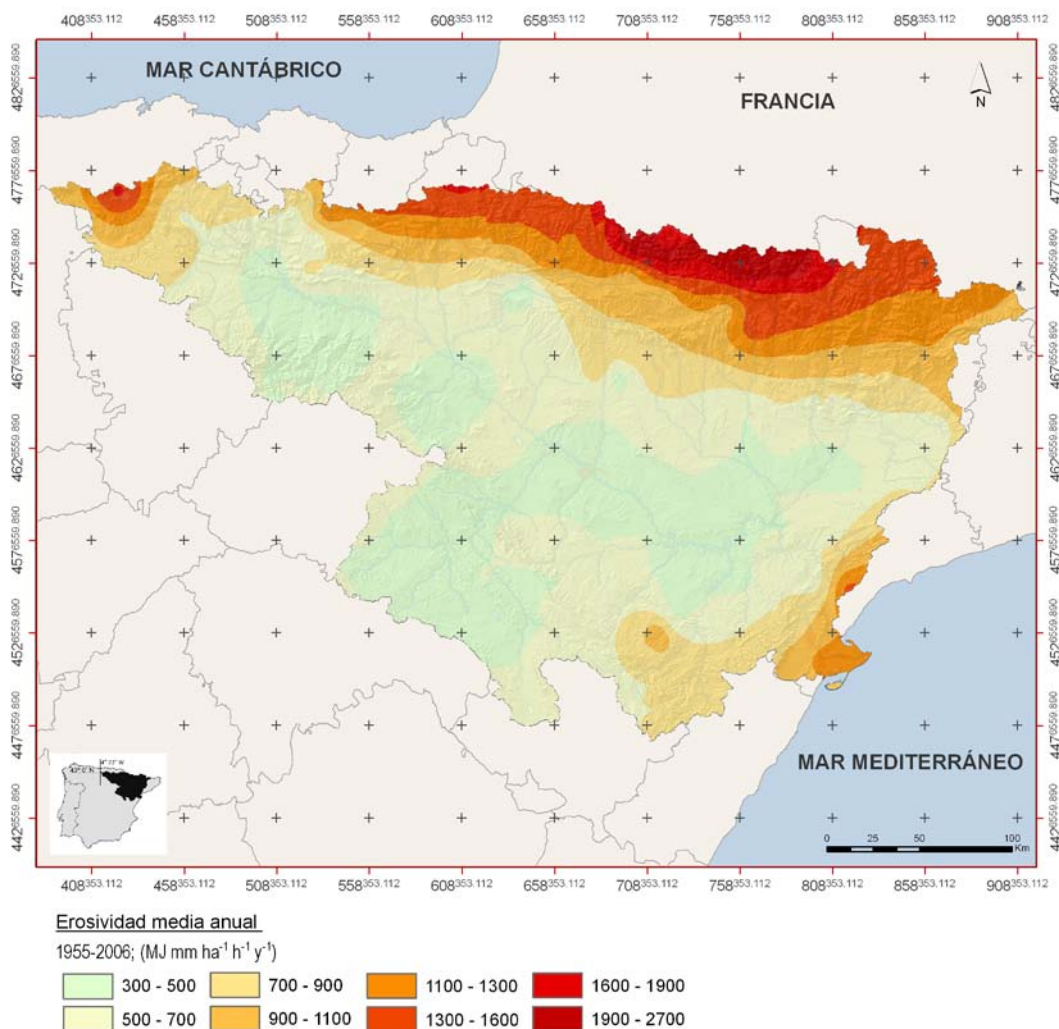


Figure 2.20: Mean annual rainfall erosivity for the period 1955-2006 ( $\text{MJ mm ha}^{-1} \text{h}^{-1} \text{y}^{-1}$ ).



The highest rainfall erosivities are reached in the Pyrenees and close to the Mediterranean coast. This last differs with the spatial distribution of rainfall since the Mediterranean area is not among the highest rainfall areas. A broad NW–SE gradient in the spatial distribution of rainfall erosivity is detected. The monthly regime of rainfall erosivity helps understanding this pattern (Figure 2.21). Cluster analysis of the station allowed distinguishing between three main regimes.

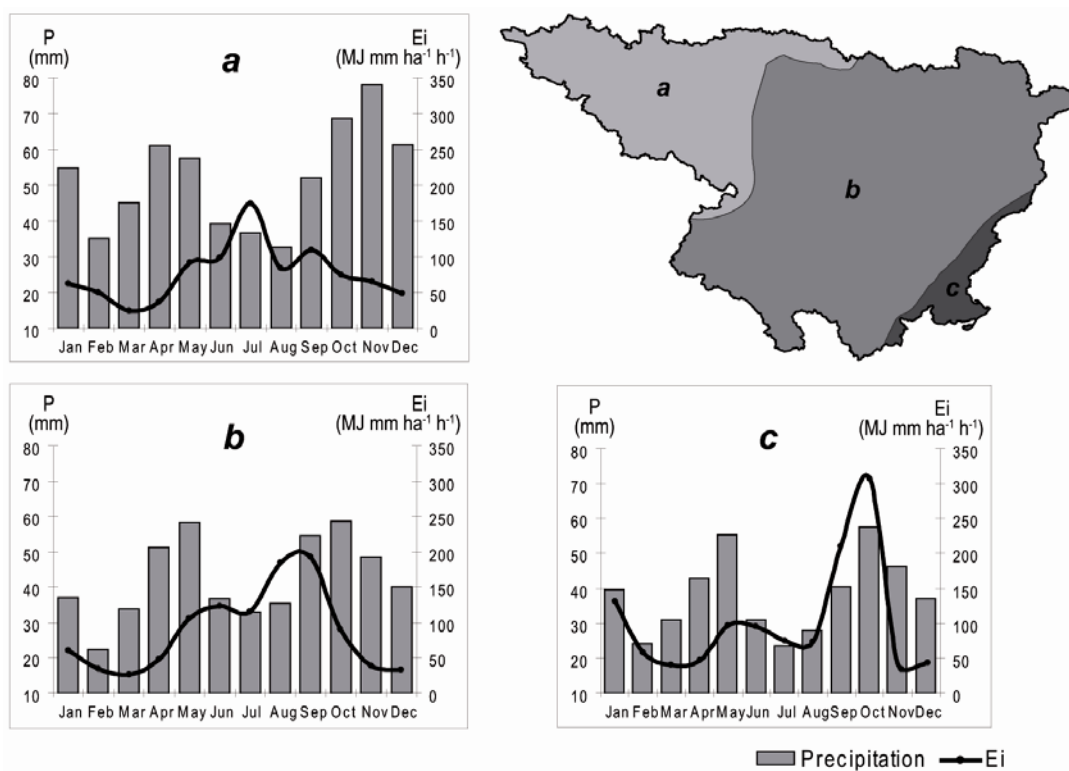


Figure 2.21: Monthly rainfall erosivity ( $Ei$ ;  $MJ\ mm\ ha^{-1}\ h^{-1}$  month $^{-1}$ ) and rainfall (mm) regimes in the study area.

The NW zone (a), which is influenced by the Atlantic Ocean, shows the highest monthly rainfall values and lowest rainfall erosivity. The highest erosivity occurs at the beginning of summer in this area. The central zone (b) includes the majority of stations. Annual precipitation is lower than in the NW zone (although still important), but erosivity is greater and shows two annual peaks, one in late spring (May–June) and a second one (the largest) at the end of the summer (August–September). The NE zone (c) has a typical Mediterranean rainfall regime, with maxima in spring and autumn. The highest erosivity occurs in autumn. The spring rainfall peaks are not as erosive as those of the autumn due to differences between these seasons in the rainfall generation mechanisms.



Rainfall in spring comes from several rainfall events of relatively low intensity. In contrast, rainfall in autumn is usually caused by a few, very intense events.

These characteristics are better shown by the monthly rainfall erosivity spatial patterns (Figures 2.22). In spring rainfall erosivity maxima are found in the mountain areas at the north, mostly in the central Pyrenees and towards the east. Mean monthly rainfall erosivity can reach  $200 \text{ MJ mm ha}^{-1} \text{ h}^{-1} \text{ month}^{-1}$  in these areas. The minimum values are always found in the middle and south west of the area, in all seasons. The summer months show similarities with the spring spatial pattern. Maximum values are reached towards the Mediterranean, and especially in the Pyrenees due to convective events. The Ebro delta also shows high rainfall erosivity values. The maximum values during the year are registered from August to October, with maxima in the interval from  $280\text{-}545 \text{ MJ mm ha}^{-1} \text{ h}^{-1} \text{ month}^{-1}$  in the Pyrenees and the Ebro delta. These areas register maximum values during Autumn. In winter, rainfall erosivity is reduced and restricted to the central Pyrenees with values progressively descending from 140 to 60  $\text{MJ mm ha}^{-1} \text{ h}^{-1} \text{ month}^{-1}$ . The Ebro delta continues showing high values during November and December.

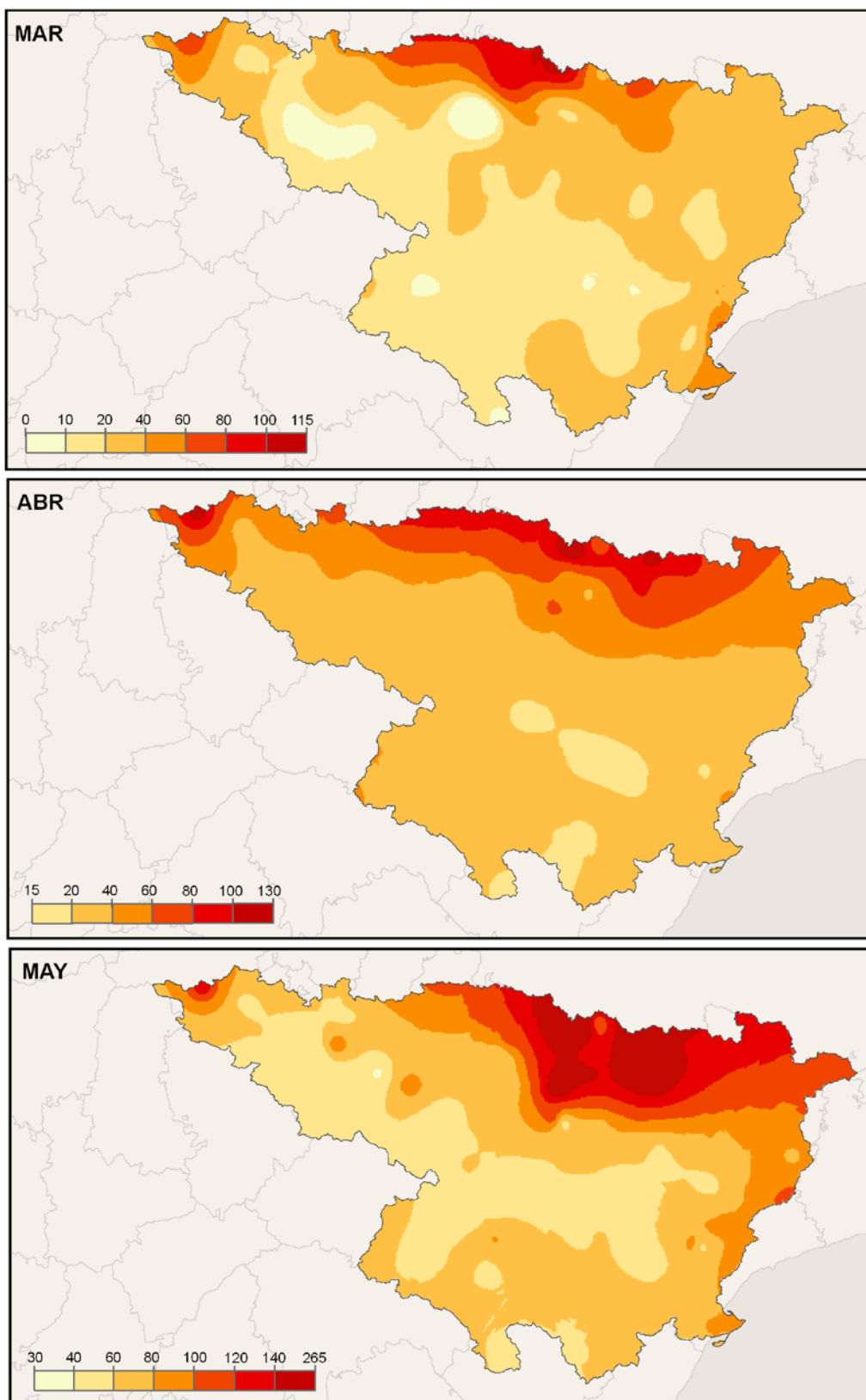


Figure 2.22: Mean monthly rainfall erosivity for spring months ( $\text{MJ mm ha}^{-1} \text{h}^{-1} \text{month}^{-1}$ ) during the period 1955-2006 in the Ebro basin (NE Spain).

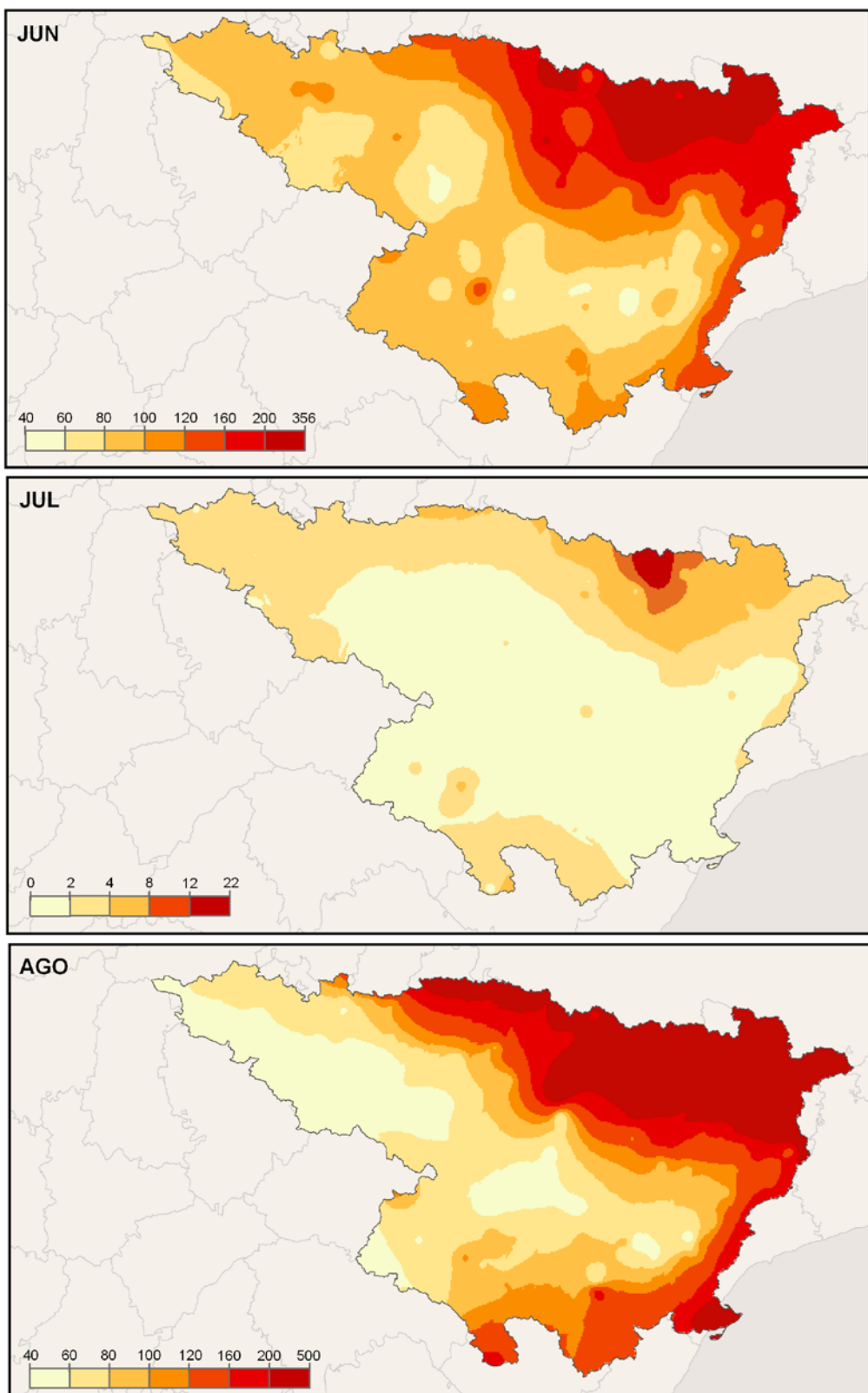


Figure 2.22 (cont.): Mean monthly rainfall erosivity for summer months ( $\text{MJ mm ha}^{-1} \text{ h}^{-1}$  month $^{-1}$ ) during the period 1955-2006 in the Ebro basin (NE Spain).

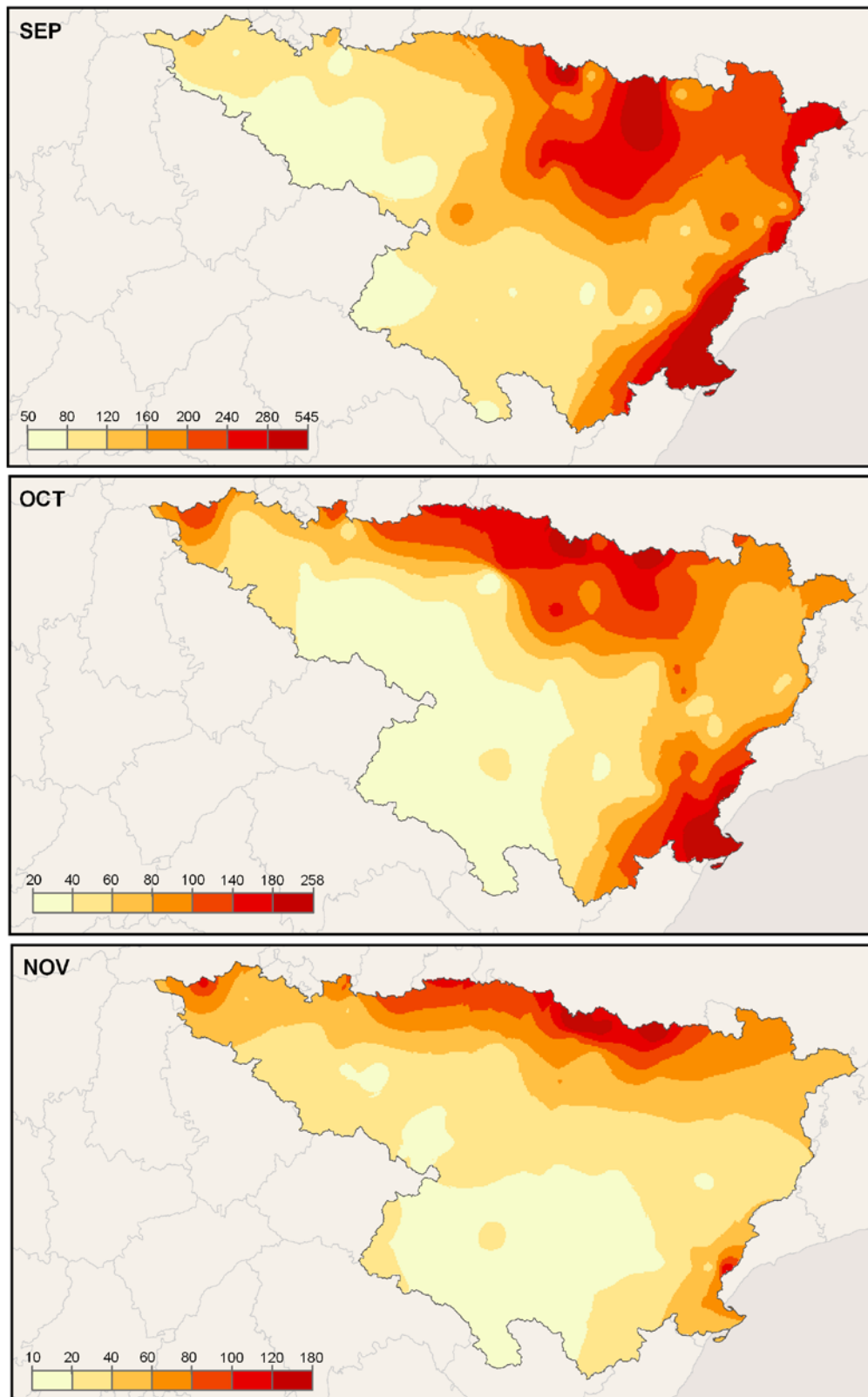


Figure 2.22 (cont.): Mean monthly rainfall erosivity for autumn months ( $\text{MJ mm ha}^{-1} \text{ h}^{-1}$  month<sup>-1</sup>) during the period 1955-2006 in the Ebro basin (NE Spain).

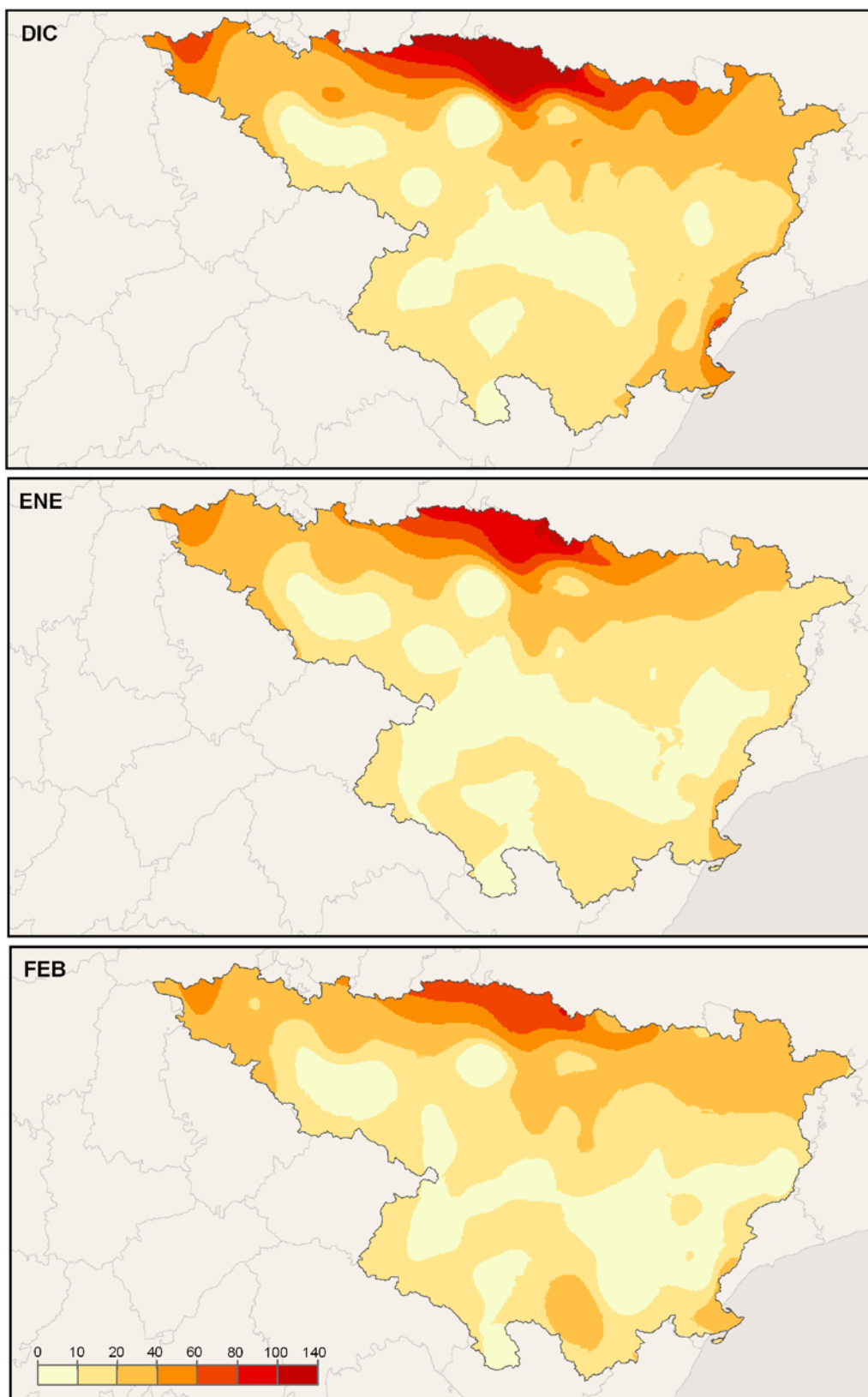


Figure 2.22 (cont.): Mean monthly rainfall erosivity for winter months ( $\text{MJ mm ha}^{-1} \text{month}^{-1}$ ) during the period 1955-2006 in the Ebro basin (NE Spain).





## 2.9. Do atmospheric teleconnection patterns influence rainfall erosivity? A study of NAO, MO and WeMO in NE Spain, 1955-2006.<sup>3</sup>

As explained earlier (bloque I), the concept of rainfall erosivity refers to the ability of any rainfall event to erode soil. It links together the physical properties of the raindrops as a consequence of rainfall-generating processes and their impact on the soil surface, and involves two main mechanisms: i) *rain splash*—the detachment of soil particles due to the kinetic energy of the rain drops—, and ii) *runoff erosion*—motion of soil particles by the shear stress exerted by surface runoff. Rainfall erosivity is responsible for changes in the soil properties due to crusting, disruption of aggregates, removal of nutrient-rich particles, etc. It represents one of the main mechanisms of soil degradation in semiarid landscapes where vegetation is scarce. Its influence depends on the soil characteristics, topography and land use, as well as on other features of the rainfall regime (D'Odorico et al. 2001). Rainfall erosivity estimates are thus of paramount importance for the estimation of soil erosion rates through space and time.

Previous work has shown that the spatial and temporal variability of rainfall intensity can be explained by coupled modes of atmospheric circulation patterns (Hurrell 1995; Jones et al. 1997; Hurrell et al. 2003). The main atmospheric circulation pattern that affects the climate of Western Europe is the North Atlantic Oscillation, NAO (Jacobeit 1987; Moses et al. 1987). The NAO is characterized by a north–south sea level pressure dipolar pattern, with one of its centres located over Iceland and the other one approximately over the Azores Islands, (Figure 2.23). The positive phase of the NAO reflects below normal heights and pressure across the high latitudes of the North Atlantic, and above-normal heights and pressure over the central North Atlantic. The NAO negative mode reflects a high-pressure blocking in the northeast Atlantic and a more meridional circulation than the opposite mode. Upper-air troughs and incursions of polar air over the Mediterranean are more frequent during negative NAO, and the Atlantic storm tracks are displaced southwards. All these factors are

---

<sup>3</sup> This section is based in the article: Angulo-Martínez, M., Beguería, S., 2012. Do atmospheric teleconnection patterns influence rainfall erosivity? A study of NAO, MO and WeMO in NE Spain, 1955-2006. *Journal of Hydrology*, (submitted).



responsible of wetter conditions in the western Mediterranean (Jacobeit 1987; Moses et al. 1987; Maheras, 1988; Kutié et al. 1996). The influence of the NAO on rainfall over the Iberian Peninsula has been recognized in many studies (Rodó *et al.*, 1997; Esteban-Parra *et al.*, 1998; Rodríguez-Puebla *et al.*, 1998; Martín-Vide and Gómez, 1999; Serrano *et al.*, 1999; Goodess and Jones, 2002; Lopez-Bustins *et al.*, 2008), and is especially strong in its south-western and central areas (Martín-Vide and Lopez-Bustins, 2006).

In contrast the Mediterranean coast of Spain is dominated by more easterly Mediterranean influences (Dünkeloh and Jacobbeit, 2003; Martin-Vide and Lopez-Bustins, 2006; González-Hidalgo *et al.*, 2009). In this area the pre-eminence of the NAO in explaining the variability of rainfall leads way to other circulation patterns such as the Mediterranean Oscillation, MO (Conte *et al.* 1989; Palutikof, 2003), and the Western Mediterranean Oscillation, WeMO (Martin-Vide and Lopez-Bustins, 2006), as several studies have revealed (Dünkeloh and Jacobbeit, 2003; González-Hidalgo *et al.*, 2009). The MO is a low-frequency variability pattern producing opposing barometric, thermal and pluviometric anomalies between the east and west extremes of the Mediterranean basin. The positive mode of MO is related to anticyclonic conditions in the western Mediterranean and a trough in the east, and with below-average rainfall rates in the entire Mediterranean basin. In its negative mode a low pressure is placed close to the Britannic isles or north of the Iberian Peninsula while anticyclonic conditions prevail in the Mediterranean. This situation is related with rainfalls in the western part of the Mediterranean basin (Dünkeloh and Jacobbeit, 2003). The Western Mediterranean Oscillation (WeMO) is defined within the synoptic framework of the western Mediterranean basin (Martín-Vide and Lopez-Bustins, 2006). The positive phase of the WeMO corresponds to the anticyclone over the Azores enclosing the southwest Iberian quadrant and low-pressure in the Liguria Gulf. This situation is related with above-average rainfall at the north and northeast of the Iberian Peninsula, especially in January when it is associated with advections from the Atlantic Ocean in the north-west. The correlation coefficient between the WeMO and monthly rainfall is 0.6 in the Bay of Biscay (Martín-Vide and Lopez-Bustins, 2006). Its negative phase coincides with central European anticyclone located north of Italy and a low-pressure centre, often cut off from northern latitudes, in the framework of the Iberian south-west. Most of the rainfalls in the eastern parts of the Iberian Peninsula, especially during December,



are associated with this situation. Its neutral phase coincides with low-pressure over the western Mediterranean basin and the surrounding areas.

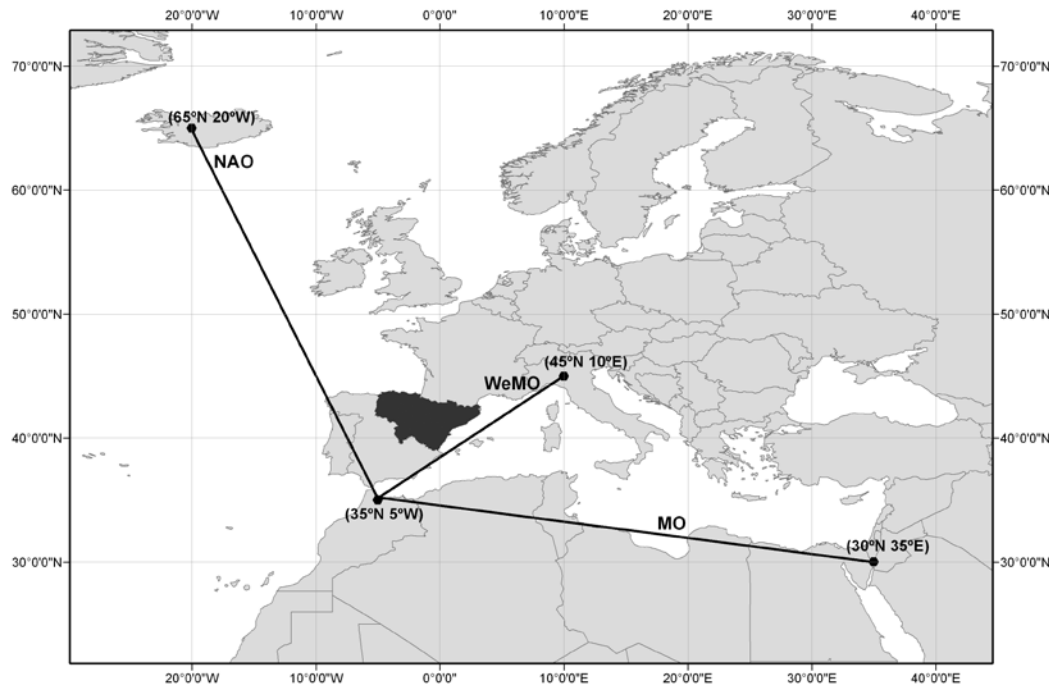


Figure 2.23: Sea-level pressure points used to calculate the daily atmospheric indices.

Despite the well-known relationships between atmospheric teleconnection patterns and rainfall amounts, very few studies have been devoted to analyze their influence on rainfall erosivity. In the eastern part of Iberian Peninsula De Luis *et al.* (2010) related monthly negative trends in rainfall erosivity—estimated by the modified Fournier Index (MFI Arnoldus, 1977) and the rainfall concentration index (PCI, Oliver 1980)—with the increase of the NAO during the period 1951-2000. Clarke and Rendell (2010) related the reduction in badland erosion rates in south Italy with the increase of the NAO since the 1980's. Other studies have addressed the influence of the El Niño-Southern Oscillation (ENSO) on rainfall erosivity in some areas of United States (D'Odorico *et al.* 2001) and Peru (Romero *et al.* 2007). No studies however have compared the varying influence of several teleconnection patterns on rainfall erosivity over a single region.

The aim of this study is to assess the influence of the NAO, MO and WeMO on daily rainfall erosivity at the annual and monthly scales in NE Spain, during the period 1955-2006. A second objective is to identify changes in the probability of



occurrence of extreme daily erosivity events as a function of daily atmospheric circulation indices.

## 2.9.1 Methods

### *Atmospheric circulation indices*

To calculate the daily indices for the atmospheric teleconnection patterns (namely NAO<sub>i</sub>, MO<sub>i</sub> and WeMO<sub>i</sub>) daily sea-level pressure grids from the ds010.0 Daily Northern Hemisphere Sea Level Pressure Grids data set (University Corporation for Atmospheric Research, 1979) were used (Figure 2.23). Following Jones *et al.* (1997) a North Atlantic Oscillation index (NAO<sub>i</sub>) was calculated as the normalized difference between time series of sea level pressure recorded at two points in the southwest Iberian Peninsula (Gibraltar, 35°N 5°W) and southwest Iceland (Reykjavik, 65°N, 20°W). MO<sub>i</sub>, as defined by Palutikof (2003), was calculated as the daily normalized difference between the SLP at Gibraltar (35°N 5°W) and Lod (Israel), 30°N, 35°E. WeMO<sub>i</sub> was calculated as the daily normalized difference between the SLP at Gibraltar (35°N 5°W) and Parma (45°N, 10°E). Positive and negative events of the atmospheric circulation indices index were identified as those days having values of the indices higher than 0.5 and lower than -0.5, respectively.

### *Differences in annual and monthly rainfall erosivity during negative and positive days of the atmospheric circulation patterns.*

In this study we have used the daily rainfall erosivity database for the period 1955-2006. The creation of this database is explained in detail in section 2.4-ii.

To evaluate the relationship between the atmospheric circulation indices—NAO<sub>i</sub>, MO<sub>i</sub> and WeMO<sub>i</sub>—and rainfall erosivity we obtained for each index two time series of daily rainfall erosivity corresponding to values of the index above 0.5 and below -0.5, respectively, (Figure 2.24).

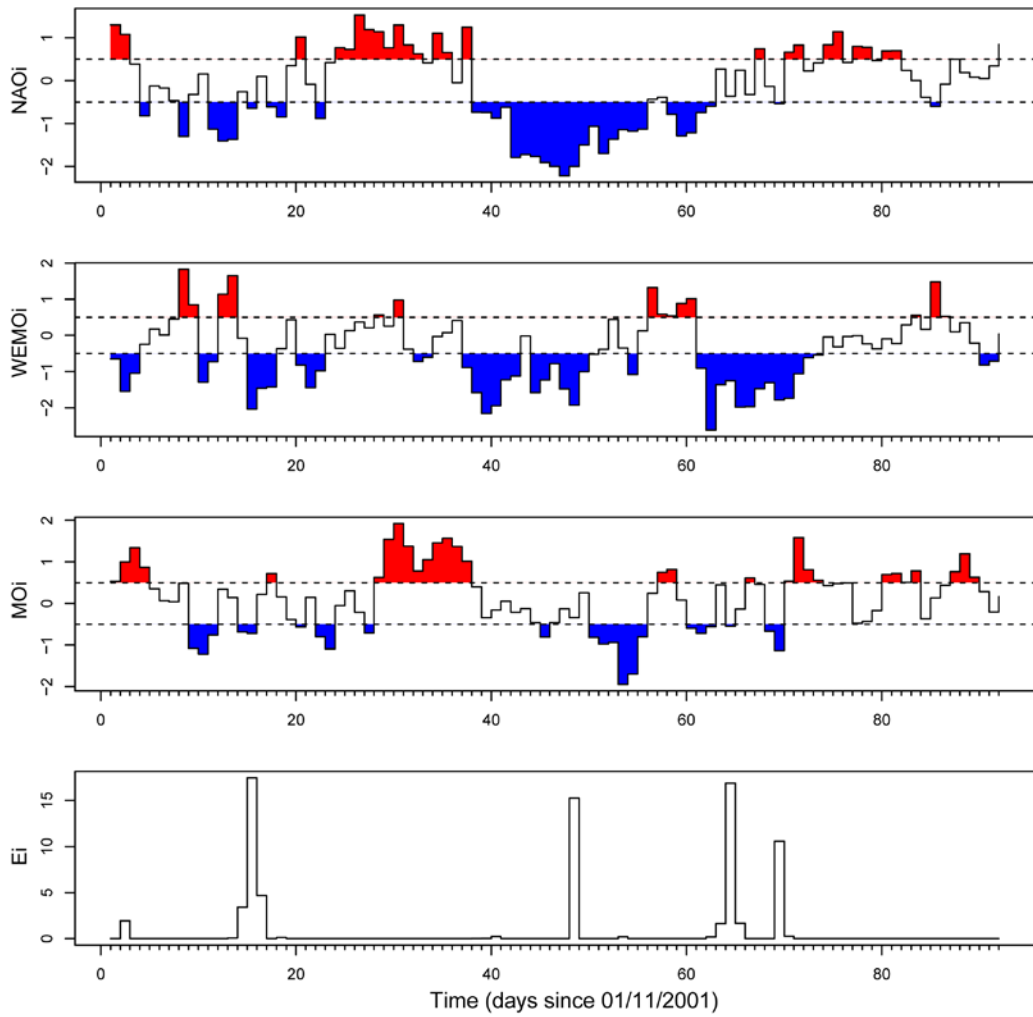


Figure 2.24: Daily time series of NAO<sub>i</sub>, WeMO<sub>i</sub>, MO<sub>i</sub> and rainfall erosivity for the observatory X9987 (Ebro Delta) between 01/01/2001 and 31/03/2001. Red and blue regions indicate positive and negative phases according to the three teleconnection indices, which were used to construct time series of daily rainfall erosivity.

Therefore, we computed the relative difference  $EI_{dif}$  between median daily erosivity registered during negative days ( $EI_-$ ) and under positive days ( $EI_+$ ) of the indices, with respect to the median of the daily erosivity registered during positive days:

$$EI_{dif} = (EI_- - EI_+)/EI_+, \quad (2.31)$$

where  $EI_-$  and  $EI_+$  are the median daily rainfall erosivity during negative and positive phases of a given atmospheric circulation index—NAO<sub>i</sub>, MO<sub>i</sub> and WeMO<sub>i</sub>—, as defined above. For example,  $(150-100)/100 = 0.5$  means that erosivity was 50% higher during negative phases than during positive phases, while  $(100-150)/150 = -0.33$  means that erosivity was 33.3% lower



during negative phases than during positive phases. The statistical significance of the relative differences was evaluated using the Wilcoxon-Mann-Whitney (WMW) rank test (Siegel and Castelan, 1988). The nonparametric WMW test—based in the median—was preferred due to its robustness against non-normality of the variables (Helsel and Hirsch, 1992). The significance level was established at  $\alpha=0.05$ . Maps of  $EI_{dif}$  for the whole period and month by month were produced to help visualizing spatial differences in the effect of atmospheric circulation indices on daily rainfall erosivity.

#### *Extreme value analysis of rainfall erosivity during positive and negative days of the atmospheric circulation patterns*

Changes in the probability distributions of extreme daily rainfall erosivity depending on the NAO, MO and WeMO phase were analyzed using the extreme value theory (Hershfield, 1973). Peaks-over-threshold (POT) series of daily rainfall erosivity were obtained for positive and negative NAO, MO and WeMO days, by selecting only those observations exceeding a threshold value  $\varepsilon$  corresponding to the 90th percentile of the series. The resulting series were fitted to a Generalized Pareto (GP) distribution by the maximum likelihood approach. GP is the limit distribution of a POT variable, provided that the POT occurrences fit a Poisson process, i.e. that the occurrences are time independent. The appropriateness of the GP distribution to model the daily erosivity POT series was checked by means of the L-moment ratios diagram and by a Kolmogorov-Smirnov test (Beguería 2005; Beguería et al. 2009). The GP distribution is described by a shape parameter  $k$  and a scale parameter  $a$ , with probability density function:

$$f(x) = \frac{1}{\alpha} \left[ 1 - \frac{k}{\alpha} (x - \varepsilon) \right], \quad (2.32)$$

and distribution function:

$$P(X \leq x) = 1 - \left( 1 - \kappa \frac{(x - \varepsilon)}{\alpha} \right)^{\frac{1}{\kappa}}, \quad (2.33)$$

where  $x$  is the daily rainfall erosivity exceeding the threshold value  $\varepsilon$ , which acts as a location parameter. The highest expected rainfall erosivity  $X_T$  over a period of  $T$  years is obtained as:



$$X_r = \varepsilon + \frac{\alpha}{\kappa} \left[ 1 - \left( \frac{1}{\lambda T} \right)^\kappa \right], \quad (2.34)$$

where  $\lambda$  is the average number of events per year.

Maps of the extreme daily rainfall erosivity events corresponding to a return period of 10 years were produced for positive and negative NAO, MO and WeMO days based on equation (30). These maps were compared in order to evaluate differences in the expected extreme events depending on each circulation pattern. The POT analysis was applied to the period between September to April, during which the influence of circulation patterns was highest, as was determined by the previous analysis.

## 2.9.2. Results

*Annual and monthly differences in median daily rainfall erosivity during negative and positive NAO, MO and WeMO days.*

The results of the WMW test comparing the daily distributions of rainfall erosivity during positive and negative NAO, MO and WeMO days yielded 154 (99%), 149 (96%) and 144 (92%) of significant differences, respectively (Table 2.7). Differences were found in almost all months, although they were especially important between September and April. Most observatories reflected this behaviour. During summer (June to August) the influence of the circulation patterns was less evident.

The relative differences in rainfall erosivity during negative and positive days of the circulation patterns varied significantly between teleconnection indices (Figure 2.25). Median rainfall erosivity was only moderately (1 to 3 times) higher during negative NAO days. The Mediterranean indices, in contrast, had a stronger influence. Thus, in the lower Ebro valley to the SE of the area the median erosivity was between 3 and 10 times higher during negative days of MO<sub>i</sub> and between 10 and 15 times higher during negative days of WeMO<sub>i</sub>. For these two teleconnection indices two areas were found—in the north in the case of MO<sub>i</sub> and in the north-northwest in the case of WeMO<sub>i</sub>—where the influence of these teleconnection patterns was reversed, i.e. erosivity was higher during



positive days. This relationship, however, was not significant according to the WMW test.

Table 2.7: Number and proportion of series with significant differences in annual and monthly erosivity between positive and negative days of the atmospheric circulation indices (Wilcoxon-Mann-Witney test)

<b>Significant series:</b>			
<b>Annual:</b>	<b>NAO</b>	<b>MO</b>	<b>WeMO</b>
Jan	144 (92%)	138 (89%)	73 (47%)
Feb	136 (87%)	136 (87%)	76 (49%)
Mar	68 (44%)	119 (76%)	81 (52%)
Apr	147 (94%)	131 (84%)	140 (90%)
May	109 (70%)	58 (37%)	99 (64%)
Jun	27 (17%)	21 (14%)	32 (21%)
Jul	40 (26%)	62 (40%)	40 (26%)
Aug	36 (23%)	39 (25%)	68 (44%)
Sep	11 (7%)	106 (68%)	139 (89%)
Oct	94 (60%)	145 (93%)	117 (75%)
Nov	152 (97%)	136 (87%)	119 (76%)
Dec	145 (93%)	135 (87%)	100 (64%)

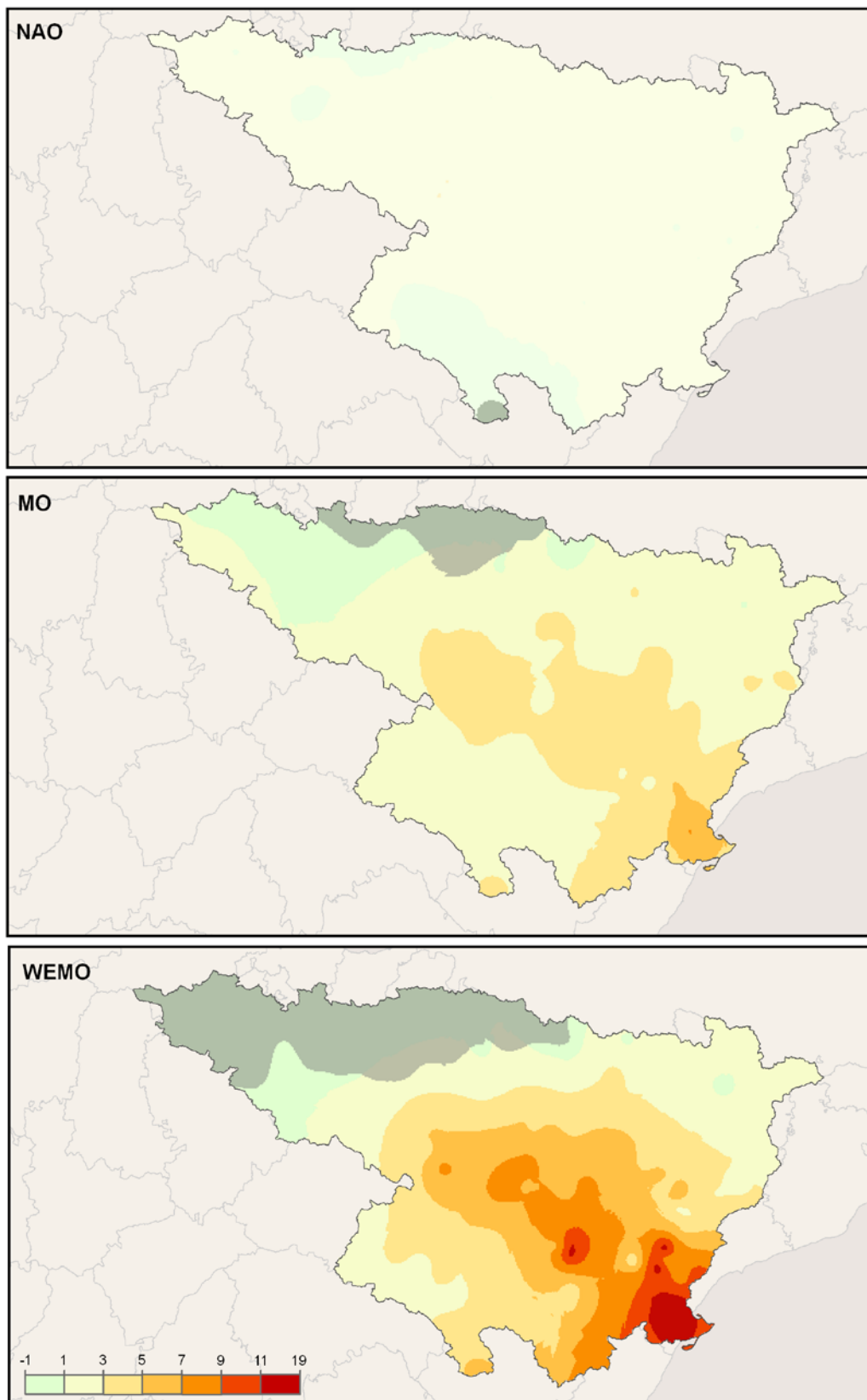


Figure 2.25: Relative differences in median daily rainfall erosivity ( $\text{MJ mm ha}^{-1} \text{ day}^{-1}$ ) at **annual** scale during negative and positive days of the atmospheric circulation indices for the period 1955-2006. Masked areas indicate no significant difference.



At the monthly basis, the highest differences took place between September and April (Figures 2.26). In general, daily rainfall erosivities in the eastern area responded most to the synoptic situations related with negative conditions of the atmospheric circulation indices. This area corresponds to the region described in Figure 2.5-C, where the highest rainfall erosivities were associated to intense rainfall events in autumn and early winter.

At the monthly scale the NAO influence was significant from October to February in most of the study area, and in April-May in some areas. From June to September the influence of the NAO on rainfall erosivity was not significant. The highest influence of NAO was found close to the Mediterranean coast, especially in the upper north-east Mediterranean area. The highest differences between positive and negative NAO days were found in November, with erosivity values up to 30 times higher during negative conditions. Again, this influence was higher in the SE of the study area. Other months (January, April, May) showed also significant influences in some areas, although much more localized spatially.

The MO revealed a higher influence than NAO, especially between September and March. This influence was highest along the Mediterranean coast, and was extended towards the inland depending on the month. The highest relative difference between positive and negative days was registered in December, for which most of the NE region had daily rainfall erosivity values which were 30 times greater under negative than under positive phase. The highest relative differences, however, were linked to the WeMO. Rainfall erosivity under negative WeMO days was up to 130 times greater than under positive days, concentrated along the Mediterranean coast between October and January. The influence of the WeMO was restricted spatially to a narrower area closer to the coast, only extending to the centre of the study area during some months.

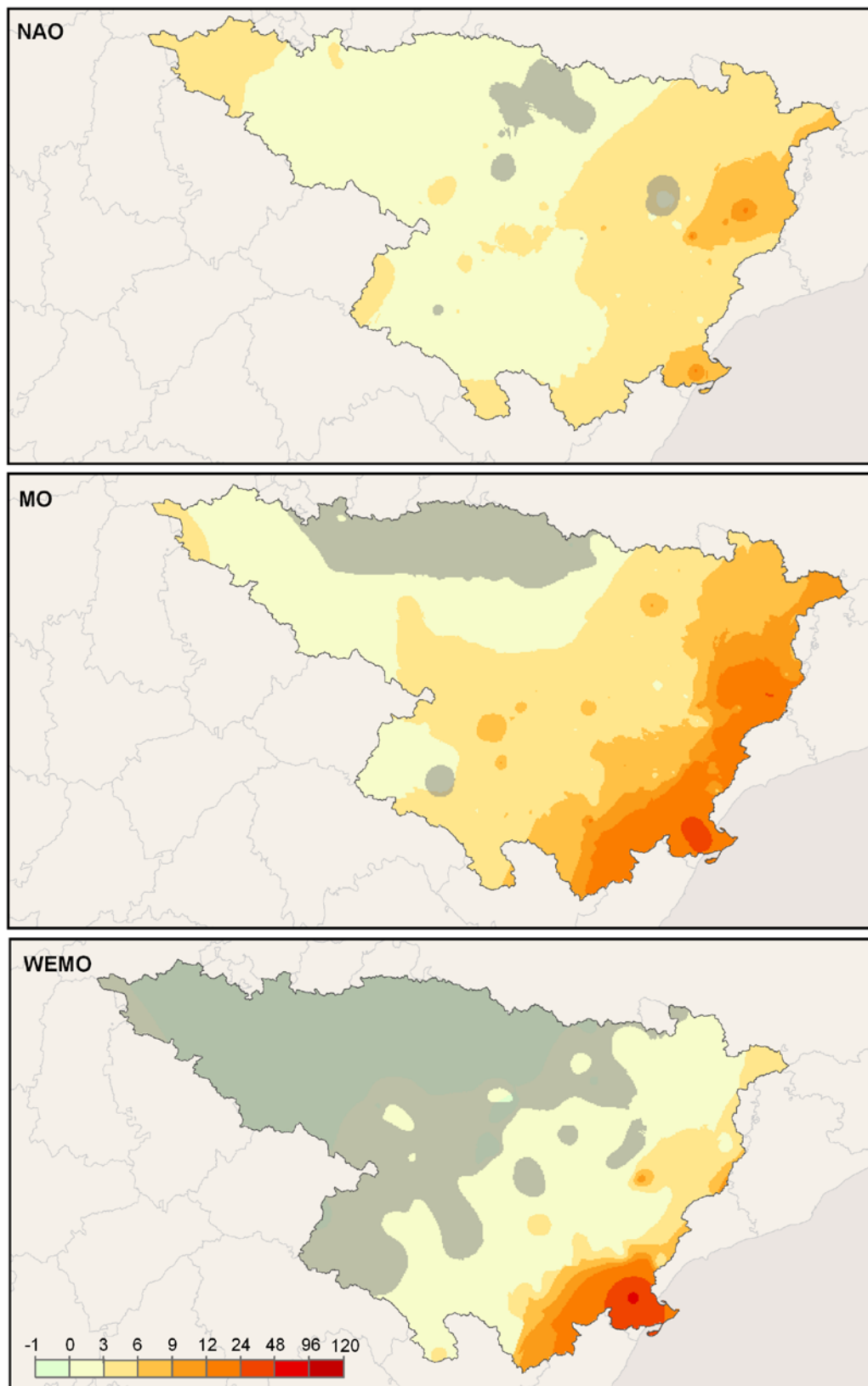


Figure 2.26: Relative differences in median daily rainfall erosivity ( $\text{MJ mm ha}^{-1} \text{ day}^{-1}$ ) for **January** during negative and positive days of the atmospheric circulation indices for the period 1955-2006. Masked areas indicate no significant difference.

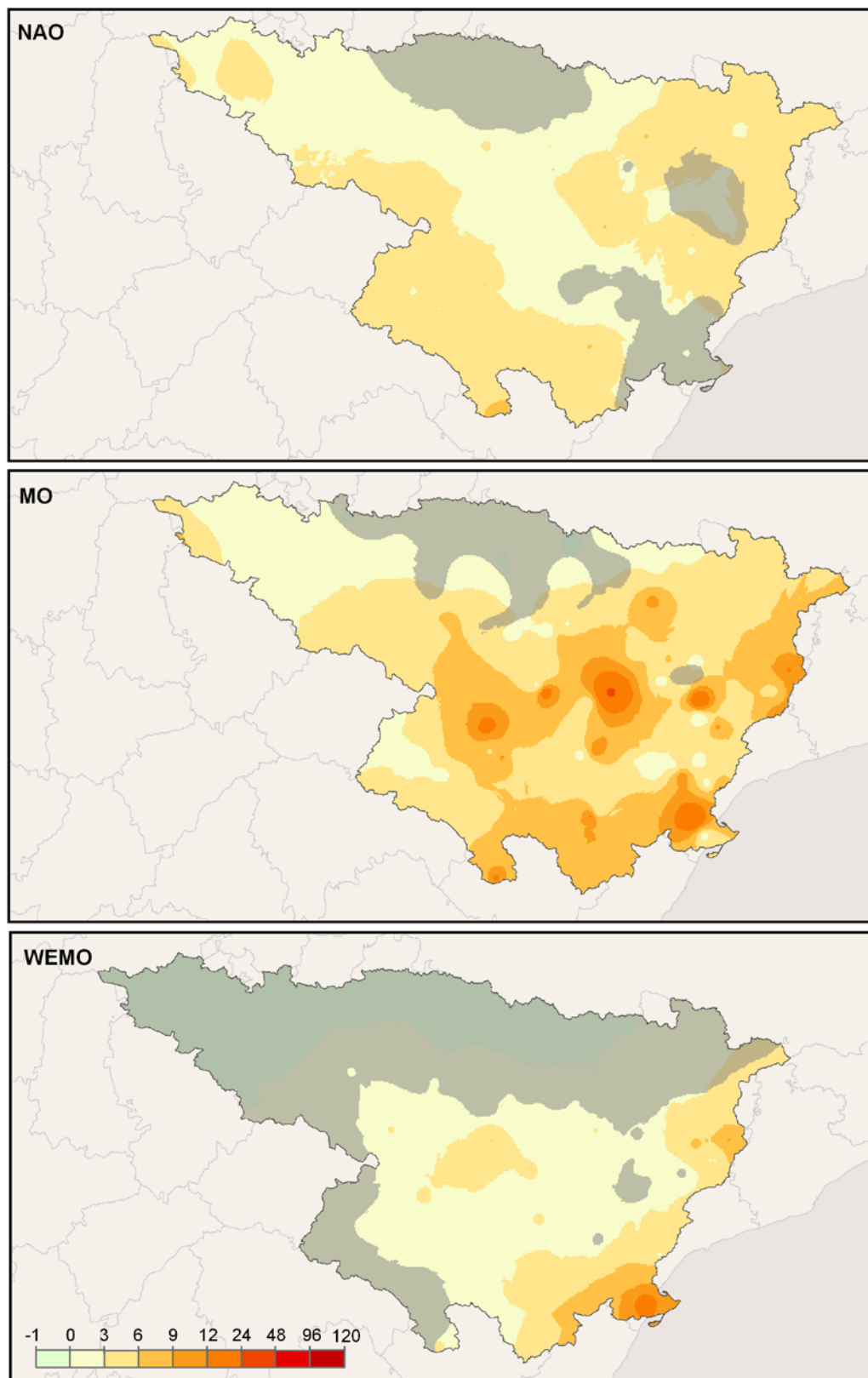


Figure 2.26 (cont.): Relative differences in median daily rainfall erosivity ( $\text{MJ mm ha}^{-1} \text{ day}^{-1}$ ) for **February** during negative and positive days of the atmospheric circulation indices for the period 1955-2006. Masked areas indicate no significant difference.

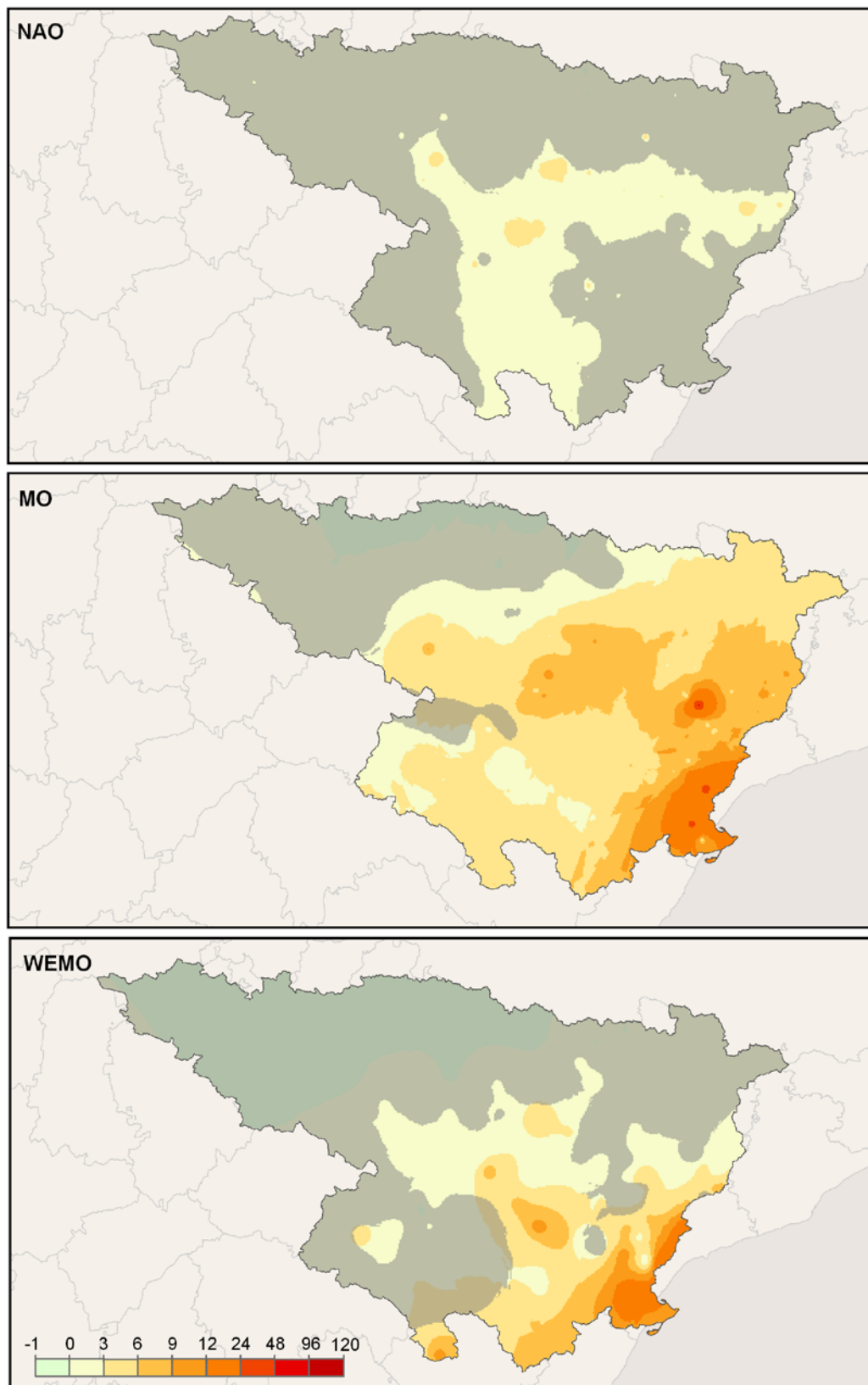


Figure 2.26 (cont.): Relative differences in median daily rainfall erosivity ( $\text{MJ mm ha}^{-1} \text{ day}^{-1}$ ) for **March** during negative and positive days of the atmospheric circulation indices for the period 1955-2006. Masked areas indicate no significant difference.

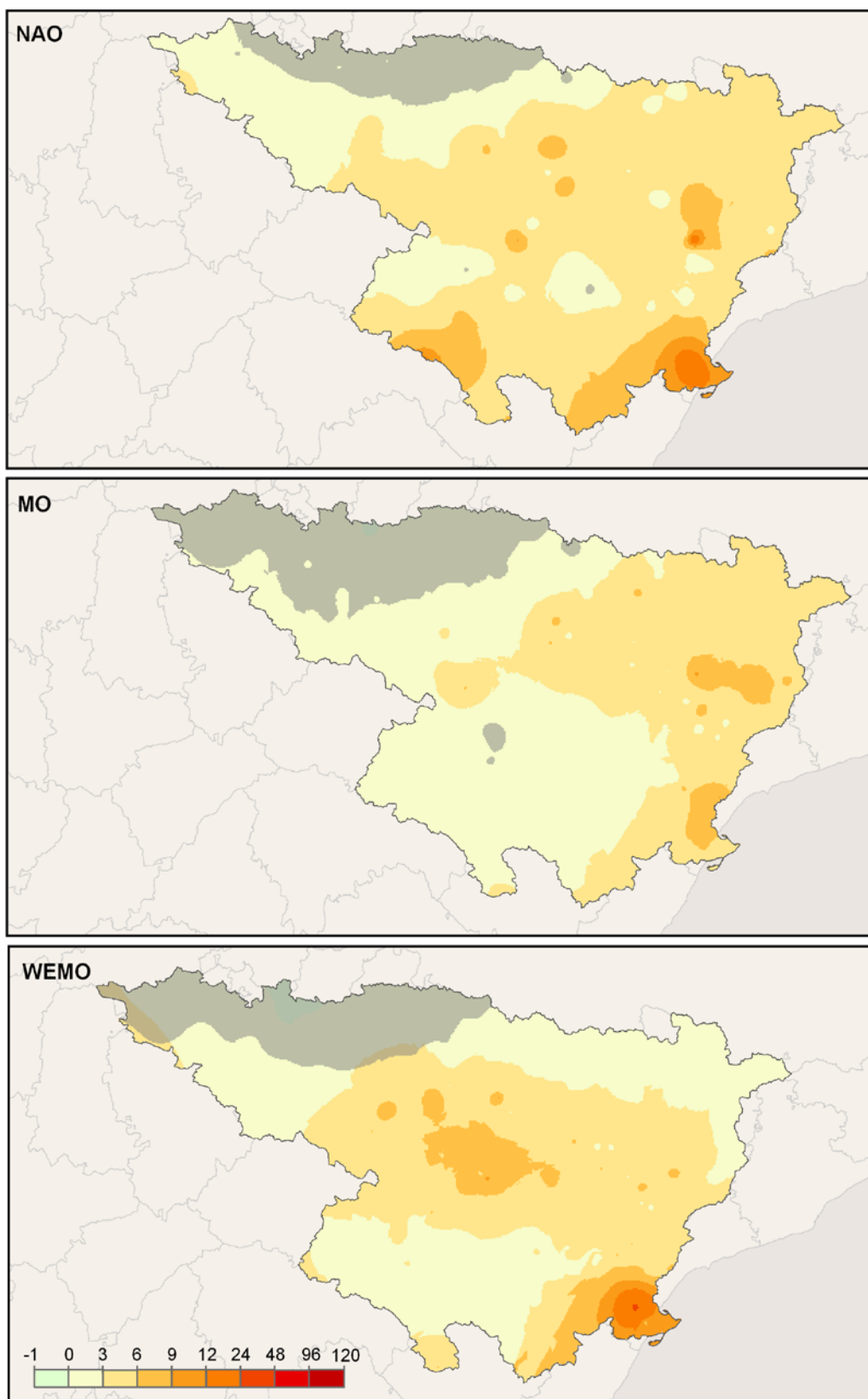


Figure 2.26 (cont.): Relative differences in median daily rainfall erosivity ( $\text{MJ mm ha}^{-1} \text{ day}^{-1}$ ) for **April** during negative and positive days of the atmospheric circulation indices for the period 1955-2006. Masked areas indicate no significant difference.

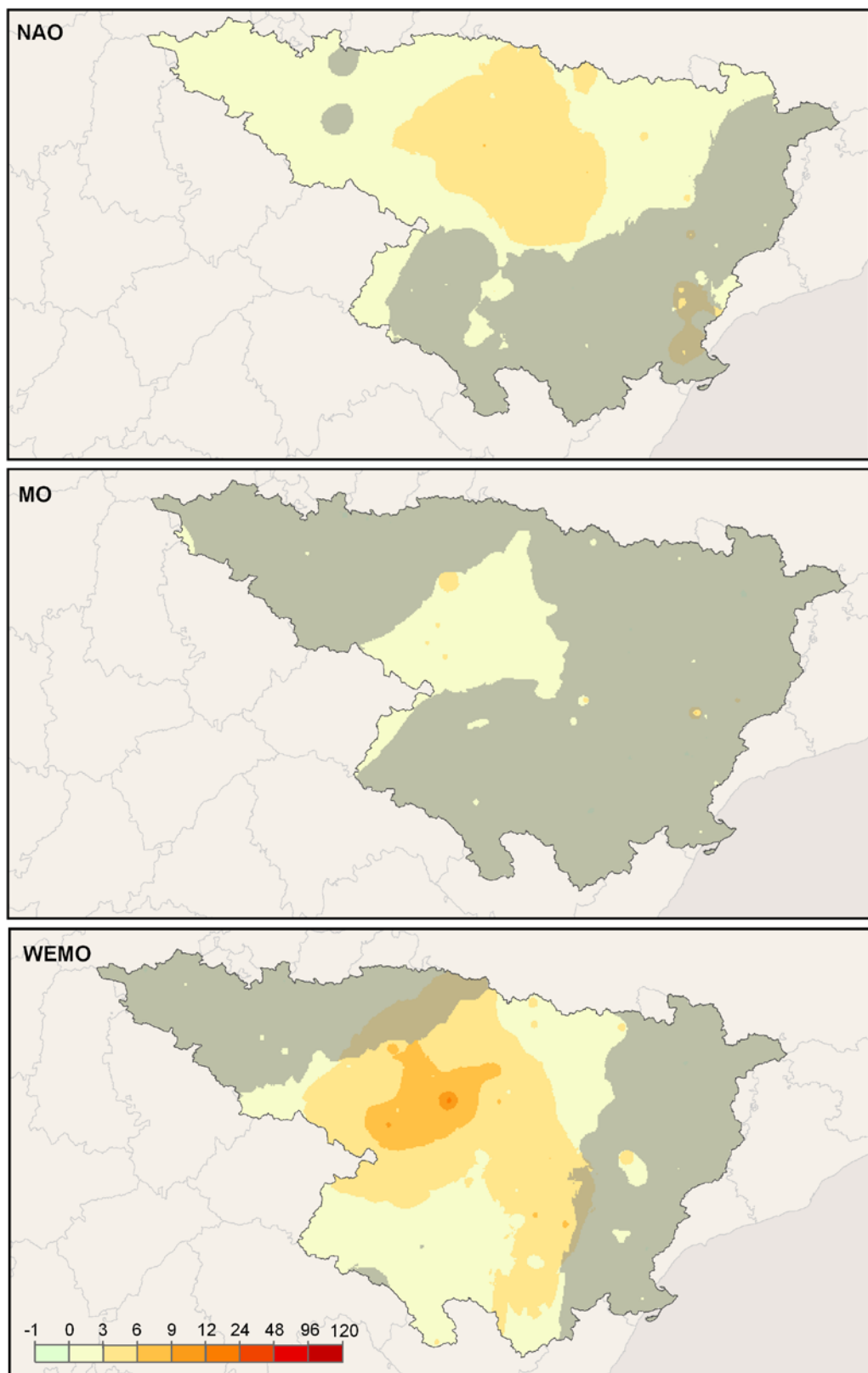


Figure 2.26 (cont.): Relative differences in median daily rainfall erosivity ( $\text{MJ mm ha}^{-1} \text{ day}^{-1}$ ) for **May** during negative and positive days of the atmospheric circulation indices for the period 1955-2006. Masked areas indicate no significant difference.

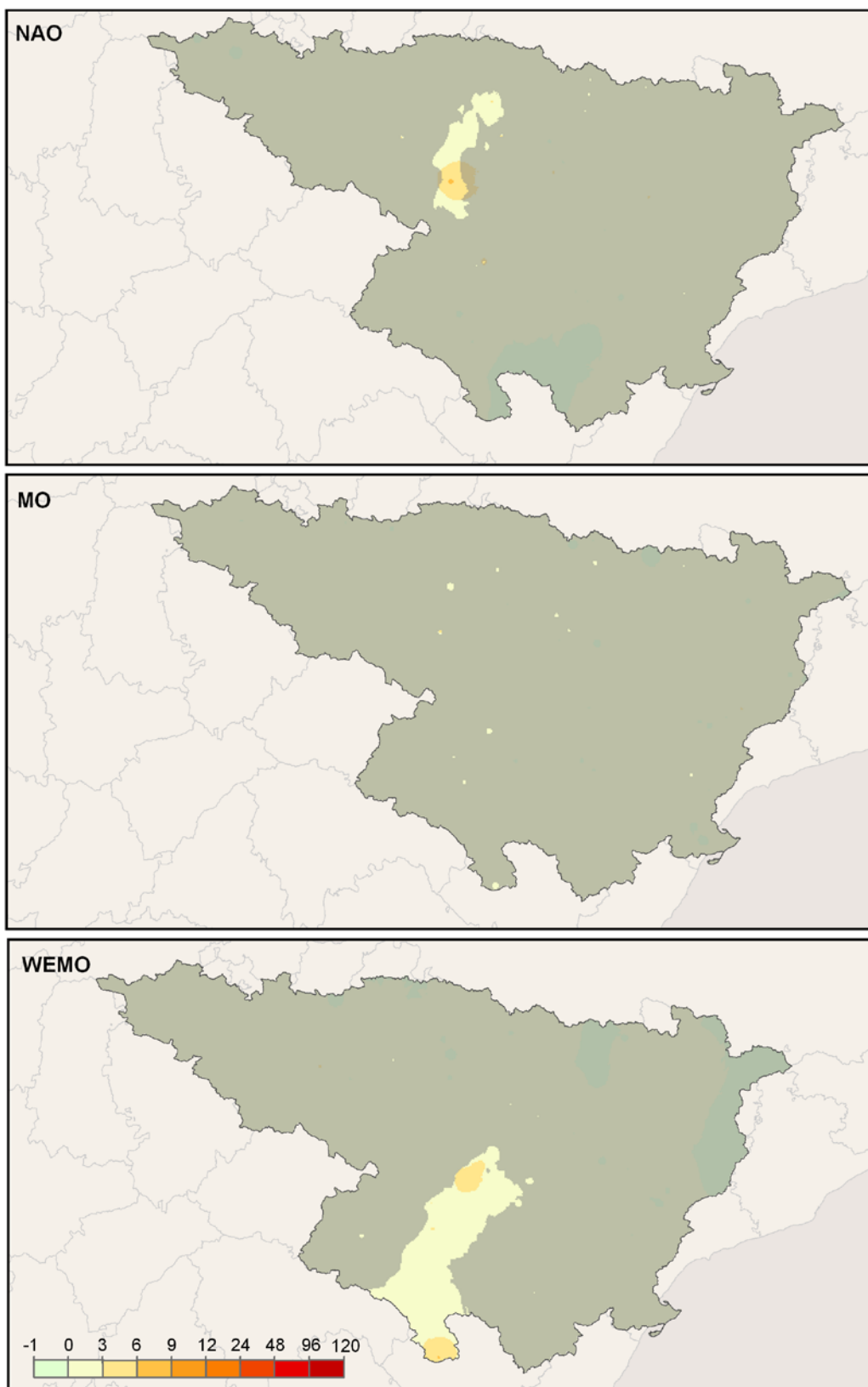


Figure 2.26 (cont.): Relative differences in median daily rainfall erosivity ( $\text{MJ mm ha}^{-1} \text{ day}^{-1}$ ) for **June** during negative and positive days of the atmospheric circulation indices for the period 1955-2006. Masked areas indicate no significant difference.

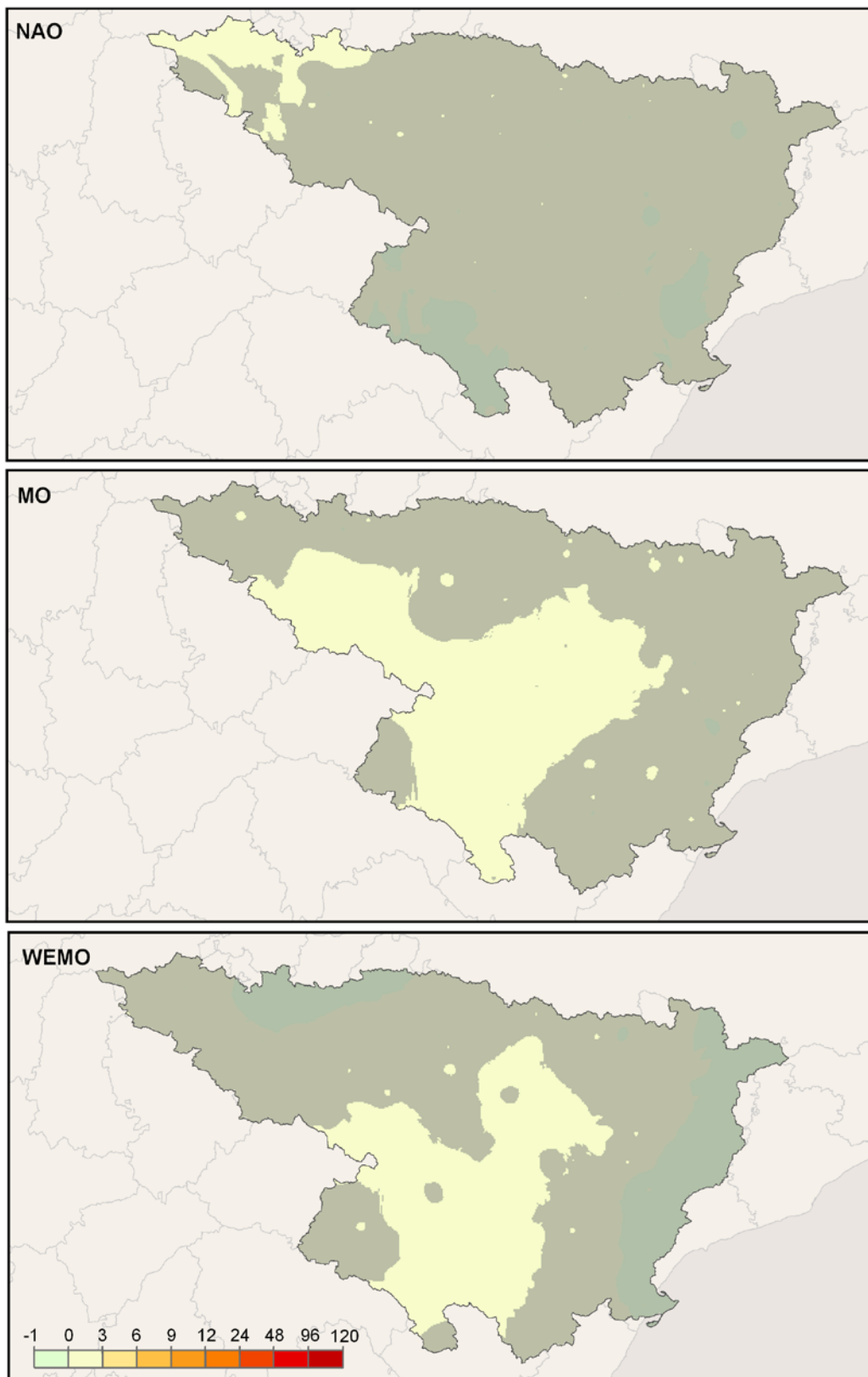


Figure 2.26 (cont.): Relative differences in median daily rainfall erosivity ( $\text{MJ mm ha}^{-1} \text{ day}^{-1}$ ) for **July** during negative and positive days of the atmospheric circulation indices for the period 1955-2006. Masked areas indicate no significant difference.

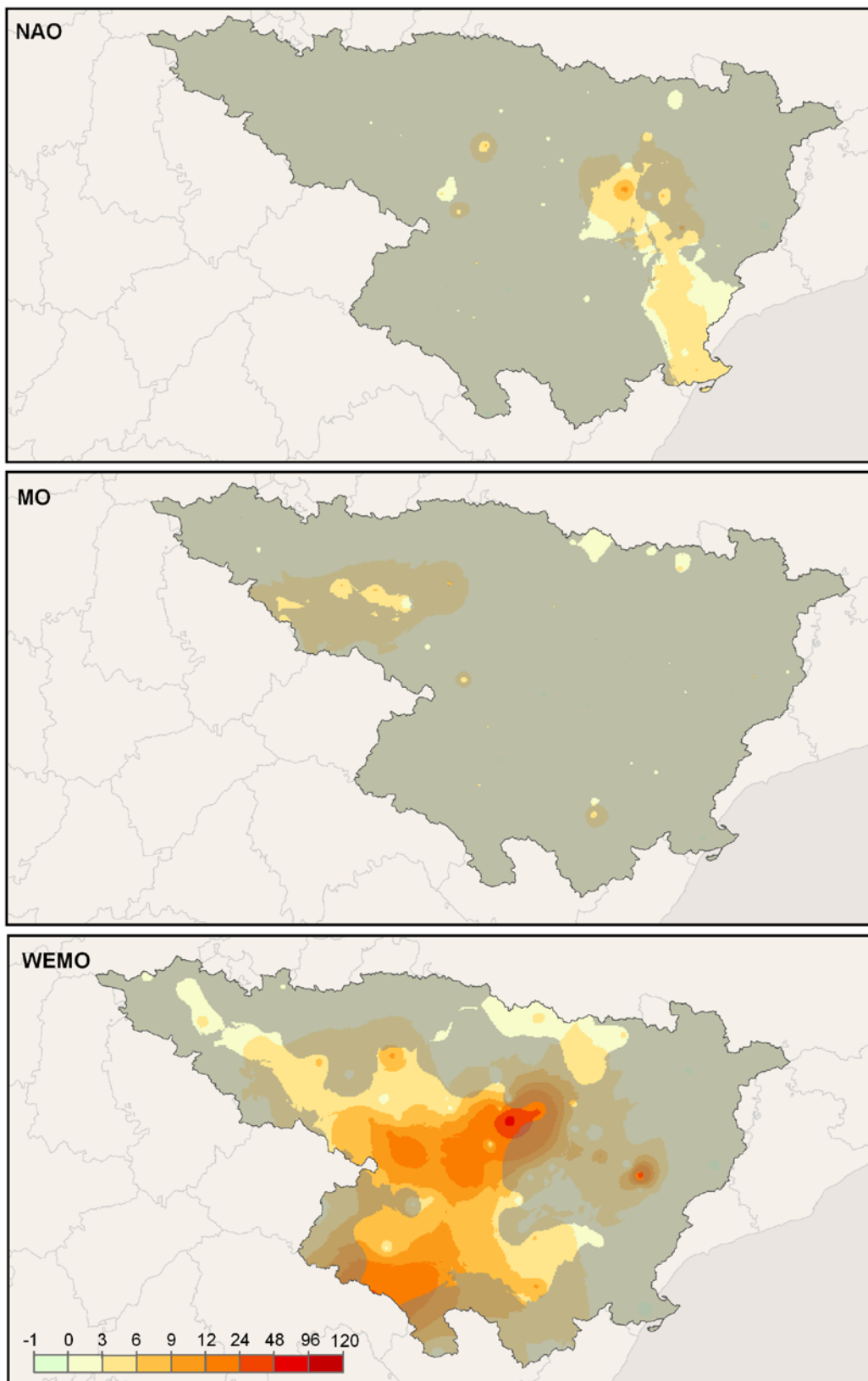


Figure 2.26 (cont.): Relative differences in median daily rainfall erosivity ( $\text{MJ mm ha}^{-1} \text{ day}^{-1}$ ) for **August** during negative and positive days of the atmospheric circulation indices for the period 1955-2006. Masked areas indicate no significant difference.

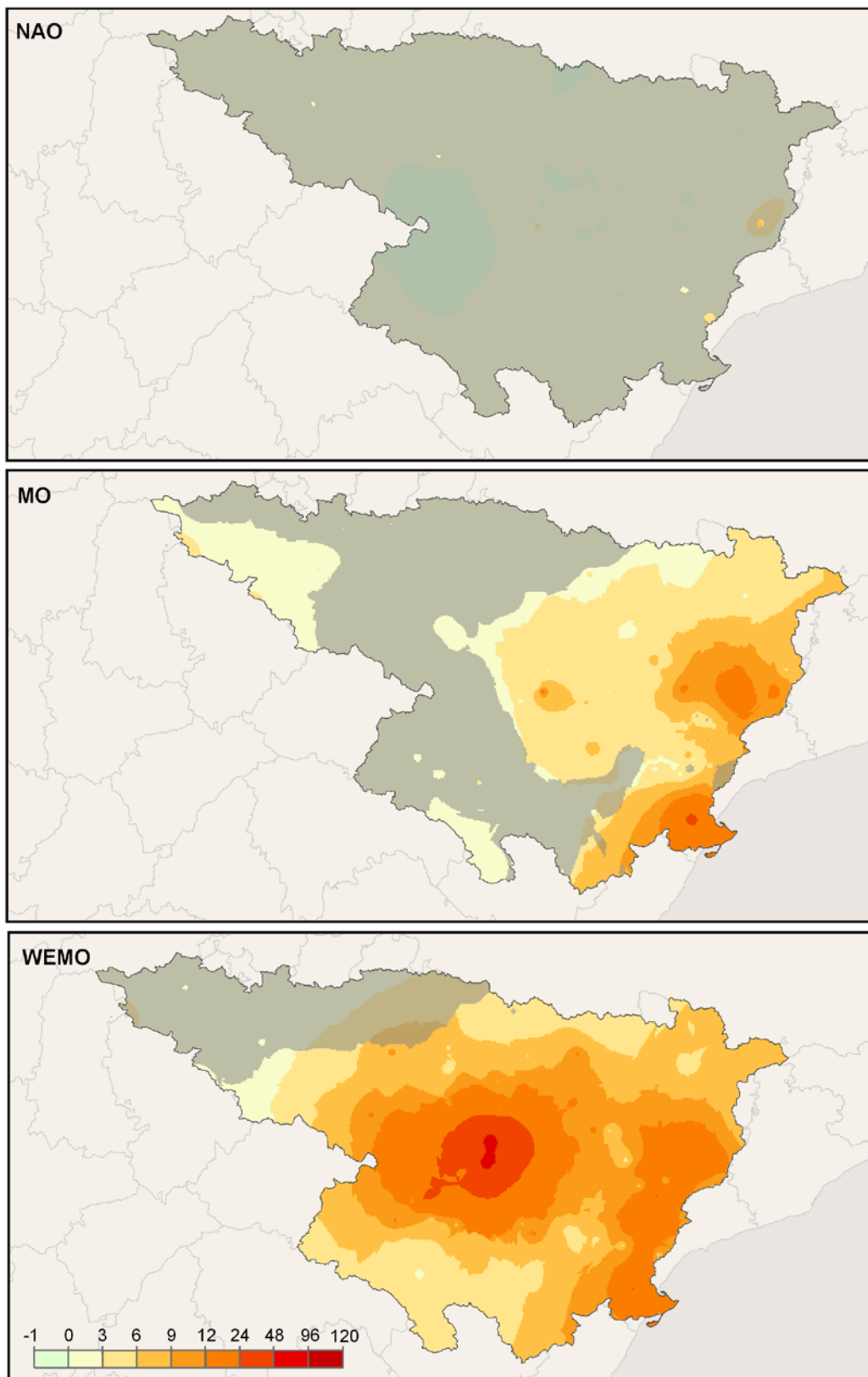


Figure 2.26 (cont.): Relative differences in median daily rainfall erosivity ( $\text{MJ mm ha}^{-1} \text{ day}^{-1}$ ) for **September** during negative and positive days of the atmospheric circulation indices for the period 1955-2006. Masked areas indicate no significant difference.

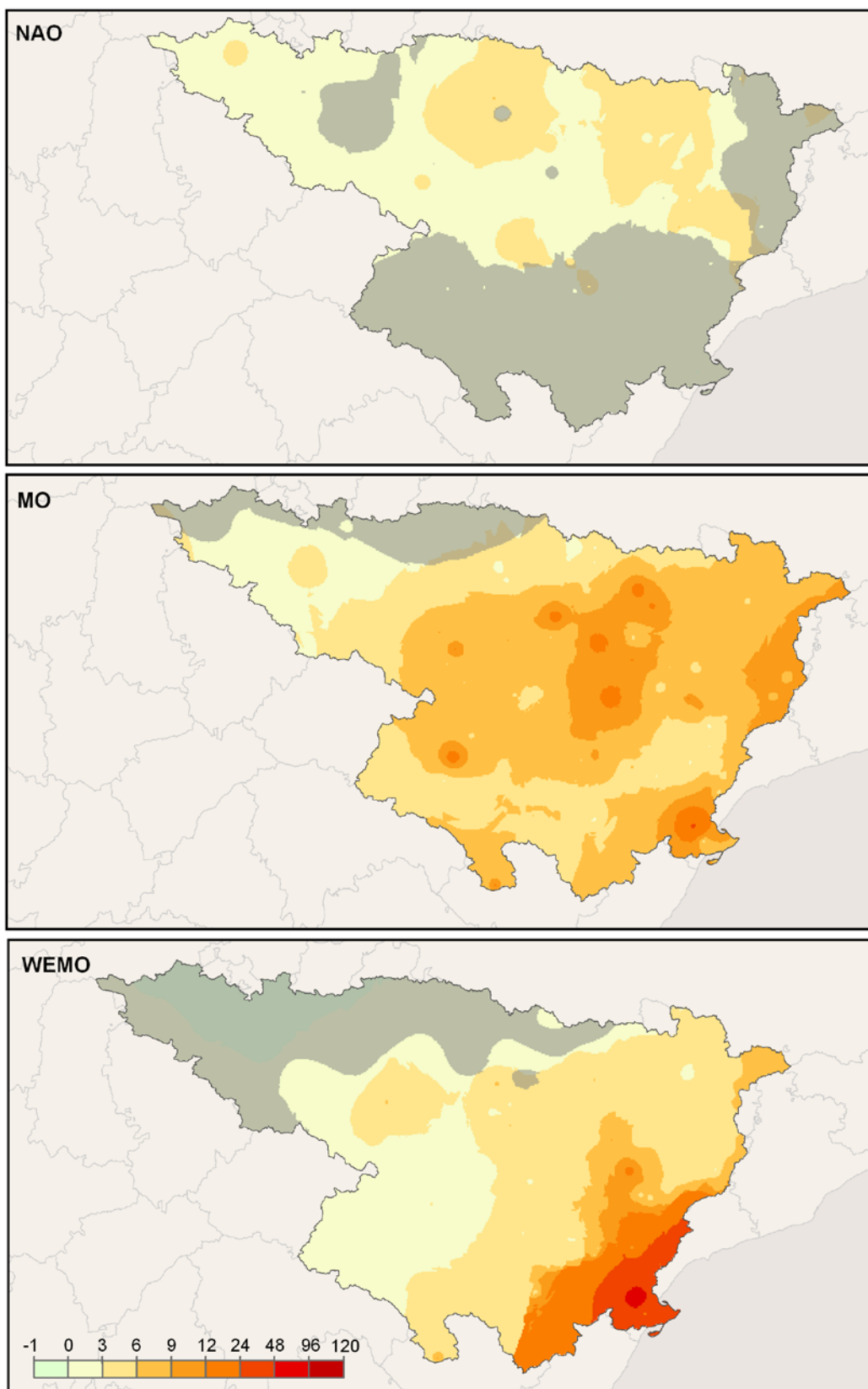


Figure 2.26 (cont.): Relative differences in median daily rainfall erosivity ( $\text{MJ mm ha}^{-1} \text{ day}^{-1}$ ) for **October** during negative and positive days of the atmospheric circulation indices for the period 1955-2006. Masked areas indicate no significant difference.

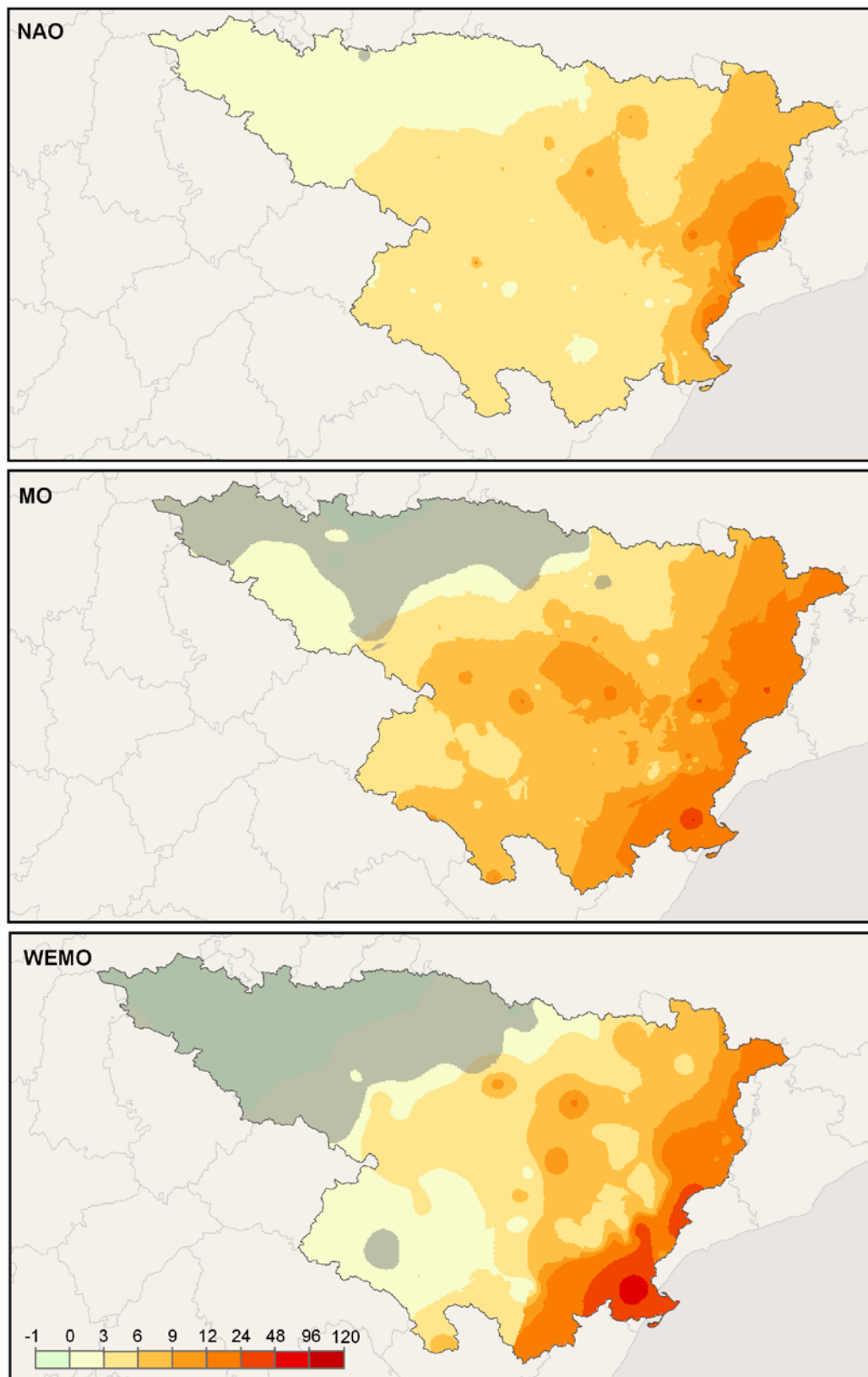


Figure 2.26 (cont.): Relative differences in median daily rainfall erosivity ( $\text{MJ mm ha}^{-1} \text{ day}^{-1}$ ) for **November** during negative and positive days of the atmospheric circulation indices for the period 1955-2006. Masked areas indicate no significant difference.

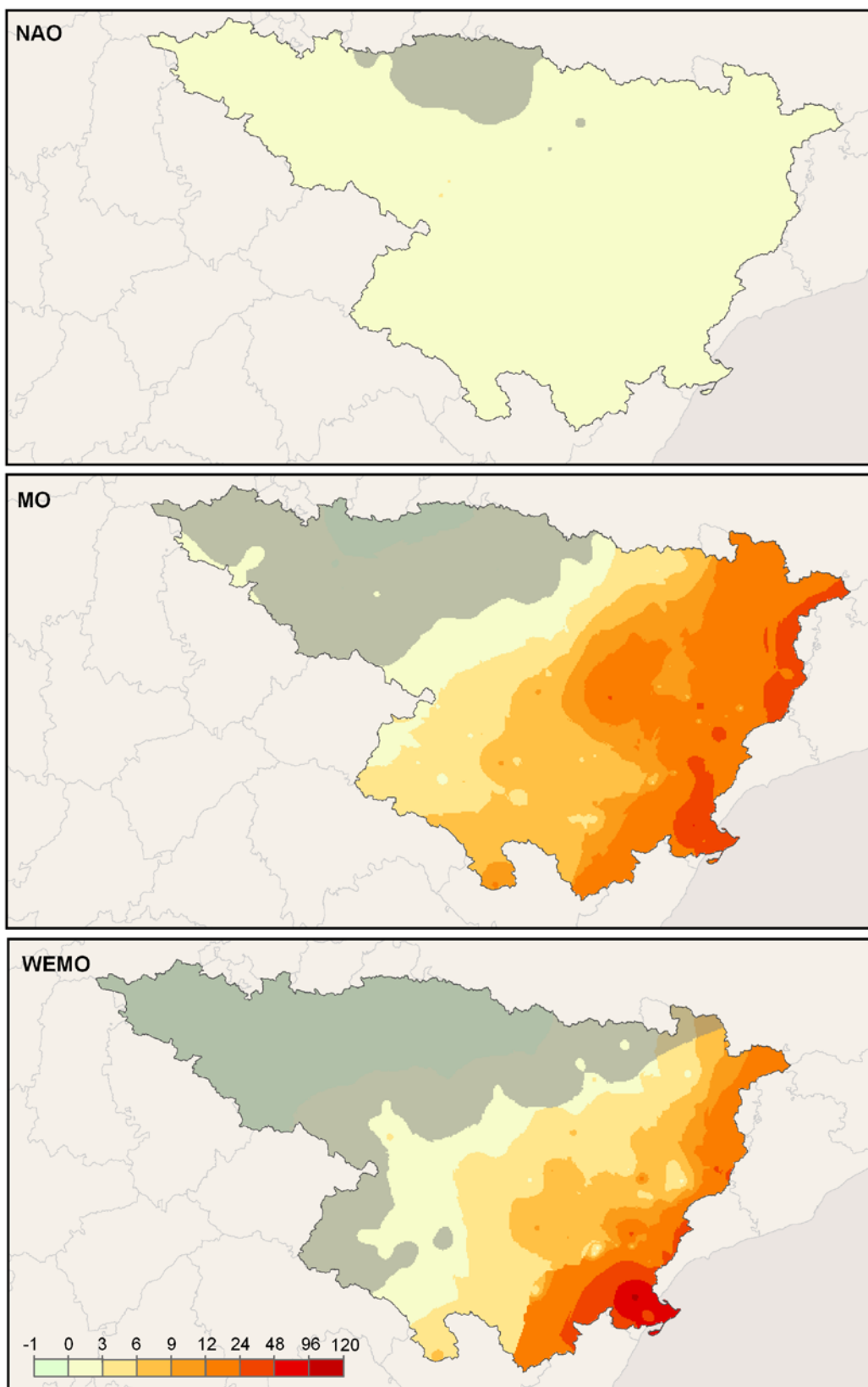


Figure 2.26 (cont.): Relative differences in median daily rainfall erosivity ( $\text{MJ mm ha}^{-1} \text{ day}^{-1}$ ) for **December** during negative and positive days of the atmospheric circulation indices for the period 1955-2006. Masked areas indicate no significant difference.



## *Differences in extreme rainfall erosivity between negative and positive NAO, MO and WEMO days*

The POT series of rainfall erosivity had a good fit to the GP distribution, as shown by the L-moment diagrams (Figure 2.27). Independently of the sign of the atmospheric circulation indices, the empirical L-moments of rainfall erosivity series plotted close to the theoretical curve of the GP distribution. This was especially evident when other possible candidate distributions were compared. The Kolmogorov-Smirnov test allowed accepting the GP distribution for the data, since only in very few cases the null hypothesis that the data came from a GP distribution was rejected at the defined significance level. This result agrees with recent studies that demonstrated the high performance of the GP distribution in fitting extreme hydrological variables using partial duration series (Hosking and Wallis, 1987; Madsen and Rosbjerg, 1997; Beguería, 2005). Here we also found that the GP distribution has a good performance in fitting daily rainfall erosivity data.

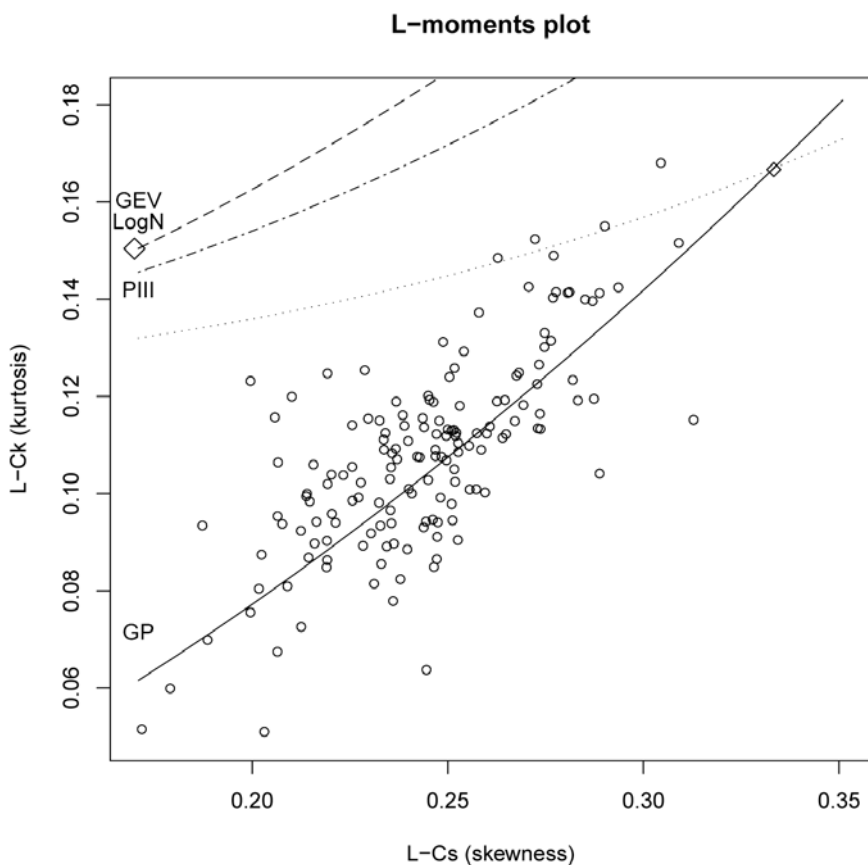


Figure 2.27: L-moments ratio diagram, comparing empirical L-moment ratios (L-skewness and L-kurtosis) with the ones of several widely used extreme value distributions: Generalized Extreme Value (GEV), Log-Normal (LN), Pearson III (PIII) and Pareto (GP).



By adjusting the daily rainfall erosivity series for the selected months to the GP probability distribution we obtained the probability of occurrence of extreme daily rainfall erosivity records associated with negative and positive NAO, MO and WeMO. Results showed greatest rainfall erosivity values expected under negative NAO, MO and WeMO conditions in most of the regions. Between the three indices the highest values were expected under negative WeMO. Differences could be found also between observatories. Those located inland to the south and south-west of the region did not show significant differences, coinciding with the results obtained in the precedent section. The Mediterranean coast and the mountains in the north and south of the area showed a high contrast between negative and positive conditions.

The rainfall erosivity expected for a return period of 10 years related with negative and positive NAO, MO and WeMO during winter are shown in Figure 2.28. Standard error maps for the predictions are shown in Figures 2.29. Under negative NAO daily rainfall erosivity values of  $50 \pm 8$  up to  $385 \pm 22$  MJ mm ha<sup>-1</sup> h<sup>-1</sup> d<sup>-1</sup> can be expected in the northern and eastern parts of the region. The highest values were concentrated in the north-east perimeter, close to the Mediterranean coast from the Ebro Delta upwards to the north and in the Central Pyrenees. Under positive NAO most of the region showed low expected daily rainfall erosivity values ranging between  $5 \pm 0.5$  and  $50 \pm 8$  MJ mm ha<sup>-1</sup> h<sup>-1</sup> d<sup>-1</sup>. High erosivity values during positive NAO were only expected in localized areas such as in the Ebro Delta and in the Central Pyrenees. Under negative MO the spatial pattern of the high daily rainfall erosivity values was similar to negative NAO, though higher values were expected. Most of the Mediterranean coast could record daily rainfall erosivity values ranging between  $150 \pm 12$  and  $250 \pm 16$  MJ mm ha<sup>-1</sup> h<sup>-1</sup> d<sup>-1</sup> with the Ebro Delta reaching values of  $385 \pm 20$  MJ mm ha<sup>-1</sup> h<sup>-1</sup> d<sup>-1</sup>. In contrast, under positive MO high erosivity values were only expected in a localized area in the north of the region, with expected values ranging between 100 and 125 MJ mm ha<sup>-1</sup> h<sup>-1</sup> d<sup>-1</sup>. Under negative WeMO the previous spatial patterns were reproduced although highest values are expected than with the other atmospheric patterns. A broader area close to the Mediterranean coast and in the central Pyrenees expected daily rainfall erosivity values ranging between  $150 \pm 8$  and  $250 \pm 16$  MJ mm ha<sup>-1</sup> h<sup>-1</sup> d<sup>-1</sup>, the highest values reaching up to  $500 \pm 16$  MJ mm ha<sup>-1</sup> h<sup>-1</sup> d<sup>-1</sup> close to the Ebro Delta and extending to the north. Positive



WeMO were related with high daily rainfall erosivity values in the mountain areas of north-west and in the central Pyrenees, with values ranging between  $100 \pm 4$  to  $150 \pm 8$  MJ mm  $\text{ha}^{-1}$   $\text{h}^{-1}$   $\text{d}^{-1}$  reaching in localised zones  $250 \pm 12$  MJ mm  $\text{ha}^{-1}$   $\text{h}^{-1}$   $\text{d}^{-1}$ .

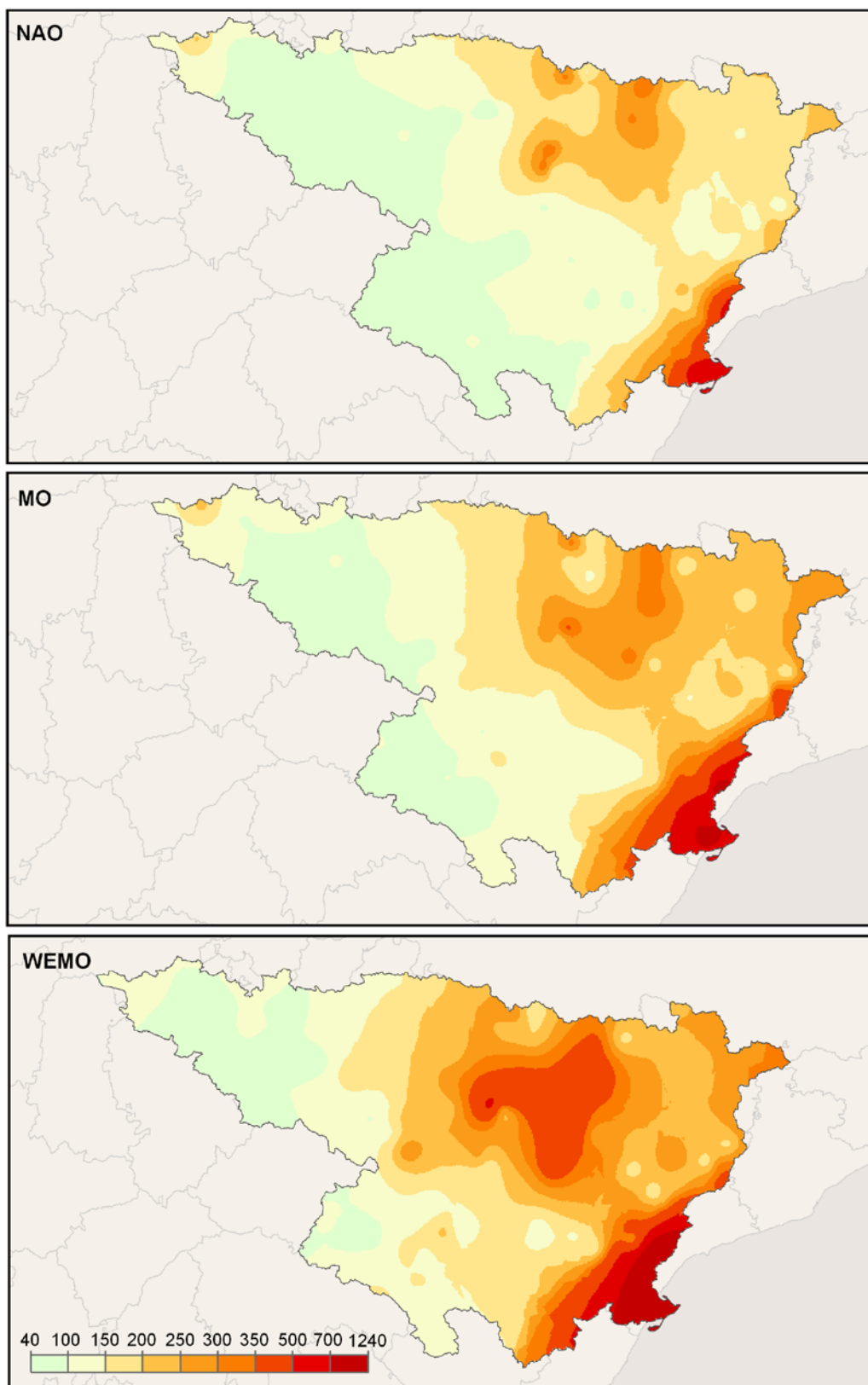


Figure 2.28: Expected extreme daily rainfall erosivity ( $\text{MJ mm ha}^{-1} \text{h}^{-1} \text{d}^{-1}$ ) during winter (September-April) corresponding to a return period of 10 years under **negative days** of the atmospheric circulation indices.

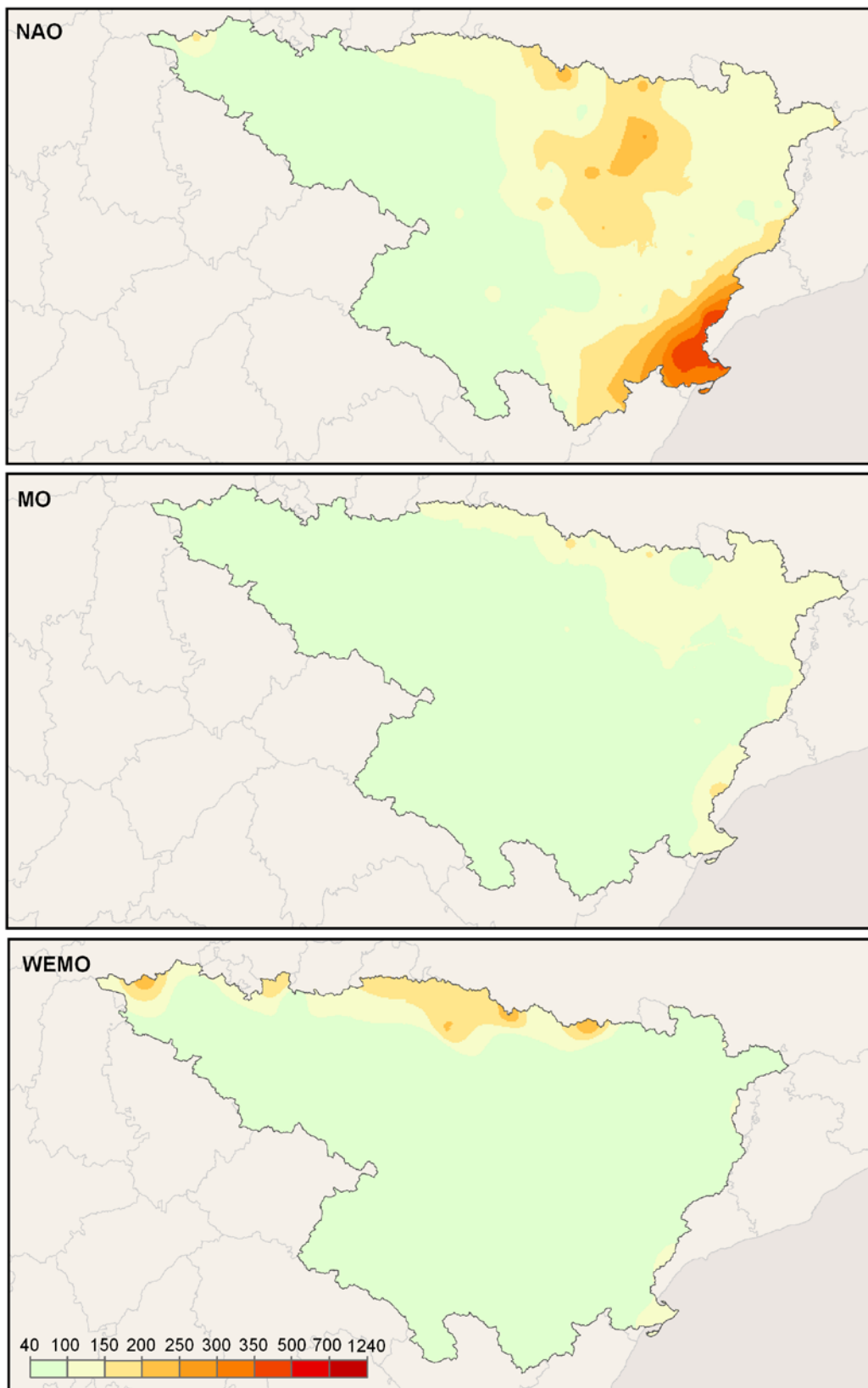


Figure 2.28 (cont.): Expected extreme daily rainfall erosivity ( $MJ \text{ mm ha}^{-1} h^{-1} d^{-1}$ ) during winter (September-April) corresponding to a return period of 10 years under **positive days** of the atmospheric circulation indices.

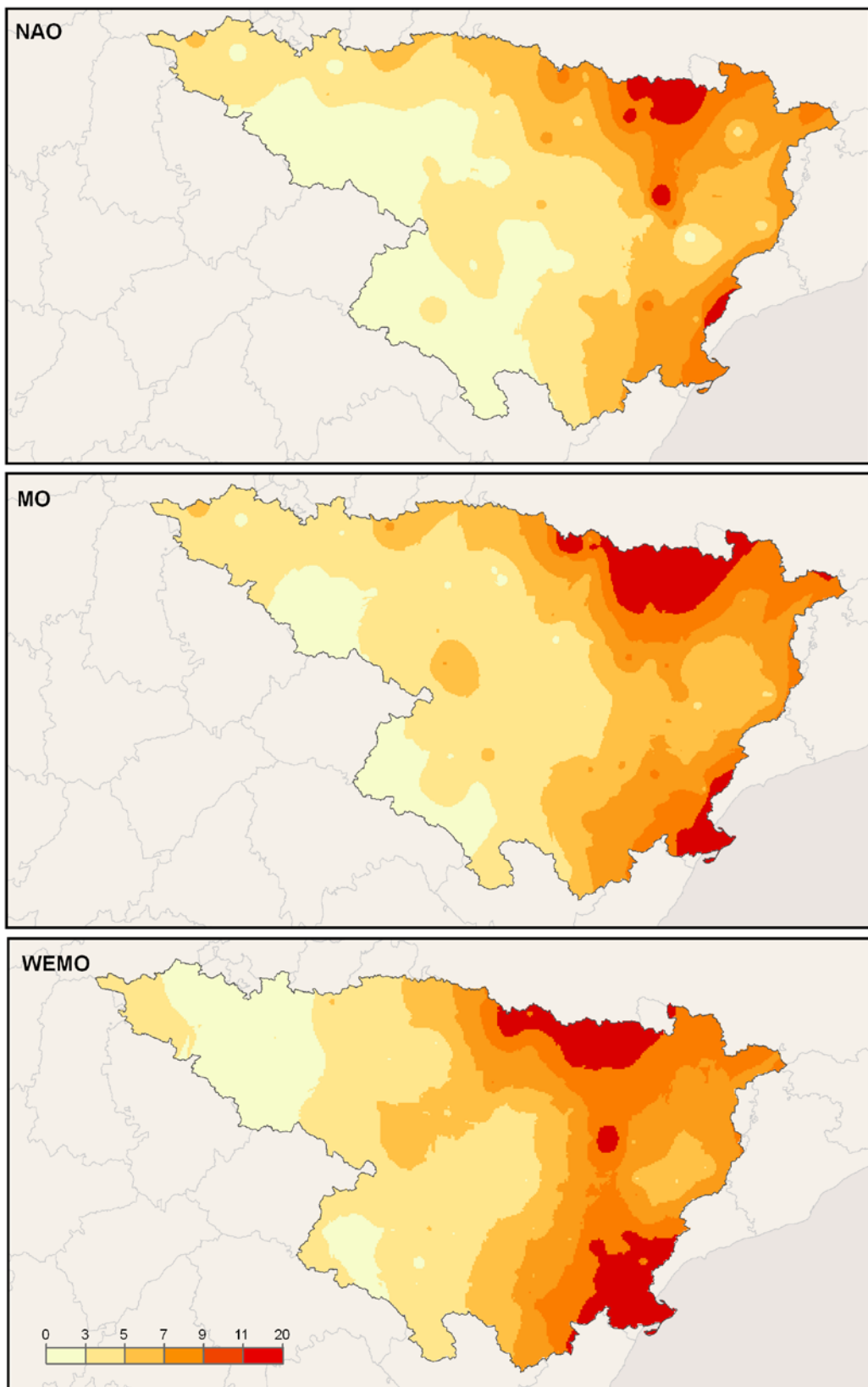


Figure 2.29: Standard error associated to the expected extreme daily rainfall erosivity ( $MJ mm ha^{-1} h^{-1} d^{-1}$ ) during winter (September-April) corresponding to a return period of 10 years under **negative days** of the atmospheric circulation indices.

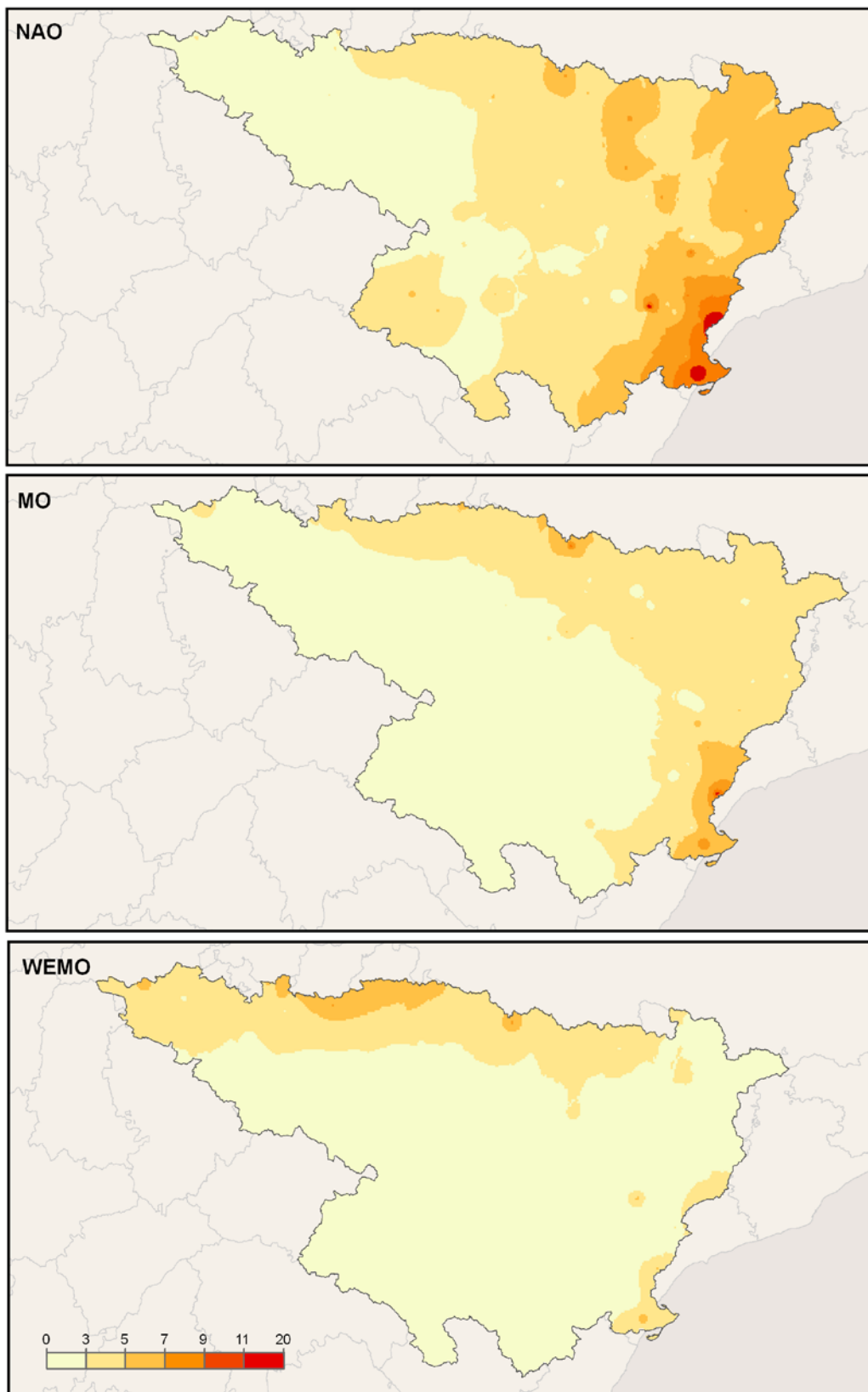


Figure 2.29 (cont.): Standard error associated to the expected extreme daily rainfall erosivity ( $\text{MJ mm ha}^{-1} \text{h}^{-1} \text{d}^{-1}$ ) during winter (September-April) corresponding to a return period of 10 years under **positive days** of the atmospheric circulation indices.



Taking as example the observatory X9987 in the Ebro delta we have generated the return period curves of the winter (September-April) extreme daily rainfall erosivity under positive and negative days of the indices (Figure 2.30). As expected from the location of the observatory in the area for which the influence of the indices is highest, the return period curves show a high contrast between the positive and negative days of the teleconnections, especially for MO and WeMO. For example, for a return period of 50 years the expected values under negative NAO are around  $1500 \text{ MJ mm ha}^{-1} \text{ h}^{-1} \text{ d}^{-1}$ , whereas under negative MO and WeMO they are higher than  $3000 \text{ MJ mm ha}^{-1} \text{ h}^{-1} \text{ d}^{-1}$ . The daily rainfall erosivity values expected under positive conditions of all of the indices are lower, especially in the case of the MO. For a return period of 50 years and positive NAO and WeMO the expected daily rainfall erosivity values are around  $1000 \text{ MJ mm ha}^{-1} \text{ h}^{-1} \text{ d}^{-1}$ , whereas under MO they are around  $500 \text{ MJ mm ha}^{-1} \text{ h}^{-1} \text{ d}^{-1}$ .

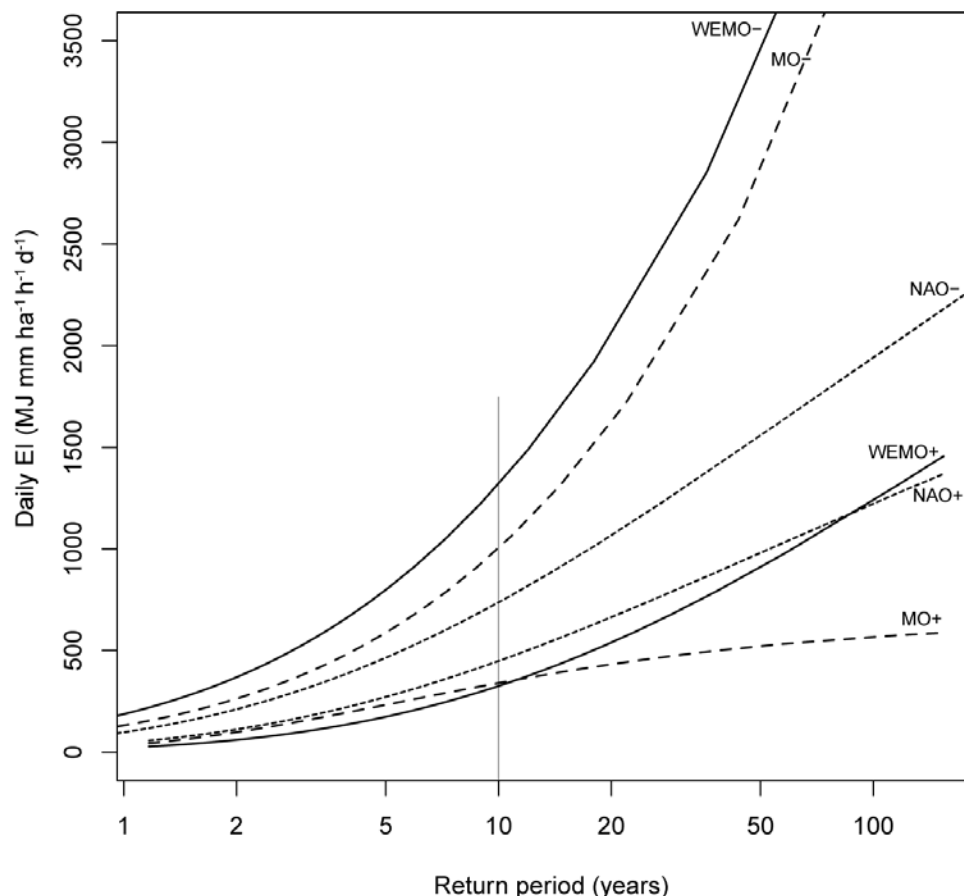


Figure 2.30: Return period curves for Ebro river delta (observatory X9987) of the winter (September-April) extreme daily rainfall erosivity under positive and negative days of the indices analysed. Grey line represents the extreme daily rainfall erosivity values under the different days of the indices for a return period of 10y, cartographed for all the observatories in figure 2.27.



### 2.9.3. Discussion

There is a general interest regarding the effects of climate dynamics, especially in a context of climate change, in the environment. However, very few studies have related the atmospheric circulation patterns to rainfall erosivity, due mostly to the lack of accurate rainfall erosivity series long enough to make this analysis possible. In this paper we investigate the differences in rainfall erosivity between positive and negative days of three well known atmospheric teleconnection patterns affecting rainfall in the Iberian peninsula: the NAO, the MO and the WeMO.

We analysed daily rainfall erosivity under positive and negative days of NAO, MO, and WeMO at the annual and monthly scales for the period 1955-2006 in 156 observatories in northeast Spain. The three teleconnection patterns had an influence on rainfall erosivity, with higher erosivities during negative modes of the three indices. This relationship was strongest between September and April, and almost no significant during the summer months. Between indices, NAO had the lowest influence on rainfall erosivity while in the cases of the MO, and especially the WeMO, the differences between positive and negative modes were greater. This is in agreement with previous studies, since the negative modes of the three teleconnections are related to increasing rainfall in the study area (Conte *et al.* 1989; Rodríguez-Puebla *et al.*, 1998; Palutikof, 2003; Dünkeloh and Jacobbeit, 2003; Martin-Vide and Lopez-Bustins, 2006; González-Hidalgo *et al.*, 2009). It has also been shown that WeMO has the highest influence of the three indices, most notably during autumn and winter, when the teleconnections control the geographic location of the major atmospheric features controlling the weather over the Iberian Peninsula.

Spatially, the influence was highest along the Mediterranean coast and decreased progressively towards the NW. The highest rainfall erosivities in the study area corresponded to negative WeMO days, and occurred around the Ebro delta. Regarding the spatial extent of the influence, the MO had the broadest extension of the significant area, while the effect of the WeMO was more restricted to the coastal zone. This also coincides with previous results analysing the influence of teleconnection indices on extreme rainfall events in the NE of Iberia (González-Hidalgo *et al.*, 2009).



The results regarding the extreme events analysis were similar. Comparison of high quantile expected values showed that the values expected under negative modes were highest for the three teleconnection patterns. The largest differences occurred along the Mediterranean coast, and WeMO showed the greatest influence between the indices. Vicente-Serrano et al. (2009) analysed extreme rainfall events in the same study area based on extreme events analysis, and found that both the Mediterranean (to the east) and the Cantabrian (to the north-west) coasts experienced the highest events, which were linked in both cases to the negative WeMO mode. This contrasts with our results, since we only found a significant relationship in the Mediterranean, but not in the NW area. This can be explained by the transformation of daily rainfall into erosivity, since the values of the parameters in equation (2.4) of this “Bloque”; section 2.4 differed notably between the two regions. Especially for certain months of the year, the same amounts of daily rainfall imply much higher erosivity values in the east than in the NW, since rainfall events of Mediterranean origin tend to be more intense and concentrated (and hence, more erosive) than frontal events of Atlantic origin.

It is a well-known fact that the NAO is responsible for most of the climatic variability in the North Atlantic, especially during winter. During its negative mode cyclones move southward increasing rainfall in most of the Iberian Peninsula. This influence, however, is reduced towards the east of the region due to the effect of the complex Iberian orography, which difficult the arrival of rainfall fronts from the Atlantic. Thus, rainfall variability close to the Mediterranean coast is more controlled by Mediterranean atmospheric dynamics. In this area, coupled modes as the MO and the WeMO have a larger influence on rainfall variability. The MO comprises those parts of the NAO linked with Mediterranean rainfall variability, and both indices are well correlated at the daily scale between September and April—Pearson correlation coefficient of 0.5 for daily values from 01/01/1955 up to 31/12/2006. The WeMO index, in contrast, is mostly uncorrelated with both indices—Pearson correlation coefficient of 0.1 with NAO, and 0.3 with MO—. Thus, it is possible that the combined effect of negative days of NAO and of WeMO, or MO and WeMO, occurring simultaneously would result in even higher rainfall erosivity values. However, the analysis of this article is restricted to the single effect of the indices, so this possibility has not been tested.



## 2.9.4 Conclusions

Expected rainfall erosivities can be two orders of magnitude higher under negative phases of the NAO, MO and WeMO in our study area, especially along the Mediterranean coast in autumn and early winter. The loss of fertile soil during this period of the year when agricultural lands are mostly bare is directly related to the rainfall erosivity and the slope gradient. Soil protection measures such as mulching help absorbing part of the kinetic energy of the rain can be effective in reducing soil splash detachment.





## 2.10. Trends in rainfall erosivity (1955-2006) over the Ebro Basin (NE Spain)<sup>4</sup>

The rainfall effect on the soil is known as rainfall erosivity. When a rainfall event occurs two erosion processes are triggering: i) *splash* or the disaggregation of soil particles by the impact forces, due to the discrete character of rainfall formed by raindrops; and ii) *runoff* erosion, once soil has reached saturation or by shear stress. This process accounts for the continuous character of rainfall as cumulative volume of water falling over the surface. Rainfall erosivity shows an exponential relation with rainfall, indicating the erosion potential of high rainfall events. Previously, it has been pointed out the difficulties on measuring rainfall erosivity, owing to them there is a need of using models to determine rainfall erosivity for its spatiotemporal analysis. The spatiotemporal study of rainfall erosivity requires long and dense databases able to capture the influences of geographical and climatological factors related with atmospheric dynamics. One of the main contributions of this study is the daily rainfall erosivity database for the period 1955-2006. This database is explained in detail in section 2.4-ii, and is the base for long term climatological studies as spatiotemporal analysis.

There is an increasing interest on assessing the impacts of climate change. Global warming is certain, but changes in rainfall parameters are not well understood (López-Moreno et al., 2010). They involve changes in atmospheric dynamics and the relative humidity; their relations with temperature and geographical factors, as topography, water masses and the heating balance between water and earth masses influencing atmospheric dynamics (Ingram, 2002). The erosivity power of the rainfall is responsible for changes in the soil properties due to crusting, disruption of aggregates, removal of nutrient rich particles, etc. (Nearing et al., 2004). Regarding rainfall erosivity, more factors have to be taking into account as soil water content in relation with rainfall and vegetation together with agriculture seasonal changes (Nearing et al., 2004, Kendon et al., 2010). The Intergovernmental Panel on Climate Change (IPCC) predicts significant changes in precipitation in the future over many areas of Europe (Christensen et al.,

<sup>4</sup> This section is extended from: Angulo-Martínez, M., Vicente-Serrano, S.M., Beguería, S., 2009. Tendencias en la erosividad de la lluvia (1955-2006) en la cuenca del Ebro. En Romero Díaz, A., Belmonte Serrano, F., Alonso Sarria, F., López Bermúdez, F. (eds). 2009. *Avances en estudios sobre desertificación. Aportaciones al congreso internacional sobre desertificación en memoria del profesor John B. Thornes*. Servicio de publicaciones de la Universidad de Murcia. 511-515.



2007). Particularly, current climate models suggest that the annual precipitation will decrease in the Mediterranean area. However, increases in variability and higher amounts of erosive rainfall are expected (Sauerborn et al., 1999) mainly as a consequence of changes in daily variability and precipitation extremes (Kendon et al., 2010). It is therefore necessary to analyse historical climate data to verify possible trends at different time scales to account for spatial and temporal variability.

A number of studies have found decreasing annual precipitation in the Iberian Peninsula since the mid 20th century, with seasonal and spatial variations (Palutikof et al., 1996; Esteban-Parra et al., 1998; Rodríguez-Puebla et al., 1998; Sauerborn et al., 1999; Trigo et al., 2000; Goodess and Palutikof, 2002; Paredes et al., 2006; Lopez-Bustins et al., 2008; González-Hidalgo et al., 2009 and 2010; Pokrovsky, 2009; Rodrigo, 2010; López-Moreno et al., 2010). These trends have been related with changes in atmospheric circulation patterns towards dryer conditions due to the northward displacement of the polar fronts, and are consistent with the evolution of major teleconnections affecting precipitation over the Iberian Peninsula such as the North Atlantic Oscillation, the Mediterranean Oscillation and the Western Mediterranean Oscillation.

De Luis et al. (2010) analysed specifically trends in rainfall erosivity in the Mediterranean basin of the Iberian Peninsula for the period 1950-2000, based on a dense and high-quality database of monthly precipitation that allowed them to compute the Modified Fournier Index (MFI). They reported an overall decrease in annual rainfall and increases in rainfall concentration, while changes in rainfall erosivity varied in space. For the Ebro basin, the study area of this analysis, they found mostly a reduction of the MFI, except in the northernmost sector (Pyrenean Range). Although interesting and valid, precipitation data at a monthly scale do not provide enough resolution to be conclusive with respect to rainfall erosivity, since a very few number of short but intense rainfall events are responsible for the largest fraction of the total annual rainfall erosivity in most climates. In this section trends in annual, monthly and daily rainfall erosivity during the period 1955-2006 in the Ebro basin are analyzed.



## 2.10.1 Methods

A daily rainfall erosivity database for the period 1955-2006 formed by 156 observatories is used in this study. Details of this database are given in section 2.4-ii. Daily rainfall erosivity series were summarized at monthly and annual scale. Temporal evolution of rainfall erosivity data were analysed by linear regression means between rainfall erosivity and time, at annual and seasonal scale. All the events corresponding to a given season or during the year are summed for that season or year, in the case of daily events they are separated according to the season. The variation is given by the increment or interest produced following the regression line or trend. The decadal change was used to quantify changes in rainfall erosivity at different scales. In the case of daily rainfall erosivity events, we analysed the evolution in the number of days with rainfall erosivity value corresponding to the quintiles at annual and seasonal scale. To help visualising spatial differences in the decadal change, maps were generated by means of local first grade polynomial interpolation. Significant variations at 95% were evaluated by Mann-Kendall test.

## 2.10.2 Results

### *Annual and seasonal rainfall erosivity*

The annual rainfall erosivity experienced a decreasing trend in most of the study area during the period 1955–2006 (Figure 2.31). Per decade change was as high as  $-200 \text{ MJ mm ha}^{-1} \text{ h}^{-1} \text{ y}^{-1}$  in some areas such as in the NE of the study area (eastern Pyrenees), but in most of the area the decrease per decade was lower than  $30 \text{ MJ mm ha}^{-1} \text{ h}^{-1} \text{ y}^{-1}$  per decade. When compared with the mean annual rainfall erosivity (Figure 2.7), the highest relative changes occurred at the NE of the study area, since the decrease of rainfall erosivity represented 60-80% of the average over the whole study period (five decades).

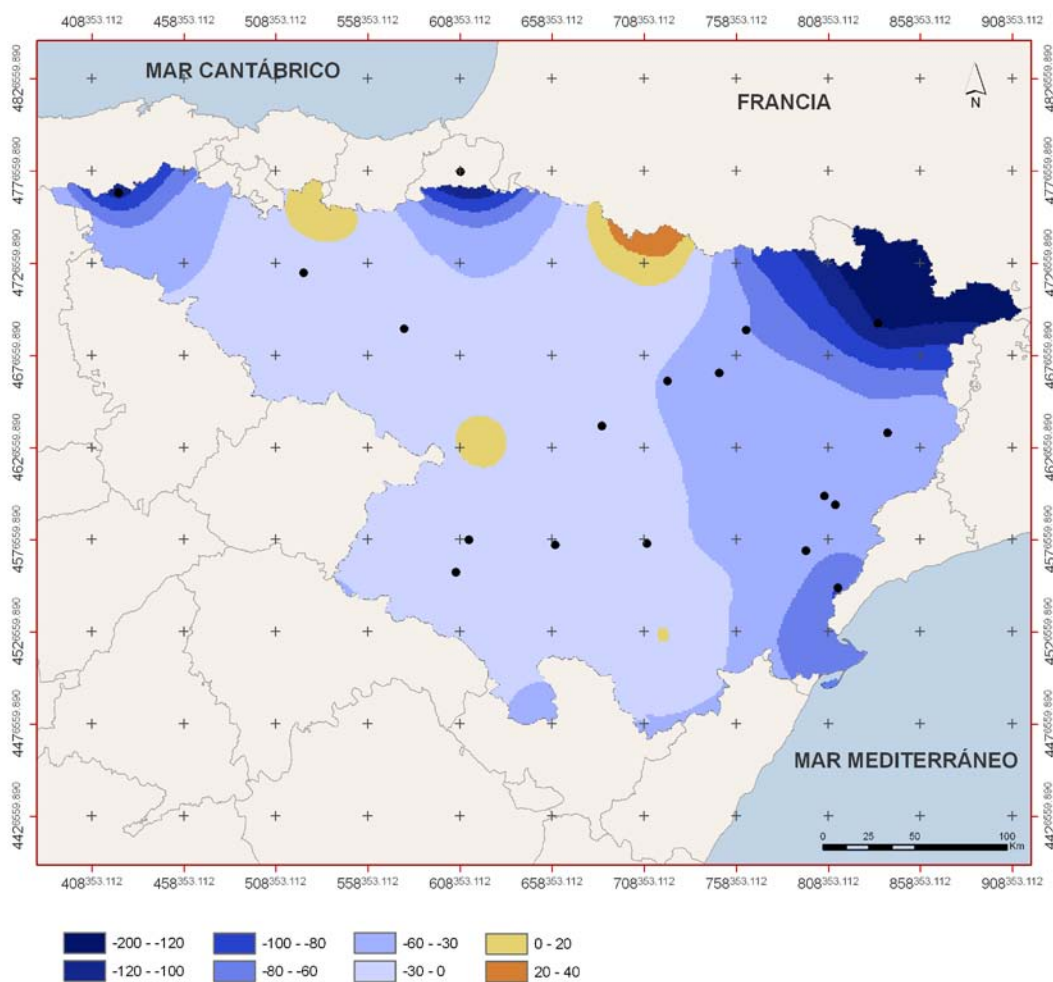


Figure 2.31: Per decade change of annual rainfall erosivity during the period 1955-2006 ( $\text{MJ mm ha}^{-1} \text{h}^{-1} \text{y}^{-1}$ ). Black circles indicate data series for which the trend was significant at the 95% confidence level.

Spatial differences were most noticeable when analysed at a seasonal basis (Figure 2.32). While in winter and spring trends were negative in most of the study area, with the most negative trends in the NE corner, in summer and autumn there were larger spatial differences. Summer yield the most heterogeneous results, since in some interior areas slightly positive trends were registered while the NE quadrant and some small areas in the North and NW experienced strong negative trends. In autumn negative trends predominated overall and were especially strong in the SE and NW corners, but positive trends were also found in the North along the Pyrenean range.

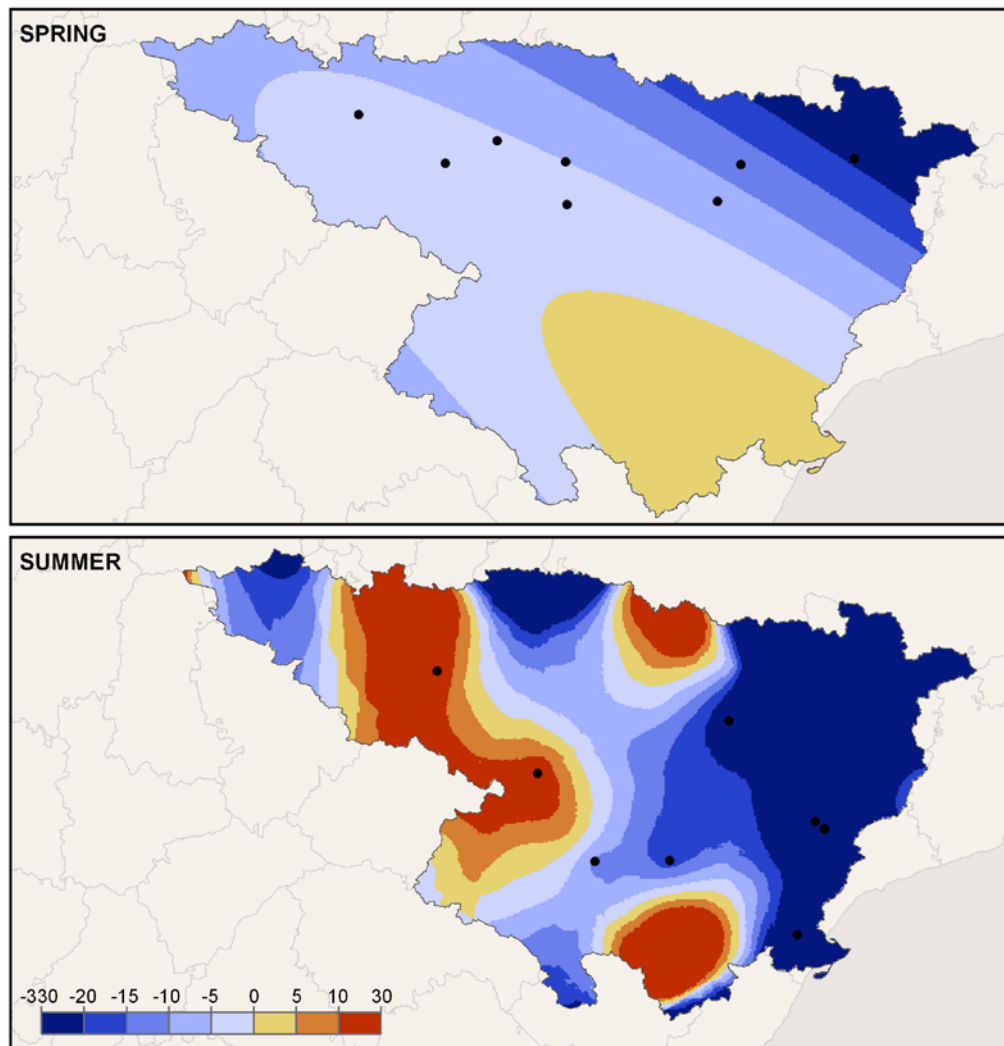


Figure 2.32: Per decade change of seasonal rainfall erosivity (spring and summer) during the period 1955-2006 ( $\text{MJ mm ha}^{-1} \text{h}^{-1} \text{y}^{-1}$ ). Black circles indicate data series for which the trend was significant at the 95% confidence level.

Although negative trends predominated overall at both annual and seasonal basis, these results should be taken with care since significance was achieved only in a small fraction of the stations (Table 2.8)

Table 2.8: Number and proportion of series with significant trends at the 95% confidence level.

Time period	Nº positive trends (%)	Nº negative trends (%)
Annual	1 (0.6%)	21 (13.5%)
Spring	1 (0.6%)	13 (8.3%)
Summer	2 (1.3%)	6 (3.9%)
Autumn	1 (0.6%)	11 (7.1%)
Winter	0	18 (11.5%)

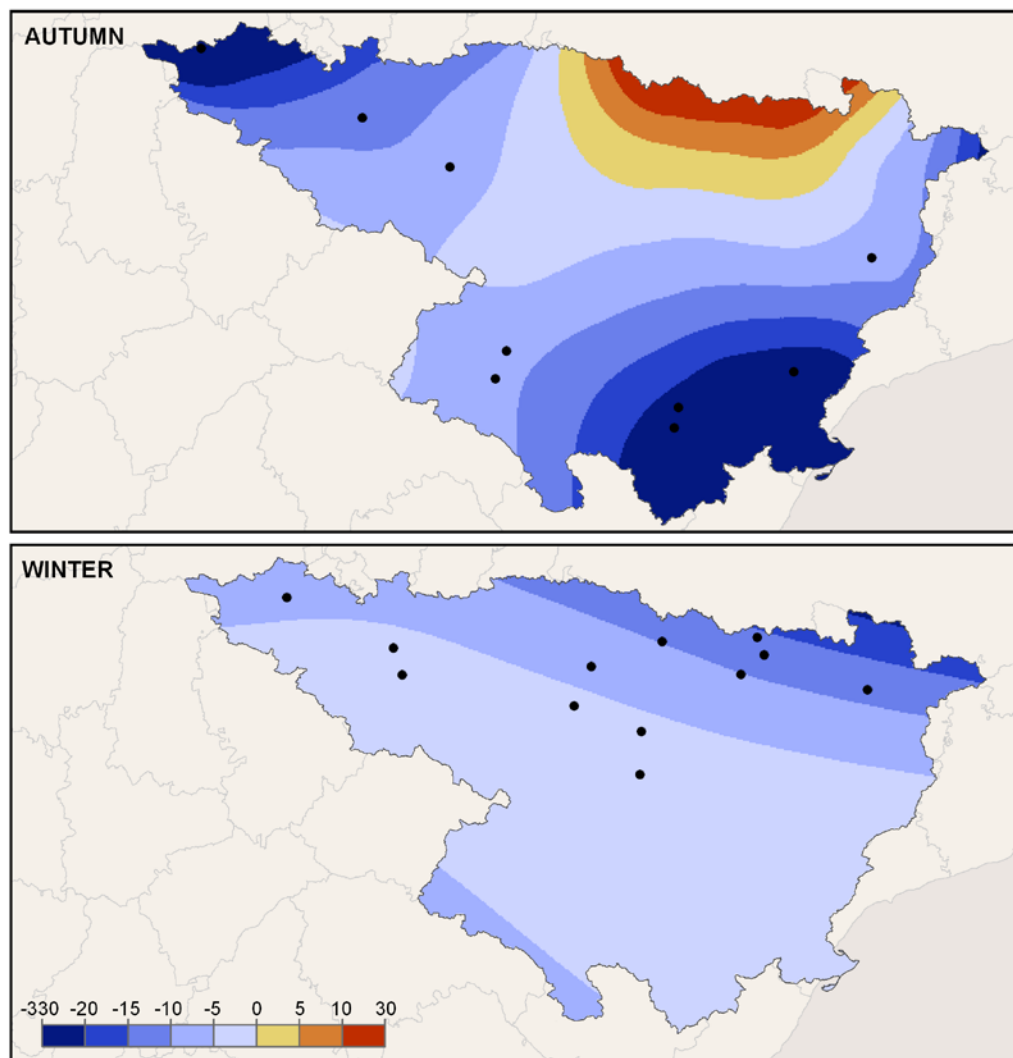


Figure 2.32 (cont.): Per decade change of seasonal rainfall erosivity (autumn and winter) during the period 1955-2006 ( $\text{MJ mm ha}^{-1} \text{h}^{-1} \text{y}^{-1}$ ). Black circles indicate data series for which the trend was significant at the 95% confidence level



Due to the paramount importance of the most erosive events in determining total erosivity, assessing trends in daily rainfall erosivity becomes highly relevant. Variations in the number of events grouped by quintiles allow assessing trends in the occurrence of rainfall erosivity events across the range of erosivity values (Figure 3.33). Since the range of the quintiles are calculated for each data series considering the whole study period (1955–2006), values below zero indicate a diminishing number of events, while positive values indicate an increasing number of events. The results show clearly that the number of very low and low erosivity events (Q1, below 20%, and Q2, between 20 and 40%) increased in a large number of stations, while the number of medium, high and very high erosivity events (Q3 to Q5) decreased.

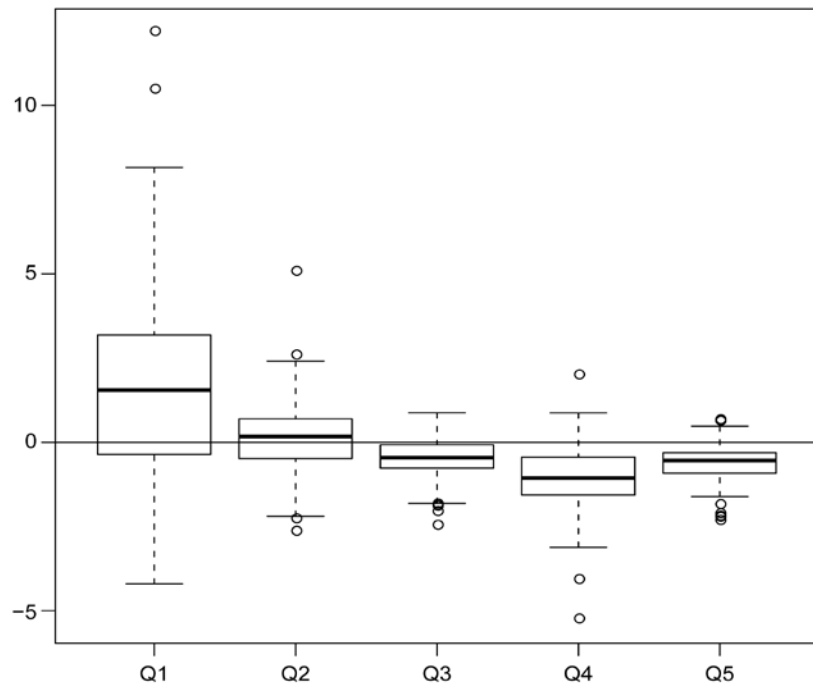


Figure 2.33: Boxplots of trends in the number of daily rainfall erosivity events classified by quintiles of daily erosivity over the whole period 1955–2006.

Spatially, the number of events in the first quintile increased between one and four events per year in most of the study area, and only in the NE corner (eastern Pyrenees) a negative trend was found (Figure 2.34). Trends were significant in the majority of stations (58.4%). The number of events in the fifth quintile, on the other hand, decreased between 0.25 and one event per year in the whole study area, with significant trends in 29.5% of the stations.

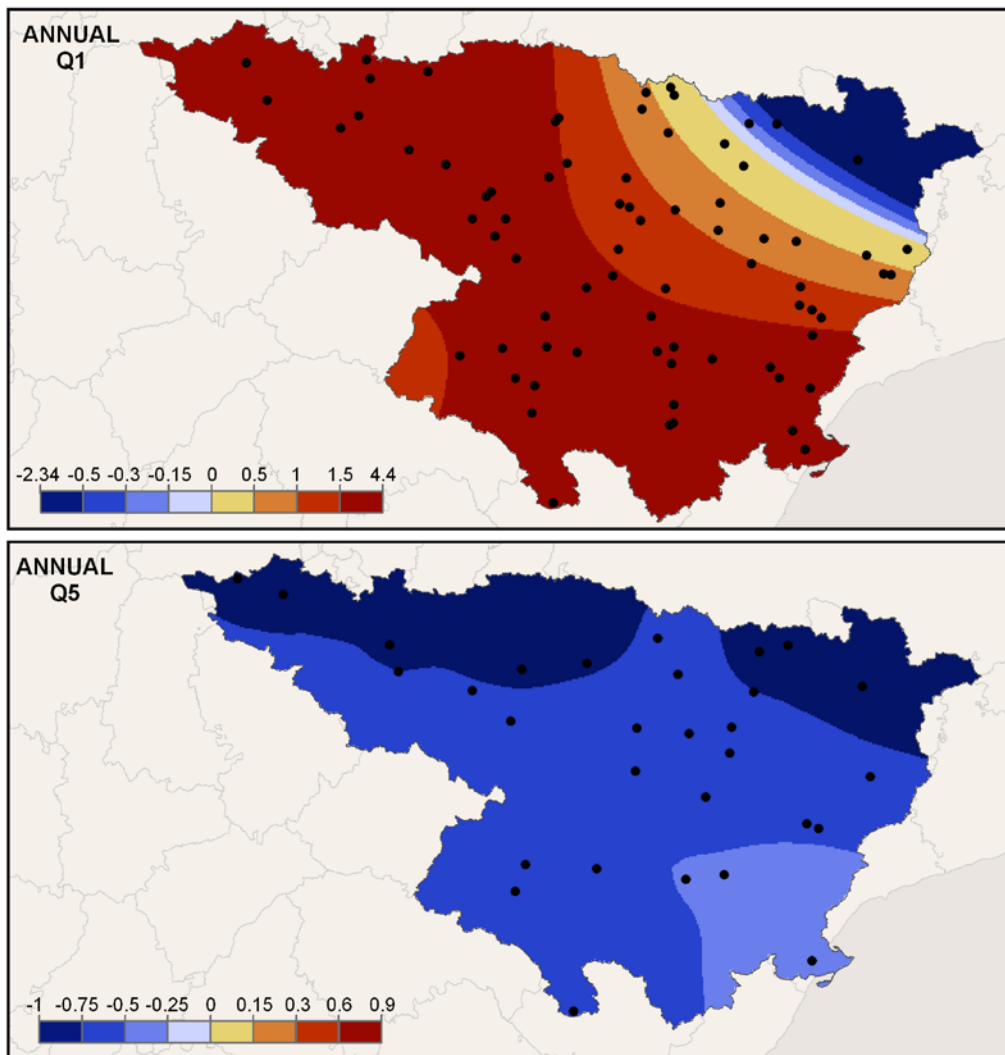


Figure 2.34: Per decade change in the number of daily rainfall erosivity events corresponding to the first (Q1) and fifth (Q5) quintiles for the period 1955-2006. Black circles indicate significant trends at the 95% confidence level.

The same pattern (increasing number of Q1 events and decreasing number of Q5 events) was found at the seasonal basis (Figure 2.35), with a few exceptions: i) the number of Q1 events decreased in winter in the NE corner; and ii) the number of Q5 events increased in autumn in a small area in the central and western Pyrenees at the N of the study area. The number and proportion of stations with significant trends is shown in Table 2.9 and Table 2.10.

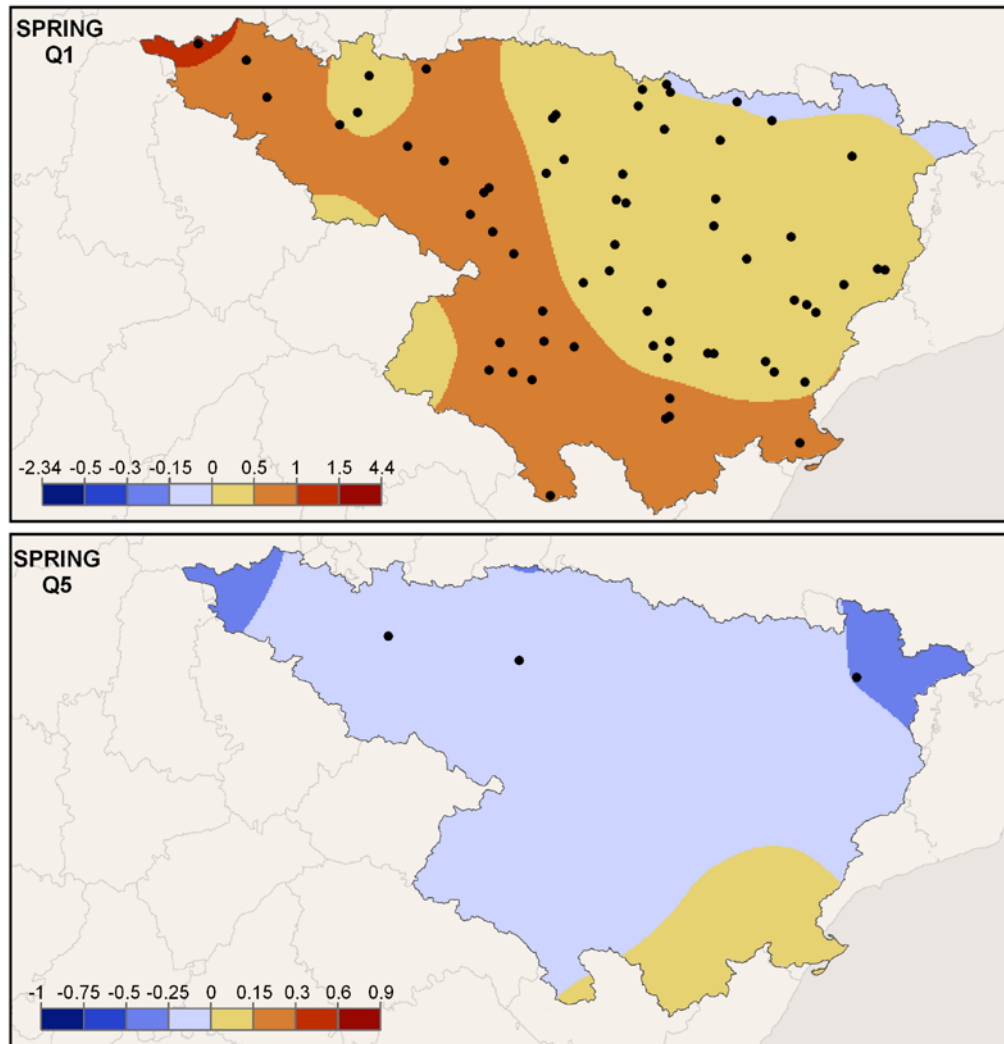


Figure 2.35: Per decade change in the number of daily rainfall erosivity events in **spring** corresponding to the first (Q1) and fifth (Q5) quintiles for the period 1955-2006. Black circles indicate significant trends at the 95% confidence level.

Table 2.9: Number and proportion of series with trends in the number of events in the first quintile (Q1) significant at the 95% confidence level.

Time period	Nº positive trends (%)	Nº negative trends (%)
Annual	70 (44.9%)	21 (13.5%)
Spring	64 (41.0%)	15 (9.2%)
Summer	59 (37.8%)	14 (9.0%)
Autumn	82 (52.6%)	11 (7.1%)
Winter	63 (40.4%)	20 (12.8%)

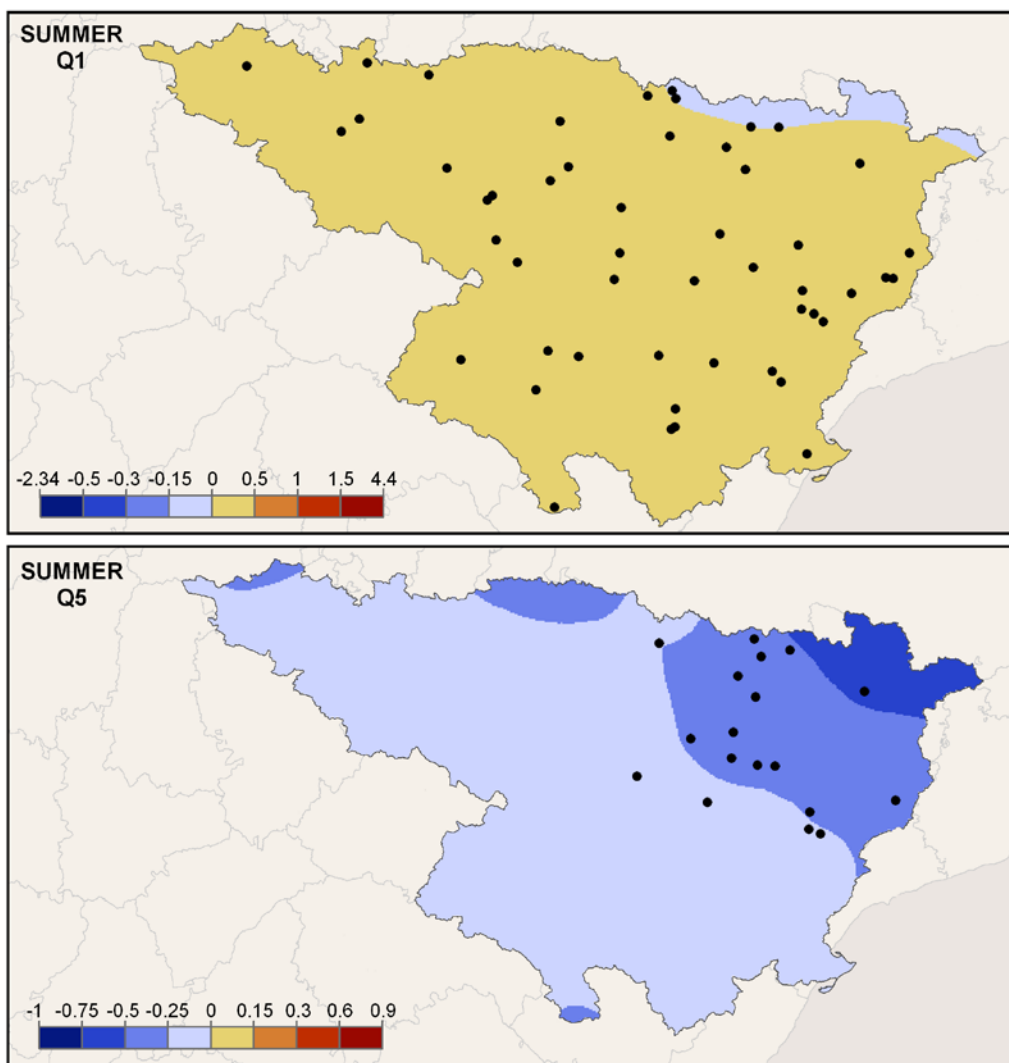


Figure 2.35 (cont.): Per decade change in the number of daily rainfall erosivity events in **summer** corresponding to the first (Q1) and fifth (Q5) quintiles for the period 1955-2006. Black circles indicate significant trends at the 95% confidence level.

Table 2.10: Number and proportion of series with trends in the number of events in the fifth quintile (Q5) significant at the 95% confidence level.

Time period	Nº positive trends (%)	Nº negative trends (%)
Annual	0	46 (29.5%)
Spring	0	6 (3.8%)
Summer	0	26 (16.6%)
Autumn	0	13 (8.3%)
Winter	0	32 (20.5%)

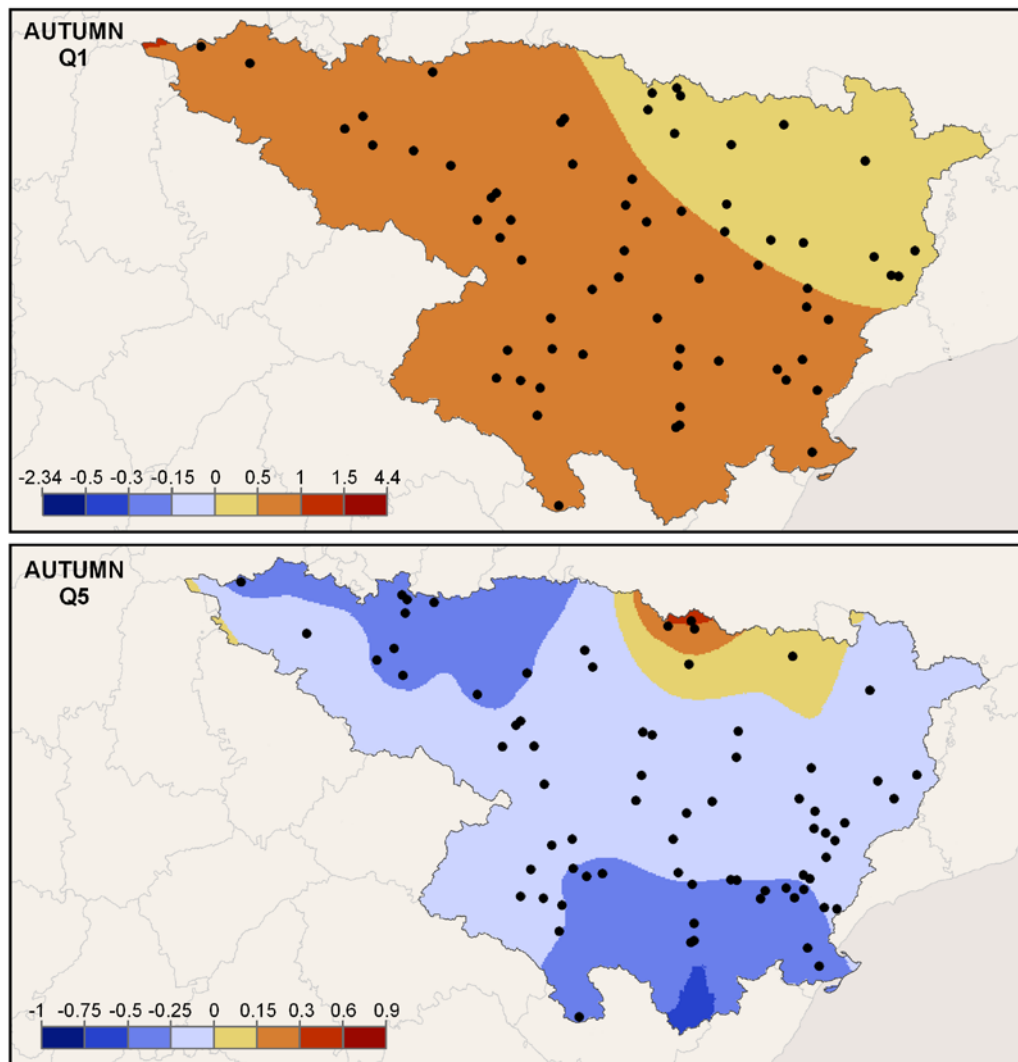


Figure 2.35 (cont.): Per decade change in the number of daily rainfall erosivity events in **autumn** corresponding to the first (Q1) and fifth (Q5) quintiles for the period 1955-2006. Black circles indicate significant trends at the 95% confidence level.

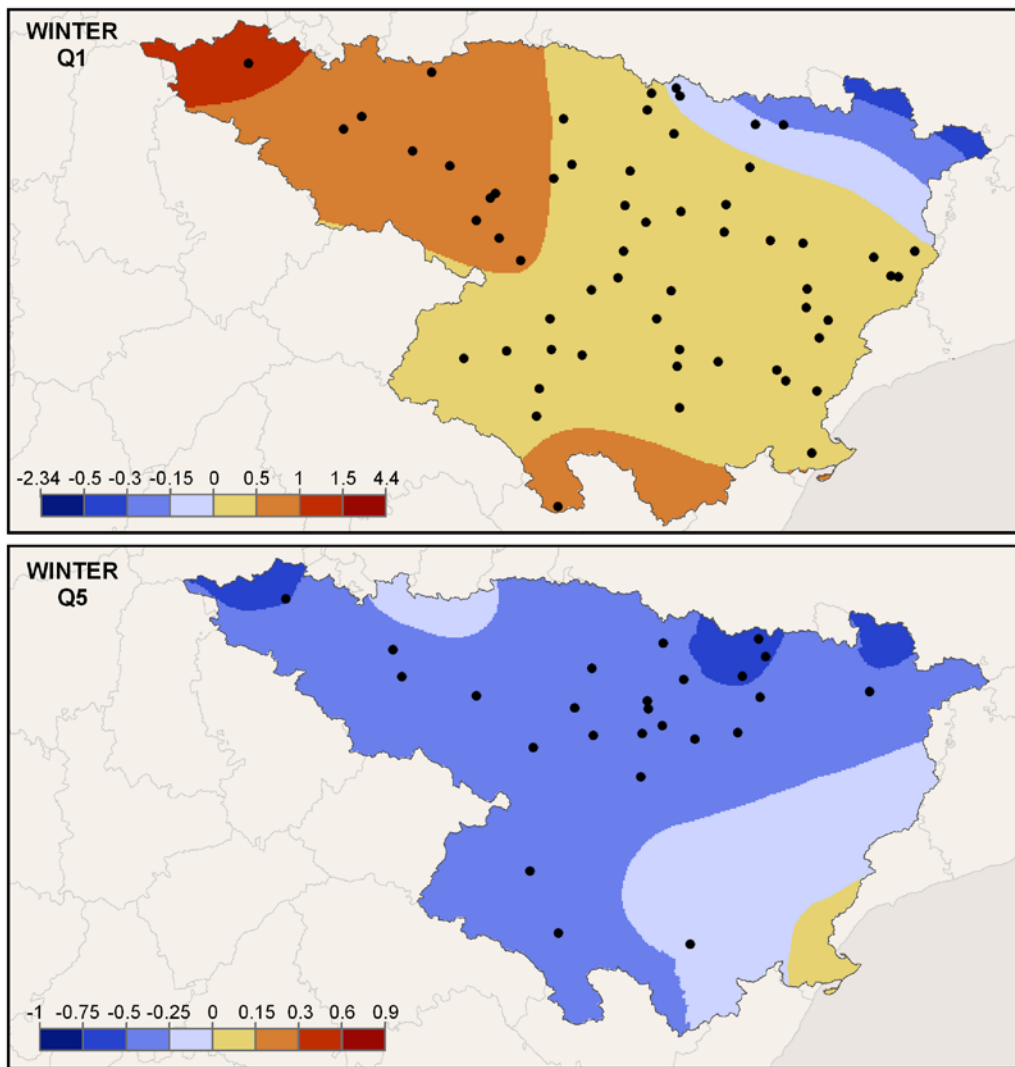


Figure 2.35 (cont.): Per decade change in the number of daily rainfall erosivity events in **winter** corresponding to the first (Q1) and fifth (Q5) quintiles for the period 1955-2006. Black circles indicate significant trends at the 95% confidence level.



### 2.10.3 Discussion

Planning of soil conservation measurements, especially concerning agriculture practices, requires a good knowledge of all factors affecting soil erosion. Among them, rainfall erosivity is one of the least studied, although its spatial and temporal dynamics can be of paramount importance when they are related to other factors such as land use and cropping practices. The development of long time series of daily rainfall erosivity (sections 2.4-ii and 2.6), even subject to uncertainty, proved being valuable in assessing the spatial and temporal dynamics of rainfall erosivity. Compared to these, data at coarser temporal resolution such as monthly precipitation series miss the importance of a few, very intense events that account for the largest fraction of total annual or seasonal rainfall erosivity.

Our results indicate a generalized decrease in annual and seasonal rainfall erosivities. This could be explained in part by decreasing precipitation trends over the Iberian Peninsula especially during the wet season from October to May (Palutikof et al., 1996; Esteban-Parra et al., 1998; Rodríguez-Puebla et al., 1998; Sauerborn et al., 1999; Trigo et al., 2000; Goodess and Palutikof, 2002; Paredes et al., 2006; Lopez-Bustins et al., 2008; González-Hidalgo et al., 2009; Pokrovsky, 2009; Rodrigo, 2010; López-Moreno et al., 2010). However, deeper inspection revealed that this trend in the annual erosivity is related to changes in the frequency distribution of erosivity events, since the number of events of low erosivity increased while the number of highly erosive events decreased. Due to the exponential distribution of rainfall erosivity the higher events account for a large part of the total cumulative erosivity, so any reduction in the frequency of high events produces a large reduction of the annual erosivity.

These results are in agreement with previous studies. In their analysis of daily precipitation in the NE of Iberia López-Moreno et al. (2010) found decreasing trends in the number of heavy precipitation events and in the relative contribution of heavy events to the annual rainfall, while the number and relative importance of light and moderate events increased. Recent results based on the non-stationary peaks-over-threshold approach to extreme events analysis found evidences of decreasing frequency and magnitude of extreme rainfall events over most of the Iberian Peninsula and in particular in its NE quadrant (Beguería et al., 2011; Acero et al., 2012).



Based on monthly precipitation data covering the Mediterranean basins of the Iberian Peninsula De Luis et al. (2010a) reported a generalized decrease in the annual precipitation. In the Ebro basin, coinciding with the study area of this study, they found that decreasing trends of the modified Fournier index (an index of rainfall erosivity based on monthly data) predominated in general, except at the North of the study area, in the Pyrenees. They did not perform seasonal analysis, but in another studies the same authors found that annual and monthly precipitation generally decreased in the Ebro basin except in February and October were a slightly increase was found along the Pyrenees (González-Hidalgo, 2009; De Luis et al., 2010b; González-Hidalgo, 2010). This coincides with our findings, since the frequency of high erosivity events (Q5) only increased in autumn in the Pyrenees.

As other authors have pointed out, strong precipitation events in the study area are significantly related to negative phases of the North Atlantic Oscillation, the Mediterranean Oscillation and the Western Mediterranean Oscillation (González-Hidalgo, 2009). The generalized decreasing precipitation along the Mediterranean basin of the Iberian Peninsula has been related to prevailing positive conditions of NAO and MO (Figure 2.36). In a previous section (section 2.8) we found a significant negative relationship between rainfall erosivity and three teleconnection indices, which was largest for the WeMO. The time evolution of the WeMO during the study period is much more stationary than the MO evolution, so it has probably contributed in a lesser extent to the evolution of rainfall erosivities.

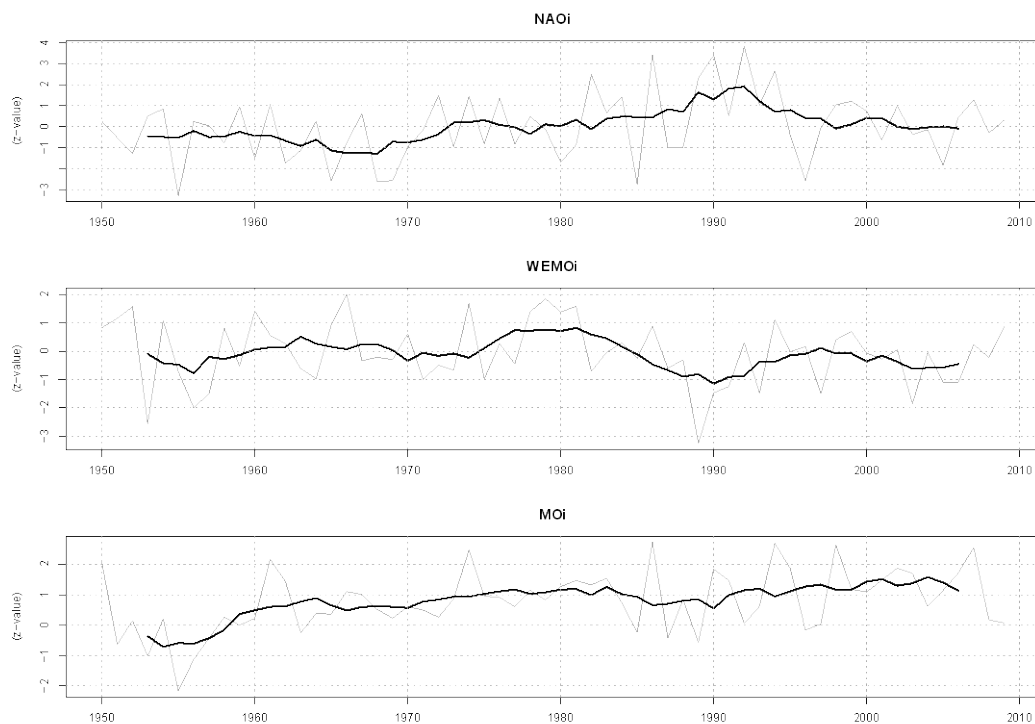


Figure 2.36: Temporal evolution of October to March NAO, WeMO and MO indices obtained from average daily indices. Source: Vicente-Serrano et al., 2009.

However, deeper inspection revealed that this trend in annual erosivity is related to changes in the frequency distribution of erosivity events, since the number of events of low erosivity increased while the number of highly erosive events decreased. Due to the exponential distribution of rainfall erosivity the higher events account for a large part of the total cumulative erosivity, therefore any reduction in the frequency of the high events produces a reduction in annual erosivity. The results of the relation between extreme rainfall erosivity events with NAO, MO and WeMO presented in section 2.8 showed more probability of extreme events occurrence under the negative phase of these indices and more probability of low rainfall erosivity events with the opposite sign, therefore the evolution of these indices in the last 55 years may explain, in a certain degree, the increase in the occurrence of Q1 rainfall erosivity events.



## 2.10.4 Conclusions

Analysis of the temporal evolution of rainfall erosivity in the study area during the period 1955-2006 revealed generalized decreasing trends at the annual and monthly scales, coinciding with a decrease in the number of daily highly erosive events and increasing number of daily low erosivity events. These trends could be explained by the displacement of the polar fronts northwards revealed by the positive tendency of the NAO and MO, whereas the increase tendency at the Mediterranean during winter months, January and February could be a consequence of the negative WeMO trend.

This study is the most complete dealing with rainfall erosivity trends in the study area. Further research is needed for a better understanding of the spatiotemporal evolution of rainfall erosivity.



## 2.11 References

- Acero, J.L., García, J.A., Gallego, M.C. 2012. Peaks-over-Threshold Study of Trends in Extreme Rainfall over the Iberian Peninsula. *Journal of Climate*, 24, 1089–1105.
- Ahmed, S., De Marsily, G. 1987. Comparison of geostatistical methods for estimating transmissivity using data on transmissivity and specific capacity. *Water Resources Research*, 23, 1717-1737.
- Angulo-Martínez, M., Beguería, S., 2009. Estimating rainfall erosivity from daily rainfall records: A comparison among methods using data from the Ebro Basin (NE Spain). *Journal of Hydrology*, 379, 111-121.
- Angulo-Martínez, M., López-Vicente, M., Vicente-Serrano, S.M., Beguería, S., 2009. Mapping rainfall erosivity at a regional scale: a comparison of interpolation methods in the Ebro Basin (NE Spain). *Hydrology and Earth Systems Science*, 13, 1907–1920.
- Apaydin, H., Erpul, G., Bayramin, I., Gabriels, D. 2006. Evaluation of indices for characterizing the distribution and concentration of rainfall: A case for the region of Southeastern Anatolia Project, Turkey. *Journal of Hydrology*, 328, 726-732.
- Arnoldus, H.M.J., 1977. Methodology used to determine the maximum potential average annual soil loss due to sheet and rill erosion in Morocco. *FAO Soils Bulletin*, 34, 39-51.
- Bagarello, V., D'Asaro, F., 1994. Estimating single storm erosion index. *Transactions of the American Society of Agricultural Engineers*, 37, 785-791.
- Banasik, K., Górska, D., 1994. Rainfall erosivity for south-east Poland. *Conserving soil resources. European perspectives* (ed. Rickson), 201-207. Lectures in soil erosion control, Silsoe College, Cranfield University, UK.
- Beguería, S., Angulo-Martínez, M., Vicente-Serrano, S. M., López-Moreno, J.I., El-Kenawy, A. 2011. Assessing trends in extreme precipitation events intensity and magnitude using non-stationary peaks-over-threshold analysis: a case study in northeast Spain from 1930 to 2006. *International Journal of Climatology*, 31, 2102–2114.



Beguería, S., Vicente-Serrano, S. M.: Mapping the hazard of extreme rainfall by peaks over threshold extreme value analysis and spatial regression techniques, *Journal of Applied Meteorology*, 45, 108-124, 2006

Beguería S, Vicente-Serrano SM, López-Moreno JI, García-Ruiz JM. 2009. Annual and seasonal mapping of peak intensity, magnitude and duration of extreme rainfall events across a climatic gradient, North-east Iberian Peninsula, *International Journal of Climatology*, 29 (12): 1759-1779

Beguería S., Pueyo Y. 2009. A comparison of simultaneous autoregressive and generalized least squares models for dealing with spatial autocorrelation, *Global Ecological and Biogeography*, 18, 273–279.

Beguería, S. 2005. Uncertainties in partial duration series modelling of extremes related to the choice of the threshold value, *Journal of Hydrology*, 303, 215–230.

Boellstorff, D., Benito, G. 2005. Impacts of set-aside policy on the risk of soil erosion in central Spain, *Agricultural Ecosystem Environment*, 107, 231-243.

Borrough, P.A., McDonnell, R.A. 1998. *Principles of geographical information systems*. Oxford University Press.

Breiman, L., Spector, P. 1992. Submodel selection and evaluation in regression: The X-random case. *International Statistical Review*, 60, 291-319.

Brown, D.P., Comrie, A.C. 2002. Spatial modelling of winter temperature and rainfall in Arizona and New Mexico, USA, *Climate Research*, 22, 115-128.

Brown, L.C., Foster, G.R., 1987. Storm erosivity using idealized intensity distributions. *Transactions of the American Society of Agricultural Engineers*, 30, 379-386.

Brunetti M, Maugeri M, Nanni T. 2001. Changes in total precipitation, rainy days and extreme events in northeastern Italy. *International Journal of Climatology*, 21, 861–871.

Casas, M.C., Herrero, M., Ninyerola, M., Pons, X., Rodríguez, R., Rius, A., Redaño, A. 2007. Analysis and objective mapping of extreme daily rainfall in Catalonia, *International Journal of Climatology*, 27, 399-409.

Charbonneau, P. 1995. Genetic algorithms in astronomy and Astrophysics. *Astrophysical Journal Supplement*, 101, 309.

Chiles, J., Delfiner, P. 1999. *Geostatistics: modelling spatial uncertainty*, Wiley, New York.



- Christensen JH, Hewitson B, Busuioc A, Chen A, Gao X, Held I, Jones R, Kolli RK, Kwon WT, Laprise R, Magana Rueda V, Mearns L, Menendez CG, Raisanen J, Rinke A, Sarr A, Whetton P (2007) Chapter 11: regional climate projections. In: *Climate change. 2007: the physical science basis*. Contribution of Working Group I to the Fourth Assessment Report of the Intergovernmental Panel on Climate Change, Cambridge University Press.
- Clarke, M.L.; Rendell, H.M. 2010. Climate-driven decrease in erosion in extant Mediterranean badlands. *Earth Surface Processes and Landforms*. 35, 1281-1288.
- Conte M, Giuffrida S, Tedesco S. 1989. The Mediterranean oscillation: impact on rainfall and hydrology in Italy. *Proceedings of the Conference on Climate and Water*, Vol. 1. Publications of Academy of Finland: Helsinki; 121–137.
- Coutinho, M.A.; Tomás, P.P. 1995. Characterization of raindrop size distributions at the Vale Formoso Experimental Erosion Centre. *Catena*, 25. 187-197.
- Cressie, N.A.C. 1993. *Statistics for spatial data rev.* (Ed.), John Wiley and Sons.
- Creus, J., 2001. Las sequías en el valle del Ebro. *Causas y consecuencias de las sequías en España*, A. Gil and A. Morales, Eds. Universidad D'Alacant, 231-259.
- Cuadrat, J.M. 1991. Las sequías en el valle del Ebro. Aspectos climáticos y consecuencias económicas. *Rev. Real Acad. Ciencias*, 85: 537-545.
- Curse, R., Flanagan, J., Frankenberger, B., Gelder, D., Herzmann, D., James, D., Krajenski, W., Kraszewski, M., Laflen, J., Opsomer, J., Todey, D. 2006. Daily estimates of rainfall, water runoff and soil erosion in Iowa. *Journal of soil and water conservation*, 61 (4): 191-199.
- Daly, C., Gibson, W.P., Taylor, G.H., Johnson, G.L., Pasteris, P. 2002. A knowledge-based approach to the statistical mapping of climate, *Climate Research*, 22, 99-113.
- D'Asaro, F., D'Agostino, L., Bagarello, V. 2007. Assessing changes in rainfall erosivity in Sicily during the twentieth century. *Hydrological processes*. DOI: 10.1002/hyp.6502.
- Deutsch, C.V., Journel, A.G. 1998. *Gstatlib: Geostatistical software library and user's guide*. Oxford university press.



- De Luis, M.; González-Hidalgo, J.C.; Longares, L.A. 2010: Is rainfall erosivity increasing in the Mediterranean Iberian Peninsula? *Land Degradation and Development*, 21, 139-144.
- De Luis M., Brunetti M., González-Hidalgo, J.C., Longares L.A., Martín-Vide L.A. 2010. Changes in seasonal precipitation in the Iberian Peninsula during 1946–2005. *Global and Planetary Change*, 74, 27–33.
- Diggle, P.J., Ribero, P.J., Cristensen, O.F. 2002. An introduction to model basis geostatistics. In: Møller, J. (Ed.). *Spatial statistics and computational methods. Lecture notes in statistics*. Springer-Verlag. New York.
- Diodato, N. 2004. Estimating RUSLE's rainfall factor in the parto of Italy with a Mediterranean rainfall regime. *Hydrology and Earth System Sciences*, 8, 103-107.
- Dirks, K.N., Hay, J.E., Stow, C.D., Harris D. 1998. High-resolution studies of rainfall on Norfolk Island. Part II: Interpolation of rainfall data, *Journal of Hydrology*, 208, 187–193.
- Domínguez-Romero, L., Ayuso Muñoz, J.L., García Marín, A.P. 2007. Annual distribution of rainfall erosivity in western Andalusia, southern Spain. *Journal of soil and water conservation*, 62, 390-401.
- D'Odorico, P.; Yoo, J.; Over, T.M. 2001. An assessment of ENSO-Induced patterns of rainfall erosivity in the Southwestern United States. *Journal of Climate*, 14, 4230-4242
- Dunkeloh, A.; Jacobbeit, J. 2003. Circulation dynamics of Mediterranean rainfall variability 1948-98. *International Journal of Climatology*, 23, 1843-1866.
- Dunkerley, D. 2008. Rain event properties in nature and in rainfall simulation experiments: a comparative review with recommendations for increasingly systematic study and reporting. *Hydrological processes*, 22, 4415-4435
- EEA, 2000. CORINE land cover 2000. European Environment Agency. <<http://image2000.jrc.it>>.
- Efron, B., Tibshirani, R.J. 1997. Improvements on cross-validation: the .632+ bootstrap method, *Journal of the American Statistical Association*, 92, 548-560.
- Elsenbeer, H., Cassel, D.K., Tinner, W. 1993. A daily rainfall erosivity model for Western Amazonia, *Journal of Soil and Water Conservation*, 48, 439-444.



- Esteban-Parra MJ, Rodrigo FS, Castro-Diez Y. 1998. Spatial and temporal patterns of rainfall in Spain for the period 1880–1992. *International Journal of Climatology*, 18, 1557–1574.
- Ferro, V., Porto, P., Yu, B. 1999. A comparative study of rainfall erosivity estimation for southern Italy and southeastern Australia, *Hydrological sciences journal*, 44, 3-24.
- Ferro, V., Giordano, G., Iovino, M. 1991. Isoerosivity and erosion risk map for Sicily, *Hydrological sciences journal*, 36, 549-564.
- Gabriels, D. 2006. Assessing the Modified Fournier Index and the Rainfall Concentration Index for some European countries. Boardman and Poesen (Ed.) *Soil Erosion in Europe*. John Wiley & sons. 675-684.
- García-Ruiz, J.M., Arnáez, J., White, S.M., Lorente, A., Beguería, S. 2000. Uncertainty assessment in the prediction of extreme rainfall events: an example from the Central Spanish Pyrenees. *Hydrological Processes*, 14, 887-898.
- Garrido J, García JA. 1992. Periodic signals in Spanish monthly rainfall data. *Theoretical and Applied Climatology*, 45: 97–106.
- Gobin, A., Jones, R., Kirkby, M., Campling, P., Govers, G., Kosmas, C., Gentile, A.R. 2004. Indicators for pan-European assessment and monitoring of soil erosion by water, *Environmental Science Policy*, 7, 25-38.
- González-Hidalgo, J.C., Brunetti, M., De Luis, M. 2010. Precipitation trends in Spanish hydrological divisions, 1946–2005. *Climate Research*, 43, 215–228.
- González-Hidalgo, J.C.; Lopez-Bustins, J.A.; Štepánek, P.; Martín-Vide, J.; De Luis, M. 2009: Monthly rainfall trends on the Mediterranean fringe of the Iberian peninsula during the second-half of the twentieth century (1951-2000). *International Journal of Climatology*, 29, 1415-1429.
- González-Hidalgo, J.C., Peña-Monnè, J.L., de Luis, M. 2007. A review of daily soil erosion in western Mediterranean areas. *Catena*, 71: 193-199
- Goodale, C.L., Aber, J.D., Ollinger, S.V. 1998. Mapping monthly rainfall, temperature and solar radiation from Ireland with polynomial regression and a digital elevation model, *Climate Research*, 10, 35-49.
- Goodess CM, Jones PD. 2002. Links between circulation and changes in the characteristics of Iberian rainfall. *International Journal of Climatology*, 22, 1593–1615.



- Goovaerts, P. 1997. *Geostatistics for natural resources evaluation*, Oxford University Press, New York.
- Goovaerts, P. 1999. Using elevation to aid the geostatistical mapping of rainfall erosivity, *Catena*, 34, 227-242.
- Goovaerts, P. 2001. Geostatistical modelling of uncertainty in soil science, *Geoderma*, 103, 3-26.
- Helsel, D.R., Hirsch, R.M. 1992. *Statistical methods in water resources*. 522pp., Elsevier, New York.
- Hengl, T., Heuvelink, G.B.M., Stain, A. 2004. A generic framework for spatial prediction of soil variables based on regression-kriging, *Geoderma*, 120, 75-93.
- Hershfield, D. M. 1973. On the probability of extreme rainfall events, *Bulletin of the American Meteorological Society*, 54, 1013 – 1018.
- Hosking, J. R. M.; Wallis, J. R. 1987. Parameter and quantile estimation for the Generalized Pareto distribution, *Technometrics*, 29, 339– 349.
- Hoyos, N., Waylen, P.R., Jaramillo, A. 2005. Seasonal and spatial patterns of erosivity in a tropical watershed of the Colombian Andes. *Journal of Hydrology*, 314, 177-191.
- Hudson, N., 1971. *Soil Conservation*. Cornell University Press, Ithaca.
- Hurrell, J. 1995. Decadal trends in North Atlantic Oscillation and relationship to regional temperature and rainfall. *Science*, 269, 676-679.
- Hurrell, J., Kushnir, Y., Ottersen, G., Visbeck, M. (Eds). 2003. *The North Atlantic Oscillation: climate significance and environmental impacts*. Geophys. Monogr. Ser., vol 134, AGU, Washington, D.C.
- ICONA. 1988. *Agresividad de la lluvia en España. Valores del factor R de la Ecuación Universal de Pérdida de Suelo*, Ministerio de Agricultura, pesca y alimentación, España.
- Ingram, W.J. 2002. On the robustness of the water vapor feedback: GCM vertical resolution and formulation. *Journal of Climatology*, 15, 917–921
- Isaaks E.H., Strivastava, R.M. 1989. *An introduction to applied geostatistics*, Oxford University Press, Oxford.



- Jacobeit J. 1987. Variations of trough positions and rainfall patterns in the Mediterranean area. *International Journal of Climatology*, 7: 453–476.
- Jones, P.D., Jónsson, T., Wheeler, D. 1997. Extension to the North Atlantic Oscillation using early instrumental pressure observations from Gibraltar and South-West Iceland. *International Journal of Climatology*, 17, 1433-1450.
- Kendon, E.J.; Rowell, D.P.; Jones, R.G. 2010. Mechanisms and reliability of future projected changes in daily rainfall. *Climate Dynamics*, 35, 489-509.
- Kinnell, P.I.A., Risso, L.M. 1998. USLE-M: Empirical modelling rainfall erosion through runoff and sediment concentration, *Soil Science Society American Journal*, 62, 1667-1672.
- Kutiel H, Maheras P, Guika S. 1996. Circulation indices over the Mediterranean and Europe and their relationship with rainfall conditions across the Mediterranean. *Theoretical and Applied Climatology*, 54: 125–138.
- Lal, R. 1976. Soil erosion on alfisols in Western Nigeria. III – Effects of rainfall characteristics. *Geoderma*, 16, 389-401
- Lana X, Burgueño A. 1998. Spatial and temporal characterization of annual extreme droughts in Catalonia (Northeast Spain). *International Journal of Climatology*, 18, 93–110.
- Lasanta, T. 2003. Gestión agrícola y erosión del suelo en la cuenca del Ebro: el estado de la cuestión. *Zubía*, 21, 76-96.
- Llasat, M.C., Barriendos, M., Barrera, A., Rigo, T. 2005. Floods in Catalonia (NE Spain) since the 14th century. In Benito, G, Ouarda, T.B.M.J., Bárdossy, A (Eds.) Palaeofloods, historical data & climate variability: Applications in flood risk assessment. *Journal of Hydrology*, 313 (1-2), 32-47.
- Llasat, M.C. 2001. An objective classification of rainfall events on the basis of their convective features: Application to rainfall intensity in the northeast of Spain. *International Journal of Climatology*, 21, 1385-1400
- Llasat, M.C. and Puigcerver, M. 1994. Meteorological factors associated with floods in the north-eastern part of the Iberian Peninsula, *Natural Hazards*, 5, 133-151.
- Leek, R., Olsen, P. 2000. Modelling climatic erosivity as a factor for soil erosion in Denmark: changes and temporal trends, *Soil use Management*, 16, 61-65.



- Lim, K.J., Sagong, M., Engel, B.A., Tang, Z., Choi, J., Kim, K. 2005. GIS-based sediment assessment tool, *Catena*, 64, 61-80.
- Lopez-Bustins, J.A.; Martin-Vide, J.; Sanchez-Lorenzo, A. 2008. Iberia winter rainfall trends based upon changes in teleconnection and circulation patterns. *Global and Planetary Change*, 63, 171-176.
- López-Moreno, J.I., Vicente-Serrano, S. M., Angulo-Martínez, M., Beguería, S., El-Kenawy, A. 2010. Trends in daily precipitation on the north eastern Iberian Peninsula, 1955–2006. *International Journal of Climatology*, 30, 1026–1041.
- López-Vicente, M., Navas, A., Machin, J. 2008. Identifying erosive periods by using RUSLE factors in mountain fields of the Central Spanish Pyrenees, *Hydrology Earth System Science*, 12, 1-13.
- Madsen, H., Rosbjerg, D. 1997. The partial duration series method in regional index-flood modeling, *Water Resources Research*, 33, 737 – 746.
- Maheras, P. 1988. Changes in rainfall conditions in the western Mediterranean over the last century. *Journal of Climate*, 8, 179–189.
- Marazzi, A. 1993. *Algorithms, Routines and S Functions for Robust Statistics*. Wadsworth & Brooks/Cole.
- Martín-Vide, J., Lopez-Bustins, J.A. 2006. The Western Mediterranean Oscillation and rainfall in the Iberian Peninsula. *International Journal of Climatology*. 26, 1455-1475.
- Martin-Vide, J., Gomez, L. 1999. Regionalization of peninsular Spain based on the length of dry spells. *International Journal of Climatology*, 19, 537–555.
- Martín-Vide, J. 1994. Diez características de la pluviometría española decisivas en el control de la demanda y el uso del agua. *Boletín de la AGE*, 18: 9-16.
- Martínez, M.D., Lana, X., Burgueño, A., Serra, C., 2007. Spatial and temporal daily rainfall regime in Catalonia (NE Spain) derived from four precipitation indices, years 1950–2000. *International Journal of Climatology*, 27, 1527–1632.
- Martínez-Casanovas, J.A., Ramos, M.C., Ribes-Dasi, M. 2002. Soil erosion caused by extreme rainfall events: mapping and quantification in agricultural plots from very detailed digital elevation models. *Geoderma*, 105, 125-140.
- McBratney, A., Mendoça-Santos, M., Minasny, B. 2003. On digital soil mapping, *Geoderma*, 117, 3-52.



- McBratney, A.B., Webster, R. 1986. Chosing functions for semi-variograms of soil properties and fitting them to sampling estimates, *Journal of Soil Science*, 37 (4), 617-639.
- Metcalfe, T.S., Charbonneau, P. 2003. Stellar structure modelling using a parallel genetic algorithm for objective global optimization. *Journal of computational physics*, 185, 176-193.
- Millward, A.A., Mersey, J.E. 1999. Adapting the RUSLE to model soil erosion potential in a mountainous tropical watershed, *Catena*, 38, 109-129.
- Mitasova, H., Mitas, L., Brown, W.M., Gerdes, D.P., Kosinovsky, I., Baker, T. 1995. Modelling spatially and temporally distributed phenomena: new methods and tools for GRASS GIS, *International Journal of Geographic Information Systems*, 9, 433-446.
- Moses, T., Kiladis, G.N., Diaz, H.F., Barry, R.G. 1987. Characteristics and frequency of reversals in mean sea level pressure in the North Atlantic sector and their relationship to long-term temperature trends. *International Journal of Climatology*, 7, 13–30.
- Mutua, B.M., Klik, A., Loiskandl, W. 2006. Modeling soil erosion and sediment yield at a catchment scale: the case of masinga catchment, Kenya, *Land Degradation and Devolpement*, 17, 557-570.
- Nash, J.E., Sutcliffe, J.V., 1970. River flow forecasting through conceptual models part I – A discussion of principles. *Journal of Hydrology*, 10, 282-290.
- Nearing, M.A., Pruski, F.F., O'Neal, M.R. 2004. Expected climate change impacts on soil erosion rates: A review. *Journal of Soil and Water Conservation*, 59, 1, 43-50.
- Ninyerola, M., Pons, X., Roure, J.M.: Objective air temperature mapping for the Iberian Peninsula using spatial interpolation and GIS, *International Journal of Climatology*, 27, 1231-1242, 2007.
- Ninyerola, M., Pons, X., Roure, J.M.: Monthly rainfall mapping of the Iberian Peninsula using spatial interpolation tools implemented in a Geographic Information System, *Theoretical and Applied Climatology*, 89, 195-209, 2007.
- Ninyerola, M., Pons, X. and Roure, J.M. 2000. A methodological approach of climatological modelling of air temperature and rainfall through GIS techniques, *International Journal of Climatology*, 20, 1823-1841.



- Norrant C, Douguédroit A. 2006. Monthly and daily precipitation trends in the Mediterranean (1950–2000). *Theoretical and Applied Climatology*, 83, 89–106.
- Odeh, I.O.A., McBratney, A.B., Chittleborough, D.J. 1995. Further results on prediction of soil properties from terrain attributes: heterotopic cokriging and regression-kriging, *Geoderma*, 67 (3-4), 215-226.
- Odeh, I.O.A., McBratney, A.B., Chittleborough, D.J. 1994. Spatial prediction of soil properties from landform attributes derived from a digital elevation model, *Geoderma*, 63, 197-214.
- Onori, F., De Bonis, P. Grauso, S. 2006: Soil erosion prediction at the basin scale using the revised universal soil loss equation (RUSLE) in a catchment of Sicily (southern Italy). *Environmental Geology*, 50: 1129-1140.
- Palutikof, J.P. 2003. Analysis of Mediterranean climate data: measured and modelled. In *Mediterranean Climate-Variability and Trends*, Bolle HJ (ed.). Springer-Verlag: Berlin; 133–153.
- Paredes, D.; Trigo, R.M.; García-Herrera, R.; Franco-Trigo, I. 2006. Understanding rainfall changes in Iberia in early spring: weather typing and storm-tracking approaches. *Journal of Hydrometeorology*, 7, 101-113.
- Peñarrocha, D., Estrela, M.J., Millán, M. 2002. Classification of daily rainfall patterns in a Mediterranean area with extreme intensity levels: the Valencia region. *International Journal of Climatology*, 22, 677–695.
- Petkovsek, G., Mikos, M. 2004. Estimating the R factor from daily rainfall data in the sub-Mediterranean climate of southwest Slovenia. *Hydrological sciences journal*, 49 (5), 869-877.
- Pokrovsky, O.M. 2009: European rain rate modulation enhanced by changes in the NAO and atmospheric circulation regimes. *Computers and Geosciences*, 35, 897-906.
- Pons, X., Ninyerola, M. 2008. Mapping a topographic global solar radiation model implemented in a GIS and calibrated with ground data, *International Journal of Climatology*, 28, 1821-1834.
- Pons, X. 2006. *Manual of miramon*. Geographic Information System and Remote Sensing Software, Centre de Recerca Ecològica i Aplicacions Forestals (CREAF): Bellaterra, (<http://www.creaf.uab.es/miramon>).



- Posch, M., Rekolainen, S. 1993. Erosivity factor in the Universal Soil Loss Equation estimated from Finnish rainfall data. *Agricultural Science in Finland*, 2, 271-279.
- Prudhome, C, Reed DW. 1999. Mapping extreme rainfall in a mountainous region using geostatistical techniques: A case study in Scotland, *International Journal of Climatology*, 19, 1337–1356.
- R Development Core Team, 2008. R: *A Language and Environment for Statistical Computing*. Vienna (Austria), R Foundation for Statistical Computing
- Rao, A. R., Hamed, K. H. 2000. *Flood Frequency Analysis*, CRC Press, Boca Raton, Fla.
- Renard, K.G., Foster, G.R., Weesies, G.A., McCool, D.K., Yoder, D.C., 1997. *Predicting Soil Erosion by Water: A Guide to Conservation Planning with the Revised Universal Soil Loss Equation (RUSLE)*. Handbook #703. US Department of Agriculture, Washington, DC.
- Renard, K.G., Freimund, J.R., 1994. Using monthly rainfall data to estimate the R factor in the revised USLE. *Journal of hydrology*, 157 (1-4): 287-306.
- Richardson, C.W., Foster, G.R., Wright, D.A., 1983. Estimation of Erosion Index from Daily Rainfall Amount. *Transactions of the American Society of Agricultural Engineers*, 26, 153-160.
- Rodó, X., Baert, E., Comin, F.A., 1997. Variations in seasonal rainfall in southern Europe during the present century: relationships with the North Atlantic oscillation and the El Niño–Southern oscillation. *Climate Dynamics*, 19, 275–284.
- Rodríguez-Puebla, C., Encinas, A.H., Nieto, S., Garmenia, J. 1998. Spatial and temporal patterns of annual rainfall variability over the Iberian Peninsula. *International Journal of Climatology*, 18, 299–316
- Romero, C.C., Baigorriá, G.A., Stroosnijder, L. 2007. Changes of erosive rainfall for El Niño and La Niña years in Northern Andean highlands of Peru. *Climatic Change*. 85, 343-356.
- Romero, R., Guijarro, J.A., Ramis, C. and Alonso, S. 1998. A 30-year (1964-1993) daily rainfall data base for the Spanish Mediterranean regions: first exploratory study. *International Journal of Climatology*, 18, 541-560



- De Santos Loureiro, N., De Azevedo Coutinho, M. 2001. A new procedure to estimate the RUSLE  $El_{30}$  index, based on monthly rainfall data and applied to the Algarve region, Portugal, *Journal of Hydrology*, 250, 12-18.
- Sauerborn, P., Klein, D.A., Botschek, J., Skowronek, A. 1999. Future rainfall erosivity from large scale climate models – methods and scenarios for a humid region. *Geoderma*. 93, 269-276.
- Selker, J.S., Haith, D.A., Reynolds, J.E., 1990. Calibration and testing of Daily Rainfall Erosivity Model. *Transactions of ASAE*, 33, 1612-1618.
- Serrano, A., J. A. García, V. L. Mateos, M. L. Cancillo, and J. Garrido, 1999. Monthly modes of variation of rainfall over the Iberian Peninsula. *Journal of Climate*, 12, 2894–2919.
- Shi, Z.H., Cai, C.F., Ding, S.W., Wang, T.W., Chow, T.L., 2004. Soil conservation planning at the small watershed level using RUSLE with GIS. *Catena*, 55, 33-48
- Siegel, S., Castelan, N.J. 1988. *Nonparametric statistics for the behavioural sciences*. McGraw-Hill, New York.
- Tobler, W.R. 1970. A computer movie simulating urban growth in Detroit region. *Economic Geography*, 46, 234-240.
- Van der Knijff, J.M., Jones, R.J.A., Montanarella, L., 2000. *Soil Erosion Risk Assessment in Italy*. European Commission—European Soil Bureau. 52 pp.
- Venables, W. N., Ripley, B. D. 2002. *Modern Applied Statistics with S*. Fourth edition. Springer.
- Verstraeten, G., Poesen, J., Demarée, G., Salles, C. 2006. Long-term (105 years) variability in rain erosivity as derived from 10-min rainfall depth data for Ukkel (Brussels, Belgium): implications for assessing soil erosion rates, *Journal of Geophysical Research*, 111, D22109. doi: 10.1029/2006JD007169.
- Vicente-Serrano, S.M., Beguería, S., López-Moreno, J.I., El Kenawy, A. & Angulo, M. 2009. Daily atmospheric circulation events and extreme rainfall risk in Northeast Spain: the role of the North Atlantic Oscillation, Western Mediterranean Oscillation, and Mediterranean Oscillation. *Journal of Geophysical Research-Atmosphere*. 114, D08106, Doi: 10.1029/2008JD011492.
- Vicente-Serrano, S.M., Beguería, S., López-Moreno, J.I., García-Vera, M.A., Stepanek, P. 2009. A complete daily rainfall database for north-east Spain:



Reconstruction, quality control and homogeneity. *International Journal of Climatology*, DOI: 10.1002/joc.1850

Vicente-Serrano, S.M., Lanjeri, S., López-Moreno, J.I.: Comparison of different procedures to map reference evapotranspiration using geographical information systems and regression-based techniques, *Int. J. Climatol.*, 27, 1103-1118, 2007.

Vicente-Serrano, S.M. 2005. *Las sequías climáticas en el valle medio del Ebro: factores atmosféricos, evolución temporal y variabilidad espacial*. Publicaciones del Consejo de Protección de la Naturaleza de Aragón, 277p.

Vicente-Serrano, S.M., Saz-Sánchez, M.A., Cuadrat, J.S. 2003. Comparative analysis of interpolation methods in the middle Ebro Valley (Spain): application to annual rainfall and temperature, *Climate Research*, 24, 161-180.

Vogt, J.V., Viau, A.A., Paquet, F. 1997. Mapping regional air temperature fields using satellite derived surface skin temperatures, *International Journal of Climatology*, 17, 1559–1579.

Wackernagel, H. 1998. Multivariate Geostatistics: an introduction with applications, vol. xiv, Springer, Berlin/London.

Weisse, A.K., Bois, P. 2002. A comparison of methods for mapping statistical characteristics of heavy rainfall in the French Alps: The use of daily information, *Hydrology Science Journal*, 47, 739–752.

Weiss, S.M. and Kulikowski, C.A. 1991. *Computer Systems That Learn*, Morgan Kaufmann.

Willmott, C.J., Matsuura, K. 2005. Advantages of the mean absolute error (MAE) over the root mean square error (RMSE) in assessing average model performance. *Climate Research*, 30, 79–82.

Willmott, CJ. 1981. On the validation of models, *Physical Geography*, 2, 184–194.

Winchell, M.F., Jackson, S.H., Wadley, A.M., Srinivasan, R. 2008. Extension and validation of a geographic information system-based method for calculating the Revised Universal Soil Loss Equation length-slope factor for erosion risk assessments in large watersheds, *Journal of Soil and Water Conservation*, 63, 105-111.

Wischmeier, W.H., Smith, D.D., 1978. Predicting rainfall erosion losses: a guide to conservation planning. *USDA Handbook 537*, Washington, DC.



Wischmeier, W.H., 1959. A rainfall erosion index for a universal soil-loss equation. *Soil Science Society of America Proceedings*, 23, 246-249.

Yu, B., Hashim, G.M., Eusof, Z., 2001. Estimating the R-factor with limited rainfall data: a case study from peninsular Malaysia. *Journal of Soil and Water Conservation*, 56, 101-105

Yu, B., Rosewell, C.J., 1996a. An assessment of daily rainfall erosivity model for New South Wales. *Australian Journal of Soil Research*, 34, 139-152

Yu, B., Rosewell, C.J., 1996b. A robust estimator of the R factor for the Universal Soil Loss Equation. *Transactions of ASAE*, 39, 559-561

Yu, B., Rosewell, C.J., 1996c. Rainfall erosivity estimation using daily rainfall amounts for South Australia. *Australian Journal of Soil Research*, 34, 721-733



## Bloque III

### Estudio experimental de la erosividad de la lluvia; validación de índices a partir de datos empíricos

"The limited data we had led one to reasonably conclude this. I now see that there's another explanation for it".—David Kay.

#### Resumen

En este bloque se aborda el análisis experimental de la erosividad de la lluvia. En primer lugar se evalúa la relación entre la erosividad de 45 eventos de lluvia natural, obtenida a partir de mediciones de campo con un disdrómetro óptico, y la erosión de suelo por salpicadura medida a partir de tazas de erosión sobre tres suelos característicos de la región. En segundo lugar se comparan las metodologías de la RUSLE (Renard *et al.*, 1997), la propuesta universal de Van Dijk *et al.* (2002) y la propuesta de Cerro *et al.* (1998) para la estimación de la erosividad de la lluvia a partir de datos de intensidad de precipitación con los valores más precisos obtenidos a partir de la observación en campo. Los resultados de este apartado muestran un buen grado de ajuste entre la erosividad de la precipitación y la erosión por salpicadura, con variaciones no significativas entre suelos. Respecto a la estimación de la erosividad a partir de registros de intensidad de precipitación, se observa una generalizada subestimación de la erosividad con la aplicación de estos modelos en el centro del valle del Ebro, que puede ser atribuida a diferencias entre las características esperables (teóricas) y observadas de la relación entre masa y velocidad de caída de las gotas de lluvia.



## Abstract

This part deals with the experimental analysis of rainfall erosivity. First of all, the relationship between natural rainfall erosivity characteristics of 45 events, measured with an optical disdrometer in the experimental field, and splash erosion, measured with splash cups, in the three soil types dominant in the study area is evaluated. Secondly, RUSLE methodology together with the proposals from Van Dijk et al. (2002) and Cerro et al. (1998) for the estimation of rainfall erosivity from intensity data are compared with more precise natural rainfall measures. Rainfall erosivity and splash erosion show good agreement, without significant variations between soil types. Regarding rainfall erosivity estimates from intensity data, a generalized underestimation in rainfall erosivity occurs when using these models in the centre of the Ebro basin, which might be attributed to different expected characteristics (from theoretical models) in relation with raindrops mass and terminal velocity.



### 3.1 Introduction

The estimation of soil loss due to rainfall erosion has been a great concern since long ago. As a result of a great empirical effort, seminal studies concluded in simplified equations synthesizing the erosive effects of rainfall energy on the soil surface. The development of new instruments made possible obtaining an accurate description of natural rainfall characteristics like the drop size spectra, drop velocity, type of precipitation, precipitation amount and intensity, at very detailed time intervals of 1 minute or less. However, such instruments are still rare, so no climatological databases exist with a high spatial or temporal coverage.

In order to obtain a deeper understanding of rainfall erosivity, an experimental design was developed and implemented in the Aula Dei Experimental Station in Zaragoza ( $41^{\circ}43'30''\text{N}$ ,  $0^{\circ}48'39''\text{O}$ ., 230 m. a.s.l.) during the period between 04/03/2010–30/10/2011. The experiment monitored the rainfall properties with a laser precipitation monitor, allowing rainfall energy calculation at one-minute time intervals. In addition, splash erosion was measured after each rainfall event in three soils typical of the Ebro basin. This section presents the results obtained from this experiment.

In section 3.2 the experimental set up is explained including: i) the experimental design; ii) the characteristics of the laser precipitation monitor; iii) the calculation of rainfall energy; iv) the soil characteristics; and v) the splash monitoring.

Section 3.3 presents the results relating rainfall erosivity and splash erosion under natural rainfall conditions in three soils of the inner Ebro valley, proposing an empirical equation.

In section 3.4 the reliability of rainfall erosivity indices based on rainfall intensity data is analysed.



### 3.2. Experimental setup

In order to evaluate the relationship between rainfall erosivity parameters and the amount of soil particles detached and transported by splash, we designed an experiment to monitor rainfall characteristics under natural conditions and splash erosion produced by natural rainfall events over three typical soils types commonly found in the Ebro valley (NE Spain). The monitoring period was 04/03/2010–30/10/2011. The experiment was located at 41°43'30"N, 0°48'39"O., 230 m. a.s.l. Rainfall characteristics were monitored using a THIES Klima Laser Precipitation Monitor, which had a very good performance during the experiment.

The Laser Precipitation Monitor (LPM, also known as Optical Spectro Pluviometer) was designed to measure the size and fall velocity of every raindrop  $\geq 0.16$  mm diameter at ground level. Initially developed by Donnadieu et al. (1969), the LPM derives fall velocity and diameter of hydrometeors from the duration and amplitude of obscurations in the path of an infrared laser beam, between a light emitting diode and a receiver, with a sampling area of  $51.4\text{ cm}^2$ . The geometry of the beam limits the estimation of fall velocity to the vertical component (Salles and Poesen, 1999), so velocity measures can be overestimated with strong wind. The size and velocity of measured drops are grouped into 22 and 20 classes, respectively (Table 3.1).

From these data several rainfall variables are integrated every minute. For each rainfall period we calculated the cumulative rainfall ( $P$ , mm); effective duration ( $D_{\text{eff}}$ , minutes); maximum intensity in 30 minutes ( $I_{30}$ , mm h $^{-1}$ ) and kinetic energy per minute ( $e_r$ , J m $^2$  mm $^{-1}$ ), (Table 3.2). We considered the beginning of every event since the moment when splash cups were placed at the experimental site, and the end of it, once splash sediment was found and splash cups were removed. Hence the total duration of the event corresponds to the time during which splash cups were in the field, and effective duration was calculated from the period in which actual rainfall was recorded. As an example, the disdrometric record of the first event registered during the measuring period is provided in Figure 3.1.



Table 3.1. Laser Precipitation Monitor classification of drop diameter and velocity

Particle diameter class			Particle speed class				
Class	Diameter from (mm)	To (mm)	Class width (mm)	Class	Speed from (m s <sup>-1</sup> )	Speed to (m s <sup>-1</sup> )	Class width (m s <sup>-1</sup> )
1	0.125	0.250	0.125	1	0.00	0.20	0.20
2	0.250	0.375	0.125	2	0.20	0.40	0.20
3	0.375	0.500	0.125	3	0.40	0.60	0.20
4	0.500	0.750	0.250	4	0.60	0.80	0.20
5	0.750	1.000	0.250	5	0.80	1.00	0.20
6	1.000	1.250	0.250	6	1.00	1.40	0.40
7	1.250	1.500	0.250	7	1.40	1.80	0.40
8	1.500	1.750	0.250	8	1.80	2.20	0.40
9	1.750	2.000	0.250	9	2.20	2.60	0.40
10	2.000	2.500	0.500	10	2.60	3.00	0.40
11	2.500	3.000	0.500	11	3.00	3.40	0.40
12	3.000	3.500	0.500	12	3.40	4.20	0.80
13	3.500	4.000	0.500	13	4.20	5.00	0.80
14	4.000	4.500	0.500	14	5.00	5.80	0.80
15	4.500	5.000	0.500	15	5.80	6.60	0.80
16	5.000	5.500	0.500	16	6.60	7.40	0.80
17	5.500	6.000	0.500	17	7.40	8.20	0.80
18	6.000	6.500	0.500	18	8.20	9.00	0.80
19	6.500	7.000	0.500	19	9.00	10.00	1.00
20	7.000	7.500	0.500	20	10.00	$\infty$	$\infty$
21	7.500	8.000	0.500	-	-	-	-
22	8.000	$\infty$	$\infty$	-	-	-	-

Table 3.2. Laser Precipitation Monitor variables recorded in real time every minute

Name	Unit	Description
Synop code 4677	-	Hydrometeor code
Rain intensity	mm h <sup>-1</sup>	Amount of drops falling in a minute
Precipitation amount	mm	
Water content	g m <sup>-3</sup>	
Kinetic energy	J m <sup>-2</sup> mm <sup>-1</sup>	Estimated from the LPM classes.



The kinetic energy  $ke_{i,j}$  (J) of a drop pertaining to diameter class  $i$  and velocity class  $j$  was estimated following the formula:

$$ke_{i,j} = \frac{1}{2} m_i v_j^2 = \frac{1}{12} 10^{-3} \pi \rho v_j^2 D_i^3 , \quad (3.1)$$

where  $m_i$  is the mean mass corresponding to drop diameter class  $i$  (g);  $\rho$  is the density of water ( $1 \text{ g cm}^{-3}$ );  $v_j$  is the mean speed for the velocity class  $j$  ( $\text{m s}^{-1}$ ); and  $D_i$  is the mean diameter for class  $i$  (mm). The mass of raindrops was calculated from the diameter measured by the LPM, by assuming a spherical drop shape. Total kinetic energy  $ke_{\text{sum}}$  per minute was determined by multiplying  $ke_{i,j}$  by the number of drops registered in each size and velocity class. Finally, the unit energy ( $e_r$ ) was obtained by dividing the sampling area of the device ( $a$ ) (in our case  $0.00514 \text{ m}^2$ ) by rainfall amount per minute ( $p_r$ ) for obtaining energy rates per unit surface and precipitation amount ( $\text{J m}^{-2} \text{ mm}^{-1}$ ), and then transformed into  $\text{MJ ha}^{-1} \text{ mm}^{-1}$ :

$$e_r = \frac{ke_{\text{sum}}}{a p_r} = e_r (\text{J m}^{-2} \text{ mm}^{-1}) \frac{10^6}{10^4} = e_r (\text{MJ ha}^{-1} \text{ mm}^{-1}) , \quad (3.2)$$

where  $e_r$  and  $v_r$  are, respectively, the unit rainfall energy ( $\text{MJ ha}^{-1} \text{ mm}^{-1}$ ), obtained from eq. (2), and the rainfall amount (mm) during a time period  $r$  (one minute), and  $I_{30}$  is the maximum rainfall intensity during a period of 30 consecutive minutes in the event ( $\text{mm h}^{-1}$ ).

The event's rainfall erosivity  $EI_{30}$  ( $\text{MJ mm ha}^{-1} \text{ h}^{-1}$ ) (Renard et al., 1997) was obtained as follows:

$$EI_{30} = \left( \sum_{r=1}^0 e_r v_r \right) I_{30} . \quad (3.3)$$

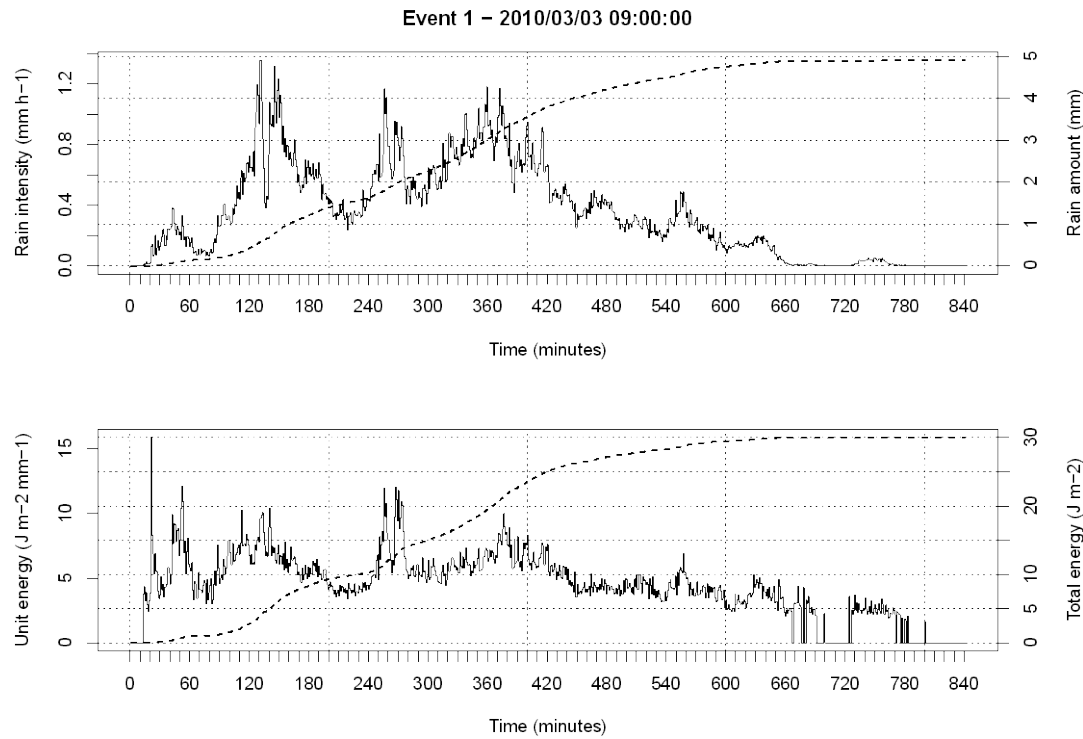


Figure 3.1: Example of a disdrometric record: one-minute values of rainfall intensity and unit energy flow (left axis) and cumulative rain and energy (dotted line and red axis) for one rainfall event.

### 3.2.1 Soil characteristics

The three types of soils used in this study were Cambisol, Gipsisol and Solonchak (FAO, 1989). They are representative of the central Ebro valley in NW Spain, and they are subject to accelerated erosion rates because they are either occupied by agricultural lands that remain bare during several months every year (Machín and Navas, 1998) or else they sustain low-coverage plant communities due to their restrictive conditions for vegetation and semi-arid climate (Guerrero et al., 1999; Pueyo et al., 2007).

The soils were brought to the experimental site from a nearby location taken from the upper 30 cm of the topsoil horizon. Cambisols are developed over glaci and terraces from fluvial deposits and marls. Its texture is sandy-loam with 25% pebbles, alkaline pH and low salinity. They show good drainage, low organic matter content (< 2%) and low gypsum content (2.5%), and 35.4% carbonate content. Gipsisols are located in colluvial-alluvial valley areas developed over deposits from nearby gypsiferous hills. They have a silty texture, alkaline pH and



higher salinity than Cambisols. They have a low organic matter and carbonate content and high gypsum content. Solonchaks are found in depressions or level areas. Their texture is clay-loam, and they have poor drainage. Detailed descriptions of the soils are given by Bermúdez (1997). Their main properties are summarized in Table 3.3. Data on this table was based on one sample of the upper 20 cm of soil for each soil type. The samples were air-dried, grinded, homogenized and quartered, to pass through a 2 mm sieve. The following properties were determined for each sample: i) bulk (considering the soil pores) and real (considering only the solid phase) density; ii) porosity; iii) fraction of sand ( $>2 \mu\text{m}$ ), silt (50 to  $2 \mu\text{m}$ ) and clay ( $< 2 \mu\text{m}$ ) particles and texture classification according to USDA (1973); iv) pH; v) electric conductivity; vi) cation exchange capacity; vii) organic matter, Carbon and Nitrogen content, Carbon / Nitrogen ratio; viii) carbonates and gypsum content. The properties were measured following standard techniques. Grain size was determined by a Coulter LS 230 equipment after chemical elimination of the organic matter. The pH (1:2.5 soil:water) was measured using a pH-meter. Electric conductivity was determined by a Crison 522 conductivimeter. Organic matter was determined by titration. Carbonates were measured using a pressure calcimeter. Total nitrogen was measured using the Kjeldhal Method. The cation exchange capacity was determined by a Mg  $(\text{NO}_3)_2$  solution followed by ICP-OES analysis.



Table 3.3. Soil type properties

Parameters	Units	Cambisol	Gypsisol	Solonchak
Real density	g cm <sup>-3</sup>	2.52	2.01	2.52
Apparent density	g cm <sup>-3</sup>	1.31	1.18	1.31
Total porosity	%	47.88	41.26	47.94
Granulometry				
Sand	%	30.01	13.88	26.35
Coarse silt	%	12.36	18.18	12.15
Fine silt	%	33.87	45.65	33.76
Clay	%	23.79	22.29	27.74
Texture		Sandy loam	Silt	Clay loam
pH		8.63	8.35	8.13
EC 1/5	dSm <sup>-1</sup>	0.37	2.4	2.33
EC (es)	"		3.84	5.92
C.I.C.	meqL <sup>-1</sup>	149.4	119.88	155.99
Carbon	%	1.02	0.49	1.03
Organic matter	%	1.73	0.84	1.78
Nitrogen	%	0.11	0.07	0.06
C/N		9.19	7.54	17.76
CO3=	%	35.41	15.72	35.7
Gypsums	%	2.5	61.79	3.81

### 3.2.2. Splash monitoring

Splash erosion was monitored with Morgan's splash cups (Morgan, 1981). This simple device consists in a circle with another smaller circle inside in contact with the soil, with a soil sampling area of 0.0085 m<sup>2</sup>. Soil particles detached by raindrop impacts need to jump over a rim of 2.5 cm, and accumulate inside the splash cup. To avoid sediment loss, some drainage is allowed with small holes at the edges of cups.

The experimental design is shown in Figure 3.2. The three soils were arranged side to side in three plots of 14x1 m. The soils were kept bare during the monitoring period by manual removing of the new seedlings. The three plots are completely level to avoid slope differences.

Five splash cups were deployed in each plot. Splash cups were checked after every rain event, and if sediment was present they were replaced by clean ones and sediment was sieved and weighed. If no significant sediment was registered (<0.25g m<sup>-2</sup>), the cups were cleaned and placed again. In order to maintain



randomness and avoid sediment exhaustion effects, splash cups were placed each time in a different site within a corresponding rectangle.

CAMBISOL



GYPSISOL



LPM

SOLONCHAK



1m

Figure 3.2: Experimental scheme at the Experimental Station of Aula Dei-CSIC (41°43'30"N, 0°48'39"O. 230 m. a.s.l.). Soil plots dimensions: 14 x 1 m. The circles indicate the placement of the Morgan's splash cups. LPM is the Laser Precipitation Monitor recording rainfall properties every minute.



### 3.3. Splash erosion under natural rainfall on three soil types in NE Spain<sup>5</sup>

Splash erosion is a complex process composed by the detachment of soil particles by raindrops hitting the surface followed by splash transport of (a part of) the detached particles. Splash is responsible for initiating water erosion, since it is the first erosion to occur when an erosive rainfall event takes place (Sempere Torres et al., 1994; Hudson, 1995; Morgan, 2005). Rainfall erosivity, i.e. the capacity of rain to erode soil, depends on the kinetic energy of rain, which depends in turn on the mass and velocity of raindrops hitting the soil surface, and on rainfall intensity, which determines the number of drops per unit surface. During a rainfall event these parameters are highly variable in time and space, and so is splash erosion. The detachment of soil particles by splash depends not only on the energy of rain drops, but also on soil erodibility, which relies on soil physico-chemical characteristics, such as the soil crust, infiltration capacity, the nature of soil aggregates, organic matter content, texture, cohesion and porosity, capacity of ionic interchange and clay content (Poesen and Torri, 1988). The transport of detached particles depends mainly on the kinetic energy of raindrops and on the mass of the particles.

Measuring both (rainfall erosivity and soil erodibility) during natural rainfall events requires considerable instrumental effort and prolonged experiments to ensure a representative number of events. Consequently, scientists have concentrated in measuring rainfall erosion under simulated rainfall conditions. Most studies on splash erosion under simulated rain do not reflect the properties of natural rainfall, because usually the soil is exposed to intense, steady rainfall rates during the experiment, while in nature rainfall is characterized by very high frequency variation of intensity. In addition, little variation of drop size distribution is possible, and often the largest drops found in natural rainfall are missing (Navas et al., 1990; Navas, 1993). These experiments often result in soil loss rates higher than those produced under natural rainfall (Dunkerley, 2008). However, the results of these experiments are summarized in mathematical expressions used as erosion models and applied to natural rainfall.

---

<sup>5</sup> This section is based in the article: Angulo-Martínez, M., Beguería, S., Navas, A., Machín, J. 2012. Splash erosion under natural rainfall on three soil types in NE Spain. *Geomorphology*, (submitted).



The classical method for quantifying splash erosion relies on the use of splash cups, or small traps that collect the soil particles detached and transported by splash (Ellison, 1947; Morgan, 1978; Poesen and Torri, 1988; Salles and Poesen, 1999; Van Dijk et al., 2003; Legout et al., 2005). The data obtained by these measurements allowed the development of empirical formulae, such as the erosivity models proposed by Ellison (1944), Bisal (1960) and Meyer (1981). These early empirical models estimated soil loss as a power function of rainfall energy or rainfall intensity with a modulating multiplying coefficient determined by soil erodibility and an exponent (Park et al., 1983; Mouzai and Bouhadef, 2003). Later work showed that a certain energy threshold must be passed to initiate soil detachment, since initial energy is focused in breaking the soil crust or infiltration (Sharma and Gupta, 1991).

One of the most extensively used indices for quantify rainfall erosivity,  $EI_{30}$ ; (Renard et al., 1997) requires knowledge of the kinetic energy of rain ( $E$ ), precipitation volume per unit of time, together with the maximum intensity in 30 minutes ( $I_{30}$ ) as a measure of the saturation of the soil and starting of runoff. Since the 1960s the scientific community has developed increased interest in the size and velocity of hydrometeors, especially in relation with the development of radar methodology. This motivated the development of instruments such as optical disdrometers and laser precipitation monitors. Lately these instruments have been integrated into soil erosion studies (Salles and Poesen, 1999; Fernández-Raga et al., 2010; Scholten et al., 2011), but studies are still scarce and spatial and temporally constrained.

The purpose of this study is to evaluate and analyse the relationship between rainfall erosivity and soil erodibility under natural rainfall conditions in three soil types of the inner Ebro valley, NE Spain. Rainfall characteristics were determined using an optical disdrometer, and splash erosion was monitored in three plots using splash cups.



### 3.3.1. Methods

Previous to modelling the relationship between rainfall erosivity and splash erosion, an exploratory analysis was carried out. ANOVA tests between the amount of soil particles eroded per event by soil type was performed in order to check the statistical significance of differences between soil types. Secondly, we modelled the relationship between the  $EI_{30}$  and soil splash by soil type. The relationship between the response variable (soil splash erosion) and the covariate ( $EI_{30}$  index) takes the form of an exponential function. Therefore, we took the logarithms of all variables and evaluated their relationship with linear models.

A linear mixed-effects model (LME) was used to account for pseudo-replication. Unlike standard linear models, mixed-effects models allow incorporating both fixed-effects and random-effects in the regression analysis (Pinheiro and Bates, 2000). The fixed-effects in a linear model describe the values of the response variable in terms of explanatory variables that are considered to be non-random, whereas random-effects are treated as arising from random causes. Random effects can be associated with individual experimental units sampled from the population. Hence, mixed-effects models are particularly suited to experimental settings where measurements are made on groups of related experimental units. If the classification factor is ignored when modelling grouped data, the random (group) effects are incorporated in the residuals, leading to an inflated estimate of within-site variability. In our case, relationships were explored between the response variable (splash erosion) and the  $EI_{30}$  index, on a data set grouped according to soil type. Five measurements (pseudo-replicates) were available for each rain event and soil type. Hence, the mixed-effects model allows exploring relationships between the response variable and the covariates that are general to the soil type, regardless of local differences given by the pseudo-replicates, which are considered a random effect. The mixed-effects model combines a linear regression model with a random-effects Analysis of Variance. The mathematical formula takes the form:

$$y_{ji} = \beta_1 + \beta_2 x_{ji} + b_j + \varepsilon_{ji}, \quad (3.4)$$

$$b_j \sim N(0, \sigma^2 b_j), \quad \varepsilon_{ji} \sim N(0, \sigma^2), \quad (3.5)$$

where  $y_{ji}$  is the  $i$ th observation in the  $j$ th group of data and  $x_{ji}$  is the corresponding value of the covariates,  $\beta_1$  is a global intercept,  $b_j$  is a random effect on the



intercept for given soil type  $j$ , and  $\varepsilon_{ji}$  is a random error allowing for different variance between the soil type,  $\sigma^2$ . In our case, we counted with three soil types, i.e.  $j = 1, \dots, 3$ , and 15 observations (five pseudo-replicates per soil type, i.e.  $i = 1, \dots, 15$ ).

The LME model in Eq. (4) was fitted by generalized least squares (GLS). Function *lme* from the R library *nlme* (Pinheiro and Bates, 2011) was used for the linear mixed effects modelling. Minimization of the Akaike's Information Criterion, AIC, was used for selecting the best model, and for comparing between homoscedastic (equal error variances) and heteroscedastic (unequal error variances for different soil types) models. The AIC is a measure of goodness of fit that penalizes the complexity of the model, and hence is much suited for model selection than statistics that only measure goodness of fit such as the  $R^2$ . The fitting process started with the most complex formulae that included all interactions between the factor (soil type) and the model parameters (intercept and slope), and heterocedasticity. No significant factors were progressively eliminated until a minimum model was attained, in which all factors were significant.



### 3.3.2. Results

During the monitoring period 45 rainfall events were registered. Quality control of the rainfall events and of the corresponding soil splash allowed us to select 27 events from the total in which rainfall erosivity parameters and splash erosion were perfectly recorded (Table 3.4). The other rainfall events were rejected, due to problems with any of the monitoring devices, i.e. due to data loss during earlier stages of the experiment (thirteen events), or due to splash sediment lost by water washing or strong wind blowing after the erosive event (five events). From the twenty-seven rainfall events, twelve events did not register substantial sediment. During the monitoring period the highest splash sediment collected per rainfall event was 712.5 g m<sup>-2</sup> for Gypsisols. The same event mobilized 587.1 g m<sup>-2</sup> for Solonchaks, and 347.40.0 g m<sup>-2</sup> for Cambisols.

Variability of soil splash between events was high, while differences between soil types were lower (Figure 3.3). The variability between pseudo-replicates (i.e. within a single event and soil type) was high and increased with the amount of sediment mobilized. The “low” events (10, 19, 22, 23, 27, 40 and 45) showed smaller variability between pseudo-replicates for all soil types. Most of them had low  $I_{30}$  values ranging between 1.9>–<11.7 mm h<sup>-1</sup>, had a long effective duration, and high cumulative rainfall amounts were reached. Most of these events occurred during winter, early spring or autumn, corresponding to atmospheric dynamics typical of frontal systems. Rainfall energy, precipitation amount, and  $EI_{30}$  were relatively low during these events, although high variability was found. Energy ranged between 0.25>–<3.79 MJ ha<sup>-1</sup> mm<sup>-1</sup>,  $I_{30}$  ranged between 1.08>–<20.79 mm h<sup>-1</sup> and  $EI_{30}$  ranged between 0.27>–<45.50 MJ mm<sup>-1</sup> ha<sup>-1</sup> h<sup>-1</sup>. The events with the highest energies were 23, 19 and 40. Highest amounts of splash were found in most cases in Solonchack.

The events registering higher amounts of soil splash (2, 5, 6, 11, 13, 32, 33 and 38) showed more coincidence with rainfall parameters, but more variability between pseudo-replicates. Soil splash ranged between 113.9>–<712.5 g m<sup>-2</sup>. These events registered high precipitation amounts, between &gt;–<61.3 mm, with a short effective duration, with the exception of event n° 2 that lasted for 20.8 h. All these events occurred during late spring and summer.



Table 3.4. Properties of rainfall events registered and corresponding soil splash: n° of event; was it erosive (Y) or not (N: splash was negligible, less than  $0.25 \text{ g m}^{-2}$ ); D: total time during which splash cups were deployed (hours);  $D_{\text{eff}}$ : total time of rain registered at the monitoring site (hours); P: total rainfall (mm); E: total kinetic energy ( $\text{MJ ha}^{-1} \text{ mm}^{-1}$ );  $I_{30}$ : maximum intensity in 30 minutes ( $\text{mm h}^{-1}$ );  $EI_{30}$ : rainfall erosivity index ( $\text{MJ mm ha}^{-1} \text{ h}^{-1}$ ); mean soil splash by soil type ( $\text{g m}^{-2}$ ): CA = Cambisol, GA= Gypsisol, SA = Solonchak. Events eliminated due to loss of data are not shown.

Event	Erosive	D	$D_{\text{eff}}$	P	E	$I_{30}$	$EI_{30}$	Soil splash by soil		
								CA	GA	SA
2	Y	430.6	20.8	26.4	4.92	15.85	77.92	174.6	143.1	288.2
4	N	19.5	12.0	4.6	0.53	1.55	0.81	0	0	0
5	Y	16.3	4.9	24.3	4.34	24.25	105.21	363.3	230.8	306.8
6	Y	175.3	8.3	8.2	1.67	11.53	19.24	337.4	712.5	587.1
7	N	3.5	2.8	3.6	0.40	5.50	2.21	0	0	0
10	Y	9.8	8.3	6.7	0.87	2.34	2.02	72.0	39.1	74.6
11	Y	29.8	3.8	44.4	10.57	56.11	592.94	264.7	429.2	398.6
13	Y	25.7	3.4	61.3	11.70	92.90	1086.70	268.7	296.5	331.1
16	N	160.4	7.7	2.76	0.32	1.31	0.41	0	0	0
19	Y	741.9	56.5	20.9	2.79	11.65	32.55	91.8	52.7	110.4
21	N	1.9	1.4	0.2	0.02	0.30	0.00	0	0	0
22	Y	12	11.8	3.2	0.25	1.08	0.27	40.0	18.1	76.2
23	Y	90.2	26.6	30.0	3.79	7.31	27.73	102.6	164.2	108.5
25	N	23.5	2.7	1.1	0.11	1.13	0.12	0	0	0
26	N	4.1	3.5	1.2	0.11	0.75	0.08	0	0	0
27	Y	35.4	6.2	3	0.33	1.93	0.63	20.2	7.8	42.6
31	N	10.5	7.0	3.14	0.36	1.23	0.44	0	0	0
32	Y	26.3	7.6	27.0	4.85	26.18	126.94	113.9	229.6	145.6
33	Y	79.1	8.9	37.2	6.40	61.61	394.23	179.3	248.5	272.0
34	N	15.6	5.1	3.4	0.54	2.71	1.46	0	0	0
35	N	155.1	1.8	0.3	0.00	0.10	0.00	0	0	0
37	N	0.9	0.6	0.9	0.20	1.64	0.33	0	0	0
38	Y	8.5	3.2	30.4	7.86	35.57	279.45	456.7	381.6	350.4
40	Y	42.8	0.4	10.4	2.19	20.79	45.50	102.4	139.3	140.0
42	N	16509	2.8	0.55	0.06	0.53	0.03	0	0	0
44	N	21.0	3.0	0.5	0.07	0.34	0.02	0	0	0
45	Y	9.6	8.3	6.1	0.88	2.84	2.49	67.3	19.3	54.4



Consequently,  $EI_{30}$  also showed high variability, between  $19.24 \geq - < 1086.7$  MJ mm ha<sup>-1</sup> h<sup>-1</sup>. Event 6 can be considered an exception, since rainfall was moderate (8.2 mm) and energy,  $I_{30}$  and  $EI_{30}$  were low, but soil splash was high. In this group no differences in splash erosion were found between soil types.

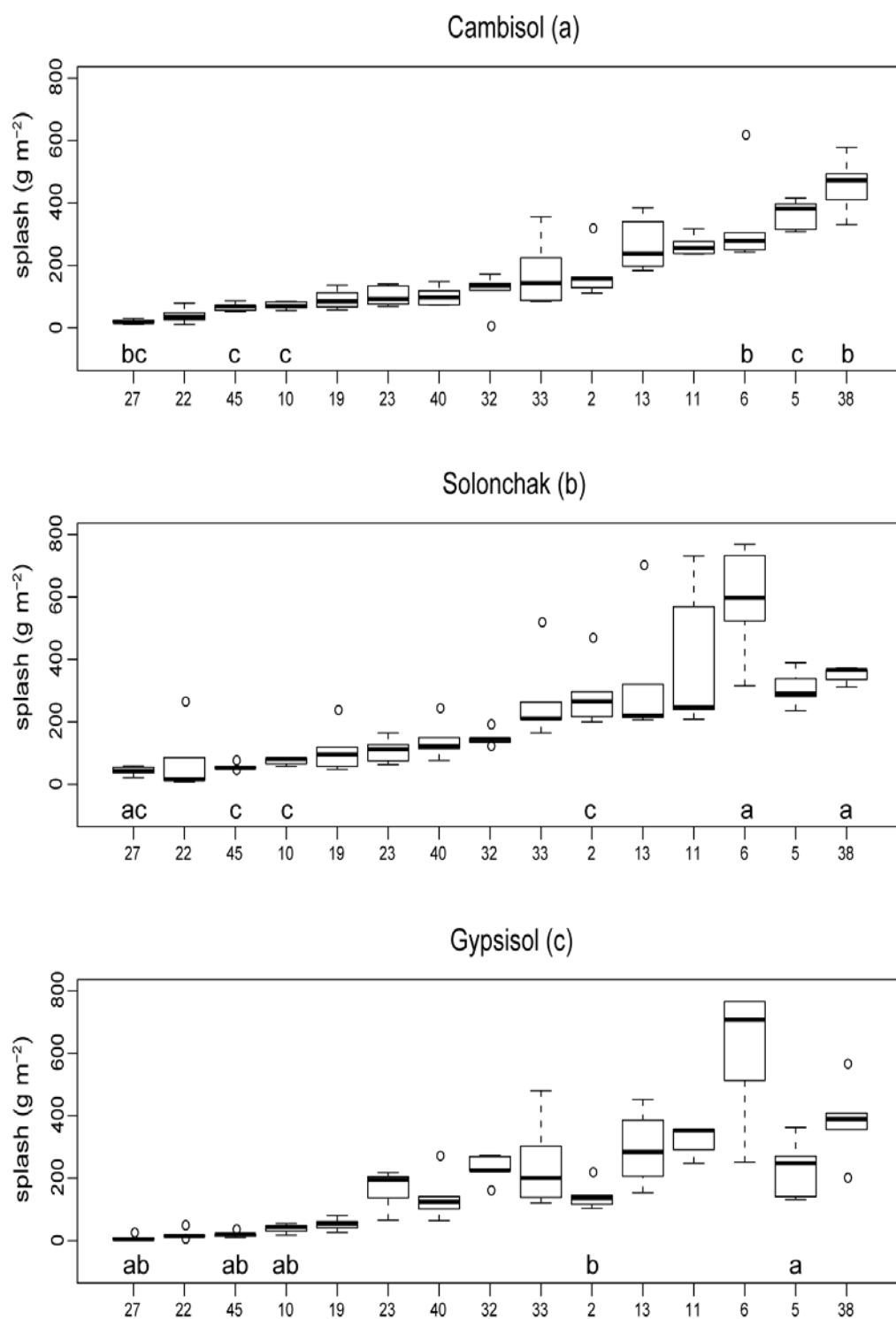


Figure 3.3: Soil splash ( $\text{g m}^{-2}$ ) boxplots by soil type sorted by the amount collected. The boxes indicate the 25<sup>th</sup> and 75<sup>th</sup> percentiles, the thick line indicates the median (50<sup>th</sup> percentile), the whiskers are extreme observations (highest/lowest observation which is not more/less than 1.5 times the interquartile range from the box), and the circles indicate outlier observations (observations which are higher/lower than 1.5 times the interquartile range from the box).



A general increasing linear relationship between splash and rainfall erosivity was found (Figure 3.4), although the high variability between the pseudo-replicates masked the global effect. LME analysis incorporated  $EI_{30}$  as the significant covariate explaining soil splash in all soil types (Table 3.5), and the soil type was not significant. Heterocedasticity was included in the model, meaning that within-group errors had a different variance, depending on soil type. The model explained 55% of variance of the measured variable ( $r^2$  coefficient). Variability between splash cups was very high, accounting for 72.4, 55.6, and 55.6% of the random variance for Cambisols, Solonchaks and Gypsisols, respectively. The remaining 27.6, 44.4, and 44.5% corresponded to random errors.

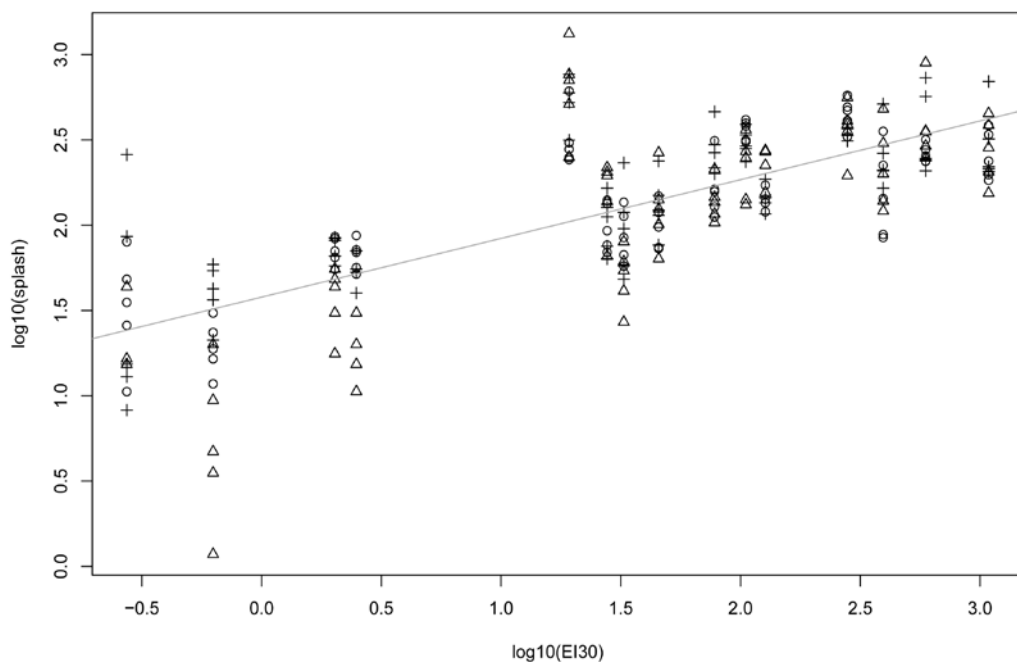


Figure 3.4: Scatter plot of soil splash vs. rainfall erosivity index  $EI_{30}$  ( $MJ \text{ mm ha}^{-1} h^{-1}$ ); Both variables are log-transformed. Soil types are indicated by symbols: Cambisol (circle), Solonchak (cross) and Gypsisol (triangle).



The results of the linear mixed-effects model yielded the following equation, in which splash erosion for soils with similar characteristics as the ones included in the study depend upon the  $EI_{30}$  index and its energy component ( $E$ ):

$$S = 38.02 (EI_{30})^{2.19}, \quad (3.6)$$

where,  $S$  is soil splash ( $\text{g m}^{-2}$ ).

Table 3.5. Linear Mixed-Effects analysis summary. Only significant covariates are shown.

Fixed effects	value	std error	df	t-value	p-value
Intercept	1.58	0.07	178	12.87	<0.001
Log( $EI_{30}$ )	0.34	0.04	43	9.18	<0.001
Akaike Information Criterium ( $AIC$ )					
	27.92				
Variance explained ( $r^2$ )	0.55				
Correlation coefficient	0.74				
Error variance components for soil type:					
	Cambisol		Solonchak		Gypsisol
Splash cups variability	72.42		55.62		55.55
Other variability	27.58		44.38		44.45

Events with zero soil splash were not included in the LME analysis due to the logarithmic transformation required. However, a plot of rainfall erosivity for events with and without splash helps in defining a threshold value for splash for the soils analysed (Figure 3.5). Such value appears to be around  $1 \text{ MJ mm ha}^{-1} \text{ h}^{-1}$ . Events 10, 22, 27 and 45 with  $EI_{30}$  values of 2.02, 0.27, 0.63 and  $2.49 \text{ MJ mm ha}^{-1} \text{ h}^{-1}$ , respectively registered splash sediment, while events 7 and 34 with  $EI_{30}$  values of 2.21 and  $1.46 \text{ MJ mm ha}^{-1} \text{ h}^{-1}$ , respectively, did not. However, considering the small number of events such a threshold should be taken as an approximate value.

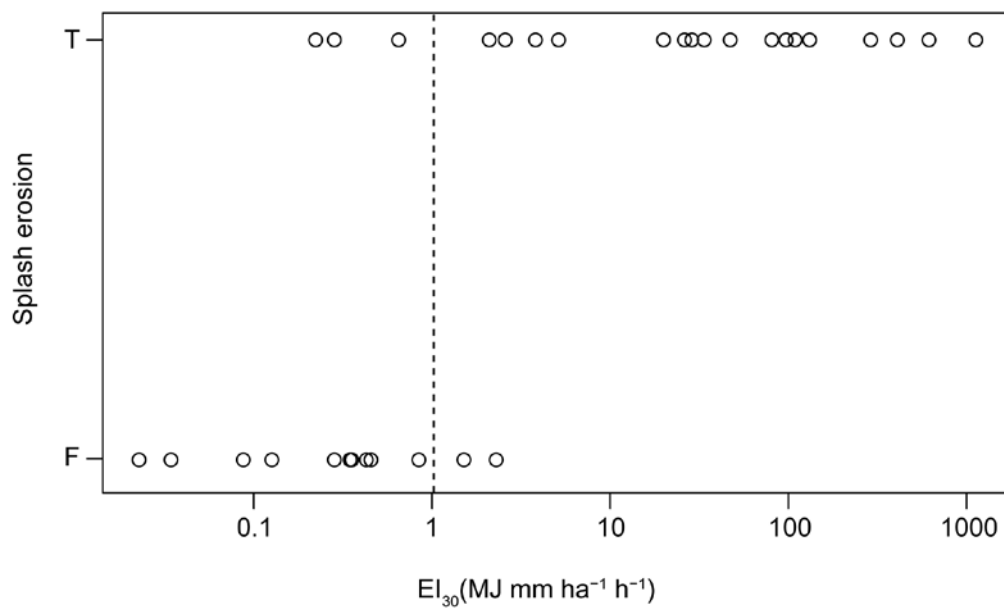


Figure 3.5: Rainfall erosivity ( $EI_{30}$ ) for events with soil splash sediment (T) and events without it (F).



### 3.3.3. Discussion

There are few similar studies evaluating the effects of natural rainfall on splash erosion, and the ones available in the scientific literature deal mostly with extreme rainfall events (Dunkerley, 2008). Most soil splash studies used simulated rainfall, and it has been argued that soil splash erosion rates obtained are highly overestimated (Poesen and Torri 1988; Dunkerley 2008). Another difference between previous studies and this one is that we were able to directly measure rainfall energy, instead of estimating it from rainfall intensity. Longer monitoring periods in different geographical regions using similar experimental designs are needed for attaining more general results. Fernandez-Raga et al. (2010) performed a similar experiment in Soutelo, northern Portugal. They found good agreement between kinetic energy and soil detachment, although they found large sources of uncertainty when undertaking experiments under natural conditions, such as the effects of rain washing or wind, leading to uncertain estimates of splash erosion. We found similar difficulties, leading to a relative high number of events that had to be discarded due to problems of rain or wind sediment washing. Splash amounts collected in the experiment of Fernandez-Raga et al. (2010) were relatively low compared with our results; this could be explained by the large contribution of small drops and low rainfall intensities.

As common in splash experiments under natural rain, the sampling intervals include several days, and in some cases more than one event occurred before the cups were removed (i.e. Shakesby et al., 1993, Terry, 1989). In our experiment we dealt with similar situations, resulting in several events that had to be rejected due to sediment wash by subsequent rains before the cups could be removed. It is possible that better results would be obtained by collecting splash cups more frequently, to isolate individual rain events, but this can be some problematic.

It has been argued that the soil conditions previous to the rainfall event and properties changes produced during the event may control splash conditions (Wainwright, 1996). In our case, the high splash amount recorded in event 6 could be explained by splash detachment prone conditions as soil crust and porosity. Inspection revealed higher levels of moisture and porosity, although no measurements were taken. The study of Singer and Le Bissonnais (1998) in 17 Mediterranean soils allowed them to distinguish two groups of soils. They found seal formation to be the main factor controlling splash and wash erosion. Other



authors also pointed to large aggregate size and high organic matter content (O.M.) as being significant for protecting against splash detachment (Luk, 1979; Ekwue, 1991). In our case differences in O. M. between the three soils were relatively low, but differences in soil texture did not lead to differences in splash.

The results of our analysis suggested that whilst  $I_{30}$  is an important parameter controlling splash erosion (Moldenhauer and Kemper, 1969; Mohammad and Kohl, 1987; Torri et al., 1999),  $E$  exerts a very important role as well. Both must be contained in  $EI_{30}$  index. A Linear-Mixed effects model between soil splash and the three rainfall erosivity covariates ( $EI_{30}$  and its components  $E$  and  $I_{30}$ ) yielded no significance for  $E$  and  $I_{30}$  alone, whereas  $EI_{30}$  was significant at the 99% confidence level. This supports the usefulness of the  $EI_{30}$  index in its original formulation. Another relevant result of our analysis is the high variability found between pseudo-replicates within the same soil type and rainfall event. This demonstrates that splash erosion is highly variable in space, and recommends the use of many splash cups per sampling unit in further experimental studies. Since these were pseudo-replicates (i.e. the samples from different splash cups within the same soil type were not statistically independent), ordinary regression was a sub-optimal model. The mixed-effects model, however, provided a convenient framework for analysing such an experimental design, since it allows incorporating fixed effects (soil type and rainfall erosivity index) and random effects (variability between splash cups within one soil type).



### 3.3.4. Conclusions

In this study, we conducted an experiment to determine relationships between rainfall erosivity parameters and soil splash erosion in three soil types under natural conditions. Linear Mixed-Effects analysis allowed us to explain most variability. Soil type did not significantly affect the amount of soil splash. Monitoring the rainfall properties relevant for soil splash erosion (kinetic energy, maximum intensity, effective storm duration and rainfall amount falling above a certain intensity threshold) and relating them to the amount of sediment mobilized is still needed in order to better understand the role of rainfall properties and soil characteristics in soil splash. Rainfall monitoring at high time resolution (e.g. every minute) is important to determine these properties, since more aggregated data (e.g. hourly or daily) are unable to capture these properties (Dunkerley, 2008, 2010).

This work has presented the experimental results of rainfall and splash erosion monitoring in three soil types under natural rainfall in NE Spain. During the measuring period (04/03/2010–30/10/2011), 27 events were evaluated. High rates of soil detachment were measured ( $\leq 712.5 \text{ g m}^{-2}$  or  $7.125 \text{ t ha}^{-1}$  per event), which stress the importance of soil splash as an erosion process in bare soils. We analysed the sources of variation of splash rates, and found significant relationships with the  $EI_{30}$  index, while no significant differences were found between the analysed soil types. The LME model explained 55% of variance, and the largest part of the residual variability ( $\leq 74\%$ ) was due to differences between splash cups within a single soil type and event (i.e. to random effects). This result has implications for further studies, since it makes clear that many pseudo-replicates (splash cups) need to be analysed to assess relationships between splash erosion, rainfall and soil characteristics. This also implies that the linear mixed-effects model, which includes both fixed and random effects, need to be used to analyse data generated by this experiment setup.



### 3.4. On the reliability of rainfall erosivity indices: a comparison between observed and estimated rainfall kinetic energy from natural rain events

The widespread application of the (R)USLE for estimating soil loss under a wide range of geographical conditions contrasts with the large criticisms which has received due to its inherent empirical nature. Its own author recommended restricting its use to zones with climatic and geographic characteristics similar to those of the region were it was calibrated (Wischmeier and Smith, 1965). Focusing on the rainfall erosivity factor (R factor) there are mainly three criticisms:

- a) Its dependence on high resolution pluviographic data (at least 15 min sampling interval), with a minimum of 20 years measuring period (Renard *et al.*, 1997; Verstraeten *et al.*, 2006). This kind of data is hardly available with a good spatial and temporal coverage.
- b) The  $EI_{30}$  establishes an energy limit in the equation for calculating the kinetic energy that may not be representative of geographical areas other than the region where it was calibrated. Several authors have developed their own equations adapted to the conditions of other geographical areas with the corresponding experimental effort (i.e. Bagarello and D'Assaro, 1994 for Sicily and south Italy; Yu and Rosewell, 1996 for south Australia; Schwertman *et al.*, 1987, for Germany; Gogichaishvili, 1981 for Georgia; Jayawardena and Rezaur, 2000 for Hong Kong; more examples are given in Table 1.4 section 1.5)
- c) The excessive simplicity of the  $EI_{30}$ , not taking into account relevant event characteristics. From the empirical studies of Seuffert *et al* (1999) carried out in Germany, Sardinia and South Africa, these authors consider the following parameters mandatory for reliable rainfall erosivity estimation: i) the spottiness or duration and distribution of rainfall pulses; ii) the relation of total to effective event duration; iii) the intensity pattern (peak and duration of high intensity rainfall pulses, as well as the ratio between the sum of the high intensity peaks and the average or total rainfall intensity); iv) the temporal occurrence within the event of high intensity peaks that are sufficiently high and long-lasting to trigger direct runoff, as well as the amount of rain falling after the first of such peaks; v)



the spatial pattern of portions of a surface that are either hit by high-intensity rainfall simultaneously or that receive no rain at all, as well as the temporal variability of this pattern in the course of a rainfall event. The authors relate all these parameters in a rainfall erosivity index, REI. However, the first critic previously commented also applies to the REI index, since data at 5-minutes time resolution or better are needed to compute it.

In this study three kinetic energy estimation models (i.e. the RUSLE equation, Van Dijk's universal equation, and the Cerro's proposal calibrated with data from Barcelona, Spain) are compared with kinetic energy values obtained from a laser precipitation monitor is carried out, with the objective of assessing their validity as indices of rainfall erosivity.



### 3.4.1 The rainfall erosivity indices

The event's rainfall erosivity index  $EI_{30}$  ( $\text{MJ mm ha}^{-1} \text{h}^{-1}$ ) has been defined earlier in this work (section 2.4), but its formulation is repeated here to enhance readability. The  $EI_{30}$  is obtained as the product of the total rainfall energy  $E$  ( $\text{MJ ha}^{-1}$ ) and the maximum 30-minutes rainfall intensity  $I$  ( $\text{mm h}^{-1}$ ):

$$EI = EI_{30} = \left( \sum_{r=1}^o e_r v_r \right) I_{30},$$

where  $e_r$  and  $v_r$  are, respectively, the unit rainfall energy ( $\text{MJ ha}^{-1} \text{mm}^{-1}$ ) and the rainfall volume (mm) during measuring time interval  $r$ .

In the absence of disdrometric data (raindrop size and velocity), the unit rainfall energy  $e_r$  needs to be estimated by means of empirical equations. Here we used three alternative formulae calibrated with raindrop data in different geographical regions, resulting in small differences. The most widely used is the  $e_{r(\text{RUSLE})}$  due to Brown and Foster (1987), based on experimental data registered at Holly Springs (USA) by McGregor and Mutcher (1976), using the method of flour pellets. This equation is used for the estimation of the rainfall erosivity index in the Revised Universal Soil Loss Equation (RUSLE, Renard *et al.*, 1997):

$$e_{r(\text{RUSLE})} = 0.29 [1 - 0.72 \exp(-0.05 i_r)], \quad (3.7)$$

Based on data from 19 previously published articles from locations around the world Van Dijk *et al.* (2002) proposed a universal kinetic energy equation— $e_{r(VD)}$ —, given by:

$$e_{r(VD)} = 0.283 [1 - 0.52 \exp(-0.042 i_r)], \quad (3.8)$$

This relationship was claimed to be a better option than the Brown and Foster one due to the wider geographical spread of the dataset employed. Due to the geographical proximity with the study area of this work, the relationship proposed by Cerro *et al.* (1998) based on disdrometric data recorded in Barcelona (Spain), is another relevant model for our case study:

$$e_{r(CERRO)} = 0.384 [1 - 0.538 \exp(-0.029 i_r)], \quad (3.9)$$

The monitoring of natural rainfall's kinetic energy was detailed in section 3.2. However, the basic information is summarized here. The raindrop spectra (number of raindrops pertaining to 22x20 classes of particle size and velocity, Table 3.1) was measured in one-minute time intervals by a Thies Klima Laser



Precipitation Monitor (LPM). The kinetic energy  $ke_{ij}$  (J) of a drop pertaining to diameter class  $i$  and velocity class  $j$  was estimated by equation (3.1), assuming a spherical drop shape. The total kinetic energy  $ke_{\text{sum}}$  per minute was determined by multiplying  $ke_{ij}$  by the number of drops recorded in each size and velocity class. Finally, the unit energy ( $e_r$ ) was obtained by dividing the sampling area of the device ( $a$ , in our case  $0.00514 \text{ m}^2$ ) and by the rainfall amount per minute ( $p_r$ , mm) in order to obtain an energy rate per unit surface and precipitation amount ( $\text{MJ ha}^{-1} \text{ mm}^{-1}$ ).

From the disdrometric data also the  $I_{30}$ , i.e. the maximum rainfall intensity during a period of 30 consecutive minutes ( $\text{mm h}^{-1}$ ), was computed. This allowed computing the  $EI_{30}$  index based on the observed data, and on the three empirical equations for  $e_r$ .

One possible source of uncertainty in the comparison relies on the different time frequency used for recording the rainfall events that yield the models in equations 3.8 to 3.10 (Figure 3.6). In the RUSLE method a time resolution of 15 minutes was used for registering the data, while Cerro recorded rainfall intensity every 30 seconds. The study of Van Dijk is based on previously published data, with differences in the methods used for recording the drop size distribution and in the time resolution employed. In our case we used a time resolution of one minute for both the observed and estimated rainfall erosivity, but we also aggregated the dataset to a time resolution of 15 minutes in order to compare the values obtained as a function of the time resolution of the record.

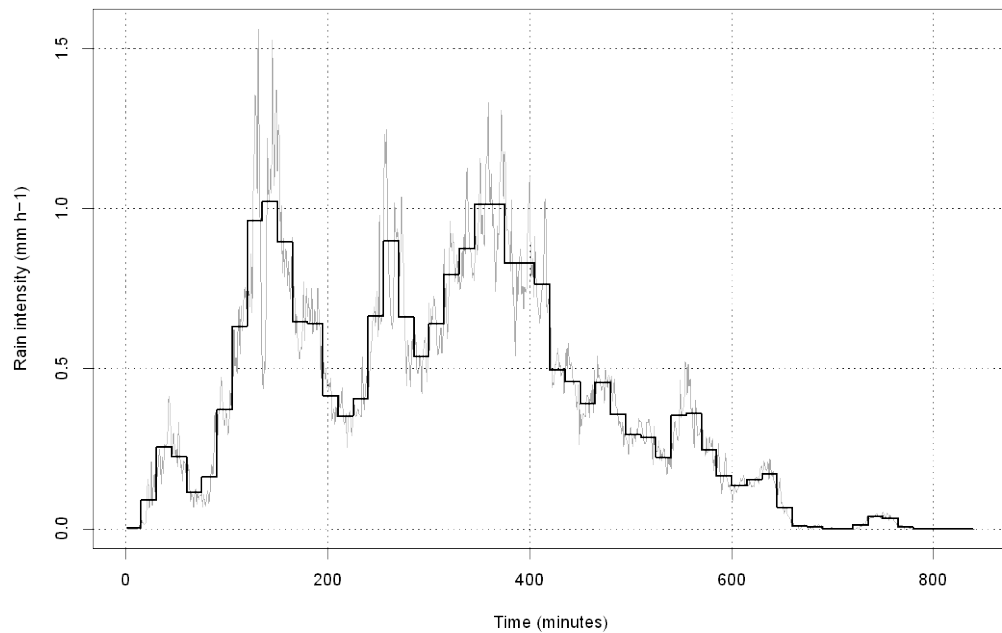


Figure 3.6: Monitoring rainfall intensity at 1-minute (grey line) and 15-minutes (black line) time resolution. Reducing the sampling frequency from one to 15 minutes has the effect of smoothing the time series of rainfall intensity, loosing the peak intensities that are shown in the high-frequency record. This could have an effect in the calculation of  $I_{30}$ , dificulting the comparison between models calibrated from records of varying time frequency.

### 3.4.2 Validation criteria

The three alternative  $E$  and  $EI_{30}$  estimations were compared to the values obtained from the disdrometric record based on standard descriptive measurements of centrality and dispersion, and on several error and goodness-of-fit statistics. Among the former we selected i) the mean bias error ( $MBE$ ), which is centered around zero and is an indicator of prediction bias; and ii) the mean absolute error ( $MAE$ ), which is a measure of the average error. As goodness-of-fit measures we used: i) the  $NS$  coefficient of efficiency (Nash and Sutcliffe, 1970), which indicates how close scatters of predicted values are to the line of best fit (this is similar to the coefficient of determination  $R^2$ , without being highly affected by outlier data); and ii) the agreement index  $D$  (Willmott, 1981), which scales the magnitude of the variables, retains the mean information and does not amplify the outliers. The equations for these statistics are shown in section 2.5.



### 3.4.3 Results

The dataset comprised 37 rainfall events of varying duration. The rainfall erosivity index components  $E$ ,  $I_{30}$  and  $EI_{30}$  were computed for each event based on observed disdrometric data, and estimations based on three empirical methods of equations 8–10 were computed. These calculations were performed based on the original 1-minute record, and on a dataset where the records were aggregated on a 15-minutes basis.

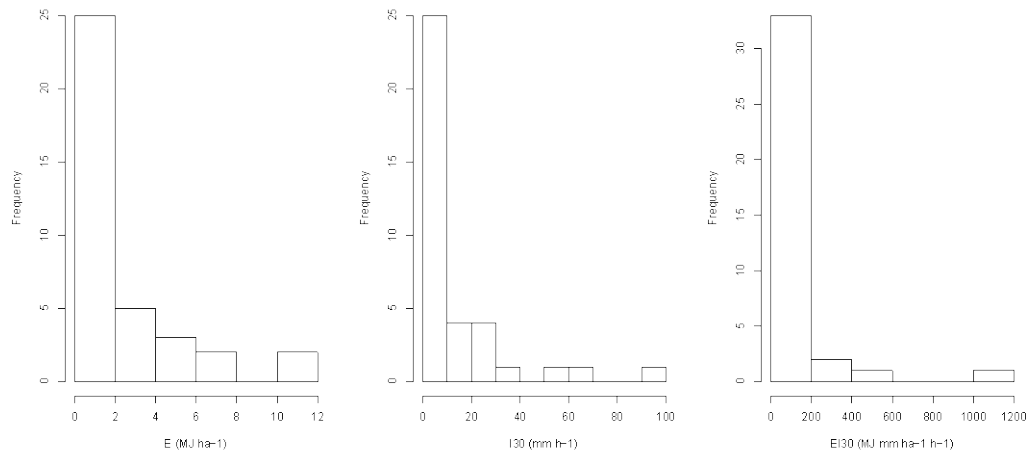


Figure 3.7: Histograms of event's kinetic energy,  $E$ , maximum 30-minutes intensity,  $I_{30}$ , and erosivity index,  $EI_{30}$ .

Rainfall erosivity varied largely across events due to differences in rainfall intensity,  $I_{30}$ , and on the cumulated kinetic energy,  $E$  (Table 3.6). The frequency distribution of the three variables showed an exponential behaviour, accentuated for  $EI_{30}$  as a product of the other two variables (Figure 3.7).

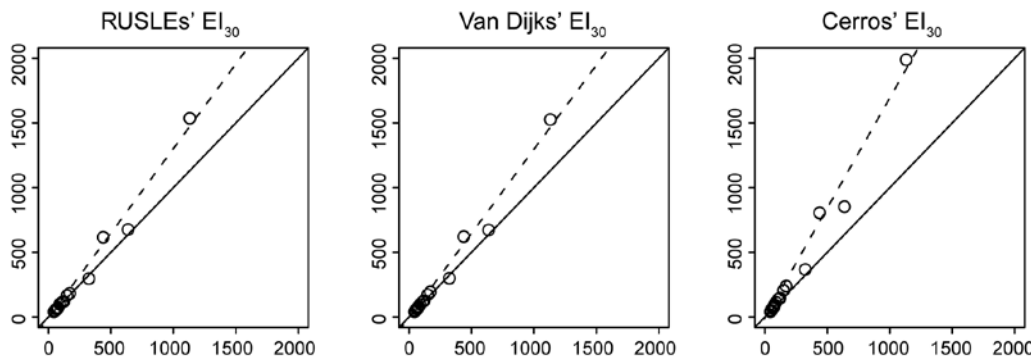


Figure 3.8: Comparison between observed (ordinate axis) and predicted (abscissa axis) values of rainfall erosivity,  $EI_{30}$  (circles). Line of perfect fit (continuous) and regression line (dashed).

Overall, the three empirical models provided grossly satisfactory results for the estimation of  $E$ , and therefore for  $EI_{30}$  (Table 3.8). The comparison between observed and estimated values of  $EI_{30}$  yielded very high goodness-of-fit statistics (correlation,  $r^2$ , Willmott's  $D$  and Nash-Sutcliffe). However, the mean absolute errors ranged between 25 (for RUSLE and Van Dick) and 60% (for Cerro) of the observed values and the three models had a tendency to overestimate rainfall erosivity, as shown by higher mean and standard variation values and by positive mean bias error in all cases. Among the three methods, the Cerro equation resulted in higher overestimation. The reason of this apparent paradox in the validation statistics (very high goodness-of-fit values and a marked bias) is explained when the estimated and observed values are plotted together (Figure 3.8). The three models showed a clear tendency to overestimate rainfall erosivity across the range of observed values, but the circles fit very well to a linear regression, explaining the very high goodness-of-fit statistics.

When the data were aggregated at 15-time intervals to mimic the conditions under which some of the empirical proposals were made, the values of  $E$ ,  $I_{30}$  and  $EI_{30}$  varied slightly, as it was expected (Table 3.7 and Figure 3.8). In general, the values of kinetic energy  $E$  were not much affected by the change of the time resolution of the monitoring, but the rainfall intensity  $I_{30}$  was underestimated when it was measured at 15-minutes intervals. As a result, rainfall erosivity  $EI_{30}$  values were lower when based on 15-minutes data than when based on 1-minute data, although the difference was lower than 10% (Table 3.9).



Table 3.6. Erosivity properties of natural rainfall events registered at 1-minute time intervals: total kinetic energy  $E$  (MJ ha $^{-1}$ ), maximum intensity in 30 minutes  $I_{30}$  (mm h $^{-1}$ ) and rainfall erosivity  $EI_{30}$  (MJ mm ha $^{-1}$  h $^{-1}$ ); measured values and estimations by the RUSLE (-R), Van Dijk (-VD), and Cerro (-C) methods.

N	E	E-R	E-VD	E-C	$I_{30}$	$EI_{30}$	$EI_{30}-R$	$EI_{30}-VD$	$EI_{30}-C$
2	4.92	4.93	5.38	6.70	15.85	77.94	78.14	85.25	106.15
3	0.30	0.39	0.44	0.54	3.65	1.09	1.42	1.59	1.97
4	0.53	0.43	0.66	0.85	1.55	0.82	0.66	1.02	1.31
5	4.34	5.12	5.38	6.77	24.25	105.23	124.28	130.42	164.25
6	1.67	1.68	1.79	2.28	11.53	19.24	19.35	20.65	26.33
7	0.40	0.47	0.60	0.75	5.50	2.21	2.60	3.29	4.13
10	0.86	0.65	0.97	1.24	2.34	2.02	1.51	2.27	2.91
11	10.57	11.32	11.25	14.46	56.11	592.96	635.14	631.41	811.60
12	2.14	1.87	2.20	2.74	11.77	25.22	22.07	25.88	32.23
13	11.70	16.09	15.98	20.97	92.90	1086.64	1494.79	1484.91	1947.72
16	0.32	0.26	0.39	0.51	1.31	0.41	0.34	0.52	0.67
17	1.03	1.00	1.38	1.76	3.47	3.59	3.46	4.80	6.10
19	2.79	2.80	3.56	4.57	11.65	32.55	32.58	41.52	53.31
20	1.44	1.34	2.05	2.64	2.56	3.67	3.43	5.24	6.75
21	0.02	0.02	0.03	0.04	0.30	0.00	0.01	0.01	0.01
22	0.25	0.29	0.46	0.59	1.08	0.27	0.31	0.49	0.64
23	3.79	3.44	4.68	5.93	7.31	27.72	25.12	34.20	43.35
24	1.65	1.83	2.73	3.51	3.01	4.96	5.51	8.24	10.59
25	0.11	0.11	0.17	0.21	1.13	0.12	0.13	0.19	0.24
26	0.11	0.10	0.16	0.21	0.75	0.08	0.08	0.12	0.16
27	0.33	0.30	0.44	0.56	1.93	0.63	0.58	0.85	1.09
28	0.00	0.03	0.03	0.04	0.34	0.00	0.01	0.01	0.01
31	0.36	0.31	0.46	0.59	1.23	0.44	0.38	0.56	0.72
32	4.85	5.45	5.86	7.54	26.18	126.94	142.73	153.43	197.38
33	6.40	9.34	9.42	12.41	61.61	394.17	575.18	580.09	764.33
34	0.54	0.34	0.50	0.64	2.71	1.46	0.93	1.35	1.73
35	0.00	0.03	0.05	0.06	0.10	0.00	0.00	0.00	0.01
37	0.20	0.11	0.14	0.18	1.64	0.33	0.19	0.24	0.30
38	7.86	7.18	7.26	9.17	35.57	279.44	255.42	258.32	326.13
39	3.20	3.61	3.74	4.80	20.79	66.47	75.05	77.82	99.76
40	2.19	2.77	2.73	3.53	20.79	45.50	57.62	56.67	73.28
41	1.23	0.91	0.99	1.24	6.56	8.04	5.96	6.52	8.12
42	0.06	0.05	0.08	0.10	0.53	0.03	0.03	0.04	0.05
43	0.16	0.10	0.14	0.17	1.34	0.21	0.13	0.18	0.23
44	0.07	0.04	0.07	0.09	0.34	0.02	0.01	0.02	0.03
45	0.87	0.61	0.90	1.15	2.84	2.49	1.74	2.55	3.27
46	1.05	0.83	1.20	1.53	3.58	3.75	2.95	4.27	5.46



Table 3.7. Erosivity properties of natural rainfall events registered at 15-minute time intervals: total kinetic energy  $E$  ( $\text{MJ ha}^{-1}$ ), maximum intensity in 30 minutes  $I_{30}$  ( $\text{mm h}^{-1}$ ) and rainfall erosivity  $EI_{30}$  ( $\text{MJ mm ha}^{-1} \text{h}^{-1}$ ); measured values and estimations by the RUSLE (-R), Van Dijk (-VD), and Cerro (-C) methods.

N	$E$	$E\text{-R}$	$E\text{-VD}$	$E\text{-C}$	$I_{30}$	$EI_{30}$	$EI_{30}\text{-R}$	$EI_{30}\text{-VD}$	$EI_{30}\text{-C}$
2	4.38	4.41	5.00	6.19	15.73	68.95	69.32	78.65	97.32
3	0.20	0.29	0.37	0.46	3.60	0.72	1.05	1.33	1.67
4	0.47	0.41	0.65	0.84	1.55	0.73	0.64	1.01	1.30
5	3.84	4.42	4.85	6.00	20.57	78.97	90.82	99.67	123.41
6	1.34	1.47	1.62	2.01	11.53	15.46	16.96	18.72	23.21
7	0.38	0.44	0.58	0.73	4.92	1.89	2.14	2.83	3.57
10	0.82	0.63	0.96	1.24	2.26	1.85	1.43	2.17	2.79
11	10.42	10.96	10.94	13.82	53.77	560.18	589.17	587.96	743.19
12	1.95	1.60	2.02	2.53	10.24	19.97	16.36	20.64	25.85
13	12.27	15.93	15.80	20.40	78.97	968.80	1258.27	1248.08	1610.75
16	0.27	0.25	0.39	0.50	1.25	0.34	0.31	0.48	0.63
17	0.79	0.90	1.32	1.69	3.33	2.61	2.98	4.40	5.63
19	2.37	2.53	3.36	4.26	11.57	27.41	29.32	38.87	49.33
20	1.29	1.31	2.02	2.62	2.44	3.15	3.18	4.93	6.37
21	0.01	0.02	0.03	0.04	0.30	0.00	0.01	0.01	0.01
22	0.23	0.28	0.45	0.59	1.07	0.25	0.30	0.48	0.63
23	3.50	3.24	4.54	5.78	6.72	23.51	21.80	30.55	38.86
24	1.54	1.78	2.70	3.48	2.88	4.44	5.13	7.80	10.04
25	0.08	0.10	0.16	0.20	1.13	0.09	0.11	0.18	0.23
26	0.10	0.10	0.16	0.20	0.68	0.07	0.07	0.11	0.14
27	0.27	0.28	0.43	0.55	1.93	0.53	0.54	0.83	1.06
28	0.00	0.00	0.00	0.00	0.00	0.00	0.00	0.00	0.00
31	0.27	0.28	0.44	0.57	1.13	0.30	0.32	0.49	0.64
32	4.50	5.10	5.57	7.03	25.89	116.41	131.90	144.31	181.94
33	6.27	9.20	9.30	12.14	60.90	382.01	560.26	566.34	739.00
34	0.51	0.33	0.49	0.63	2.39	1.22	0.79	1.17	1.50
35	0.00	0.03	0.04	0.06	0.10	0.00	0.00	0.00	0.01
37	0.12	0.08	0.12	0.15	1.64	0.20	0.13	0.20	0.25
38	6.16	6.15	6.49	8.01	28.04	172.68	172.60	181.94	224.52
39	2.76	3.17	3.37	4.23	19.57	54.09	62.08	65.95	82.72
40	1.84	2.42	2.44	3.02	20.79	38.31	50.22	50.65	62.75
41	0.70	0.71	0.86	1.07	6.56	4.57	4.68	5.63	7.02
42	0.04	0.05	0.07	0.10	0.52	0.02	0.02	0.04	0.05
43	0.12	0.09	0.13	0.17	1.32	0.15	0.11	0.17	0.22
44	0.05	0.04	0.07	0.09	0.32	0.02	0.01	0.02	0.03
45	0.78	0.58	0.88	1.13	2.77	2.17	1.62	2.44	3.14
46	0.98	0.80	1.18	1.51	3.25	3.17	2.61	3.84	4.91



Table 3.8. Validation statistics of rainfall erosivity index  $EI_{30}$  estimations for 37 natural rainfall events, measured at 1-minute time frequency: bias (mean, standard deviation, mean bias error) and goodness-of-fit statistics (mean absolute error, correlation,  $r^2$ , Willmott's D, Nash-Sutcliffe).

	<i>mean</i>	<i>st. dev.</i>	<i>MBE</i>	<i>MAE</i>	<i>correl.</i>	<i>r</i> <sup>2</sup>	<i>D</i>	<i>NS</i>
Observed	78.83	209.4						
Modelled:								
RUSLE	96.48	276.0	17.65	19.57	0.99	0.99	0.98	0.93
Van Dijk eq.	97.97	274.5	19.14	20.38	0.99	0.99	0.98	0.93
Cerro	127.10	359.2	48.26	48.26	0.99	0.98	0.92	0.80

Table 3.9. Mean and standard deviation of observed and estimated erosivity  $EI_{30}$  for 37 rainfall events, recorded at 1-minute and at 15-minutes time resolution.

	1-minute		15-minutes	
	<i>mean</i>	<i>st. dev.</i>	<i>mean</i>	<i>st. dev.</i>
Observed	78.83	209.4	69.06	188.8
Modelled:				
RUSLE	96.48	276.0	83.71	238.8
Van Dijk eq.	97.97	274.5	85.75	237.6
Cerro	127.10	359.2	109.59	306.1

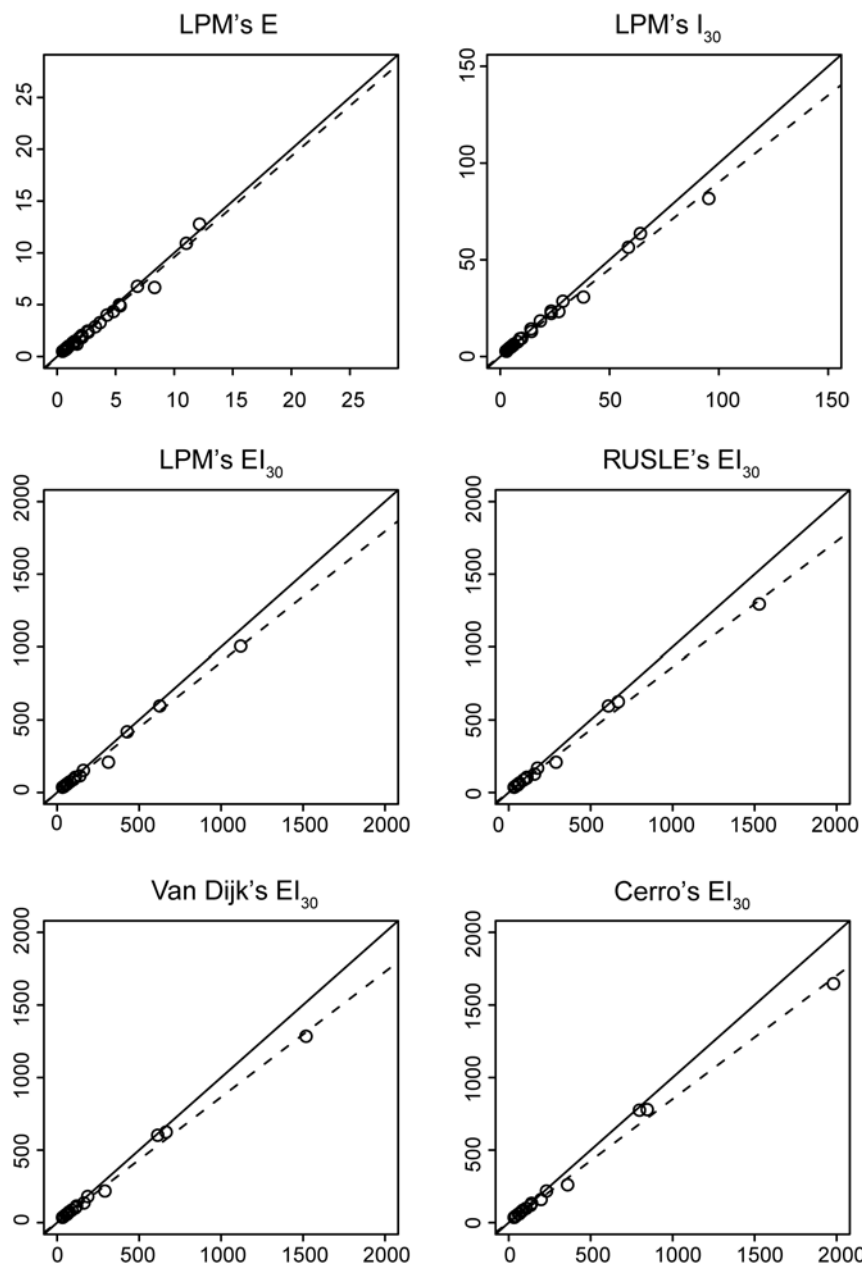


Figure 3.9: Comparison between erosivity properties ( $E$ ,  $I_{30}$  and  $EI_{30}$ ) from observations at 1-minute (ordinate axis) and 15-minutes (abscissa axis) time resolution. Observed values (LPM), and estimations by three empirical models. Line of perfect fit (continuous) and regression line (dashed).

### 3.4.4. Discussion and conclusions

We compared  $EI_{30}$  rainfall erosivity estimates by three empirical models based on rainfall intensity data (RUSLE, Van Dijk and Cerro) with observed  $EI_{30}$  values measured with a Laser Precipitation Monitor. We found that the three models produced biased estimations, resulting in overestimated rainfall erosivities by more than 25%. The fit between observations and estimations was, however,



very good, i.e. very high linear correlations existed in the three cases. This indicates that there is a source of systematic bias between observed and modelled erosivities. We tested the influence of varying sampling frequencies (time interval between measurements of rainfall properties), since the data used for calibrating several models (RUSLE, Van Dijk) had a sampling frequency lower than one minute used here. We found that reducing the sampling frequency from one to 15-minutes had the effect of reducing  $EI_{30}$  by approximately 10%. Therefore, this effect could not explain the overestimation of  $EI_{30}$  by these methods when compared to the observed values.

Another important difference between our dataset and the data used for calibrating the three empirical models relies on the characterization of raindrop velocity. Besides the distribution of drop sizes, a characterization of drop velocity is necessary for determining the kinetic energy of the rain. Manual methods such as the flour pellets or earlier disdrometers were only able to determine the drop size, so drop velocities had to be estimated based on the hypothesis that all drops fall at their theoretical terminal velocity, as given for example by the Uplinger equation (Table 1.2). In his work, Cerro et al. (1998) also used the theoretical terminal velocity of raindrops, despite the availability of direct measurements of drop velocity by an optical disdrometer. In this study we used the direct observations of drop velocity provided by the Laser Precipitation Monitor, instead of their theoretical terminal velocities. Raindrop velocity is sensitive to atmospheric conditions such as the wind speed, air pressure and temperature. Empirical studies showed that sub-terminal raindrop velocities are often the norm in natural rainfall (Laws, 1941). Cerro et al. (1998), in his analysis of disdrometer data from natural rainfall in Barcelona found that measured velocities were on average 17% lower than the theoretical ones, resulting in kinetic energy  $E$  values up to 41% lower. We believe that the bias found in this study between observed and estimated erosivities can be explained to a large extent by the fact that we used observed raindrop velocities instead of theoretical ones.



### 3.5 References

- Bagarello, V., D'Assaro, F.D., 1994. Estimating single storm erosion index. *Transactions of ASAE*, 37, 785-791.
- Bermúdez, F.G. 1997. Aplicación agronómica de lodos residuales a suelos en ambientes semiáridos y su efecto sobre propiedades físico-químicas. Tesis Doctoral, Zaragoza-Lleida. 368 pages.
- Bisal, F. 1960. The effect of raindrop size and impact velocity on sand splash. *Canadian Journal of Soil Science*, 40, 242-245.
- Brawn, D., Upton, G., 2008. Estimation of an atmospheric gamma drop size distribution using disdrometer data. *Atmospheric Research*, 87, 66–79.
- Cerro, C., Bech, J., Codina, B., Lorente, J. 1998. Modeling rain erosivity using disdrometric techniques. *Soil Science Society of America Journal*, 62 (3) 731-735
- Donnadieu, G., Dubosclard, G., Godard, S., 1969. Un pluviomètre photoélectrique pour la détermination simultanée des spectres dimensionnel et de vitesse de chute des gouttes de pluie. *Journal de Recherches Atmosphériques*, IV, 37-46.
- Dunkerley, D., 2008. Rain event properties in nature and in rainfall simulation experiments: a comparative review with recommendations for increasingly systematic study and reporting. *Hydrological Processes*, 22, 4415-4435.
- Dunkerley, D., 2010. How do the rain rates of sub-event intervals such as the maximum 5- and 15-min rates ( $I_5$  or  $I_{30}$ ) relate to the properties of the enclosing rainfall event? *Hydrological Processes*, 24, 2425-2439.
- Ellison, W.D. 1947. Soil Erosion Studies—Part II: Soil detachment hazard by raindrop splash. *Agricultural Engineering*, 28, 197–201.
- Ellison, W.D. 1944. Studies of raindrop erosion. *Agricultural Engineering*, 25, 131-136, 181-182.
- Ekwue, E.I.M. 1991. The effects of soil organic matter content, rainfall duration and aggregate size on soil detachment. *Soil Technology*, 4, 197-207.
- F.A.O. 1989. Mapa mundial de suelos. Leyenda revisada. Informes sobre recursos mundiales de suelos 60. Roma



- Fernández-Raga, M., Fraile, R., Keizer, J.J., Varela Teijeiro, M.E., Castro, A., Palencia, C., Calvo, A.I., Koenders, J., Da Costa Marques, R.L. 2010. The kinetic energy of rain measured with an optical disdrometer: an application to splash erosion. *Atmospheric Research*, 96, 225-240.
- Gogichaishvili, G.P. 1981. Reaviling of a rainfall characteristics determining the rainfall erosivity. In Laws of the display of erosion and river processes under different climatic conditions. 3th All Union Conference. Moscow, 80-81.
- Guerrero, J., Alberto, F., Hodgson, J., García-Ruiz, J.M., Montserrat, G. 1999. Plant community patterns in a gypsum area of NE Spain. 1. Interactions with topographic factors and soil erosion. *Journal of Arid Environments*, 41, 401–410.
- Hudson, N.W. 1995. Soil conservation. Third Edition. Batsford. London 304pp.
- Jayawardena, A.W., Rezaur, R.B., 2000. Drop size distribution and kinetic energy load of rainstorms in Hong Kong. *Hydrological Processes*, 14, 1069-1082.
- Laws, J.O. 1941. Measurements of the fall velocity of water drops and raindrops. *Transactions of American Geophysical Union*, 22 (3), 709-721.
- Legout, C., Leguédois, S., Le Bissonnais, Y., Malam Issa, O. 2005. Splash distance and size distributions for various soils. *Geoderma*, 124, 279–292.
- Luk, S.H. 1979. Effect of soil properties on erosion by wash and splash. *Earth Surface Processes*, 4, 241-255.
- Machín, J., Navas, A. 1998. Spatial analysis of gypsiferous soils in the Zaragoza province (Spain), using GIS as an aid to conservation. *Geoderma*, 87, 57–66.
- Meyer, L.D. 1981. How rain intensity affects interrill erosion. *Transactions of ASAE*, 24, 1472-1475.
- Mohammad, D., Kohl, R.A., 1987. Infiltration response to kinetic energy. *Transactions of ASAE*, 30, 108–111.
- Moldenhauer, W.C., Kemper, W.D., 1969. Interdependence of water drop energy and clod size on infiltration and clod stability. *Soil Science Society America Proceedings*, 33, 297–301.
- Morgan, R.P.C., 2005. *Soil Erosion and Conservation*. Third edition, Blackwell publishing, Oxford, UK. 303 p.
- Morgan, R.P.C., 1981. Field measurements of splash erosion. *I. A. S. H. P.* 133, 373–382.



- Morgan, R.P.C. 1978. Field studies of rainsplash erosion. *Earth Surface Processes and Landforms*, 3, 295–299.
- Mouzai, L. Bouhadef, M., 2003. Water drop erosivity: effects on soil splash. *Journal of Hydraulic Research*, 41, 61-68.
- Nash, J.E., Sutcliffe, J.V., 1970. River flow forecasting through conceptual models part I – A discussion of principles. *Journal of Hydrology*, 10, 282-290.
- Navas, A. 1993. Soil losses under simulated rainfall in semiarid shrublands of the Ebro valley. *Soil Use and Management*, 9(4),152–157.
- Navas, A., Alberto, F., Machín, J., Galán, A. 1990. Design and operation of a rainfall simulator for field studies of runoff and soil erosion. *Soil Technology (Soil & Tillage Research)* 3, 385–397.
- Park, S.W., Mitchell, J.K., Bubenzer, G.D., 1983. Rainfall characteristics and their relation to splash erosion. *Transactions of ASAE*, 26, 795-804.
- Pinheiro, J., Bates, D., DebRoy, S., Sarkar, D., and the R Development Core Team. 2011. *nlme: Linear and Nonlinear Mixed Effects Models*. R package version 3.1-102
- Pinheiro, J., Bates, D. 2000. *Mixed-Effects Models in S and S-PLUS*, Springer, New York, 530 pp.
- Poesen, J., Torri, D. 1988. The effect of cup size on splash detachment and transport measurements; Part I: field measurements. *Catena suppl.* 12, 113-126.
- Pueyo, Y., Alados, C.L., Maestro, M., Komac, B. 2007. Gypsophile vegetation patterns under a range of soil properties induced by topographical position. *Plant Ecology*, 189, 301–311.
- Renard, K.G., Foster, G.R., Weesies, G.A., McCool, D.K., Yoder, D.C. 1997. Predicting Soil Erosion by Water: *A Guide to Conservation Planning with the Revised Universal Soil Loss Equation (RUSLE)*. USDA Agricultural Handbook No. 703, USDA, Washington, DC, 384 pp.
- Salles , C., Poesen, J. 1999. Performance of an optical spectro pluviometer in measuring basic rain erosivity characteristics. *Jorunal of Hydrology*, 218, 142-156.
- Scholten, T., Geibler, C., Goc, J., Kühn, P., Wiegand, C. 2011. A new splash cup to measure the kinetic energy of rainfalls. *Journal of Plant Nutrition and Soil Science* 174, 596-601.



- Sempere Torres, D., Porrà, J.M., Creutin, J.D. 1994. A general formulation for Raindrop Size Distribution. *Journal of Applied Meteorology*, 33, 1494-1502.
- Seuffert, O., Busche, D., Löwe, P. 1999. Rainfall structure – rainfall erosivity: new concepts to solve old problems. *Petermanns Geographische mitteilungen*, 143 (5-6): 475-490.
- Sharma, P.P., Gupta, S.C., Rawls, W.J., 1991. Soil detachment by single raindrops of varying kinetic energy. *Soil Science Society of America Journal*, 55, 301–307.
- Shakesby, R.A., Coelho, C.O.A., Ferreira, A.J.D., Terry, J.P., Walsh, R.P.D., 1993. Wildfire impacts on soil erosion and hydrology in wet Mediterranean forest. Portugal. *International Journal Wildland Fire*, 3 (2), 95–110.
- Singer, M.J., Le Bissonnais, Y., 1998. Importance of surface sealing in the erosion of some soils from a Mediterranean climate. *Geomorphology*, 24, 79-85.
- Schwertmann, U., Vogel, W., Kainz, M., 1987. Bodenerosion durch Wasser. *Stuttgart*. 2. Aufl. 64
- Sukhanovski, Y.P., Ollesch, G., Khan, K.Y., Meiβner, R. 2002. A new index for rainfall erosivity on a physical basis. *Journal of Plant Nutrition and Soil Science*, 165, 51-57.
- Terry, J.P., 1989. The development of a new device for measuring rainsplash erosion. *Swansea Geography*, 26, 54–63.
- Torri, D., Regües, D., Pellegrini, S., Bazzoffi, P. 1999. Within-storm soil surface dynamics and erosive effects of rainstorms. *Catena*, 38, 131-150
- U.S.D.A. 1973. Manual de conservación de suelos. Ed. Limusa-Wiley, Mexico.
- Van Dijk, A.I.J.M., Bruijnzeel, L.A., Wiegman, S.E. 2003. Measurements of rain splash on bench terraces in a humid tropical steepland environment. *Hydrological Processes*, 17, 513–535
- Van Dijk, A.I.J.M., Bruijnzeel, L.A., Rosewell, C.J. 2002. Rainfall intensity-kinetic energy relationships: a critical literature appraisal. *Journal of Hydrology*, 261, 1-23.
- Verstraeten, G., J. Poesen, G. Demarée, and C. Salles (2006), Long-term (105 years) variability in rain erosivity as derived from 10-min rainfall depth data for Ukkel (Brussels, Belgium): Implications for assessing soil erosion rates, *Journal of Geophysical Research*, 111, D22109.



- Wainwright, J., 1996. Infiltration, runoff and erosion characteristics of agricultural land in extreme storm events, SE France. *Catena*, 26, 27–47.
- Wischmeier WH & Smith DD. 1965. Predicting rainfall erosion losses from cropland east of the Rocky Mountains. *Agriculture Handbook 282, USDA, Washington, DC.*
- Wischmeier, W.H., Smith, D.D., 1978. Predicting Rainfall Erosion Losses. *Agriculture Handbook 537, USDA, Washington, DC.*
- Yu, B., Rosewell, C.J., 1996c. Rainfall erosivity estimation using daily rainfall amounts for South Australia. *Australian Journal of Soil Research*, 34, 721-733
- Zanchi, C., 1993. Aspetti dell'erosione dei suoli nei diversi ambienti del bacino del Mediterraneo, in montagna ed in collina. In: La difesa del suolo in ambiente mediterranea. Atti del convengo svoltosi a Cala Gonone, 57-69.



*Bloque III: Estudio experimental de la erosividad de la lluvia*



## Bloque IV

### Valoración de los resultados de la investigación sobre el factor climático en la erosión del cuello en la cuenca del Ebro

"Sin caos, no hay conocimiento. Si no se desestima la razón con frecuencia no hay progreso." — Paul K. Feyerabend, "Contra el método".

#### Resumen

En este bloque se realiza una valoración crítica de la investigación llevada a cabo sobre la erosividad de la lluvia en la cuenca del Ebro. Se subrayan las principales aportaciones en relación con los estudios precedentes, contextualizadas dentro del marco conceptual que se desarrolló en el Bloque I. Asimismo, se evalúan de forma crítica la metodología utilizada y los resultados obtenidos, haciéndose hincapié en los aspectos que deben revisarse en futuros trabajos, a la vez que se plantean perspectivas futuras. Finalmente, se sintetizan las principales conclusiones, tanto a nivel general como específico sobre el estudio realizado en torno a la erosividad de la lluvia en la cuenca del Ebro.

#### Abstract

In this part a critical evaluation in relation with the research regarding rainfall erosivity in the Ebro basin is presented. It accounts for the main achievements acknowledged in relation with previous background summarized in "Bloque I: marco conceptual". A critical approach to the research, aimed in those points to be included or reviewed for future works and future perspectives are also raised. Finally, general and specific conclusions are summarized regarding the investigation on rainfall erosivity in the Ebro basin.





## 4.1. Introducción

Tal y como se destacó en el bloque I *la prevención de la erosión acelerada del suelo requiere la puesta en marcha de medidas de protección y conservación del suelo que exigen un sólido conocimiento de los factores y procesos que determinan la erosión.* Es claro que la erosión como fenómeno global resulta de la interacción de diversos procesos, condicionados por la concurrencia de muy diversos factores como la configuración del terreno, la cubierta vegetal, o el clima. Algunas de las metodologías más utilizadas para el estudio de la erosión, como la ecuación (R)USLE, reflejan en su propia formulación este carácter multifactorial. Sin embargo, no es posible llegar a un conocimiento global de la erosión sin abordar antes de forma aislada cada uno de sus distintos elementos. Dentro de la literatura sobre erosión del suelo han sido comparativamente escasos los trabajos dedicados al estudio de la erosividad de la lluvia más allá de zonas monitorizadas, reducidas a parcelas o pequeñas cuencas hidrográficas. La erosividad de la lluvia, sin embargo, es un elemento fundamental de la erosión, ya que constituye uno de los principales agentes erosivos al menos en ambientes mésicos como los que predominan en la mayor parte de nuestro país. Adoptando una perspectiva más amplia, la erosividad de la lluvia se relaciona con los procesos de intercambio de energía entre la atmósfera y la superficie terrestre, y ofrece información complementaria acerca de los procesos climáticos más allá de la intensidad o el volumen de la precipitación.

En España destaca el estudio titulado *La agresividad de la lluvia en España, valores del factor R de la Ecuación Universal de Pérdida de Suelo*, (ICONA, 1988), que sin embargo adolece de limitada validez debido al excesivamente breve periodo de medición en el que está basado, además de basarse únicamente en un índice de erosividad cuya validez en el territorio español no se ha contrastado. En lo que respecta a medidas puntuales sobre la erosividad de la lluvia resalta la tesis doctoral de Roldán Soriano (2006) y los estudios de Cerro et al. (1998) y Fernández-Raga et al. (2010).

La presente investigación se ha centrado en el estudio de la erosividad de la lluvia en la cuenca del Ebro, siendo ésta una zona geográfica complicada, tanto por sus peculiaridades climáticas como por su compleja geografía. El interés del trabajo no se limita sin embargo a ser un estudio regional, puesto que se ha puesto un



interés especial en el desarrollo y validación de metodologías que pueden ser extrapoladas a otras regiones.

Entre los objetivos de la Tesis que se enumeraban en el apartado 1.10, se hacía hincapié en la necesidad de construir bases de datos de erosividad de la precipitación espacialmente densas y temporalmente prolongadas para permitir un análisis climatológico de esta variable. Asimismo, se indicaba la conveniencia de la realización de estudios experimentales para valorar la conveniencia de los modelos existentes, e incluso para facilitar el desarrollo de modelos nuevos en caso necesario. Ambos aspectos han sido abordados en el desarrollo de la investigación, permitiendo realizar diversos análisis climatológicos de la erosividad de la precipitación en la zona de estudio. Los registros experimentales han permitido proponer una ecuación  $EC(I)$  para la cuenca del Ebro a partir de los datos obtenidos mediante disdrómetro óptico en el centro del valle del Ebro, así como determinar umbrales de erosividad para diversos suelos de la región.

En los siguientes apartados se describen los resultados obtenidos (sección 4.2), y se realiza una valoración crítica del grado de consecución de los objetivos propuestos y de los puntos críticos que requerirían una reevaluación o ampliación (sección 4.3). Se ofrece una perspectiva de las posibilidades de desarrollo futuro (sección 4.4), y finalmente se formulan las conclusiones generales de la Tesis (sección 4.5).



## 4.2. Principales aportaciones de la tesis doctoral.

En el primer bloque de esta monografía se realizó una revisión del estado del conocimiento sobre la erosividad de la precipitación. Aunque este trabajo no ha sido publicado, puede constituir una referencia de interés para futuras investigaciones, ya que sólo existe una revisión comparable en lengua castellana (Roldán Soriano, 2006) aunque menos completa.

En el segundo bloque de la Tesis se abordó el estudio climatológico de la erosividad de la precipitación en la Cuenca del Ebro.

El análisis de la relación entre la erosividad de la precipitación ( $EI_{30}$ ) obtenido a partir de datos de precipitación de alta resolución temporal y datos de precipitación diaria desarrollada permitió la creación de la base de datos de erosividad de la lluvia para la cuenca del Ebro durante el periodo 1955-2006 (sección 2.6). La comparación de varios modelos para la estimación de la erosividad a partir de registros diarios de intensidad de precipitación permitió discriminar el modelo de Yu y Rosewell (1996) como la solución óptima, al menos para nuestra zona de estudio. La construcción de la base de datos está así avalada por la investigación realizada sobre comparación de métodos, cuyos resultados están publicados en la revista *Journal of Hydrology* (Angulo-Martínez y Beguería, 2009) y han sido presentados en dos congresos.

A partir de la base de datos de erosividad de la precipitación se estudiaron distintas formas de interpolación espacial para estimar dos índices de erosividad (el factor R de la RUSLE y el índice  $EI_{30}$  promedio), evaluando también la incertidumbre espacial asociada (sección 2.7). La principal conclusión de este análisis fue constatar la elevada incertidumbre espacial de la erosividad de la precipitación, debido a su elevada dependencia de los episodios de precipitación de elevada intensidad. En este caso, sí existían estudios precedentes, pero ninguno de ellos contaba con una base de datos similar ni se había evaluado la incertidumbre espacial. Este estudio se ha publicado en *Hydrology and Earth System Science* (Angulo-Martínez et al., 2009).

A partir de los dos resultados anteriores (base de datos de erosividad de la precipitación y técnicas de modelización espacial) se realizó una cartografía de la erosividad de la lluvia anual y estacional (sección 2.5). Junto con la base de datos de erosividad de la precipitación, estas cartografías suponen una fuente de información nueva sobre una variable importante en la erosión del suelo.



Se estudiaron las relaciones entre la erosividad de la lluvia y los principales patrones de teleconexión atmosférica que influyen en la dinámica atmosférica y en la génesis de la precipitación del área de estudio (sección 2.8). Aunque la literatura abunda en trabajos sobre los efectos de las teleconexiones en la precipitación, no existían trabajos que analizaran sus efectos sobre la erosividad de la misma. Este trabajo ha sido aceptado para publicación en *Journal of Hydrology* (Angulo-Martínez y Beguería, aceptado). Un estudio preliminar contemplando tan sólo la relación existente entre NAO y la erosividad de la lluvia está publicado en la publicación resultante del congreso internacional sobre la oscilación del Atlántico Norte celebrado en Zaragoza en mayo de 2010, (Angulo-Martínez y Beguería (2011)).

Finalmente se estudió la dinámica temporal de la erosividad de la lluvia a escalas anual, estacional y diaria para el periodo 1955-2006 (sección 2.9). Los resultados coinciden, en cuanto a la tendencia decreciente de la erosividad de la lluvia, con otros estudios centrados en la precipitación. En el caso de la erosividad de la lluvia esta tendencia es consecuencia de un incremento en la ocurrencia de eventos menos erosivos mientras que se ha producido una reducción de los eventos elevados y extremos, en parte vinculado a la evolución positiva de los índices de teleconexión atmosférica. Este trabajo aporta nuevas evidencias de cambio climático en el patrón de las precipitaciones, y no ha sido todavía publicado.

En el tercer bloque de la Tesis se abordó un estudio experimental sobre la erosividad de la lluvia.

La monitorización de la precipitación en una parcela experimental mediante técnicas disdrométricas durante un periodo aproximado de 18 meses aportó información valiosa para abordar estudios independientes sobre la erosividad de la precipitación, más allá de la utilización de índices climáticos desarrollados en otros ámbitos geográficos.

En primer lugar se estudió la erosión por salpicadura en tres suelos característicos de la cuenca del Ebro (sección 3.3), pudiéndose formular un modelo empírico predictivo de la erosión por salpicadura en función de la erosividad de la precipitación a partir del índice  $EI_{30}$ . Este trabajo ha sido enviado a la revista *Geomorphology* (Angulo-Martínez et al., enviado).



Finalmente se abordó una validación de distintas metodologías de cálculo del índice  $EI_{30}$  por comparación con los valores medidos de forma experimental, determinándose que las tres metodologías estudiadas producían una sobreestimación de la erosividad de la precipitación que probablemente se deba a hipótesis acerca de la velocidad de caída de las gotas de lluvia, al sobreestimar la velocidad respecto a los valores reales medidos en campo. Este último trabajo permanece inédito.

### **4.3. Valoración crítica**

Como valoración positiva es importante resaltar el manejo de los métodos estadísticos en cada análisis realizado, lo que ha permitido llegar a los mejores resultados posibles. Además, se han tenido en cuenta distintas escalas de trabajo, siempre partiendo de la base diaria. Este rasgo es importante porque en el caso de la erosividad de la lluvia algunos eventos son responsables de la mayor parte de la erosividad que se produce a escala anual, estacional o mensual. Escalas temporales más agregadas enmascaran el comportamiento de esta variable y ofrecen una información sesgada. Este rasgo queda manifestado especialmente en el análisis de las tendencias.

Los principales puntos críticos o bien cuestiones que pueden mejorarse a futuro recaen especialmente sobre la construcción de la base de datos. La elevada incertidumbre espacial y temporal que muestra la erosividad de la precipitación hace necesario contar con redes pluviográficas densas y con periodos de medición prolongados. La creación de la base de datos de erosividad diaria para el periodo 1955-2006 se ha realizado con datos pluviográficos de 10 años (1997-2006) limitados temporalmente en la representación de la variabilidad climática del área de estudio. Actualmente se dispone de series más largas lo que permitiría actualizar la relación existente entre erosividad de la lluvia y precipitación y reconstruir la base de datos. Otro de los ajustes necesarios en la misma implica delimitar un umbral de temperatura para la precipitación nival, ya que de no ser así se sobreestima la erosividad en zonas donde esta es significativa. Un umbral de 0º C permitiría diferenciarla (Leek y Olsen, 2000). En cualquier caso estos ajustes modificarían sólo de forma matizada la base de datos existente, con lo que los resultados obtenidos seguirían teniendo validez.



Otra crítica pertinente se basa en la utilización de un índice empírico ( $EI_{30}$ ) calibrado con datos que reflejan dinámicas climáticas quizá no coincidentes con las que se dan en el área de estudio. En este sentido un índice de base física sería más adecuado pero la literatura científica consultada no ofrece hasta la fecha otro índice mejor. Nuestros resultados experimentales han demostrado sin embargo que el índice  $EI_{30}$  permite predecir de manera bastante precisa la erosión por salpicadura, aunque es posible que otros índices más refinados puedan arrojar resultados mejores. Respecto a la utilización de este índice, nuestros resultados muestran una divergencia entre los valores del mismo obtenidos a partir de estimaciones basadas en la intensidad de la precipitación y los valores medidos en campo mediante disdrómetro. También se han detectado diferencias originadas en la distinta resolución temporal utilizada para el registro de los datos, lo que conlleva problemas fundamentales para comparar los resultados publicados por distintos autores. Estas son cuestiones de importancia que merecen sin duda una investigación más profunda, y su debate en la comunidad científica.



#### **4.4. Perspectivas futuras**

Como perspectiva de trabajo futura, resalta el proyecto DISDROSPEC (CGL2011-24185) sobre *Monitorización y análisis del espectro disdrométrico de la precipitación y su aplicación al estudio de la erosividad y a la estimación de la precipitación por radar* (2011-2013) cuyo objetivo es el estudio de la variabilidad espacial y temporal del espectro de la precipitación en un área de estudio amplia y con contrastes climáticos y geográficos. Para ello se ampliará la red instrumental a transectos N-S y E-O en el valle del Ebro y se profundizará en las relaciones existentes entre intensidad de la precipitación y energía cinética en función de la situación meteorológica, y entre intensidad de la precipitación y lluvia radar.

Se plantea también la validación de los datos de erosividad de la lluvia obtenidos en este estudio con datos de escorrentía y exportación de sedimento en dos cuencas hidrográficas de pequeño tamaño monitoreadas en el Pirineo central (Aragüas y Arnas).

Futuros trabajos también investigarán las relaciones existentes entre erosividad de la lluvia y propiedades físico-químicas del suelo como evolución de la infiltración y cambios en la costra superficial en eventos de lluvia natural y efecto del splash sobre la cantidad de carbono orgánico, gracias a la continuidad de la campaña de experimentación iniciada durante esta tesis doctoral.



## 4.5. Conclusiones finales

El estudio que se presenta en esta tesis doctoral aporta un sólido conocimiento de la erosividad de la lluvia en la cuenca del Ebro, a partir del análisis, cuantificación y cartografía de la misma, pudiendo delimitar la zona Mediterránea, los Pirineos y pre-Pirineos como las zonas donde se alcanzan los mayores valores de erosividad de la lluvia.

La elevada variabilidad espacio-temporal que muestra esta variable la hace dependiente de redes de datos densas capaces de capturar tal variabilidad, unido al tratamiento de los datos mediante métodos estadísticos robustos con el objetivo de obtener buenos resultados. Desaconsejamos el uso de datos a resolución inferior a la escala diaria como datos de precipitación mensual, estacional o anual, ya que éstos enmascaran el comportamiento de esta variable al estar asociada fuertemente a los eventos de precipitación más intensos. El estudio climático de la erosividad de la lluvia en la cuenca del Ebro evidencia la dependencia de las dinámicas atmosféricas, especialmente en relación a eventos de precipitación elevados y extremos, con la erosividad que provocan, como consecuencia de la relación potencial entre la intensidad de la precipitación y la erosividad.

El experimento llevado a cabo para la medición de la energía de la lluvia en condiciones naturales ha permitido la validación del índice  $EI_{30}$  de la RUSLE (Brown and Foster, 1987) para la determinación de la erosividad de la lluvia empleado en el presente trabajo. El efecto de la energía cinética en la erosión por salpicadura (sección 3.3) manifiesta la importancia de la energía de la lluvia como agente erosivo, marcando un umbral de  $1 \text{ MJ mm ha}^{-1} \text{ h}^{-1}$ , correspondiente a eventos con volumen de precipitación de aproximadamente 4 mm.

Futuros trabajos han de continuar la investigación entre las dinámicas atmosféricas y condiciones genéticas de tipos de precipitación y la erosividad asociada, así como su efecto sobre el suelo.



## 4.6. Referencias

- Angulo-Martínez, M., Beguería, S., Navas, A., Machín, J. 2011. Splash detachment of soil particles under natural rainfall on three soil types of NE Spain, *Geomorphology* (en revisión).
- Angulo-Martínez, M., Beguería, S. 2011. Evaluation of the Relationship Between the NAO and Rainfall Erosivity in NE Spain During the Period 1955–2006, pag 183-198; in Vicente-Serrano, S. M. and Trigo, R. M. (eds.) *Hydrological, Socioeconomic and Ecological Impacts of the North Atlantic Oscillation in the Mediterranean Region*. Springer Verlag, Dordrecht Heidelberg London New York. ISBN 978-94-007-1371-0. DOI 10.1007/978-94-007-1372-7.
- Angulo-Martínez, M., Beguería, S. 2011. Do atmospheric teleconnection patterns influence rainfall erosivity? A comparison between NAO, MO and WeMO in NE Spain, 1955-2006, *Journal of Hydrology* (aceptado para publicación).
- Angulo-Martínez, M., Beguería, S. 2009. Estimating rainfall erosivity from daily precipitation records: a comparison among methods using data from the Ebro Basin (NE Spain). *Journal of Hydrology*, 379 (1-2), 111-121
- Angulo-Martínez, M., López-Vicente, M., Vicente-Serrano, S.M., Beguería, S. 2009. Mapping rainfall erosivity at a regional scale: a comparison of interpolation methods in the Ebro Basin (NE Spain). *Hydrology and Earth Systems Science*, 13, 1907-1920.
- Cerro, C., Bech, J., Codina, B., Lorente, J. 1998. Modeling rain erosivity using disdrometric techniques. *Soil Science Society of America Journal*, 62 (3) 731-735
- Fernández-Raga, M., Castro, A., Palencia, C., Calvo, A.I., Fraile, R. 2009. Rain events on 22 October 2006 in León (Spain): Drop Size Spectra. *Atmospheric Research*, 93, 619-635
- Leek, R., Olsen, P. 2000. Modelling climatic erosivity as a factor for soil erosion in Denmark: changes and temporal trends, *Soil Use and Management*, 16, 61-65
- Roldán Soriano, M. 2006. El poder de la lluvia. Características de la precipitación y erosividad. Nueva formulación para la estimación de la erosividad. Aplicación al cálculo del factor «R » de la USLE. Serie Técnica. Dirección General para la Biodiversidad. Ministerio de Medio Ambiente.



Yu, B., Rosewell, C.J., 1996. A robust estimator of the R factor for the Universal Soil Loss Equation. *Transactions of the ASAE*, 39, 559-561